Design, Synthesis and Characterization of Ti-containing Ordered Mesoporous Materials for Epoxidation of Vernonia Oil

Yaregal Awoke Genet

A Thesis Submitted to

The Department of Chemistry

Presented in Fulfillment of the Requirements for the Degree of Doctor of Philosophy (Inorganic Chemistry)

Addis Ababa University

Addis Ababa, Ethiopia

Addis Ababa University

School of Graduate Studies

This is to certify that the thesis prepared by Yaregal Awoke, entitled: "**Design, Synthesis and Characterization of Ti-containing Ordered Mesoporous Materials for Epoxidation of Vernonia Oil**" submitted in fulfillment of the requirements of degree of Doctor of Philosophy (Inorganic Chemistry) complies with the regulation of the University and meets the accepted standards with respect to originality and quality.

Signed by the Examining Committee

Examiner _____Signature _____Date _____

Examiner _____Signature _____Date _____

Examiner _____Signature _____Date _____

Advisor _____Signature _____Date _____

Advisor _____Signature _____Date _____

_____

Chair of Department or Graduate Program Coordinator

ABSTRACT

Design, Synthesis and Characterization of Ti-containing Ordered Mesoporous Materials for Epoxidation of Vernonia Oil

Yaregal Awoke

Addis Ababa University, 2020

This study focusses on obtaining heterogeneous Ti-containing catalysts through the design and optimization of pure silica SBA-15 and hybrid organic-inorganic PMO mesostructured materials in which the pore size, the particle morphology, and the surface chemistry are controlled to enhance the accessibility of the active sites and to avoid diffusion problems of substrates and products. The synthesis conditions of pure silica SBA-15 and hybrid organosilica PMO materials with different particle morphologies and pore sizes have been optimized. Ti has been incorporated in the framework/on the channel of both types of ordered mesoporous materials by using either co-condensation or grafting methods. To do this, the optimum SBA-15 and PMO materials, which have different pore diameters have been selected for Ti-grafting. A strategy has been designed to incorporate Ti in the framework of the mesoporous material during the support synthesis step (co-condensation). A detailed study has been undertaken to analyze the use of different surfactants, different Ti-source precursors, additives and different Ti/Si ratios of the synthesis gel to obtain Ti-incorporation in the T_d structure and thereby avoiding or minimizing the agglomeration of TiO_2 species. The prepared samples were characterized by X-ray diffraction (XRD), Thermogravimetric Analysis (TGA), N_2 adsorption-desorption isotherms, Scanning Electron Microscopy (SEM), Transmission Electron Microscopy (TEM), Inductively Coupled Plasma Optical Emission Spectroscopy (ICP-

OES) and Diffuse Reflectance UV-vis Spectroscopy (DRS UV-vis). The following Ti-containing SBA-15 and PMO with different particle morphologies and pore sizes with isolated Ti (IV) species have been synthesized:

- Ti-containing SBA-15 and PMO materials with hexagonal plate-like and fiber-like particle morphology using Pluronic P104 and P123 surfactants;
- Ti-containing SBA-15 materials with hexagonal pore structure and large pore diameters (> 10 nm) using TIPB micelle expander;
- Ti-containing PMO materials with moderately ordered hexagonal pore structure and large pore diameters (> 8.5 nm) using TIPB micelle expanders;
- Ti-grafted SBA-15 and PMO materials with highly populated isolated T_d Ti (IV) species and without formation of anatase TiO_2 species.

The catalytic activities of selected catalysts were tested for the epoxidation of cyclohexene using TBHP (5.5 M in decane solution) as an oxidant. The catalysts which give good conversion and epoxide selectivity in the epoxidation of cyclohexene were selected for epoxidation of vernonia oil. Solvent-free epoxidation of vernonia oil with anhydrous TBHP (5.5 M TBHP in decane solution) in the presence of selected Ti-containing SBA-15 and PMO catalysts was investigated. Ti-grafted materials show better catalytic activity than their corresponding Ti-containing materials, synthesized by the co-condensation method. Ti-containing SBA-15 materials are better in conversion when compared to PMO type of materials. Among them, Ti-grafted SBA-15 with large pore diameter (TiG-ESBA-L) gives the highest conversion (71%) with 80% of epoxide selectivity. Ti-containing PMO materials are better in epoxide selectivity in epoxidation of vernonia oil (achieving more than 90% epoxide selectivity) when compared to their corresponding Ti-SBA-15 materials.

ACKNOWLEDGMENT

First of all, I would like to express my sincere gratitude and deepest respect to my advisors Prof. Isabel Diaz and Dr. Yonas Chebude for giving a chance to study my PhD under their supervision. Their thoughtful guidance, invaluable advice, continuous supervision, valuable comments, encouragement, and assistance that greatly encouraged me during all stages of my PhD study. I am very thankful for their utmost dedication in providing research facilities and materials necessary for my research work. I extend my gratitude to all chemistry department staff members of Addis Ababa University for their invaluable help at every stage of my PhD study directly and/or indirectly.

I am also thankful to Dr. Carlos Marquez-Alvarez, Prof. Joaquín Pérez-Pariente, and Dr. Manuel Sánchez-Sánchez, for their invaluable suggestions and comments during my laboratory work. All the people at Institute of Catalysis and Petrochemistry (ICP-CSIC), especially the Molecular Sieves Group: Dr. Enrique Sastre, Dr. Luis Gómez-Hortigüela, Dr. Rosa M. Blanco, Marisol Grande, Dr. Alba Estrella Diaz Alvarez, Raquel, Gabriel and all others whose names are not mentioned are also acknowledged for their unreserved help in all aspects during my stay in CSIC-ICP, Madrid.

My sincere thanks go to all laboratory technicians of CSIC-ICP, Isabel Pacheco for giving me training for TGA analysis, Conchi and Javier Agúndez for running powder XRD and DRS UV-vis, and all technicians who are working in N_2 adsorption/desorption isotherm, ICP-OES, SEM, TEM, and ^{1}H-NMR.

I acknowledge the Spanish Research Council, CSIC, for sponsoring me nearly a year to stay in Spain via de iCOOP Program iCOOP+2016 COOPA20136. I also acknowledge the

School of Chemistry, University of Nottingham, for supplying $scCO_2$-extracted vernonia oil. I would like to extend my acknowledgment to IUPAC for sponsoring me for nearly a week to take training in Postgraduate summer school on Green Chemistry in Tanzania. I would like also to thank Addis Ababa University for hosting me as a PhD student and Assosa University for granting this study leave.

My entire lab mates, Dr. Guta Gonfa, Dr. Tesfaye Haile and Dr. Masresha Amare are also acknowledged for their helpful discussion and comments, which added value to my work.

Lastly but not least, I extend my greatest appreciation and hearty gratitude to my relatives especially Dr. Abere Genetu, my parents, my brother and sisters for their love and encouragement and also my very special thanks extends to my family, my wife Zoma Awoke Alene and my daughter Nuhamin Yaregal Awoke for their love, encouragement and understanding me throughout the ups and downs of the entire my PhD study.

TABLE OF CONTENTS

LIST OF FIGURES

LIST OF TABLES

LIST OF ABBREVIATIONS

SBA-15	Santa Barbara Amorphous number 15
PMO	Periodic mesoporous organosilica
Ti-SBA-15	Titanium containing SBA-15
Ti-PMO	Titanium containing PMO
OMM	Ordered Mesoporous Materials
MCM-41	Mesoporous Catalytic Materials 41
CTAB	Cetyl Trimethyl Ammonium Bromide
LCT	Liquid Crystal Templating
TEOS	Tetraethyl orthosilicate
TMOS	Tetramethyl orthosilicate
PEO	Polyethylene oxide
PPO	Polypropylene oxide
TIPB	1, 3, 5-Triisopropylbenzene
TMB	1, 3, 5-Trimethylbenzene
P123	Pluronic P123
P104	Pluronic P104
BTMSE	1, 2-Bis (trimethoxysilyl) ethane
BTESE	1, 2-Bis (triethoxysilyl) ethane
T_d	Tetrahedral
EVOs	Epoxidized vegetable oils
PVC	Polyvinyl Chloride
a. s. l.	Above sea level

FAMEs	Fatty Acid Methyl Esters
TS-1	Titanosilicate
AESO	Acrylated epoxidized soybean oil
SEM	Scanning Electron Microscope
TEM	Transmission Electron Microscope
TGA	Thermogravimetric Analysis
DRS UV-vis	Diffuse reflectance Ultraviolet-visible spectroscopy
XRD	X-ray Diffraction
BET	Brunauer-Emmett-Teller
BJH	Barrett-Joyner-Halenda
^{1}H NMR	Proton Nuclear Magnetic Resonance spectra
^{13}C NMR	Carbon-13 Nuclear Magnetic Resonance spectra
DTG	Derivatives of Thermogravimetric Analysis
ATR-FTIR	Attenuated total reflection-Fourier transform infrared spectroscopy
S_{BET}	BET Surface Area
VO	Vernonia Oil
$scCO_2$	Supercritical carbon dioxide
ICP-OES	Inductively coupled plasma optical emission spectroscopy
DR UV-Vis	Diffusion reflectance UV-Vis spectroscopy
a_o	Unit cell size
d	Interplanar spacing
nm	Nanometer
IUPAC	International union of pure and applied chemistry

GC-FID	Gas chromatography with flame ionization detector
TIP	Titanium (IV) isopropoxide
PMO-L	PMO materials synthesized using P123 surfactant
PMO-S	PMO materials synthesized using P104 surfactant
SBA-L	SBA-15 materials synthesized using P123 surfactant
SBA-S	SBA-15 materials synthesized using P104 surfactant
E-PMO-L	Large pore PMO-L material synthesized using TIPB as swelling agent
E-PMO-S	Large pore PMO-S material synthesized using TIPB as swelling agent
M-PMO-L	Large pore PMO-L material synthesized using TMB as swelling agent
M-PMO-S	Large pore PMO-S material synthesized using TMB as swelling agent
E-SBA-L	Large pore SBA-L material synthesized using TIPB as swelling agent
E-SBA-S	Large pore SBA-S material synthesized using TIPB as swelling agent
M-SBA-L	Large pore SBA-L material synthesized using TMB as swelling agent
M-SBA-S	Large pore SBA-S material synthesized using TMB as swelling agent
Cp	Cyclopentadienyl
CP_2TiCl_2	Titanocene dichloride
Ti-ESBA-L	Titanium containing E-SBA-L
Ti-ESBA-S	Titanium containing E-SBA-S
Ti-EPMO	Titanium containing E-PMO
TBHP	Tert-butylhydroperoxide
TiSBAL1	Ti/Si ratio of the synthesis gel is 0.01
TiSBAL5	Ti/Si ratio of the synthesis gel is 0.05
TiSBAL10	Ti/Si ratio of the synthesis gel is 0.1

CHAPTER ONE

1. INTRODUCTION

1.1. Background of the study

Over the last century our dependency on the petroleum oil resources for the synthesis of different products from industry, which is important in our daily lives, and used as energy source for transportation has increased dramatically. The growing demand of petroleum-based products, depletion of fossil oil reservoirs, escalating oil price and the negative impact of petroleum based products on the environment (their non-biodegradability & rising concentration of greenhouse gases like CO_2) are the driving force in searching for alternative, sustainable and renewable resources of energy and industrial feedstocks. Using renewable raw materials in chemical industry could generate a sustainable development to meet the needs of current and future generations. As a result, bio-based polymers derived from renewable feedstocks receive more and more attention for their eco-friendly properties, including reducing the consumption of non-renewable sources like petroleum and lowering the greenhouse gas emission. The most common renewable sources used are vegetable oils, polysaccharides, lignocellulose and proteins. Among these, vegetable oils are one of the most promising candidates to substitute petroleum derivatives as the monomers of polymers. Currently different scholars in many countries are motivated to investigate the bio-based resources and they report their investigation in different ways[1, 2]. Plant oils are often modified to increase their reactivity and therefore facilitate further conversion to higher value-added products to produce biodegradable and cost effective materials [3]. Bio-based epoxy resins are promising alternatives to petroleum-based epoxies, due to their lower toxicity and their availability from renewable resources. Epoxy oils are

widely used as raw materials for manufacturing of plastic formulations, protective coatings, lubricants, production of surfactants, polyurethanes and various types of composite materials[4]. Seeds from crops, such as soybean and linseed, are currently used as major sources of unsaturated oils for the synthesis of epoxy oils. However, these oils are edible and the chemical epoxidation process is expensive.

Ethiopia celebrates a large diversity in natural resources including non-edible seed oils. This richness offers tremendous opportunities for our country to pursue novel routes towards sustainability. In the mid-50s, the United States Department of Agriculture conducted extensive research to identify plants not competing with existing crops as new sources of industrial raw materials. Among the many species examined, *Vernonia galamensis*, native to East Africa, received much attention due to the high concentration of naturally epoxidized oil in its seeds, which could be used as a potential substitute for currently used epoxy oils. These seeds contain more than 40% oil, composed of vernolic (72 - 80%), oleic (4 - 6%) and linoleic (12 – 14%) esters. This showed that vernonia oil is composed from both epoxy and unsaturated carbon groups in the fatty acid chain. Therefore, full epoxidation of vernonia oil may lead to an oxirane value of about 10%[5, 6]. Although there are several methods available to epoxidize double bonds of unsaturated fatty acids, epoxy fatty acid compounds are obtained at industrial scale mainly by the peracid process. The peracid oxidant acts as the catalytic species *in situ* when a carboxylic acid (usually formic acid) reacts with hydrogen peroxide[7, 8]. However, soluble mineral acids are essential for this process and these acidic components have several drawbacks: i) side reactions because of acid-catalyzed epoxide ring opening; ii) difficult separation of acidic by-products; iii) production of abundant neutralized salts that have to be disposed;

iv) corrosion problems due to the strong acids present in the process. For these reasons, selectivity to the desired products is low. Additionally, the process does not comply with the principles and processes underlying green chemistry[9]. Due to these disadvantages, several recent studies have been undertaken paving the way to large scale, catalysis-based sustainable processes to be applied for the epoxidation of unsaturated fatty acid derivatives[10]. Herein we report our results on the selective epoxidation of cyclohexene and vernonia oil, using Ti-incorporated SBA-15 and PMO materials which have tunable pore size, suitable particle morphology and convenient surface chemistry as catalysts.

Heterogeneous solid catalysts that can generate desired products selectively and effectively are both economical and sustainable. Metallosilicate catalysts such as zeolites and mesoporous silica with tetrahedrally coordinated transition metal species covalently linked into silica frameworks have attracted attention as oxidation catalysts because of the specific nature of the active sites and the relative natural abundance of their composition elements[11-14]. Siliceous mesoporous materials of SBA-15 type possess a regular two-dimensional array of tubular channels. In comparison with other regular mesoporous materials, SBA-15 can be prepared with larger pores, resulting in a more stable structure due to the thicker pore walls[15, 16]. Titanium containing and organically modified SBA-15 mesoporous materials attracted our attention because of their promising application as selective oxidation catalysts for unsaturated organic compounds[17]. Their catalytic activity is highly affected by their composition, structure, and method of preparation. Functionalization of SBA-15 with isolated titanium sites either through co-condensation[18, 19] or grafting[20] has been an active area of research in the last decade. The loading amount and the dispersion of Ti greatly affect its reactivity[21]. The reactivity of the Ti source in the strong acidic media

required to prepare SBA-15 is the key parameter analyzed in the literature. Titanocene dichloride seems to be an efficient source to incorporate isolated Ti (IV) centres preventing TiO_2 oligomerization[22]. Moreover, following the same approach and aiming at enhancing the hydrophobicity of the pore surface, in this study titanium was incorporated successfully in Periodic Mesoporous Organosilica (PMO) with ethane groups forming the pore walls[23]. These works inspired us to proceed with the direct synthesis of Ti-SBA-15 and Ti-PMO using Cp_2TiCl_2 in the presence of non-ionic surfactants while developing tunable oxidation catalysts for bulkier molecules that may imply both larger pore size and short diffusion paths. Limited number of papers have been published on controlling the pore size and particle morphology during functionalization of Ti active sites in SBA-15 materials. The morphology of OMM particles plays a significant role in diffusion and adsorption of molecules[24, 25]. Thus our aim is to synthesize Ti containing SBA-15 and PMO materials by either direct hydrothermal synthesis or grafting method with different pore sizes and particle morphology and to evaluate their catalytic activity in epoxidation of unsaturated organic compounds.

1.1.1. Ordered Mesoporous Materials

In chemical catalysis, environmentally benign technologies are always been sought due to the strict environmental regulations. In recent years porous materials have attracted the attention of researchers and material scientists due to commercial interest in their applications in various fields especially in heterogeneous catalysis. Porous silicates are a huge family of inorganic materials, possessing open – pore frameworks and large surface area[26]. The synthesis, characterization, and application of novel porous materials have been strongly encouraged due to their wide range of applications in adsorption, separation,

catalysis, and sensors. The design and functionalization of porous materials suitable for specific application is still a challenge for the chemist. After the discovery of zeolitic materials as catalysts, several reactions of organic substrates using dilute solution of hydrogen peroxide were studied under mild reaction conditions. These zeolitic catalysts have some limitations in the case of bulky reactant molecules, due to their narrow pore sizes[13]. To overcome the limitations of microporous zeolite type materials, studies have been conducted in the field of mesoporous molecular sieves which have pore diameters between 2-50 nm, beginning with the M41S family[27]. Ordered mesoporous materials are nowadays an established class of materials characterized by large and uniform pore sizes, highly regular nanopores and a large surface area[28]. A large variety of structures and pore sizes have been investigated showing a wide range of uses as supports in various catalytic applications, including acidic/basic catalysis, hydrogenation, desulfurization, oxidation, asymmetric synthesis or enzyme catalysis[29]. In the early 1990s, Japanese scientists and Mobil scientists separately reported the synthesis of mesostructured silicates. Ordered mesoporous materials (OMM) were first synthesized by scientists of the Mobil Oil Company in 1992[27] . The prominent characteristics of these materials are high surface areas, narrow pore size distribution along with uniform pore size, typically in the range of 3 – 10 nm. Initially three mesophases were synthesized collectively known as M41S materials, and are described as mesoporous per the IUPAC nomenclature because of their pore diameters ranging between 2 nm < d < 50 nm. Perhaps the most widely recognized and used OMM is known as MCM-41 (a Mobil code for mesoporous catalytic material), with a regular hexagonal packed pore structure formed by 1D channels. The other two phases have cubic (MCM-48), or lamellar structures (MCM-50). Because of their unique

properties, MCM-41 have found uses in many biological applications such as drug delivery or cell imaging, cell labeling, and catalysis for catalyst adsorption and enzyme immobilization. A remarkable contribution in the synthesis of ordered mesoporous materials was made by Zhao *et al* [15] in 1998, who used triblock copolymer surfactants to template the formation of ordered large pore mesoporous silica with different structures under strongly acidic conditions. The synthesized mesoporous SBA-15 material exhibit interesting features like large pore openings (5-30 nm) and high porosity. SBA-15 is a hexagonally ordered silica material with tailorable uniform mesopores and micropores in the mesopore walls, uniform hexagonally arrayed channels with a narrow pore size distribution and good thermal and mechanical stability due to its thicker amorphous silica walls and it may exhibit a large variety of morphologies depending on the synthesis conditions. These properties of SBA-15 makes it a preferable choice to use as a support for different catalysts[15, 16].

The formation of mesoporous materials could be explained by using three main synthetic approaches (Figure 1). All these models are proposed on the basis of surfactants in the solution forming micelles that act directing the structure of the final material. Surfactants are amphiphilic molecules composed by hydrophilic head and hydrophobic tail groups within the same molecule that self-assemble so as to minimize the contact with incompatible ends. The way of interaction between the surfactants with inorganic species is the main difference among the various synthetic routes and is marked by the pH of the approach. Condensation followed by polymerization is a common step in all proposed mechanisms to produce mesostructured materials. In “true” liquid crystal templating method (route A), the surfactants are present in high concentrations forming micelles in

the synthesis media from the beginning and the self-assembly process of the surfactants results the formation of liquid crystal mesophases, which is followed by the formation of mineral network deposited around the self assembled substrate. This pathway had already been suggested as one possible mechanism for the formation of MCM-41 in the original publication by the Mobil group. The second proposed mechanism is called cooperative self-assembly in which the surfactants and the mineral network precursors produce the organized architectures (route B). The surfactant-inorganic composite mesophase forms cooperatively from the species present in solution (i.e., cooperative self-assembly), which are not in a liquid crystalline state prior to mixing of the precursors. In many cases, a cooperative self-assembly takes place *in situ* between the templating species and the mineral network precursors, with synchronized self-assembly and inorganic network formation, yielding the highly organized mesoscopic architectures. A two-dimensional (2-D) hexagonal mesoporous material (denoted as SBA-15 for Santa Barbara No. 15) was formed via this pathway[30]. A third approach was also proposed in which a nanometric inorganic component (nanometric building block) is present and can be subsequently assembled and linked by the organic connectors (route C). Here, no ‘‘soft’’ surfactant template is used, but instead the pore system of an ordered mesoporous silica is used as a hard template serving as a true mold for preparing compositions such as metals, carbons, or transition metal oxides. This nanocasting route is very suitable for creating frameworks that are difficult to access using liquid crystal-based templates (i.e., reactive oxides, polymers, carbons, non-oxides, metals, etc.)[30, 31].

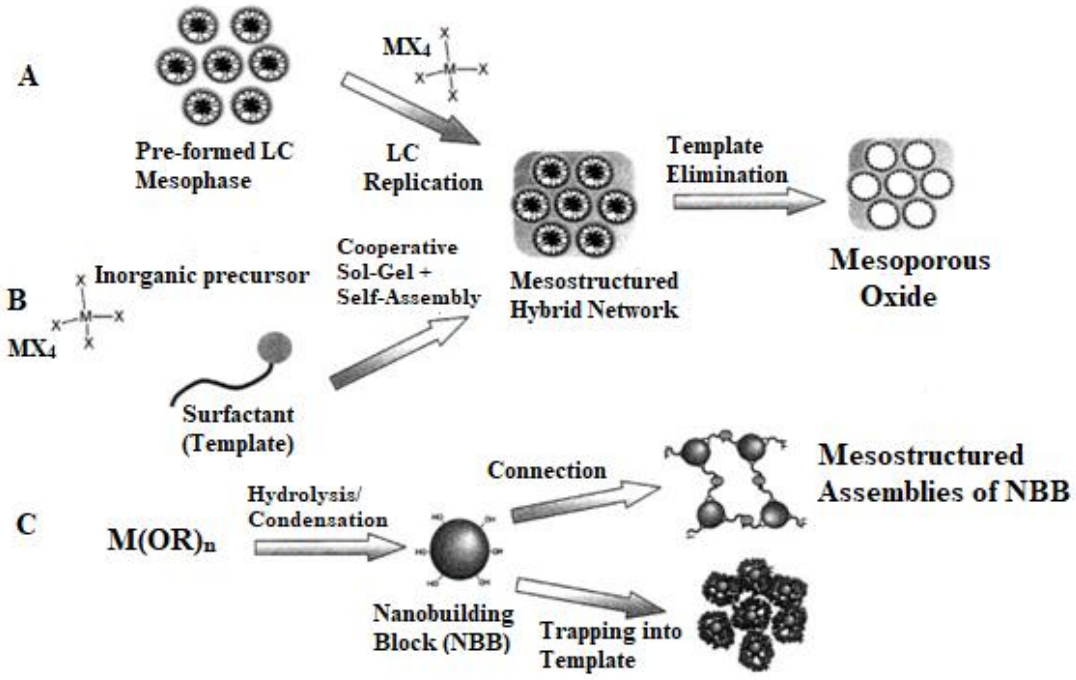

Figure 1. Main synthetic approaches for the mesostructured materials[32]

The synthesis of mesostructured materials could be directed by both the surfactant and inorganic soluble species. The interaction between the surfactants and inorganic precursors is the main factor for the formation of ordered mesoporous materials (Figure 2). Table 1 lists the main synthesis routes and the corresponding surfactants and classical products. When using cationic surfactants such as CTAB as a structure directing agent in alkaline media, the formation of the mesostructured material is mainly governed by electrostatic interaction. This means the charges of the surfactant (S) and the inorganic species (I) are opposite, in the given pH of the synthesis condition. The proposed synthesis path in the presence of electrostatic interaction could be direct synthesis route (S^+I^- & S^-I^+) or indirect synthesis path (the self-assembly of inorganic and surfactant species bearing the same charge). In the indirect synthesis path counterions used as charge compensation species. The choice of the counterion depends on the pH of the synthesis condition, in acidic

solutions, the $S^+X^-I^+$ path takes place in the presence of halide anions ($X^- = Cl^-$, Br^-) and in basic media, the $S^-M^+I^-$ path takes place in the presence of alkaline cations ($M^+ = Na^+$, K^+) (Figure 2 (A-D))[32]. Hydrogen-bonding interaction mechanisms, namely, S^0I^0 or N^0I^0, were proposed by Pinnavaia and co-workers for preparing mesoporous silicates under neutral conditions[33]. N^0 are neutral amines, S^0 are nonionic surfactants, and I^0 are hydrated silicate oligomers from TEOS. It should be noted that amines and PEO-derived molecules are different. Organic long-chain alkyl amines, which have hydrophobic hydrocarbon chains and hydrophilic amine groups, similar to surfactants. However, ethanol has to be added in the synthesis batch for mesoporous silicas due to the insolubility of these amines. Only disordered worm-like mesoporous silicas were obtained. Silicate oligomers are negatively charged in neutral solution. Neutral amines (N^0) and nonionic surfactants (S^0) are probably partially protonated or charged. Later on, the synthesis of mesoporous silica SBA-15 was carried out under a strongly acidic conditions by using triblock copolymer P123 as a template. It is more likely a double-layer hydrogen-bonding $S^0H^+X^-I^+$ interaction.

Table 1. Summary of synthesis routes to mesoporous materials with the emphasis on silicates[31]

Route	Interactions	Symbols	Conditions	Classical products
S^+I^-	electrostatic coulomb force	S^+, cationic surfactant I^-, anionic silicate species	basic	MCM-41, MCM-48, MCM-50, SBA-6, SBA-2, SBA-8, FDU-2, FDU-11, FDU-13, etc.
S^-I^+	electrostatic coulomb force	S^-, anionic surfactants, $C_nH_{2n+1}COOH$, $C_nH_{2n+1}SO_3H$,	aqueous	Mesoporous alumina

		$C_nH_{2n+1}OSO_2H$, $C_nH_{2n+1}OPO_2H$ I^+, metal ions such as Al^{3+}		
$S^+X^-I^+$	Electrostatic Coulomb force, double layer H bond	S^+, cationic surfactants I^+, silicate species X^-, Cl^-, Br^-, I^-, SO_4^{2-}, NO_3^-	acid	SBA-1, SBA-2, SBA-3
$S^-X^+I^-$	electrostatic Coulomb force, double layer H bond	S^-, anionic phosphate surfactants, $C_nH_{2n+1}COOH$, $C_nH_{2n+1}SO_3H$, $C_nH_{2n+1}OSO_2H$, $C_nH_{2n+1}OPO_2H$ I^+, transition metal ions, WO_4^{2-}, $Mo_2O_7^-$ X^+, Na^+, K^+, Cr^{3+}, Ni^{2+}, etc.	basic	W, Mo oxides
S^0I^0 (N^0I^0)	H bond	S^0, nonionic surfactants, oligomeric alkyl PEO surfactants, and triblock copolymers N^0, organic amines, $C_nH_{2n+1}NH_2$, H_2N $C_nH_{2n+1}NH_2$; I^0, silicate species, aluminate specie,	neutral	HMS, MSU, disordered, worm-like mesoporous silicates
$S^0H^+X^-I^+$	electrostatic Coulomb force and double layer H bond	S^0, nonionic surfactants I^+, silicate species X^-, Cl^-, Br^-, I^-, SO_4^{2-}, NO_3^-	acidic, pH < 2	SBA-n (n = 11, 12, 15, and 16)[34, 35], FDU-n (n= 1, 5 and 12), KIT-n (n = 5 and 6)

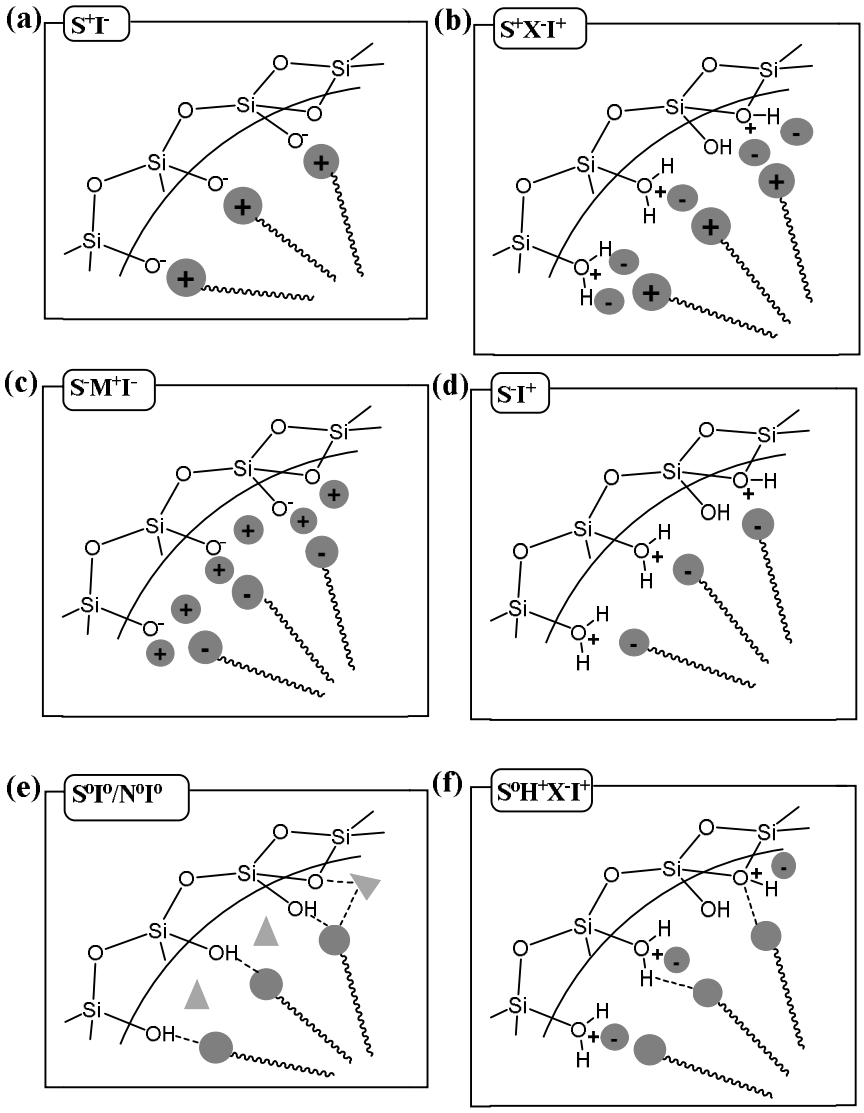

Figure 2. Schematic representation of the different types of precursor surfactant interfaces

As shown in Figure 3 the silica precursor sources hydrolyze in aqueous solution for the formation of silanol groups. During the hydrolysis step, water is used as a nucleophile in the presence of acid or base catalysts. The silanol molecules further condense with other silanol molecule (water condensation) or with other silica precursor (alcohol condensation) for the formation of siloxane group which could polymerize on the wall of the micelle. The hydrolysis and condensation of silica precursor sources and the interaction of these species

with each other as well as with the head of the surfactant produces ordered mesoporous materials with different structure, textural properties and particle morphologies.

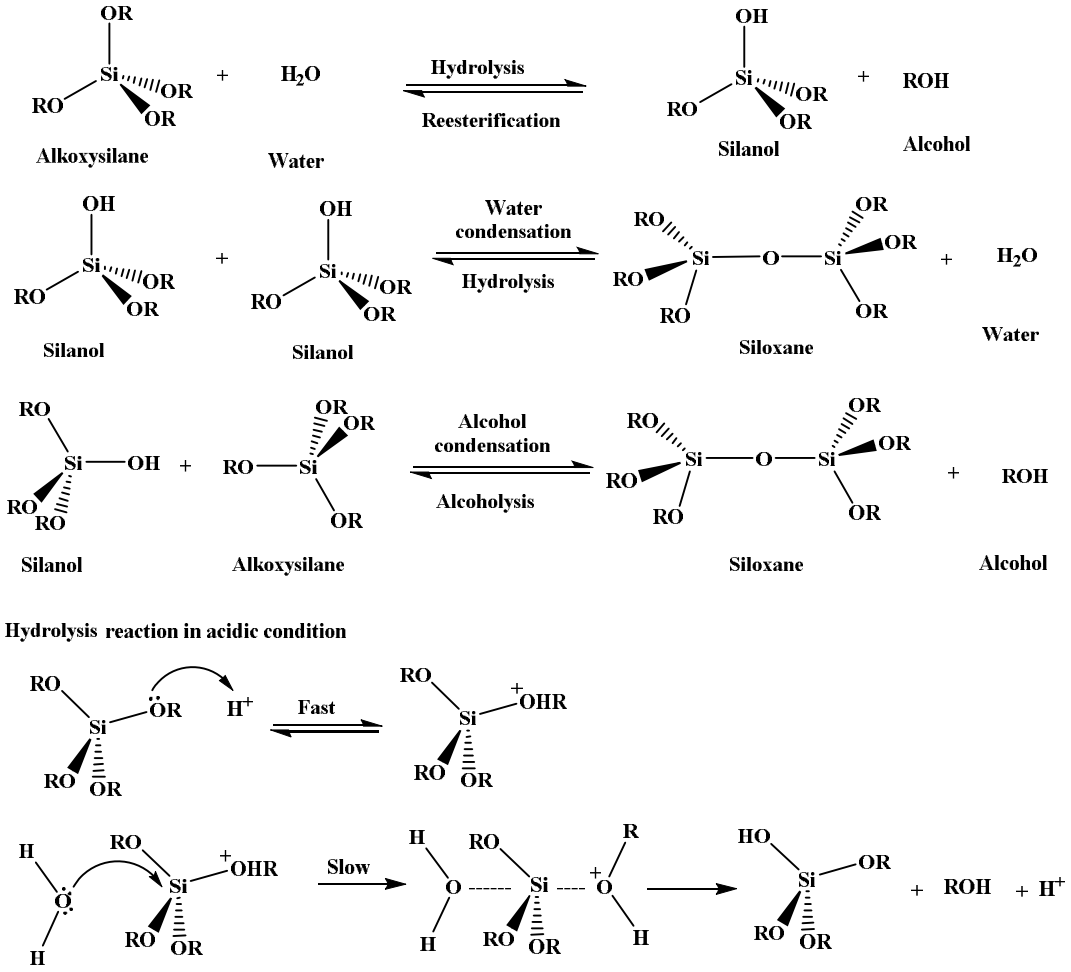

Figure 3. Mechanism of hydrolysis and condensation of silica precursor

1.1.2. Mechanism of SBA-15 formation

SBA-15 materials commonly synthesized using non-ionic surfactants such as Pluronic P123 ($(EO)_{20}(PO)_{70}(EO)_{20}$) (Figure 4) as a structure-directing agent in aqueous highly acidic solution to direct the formation of structured materials from the inorganic precursor through condensation reactions.

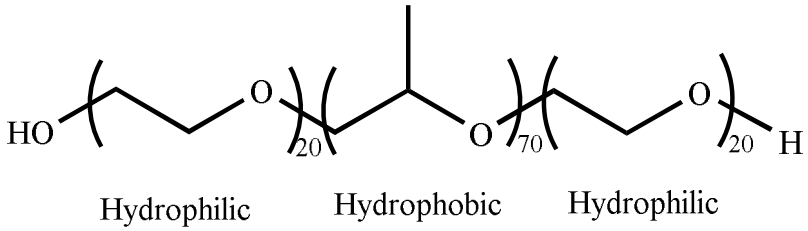

Figure 4. Pluronic P123 nonionic surfactant[36]

During the synthesis of SBA-15, the interaction mechanism of surfactant to inorganic species were proposed (Figure 2 f), where the main interactions between the surfactant and the inorganic species are H-bonding or dipolar which is denoted as $[S^0H^+X^-I^+]$[37]. The surfactant Pluronic P123 dissolved in acidic aqueous solution to form a micelle, both the surfactant and silica species protonated under acidic conditions and suitable for formation of electrostatic Coulomb force and double layer H bond between them.

- Ethylene oxide (EO) moieties of the surfactant in strong acid media associated with hydronium ions

  $REOm + yHX \rightarrow REOm\text{-}y[(EO).H_3O^+]y.....YX^-$

- Alkoxy silane species are hydrolyzed

  $Si(OEt)_4 + nH_3O^+ \rightarrow Si(OEt)_{4-n}(OH_2^+)_n + nEtOH$

Organic inorganic self-assembly is driven by weak non covalent bonds such as H- bonds, Van der Waals forces and electrovalent bonds between the surfactants and inorganic species.

$$REO_{m-y}\,[(EO).H_3O^+]y\ldots YX^-...I^+ \equiv S^0H^+X^-I^+$$

Based on hydrogen bonding interactions the neutral templating mechanism $S^0H^+X^-I^+$ (S^0H^+ being the surfactant hydrogen-bonded to a hydronium ion, X^- the chloride ion, and I^+ the protonated silica) has been proposed to synthesize mesoporous SBA-15 materials, in which

the randomly ordered rod like micelles (formed from the self organized surfactants) interact with the silica species to yield tubular silica deposited around the external surface of the micelle rods. The spontaneous ordering of these composite species result in the formation of hexagonal packed structure (Figure 5)[38].

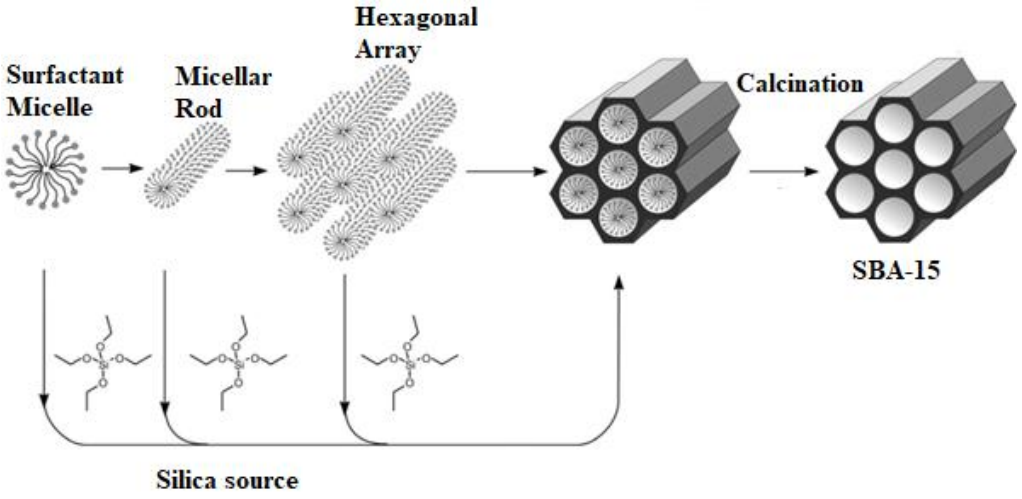

Figure 5. Formation of SBA-15 materials by cooperative self-assembly mechanism[39]

The main advantage of Pluronic P123 surfactant is that it is non-toxic and convenient to synthesize SBA-15 materials with standard pore sizes and ordered cylindrical pore structure with hexagonally arranged channels. However, the conventional particle morphology of the final material produced using Pluronic P123 surfactant is very long fibers. This may be due to the presence of more hydrophobic PPO groups in the surfactant molecule assisting the end to end hydrophobic micelle interaction in one dimension. Such type of particle morphology may hinder the diffusion of bulky molecules or the accessibility of the active sites towards the reagents. This limitation could be avoided either by increasing the pore diameter or controlling the particle morphology.

The pore size and particle morphology of SBA-15 materials can be controlled by using different methods. The pore size of SBA-15 may be increased up to 30 nm using alkanes from hexane to dodecane, 1, 3, 5-trimethylbenzene (TMB) and 1, 3, 5-triisopropylbenzene (TIPB) as a swelling agent. An alternative way to enlarge the pores is to reduce the shrinkage during calcination by increasing the hydrothermal treatment time or temperature. Another way is to avoid the calcination step altogether and use other methods for template removal (extracting with ethanol in acidic solution or with H_2O_2). Different morphologies of SBA-15 such as fibers, platelets, pearls, monoliths, films, etc. can be synthesized by variations in the reaction conditions during the synthesis or by additions of salts such as KCl, NH_4F or Na_2SO_4. Different alkanes in combination with NH_4F have yielded morphologies such as sheets, fibers and nanosized slices depending on the alkane used and reagent concentrations. Accessibility of the pores depends on the morphology which makes different morphologies suitable for different applications. When alkanes are used as co-solvents in the synthesis, the pore length is decreased and short channel materials are produced as illustrated in Figure 6. The micelle expander added into the synthesis solution either enter the micelle cores to increase the pore size or it could be found in the solution as droplets stabilized by the crystallites to change the morphology from fiber to sheets[40]. At the point of morphological transition, the material may lose its hexagonal structure. Therefore, appropriate amount of micelle expander should be added to increase the pore size without affecting the pore structure, the ratio of micelle expander to P123 will be increased only until the pores are saturated (Figure 6 (b)).

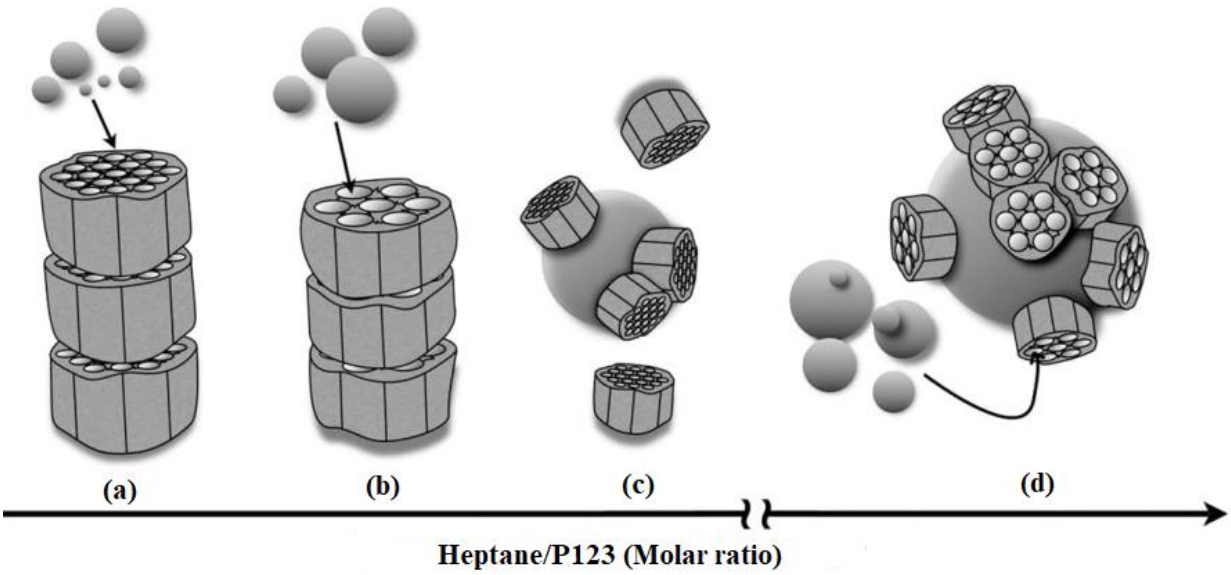

Figure 6. Schematic representation of the role of heptane in the formation of different morphologies of SBA-15 due to the hydrophobic ends of the crystallites. In (a) and (b) X < 470, (c) 470 < X < 920 and (d) X = 920 (X is molar ratio of heptane/P123)[40]

One of the common methods used to control the particle morphology of SBA-15 materials is using surfactants which have balanced hydrophilic (PEO) and hydrophobic (PPO) groups as a structure-directing agent. Pluronic P104 ($(EO)_{27}(PO)_{61}(EO)_{27}$) (Figure 7) is one of commonly known structure-directing agent used to synthesize SBA-15 materials with short channel and plates-like particle morphology.

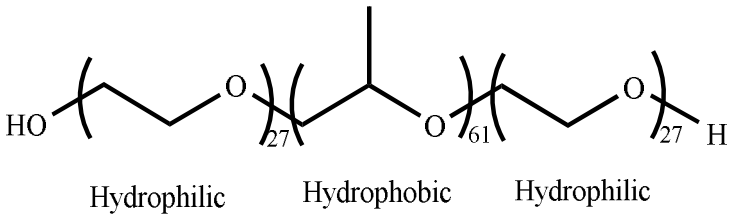

Figure 7. Pluronic P104 nonionic surfactant[41]

This may be due to the presence of balanced hydrophobic and hydrophilic groups in the surfactant molecule give equal probability to the end-to-end as well as side-to-side micelle interaction produces plates-like particles. The synthesis condition (acidic solution) as well as the mechanism of its interaction with the silica species (H-bonding) is similar with Pluronic P123, as a result produces materials with similar pore structure, ordered pore structure with hexagonal array of channels. However, its pore structure and its textural properties are highly sensitive towards the synthesis condition when using Pluronic P104 as a structure-directing agent.

The applicability of pure silica SBA-15 is based on the presence large number of silanol (Si-OH) groups on the surface of the material, and the potential for surface functionalization (Figure 8) [42]. The advantages of such a reactive pore surface relies on the capacity to functionalize to a targeted application.

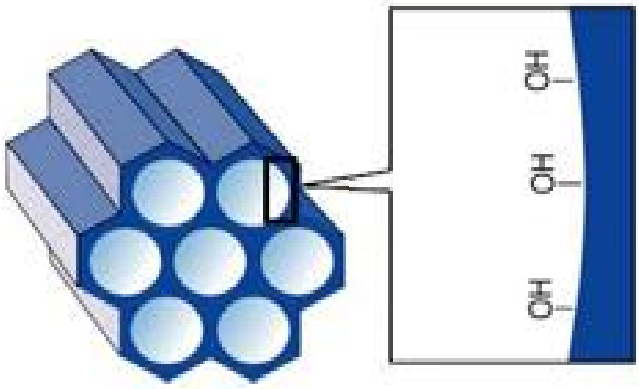

Figure 8. Hexagonal symmetry and hydrophilic surface of SBA-15 type of materials

1.2. Surface modification of ordered mesoporous materials

Pure silica ordered mesoporous materials are not active to catalyze chemical reactions unless they are functionalized with catalytically active functional groups[43]. The degree of

surface acidity and surface hydrophobicity of the porous materials are the two important parameters in catalysis of oxidation reactions. Functionalized with catalytically active groups and improving the surface hydrophobicity by minimizing surface hydroxyl groups are very important surface modification methods of ordered mesoporous materials to make it a powerful catalyst in oxidation reactions. The catalytic properties of molecular sieves rely on the presence of active sites in their frameworks/channels. In industrial manufacturing of fine chemicals, the selective oxidation transformations are widely performed in the presence of organic peroxides and are catalyzed by metallosilicate-based heterogeneous catalysts. The literatures concerning successful incorporation of metal hetero atoms into MCM-41 materials have been developing for industrial application to catalyze such type of reactions[44]. With the incorporation of various metals including Ti, it was found that the catalytic properties of these materials could be improved. The field of mesoporous titanium silicates is one of the fastest developing areas of porous materials. The attempts to obtain titanium materials with high catalytic activity and tunable catalytic behavior lead to the development of various processes for their synthesis. A combination of the large pore dimensions of mesoporous materials with the catalytic active sites in these structures would be highly advantageous leading to novel and probably useful catalysts or catalyst carriers. A good accessibility of reactant to the active sites and rapid departure of the desired products could be possible with anchoring of metal oxide species onto the inner walls of the mesopores[45]. Soon after the reports for mesoporous silicas synthesized by the surfactant-templating approach, Ti-containing mesoporous materials including Ti-MCM-41, Ti-MCM-48, Ti-SBA-1, Ti-SBA-15 and so on have been found to be used as versatile catalysts for the conversion of bulky molecules[46]. Among them, Ti-SBA-15 with a large

pore size ranging from 6 to 10 nm attracts much attention, its large pore diameter may improve the diffusion of reagents or the accessibility of the active sites.

1.2.1. Titanium incorporation in SBA-15 materials

Formation of highly dispersed metallic nanoclusters in SBA-15, provide a significant and valuable contribution to the area of mesoporous material synthesis and the resulted catalysts have the advantage of higher stability and the excellent control of the pore size and shape. Pure silica SBA-15 can be used as a versatile catalyst support material or catalytic site via partial substitution of Si^{4+} by other cations. The incorporation of heteroatoms into the walls of mesoporous silica material is of great importance in the field of catalysis. However, in the case of metal incorporated SBA-15, only a small fraction of the metal precursor added was retained into the mesoporous structure, which might be due to the easy dissociation of metal–O–Si bonds under strongly acidic conditions. Transition metal ions like Mo[47], Ti[19], V[48], Nb[49] incorporated into silica materials due to their interesting catalytic properties in many reactions.

The discovery of titanosilicate molecular sieves opened up a new chapter in the selective oxidation of several substrates under mild conditions. However, the intrinsic pore geometry of this molecular sieve limits the range of substrates for which it can be used, which has led to increased efforts to find ways around this restriction. To overcome the diffusion limitations and to facilitate easy access to the active sites of these molecular sieves, several authors have used titanium based large pore molecular sieves[50]. Titanium-containing ordered mesoporous silicates have attracted much attention because of their potential as selective oxidation catalysts for bulky organic substrates (triglyceride molecules)[51]. It is widely known that the dispersion of the titanium centers, the accessibility of the substrates

to them and the porous structure of the final material play a role on the catalytic properties of these catalysts. Moreover, these features can be controlled through the choice of the proper synthetic procedure and the titanium source[52]. In general, there are two well-known methods to incorporate Ti in the framework/channel of SBA-15: (i) Co-condensation: the simultaneous condensation of corresponding silica and titanium precursors[53] (ii) Grafting: a post synthesis treatment, by which metal sources incorporate on mesoporous silica from vapor deposition or impregnation and subsequent calcination (Figure 9)[20]. Grafting method is more advantageous in terms of accessibility of the active sites towards the reagents, most of the active sites could be on the pore surface. The limitation of this method may be the dispersity of the active sites and the leaching problem during the reaction. Appropriate selection of solvents during grafting and calcination at the end of the grafting process may improve the dispersity and stability of the active sites, respectively. By comparison, titanium can be directly incorporated into the silica framework by one-step condensation. One-step synthesis also shows the advantage in the possibly uniform distribution of titanium species, the avoidance of pore blockage and Ti leaching is minimized during the reaction. However, the less accessibility of the active sites due to the buried Ti species in the amorphous pore wall of the SBA-15 materials is the drawback of this method. The co-condensation synthesis involves the cooperative assembly between surfactant templates and inorganic precursors. Besides interaction between organic and inorganic species, the interaction inside the inorganic species themselves should be considered. In the synthesis of Ti-containing mesoporous silicas, the hydrolysis and condensation of titania should be fully considered because of much faster rates than those of silica. Several methods have been used to reduce the hydrolysis and condensation rates of Ti precursors or improve the

hydrolysis rate of silica sources. Expensive organic titanium sources are normally applied. For example, the initial reports on titanium-containing mesoporous silicas used chemically modified Ti-alkoxide to control over the rate of hydrolysis of the metal precursor. Melero et al. prepared Ti-containing mesoporous silica by using titanocene dichloride as a titanium source[52].

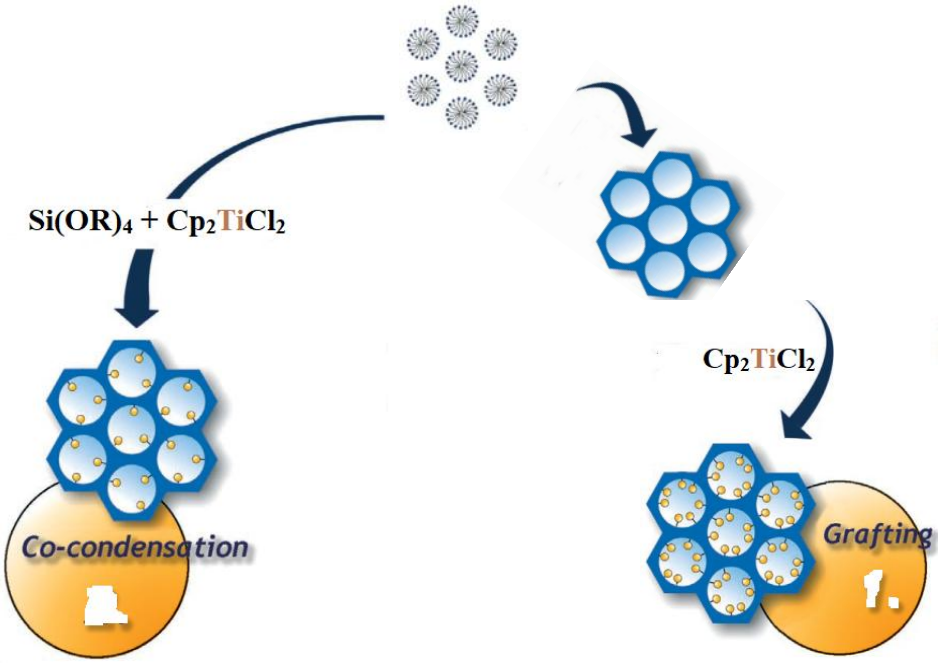

Figure 9. Synthesis methods of Ti-SBA-15 materials

The synthesis of SBA-15 materials with a high content of Ti in its framework with avoiding agglomeration of TiO_2 species by using the co-condensation method is a challenging job. Until now, reports on the successful preparation of Ti-containing mesoporous materials under acidic conditions are very few and this might be due to the easy dissociation of Ti–O–Si bonds under acidic and hydrothermal conditions[18]. In the direct synthesis of Ti-SBA-15 materials, the concentration of the acid, the concentration of the titanium precursor and

the hydrothermal synthesis temperature and time greatly influence the Ti incorporation ratio and its chemical environment[53].

1.2.2. Improving surface hydrophobicity of SBA-15

Although Ti-incorporated SBA-15 materials are good catalysts to catalyze different oxidation reactions, the presence of excessive surface hydroxyl groups make the surface more hydrophilic. This surface property may hinder the adsorption and diffusion of hydrophobic reagents and decrease the selectivity of epoxides during epoxidation reaction due to ring opening reaction facilitated by surface hydroxyl groups. To improve the hydrophobic properties of pure silica mesoporous materials (SBA-15), it should be modified by using surface functionalizing agents (hydrophobic groups). The combination of the properties of organic and inorganic building blocks within a single material is particularly attractive from the viewpoint of materials scientists because of the possibility to combine the enormous functional variation of organic chemistry with the advantages of a thermally stable and robust inorganic substrate. This is particularly applicable to heterogeneous catalysis. The symbiosis of organic and inorganic components can lead to materials whose properties differ considerably from those of their individual, isolated components[54, 55].

In general, there are three well known methods to synthesize porous organic-inorganic hybrid materials: (i) grafting of the purely inorganic silica materials by organic groups to modify the pore surfaces of the material[56] (ii) co-condensation: the simultaneous condensation of corresponding silica and organosilica precursors, (iii) production of periodic mesoporous organosilica (PMO) through the incorporation of organic groups as

bridging components directly and specifically into the pore walls by using bissilylated single-source organosilica precursors[39].

The application of the grafted hybrid materials is highly limited due to the nonhomogeneous distribution of the organic groups within the pores due to the restriction of diffusion of reagents further into the center of the pores. In extreme cases (e.g., with very bulky grafting species), this can lead to complete closure of the pores (pore blocking). The problem of pore blocking could be avoided by synthesizing the hybrid materials through co-condensation of the pure silica sources (TEOS & TMOS) and terminal trialkoxyorganosilanes of the type $(RO)_3SiR$ in the presence of structure-directing agents leading to materials with organic residues anchored covalently to the pore walls. In this synthesis method organic units are generally more homogeneously distributed than in materials synthesized with the grafting process[57]. However, the co-condensation method also has disadvantages derived from the degree of mesoscopic order of the produced materials decreasing with increasing the concentration of $(RO)_3SiR$ in the reaction mixture, which ultimately leads to totally disordered products. Furthermore, the proportion of terminal organic groups that are incorporated into the pore-wall network is generally lower than would correspond to the starting concentration of the reaction mixture. While increasing the concentration of $(RO)_3SiR$ in the initial reaction mixture the tendency towards homocondensation reactions, which is caused by the different hydrolysis and condensation rates of the structurally different precursors, is a constant problem in co-condensation because the homogeneous distribution of different organic functionalities in the framework cannot be guaranteed. Due to this reason, another synthesis method of organic–inorganic hybrid materials (PMO) by hydrolysis and condensation reactions of

bridged organosilica precursors of the type $(RO)_3Si\text{-}R\text{-}Si(OR)_3$ has been known for a long time from sol–gel chemistry.

Periodic Mesoporous Organosilicas (PMOs) are characterized by a periodically organized pore system and a very narrow pore size distribution. The first PMO was synthesized in 1999 by three research groups working independently of one another[58]. In PMO materials the organic units are incorporated in the three-dimensional network structure of the silica matrix through two covalent bonds and thus distributed totally homogeneously in the pore walls[57]. In this approach, 100% of the Si-are holding a Si-C bond, increasing notably the degree of hydrophobicity of the material. PMO materials could be synthesized by following the concept of the synthesis of pure silica SBA-15 materials but using bissilylated organosilica precursors, $(R'O)_3Si\text{-}R\text{-}Si(OR')_3$, — in which the organic bridges are integral components of the silica network. The synthesis mechanism of PMO materials is similar to the synthesis mechanism of pure silica SBA-15 materials, except that the interactions are not well defined, the structure of the final material strongly depend on the surfactant to organosilica precursor interaction. During the synthesis of PMOs materials, inorganic salts like KCl have been used to improve the condensation rate and thus the hydrothermal stability, control the morphology, extend the synthesis domain, and tailor the framework porosity, results that can be attributed to the specific effect of inorganic salts on the self-assembly interaction between surfactant head groups and organosilica species[59]. This type of materials offer the possibility to adjust the surface hydrophobicity and reactivity, as well as their mechanical and hydrothermal stability through the incorporation of different functional organic moieties in their pore walls[57, 60]. With uniformly distributed bridging functional groups (R) in their frameworks, PMOs possess ordered mesopores as well as

various functional groups, offering a wider application potential over their pure inorganic counterparts (SBA-15)[61].

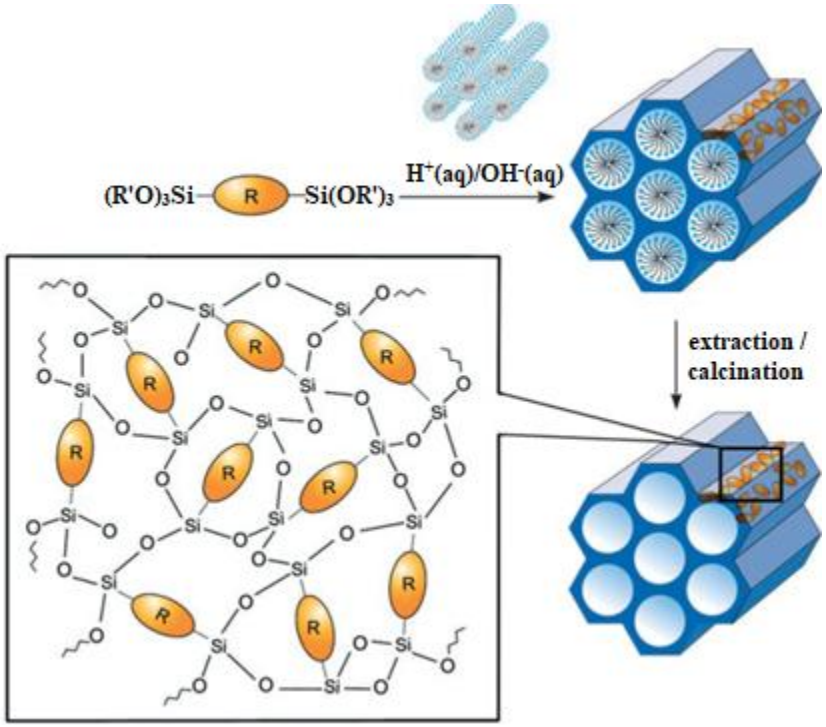

Figure 10. General synthetic pathway to PMOs that are constructed from bissilylated organic bridging units[39]

The main steps for the synthesis of PMOs are shown in Figure 10, where R is commonly ethane, vinyl or phenyl group. Such a method results in higher loading of the bridged precursor with no problem of pore blocking and leaching[62]. Currently, PMOs are considered a class of materials which have potential applications in catalysis[63], chromatography, electronics[64], metal adsorption[65] and immobilization of biomolecules[59, 66].

1.2.3. Titanium incorporation in PMO materials

As mentioned above, the introduction of transition metal ions like Ti (IV) ion through co-condensation or grafting method improves the surface acidity and the catalytic activity of the material. According to Bhaumik, *et al*[67] and Chu *et al*[68] report, Ti can be incorporated within the framework of PMO materials by using the direct synthesis method. In alkaline conditions, Ti-containing ethane-bridged hybrid mesoporous materials Ti-HMM with a high content of Ti (2 wt. %) was synthesized. However, the pore size is limited to 3 nm, this may hinder the accessibility of active sites during the reaction with bulky molecules[67]. A relatively large pore size Ti-containing PMO was synthesized by using Pluronic P123 surfactant in acidic media. However, the maximum amount of Ti incorporation was only about 0.34 wt.% regardless of the initial Ti/Si ratio[68]. This may be due to the fast hydrolysis of Ti-O-Si from the wall of the material in acidic conditions. As a result, only a limited number of papers have been published in the area of this study. Thus, optimizing conditions to synthesize Ti-PMO materials with highly dispersed T_d Ti (IV) active sites is a currently active research area.

1.3. Plant seed oils: Vernonia galamensis

Plant oils composed predominantly of triglycerides (Figure 11) are playing an important role in the chemical industry, thanks to their inherent biodegradability, accessibility, and versatile modifications as well as environmental issues and scarcity of petroleum sources[69]. According to Statista, vegetable oil production is growing constantly and amounted to some 203.83 million metric tons worldwide in 2018–2019[70]. Most of the plant oils (Table 2) could be used in food industry as well as a raw materials to produce different products. Due to their high consumption in recent years, approximately 80 % of plant oils were

utilized for food application, whereas only about 20% are used as industrial feedstocks for biofuels, coatings, paints, lubricants, plasticizers, surfactants, etc[71]. On the other hand, the industrial products based on plant oils and their derivatives have been rapidly expanding due to the depletion of petroleum oil resources and their toxicity[10]. The industrial application of plant oils is mostly based on chemical modification of the carboxyl and the unsaturated carbon present in triglyceride.

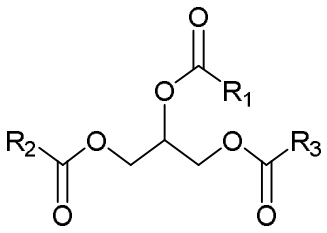

Figure 11. Triglyceride structure of vegetable oils

R represents the fatty acid chains which may have different number of carbon atoms, number of unsaturated carbons (Table 2) and in the possible presence of naturally formed functional groups, like hydroxyl or epoxy groups and in the possible presence of naturally formed functional groups. To synthesize polymers from triglyceride oils, the presence of reactive positions like ester, unsaturated carbons, allylic hydrogen atoms and the α-position of ester groups in the fatty acid chains used to modify the triglyceride structure (Figure 12)[72]. Epoxidation of the unsaturated carbon is one of the most interesting chemical modifications of the plant oils to increase their reactivity during polymer synthesis[69, 73].

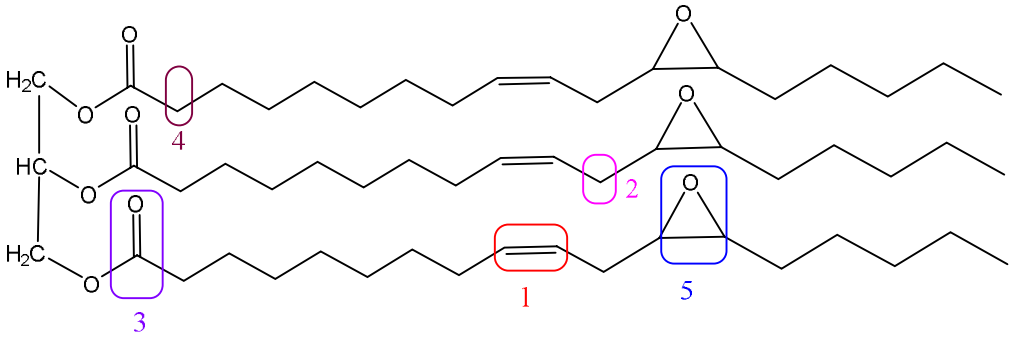

Figure 12. Reactive sites exploited for the preparation of macromolecular materials from unsaturated plant oils (e.g. vernonia oil)

According to different reports[4], one of the most promising routes of vegetable oil utilization is the production of epoxidized vegetable oils (EVOs). EVOs were commonly used as polyvinyl chloride (PVC) stabilizers, plasticizers for plastics, lubricants and starting materials to produce polyols and prepolymers in surface coating formulations and to synthesize polyurethane foams. Polymers obtained from epoxidized plant oils have better mechanical, electrical and thermal properties than those of the polymers obtained from petrochemical products. Generally epoxidized plant oils are important intermediates in organic synthesis as they participate in many reactions due to the presence of highly reactive oxirane rings[74].

Table 2. Typical properties and fatty acid compositions of common vegetable oils

Vegetable oil	Double bonds[a]	Iodine value[b]	Oleic	Linoleic	Linolenic	Palmitic	Stearic
Canola	3.9	110-126	61	21	9	4	2
Cottonseed	3.9	90-119	19	54	1	22	3
Corn	4.5	102-130	25	60	1	11	2
Linseed	6.6	168-204	22	17	52	5	4
Olive	2.8	75-94	71	10	1	14	3
Palm	1.8	44-58	39	10	-	44	4
Peanut	3.4	80-106	48	32	-	11	2
Soybean	4.6	117-143	23	53	8	11	4
Sunflower	4.7	110-143	42	47	1	6	4

* Note: percentages may not add to 100% due to rounding and/or presence of other minor fatty acid contents, which are not listed; [a] average number of double bonds per triglyceride; [b] Iodine value = grams of iodine consumed by 100 g of oil samples.

Vernonia galamensis is a new potential industrial oilseed crop (Figure 13) with origin in East Africa including Ethiopia[75]. It was identified for the first time in Eastern Ethiopia by Perdue in 1964 at 7 km south east of Harar town, 9º14'N and 42º35'E at 1700 m a.s.l.[76]. It is known to naturally grow as weeds in fields or in wood lands under a wide range of agro ecological conditions of Africa. In the 1950s *Vernoniaanthelmintica* (L.) Wild was noted as a potential source of vernolic acid, but efforts to domesticate it has failed. In 1964 in semi-arid areas of Eastern Ethiopia, specimens of *Vernonia galamensis* were collected that combined a high vernolic acid content with a promising seed yield and good seed retention[77, 78]. Reports have witnessed that different parts of Ethiopia are habitats of *vernonia galamensis* weed[79]. The seed oil has unique chemical and physical properties that will permit its use in the formulation of reactive diluents, products to serve as solvents that

become part of the dry paint surface and do not evaporate to pollute the air[6]. Seeds of vernonia produce triglyceride oil, rich in vernolic acid, a naturally epoxidized[80] fatty acid which is environmentally friendly, less expensive and less viscous compared to other artificial epoxy oils.

Figure 13. Vernonia galamensis weed and its seed[81]

1.3.1. Structure, composition and reactivity of vernonia oil

The seeds of *Vernonia galamensis* contain more than 40% triglyceride oil, composed from vernolic acid (72 – 80%), linoleic acid (12 – 14%), oleic acid (4 – 6%), stearic acid (2 – 3%), palmitic acid (2 – 3%) and a trace amount of arachidic acid (Figure 14)[77, 78, 82]. The trivernolin is composed of three fatty acids from the above type and glycerol juncture. The free fatty acids could be formed by the hydrolysis of triglyceride of vernonia oil[72]. The commercial importance of vernonia oil includes its use as a reactive diluent in coatings, in plastic formulations, chemical coatings, epoxy resin, adhesives, plasticizers and stabilizers and as a chemical intermediate.

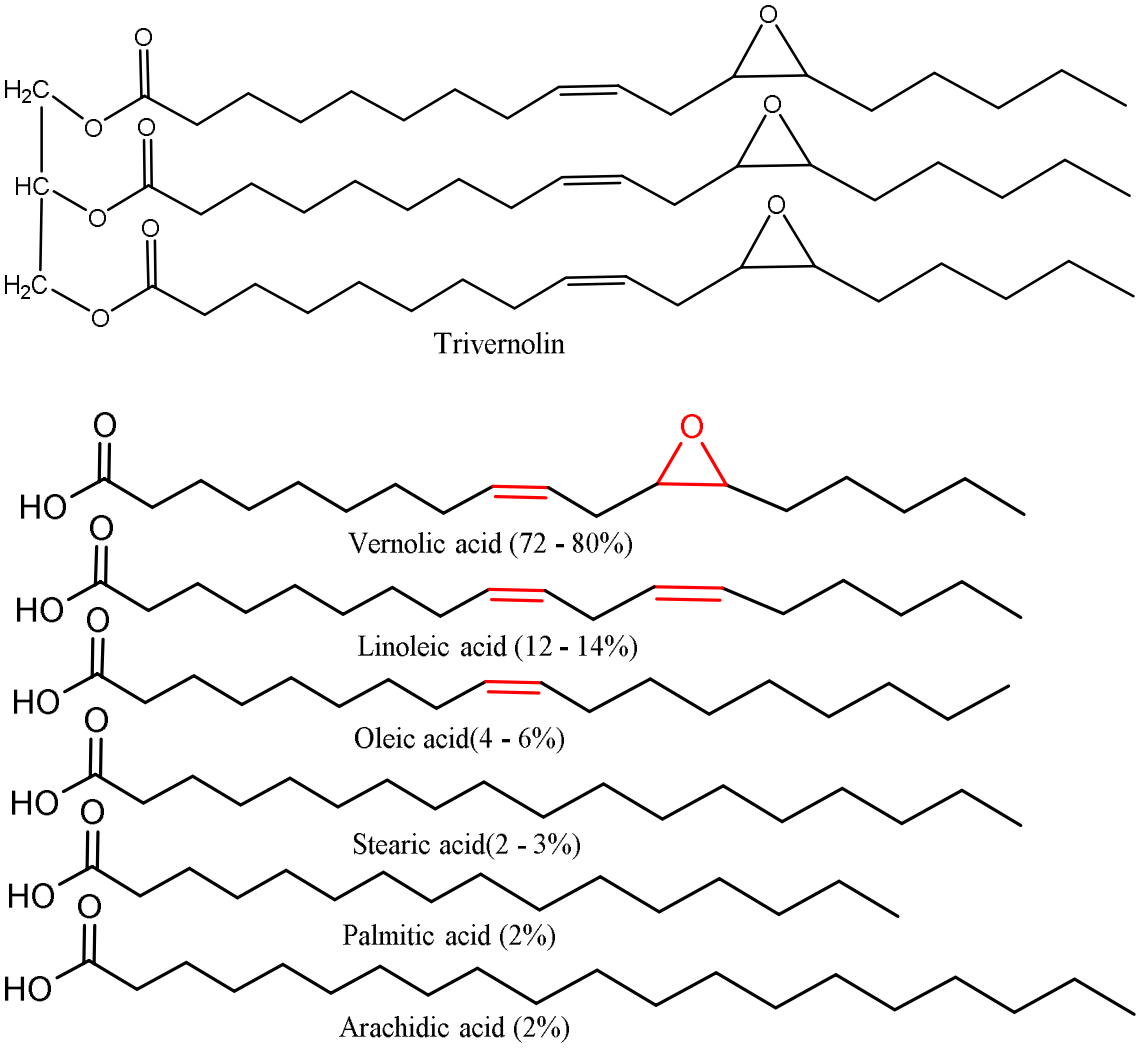

Figure 14. Structures of trivernolin and the fatty acid chains

Vernonia oil has a variety of reactive groups suitable for functionalization and to modify its chemical and physical property. The presence of reactive epoxy groups and double bonds in the vernonia oil molecule makes it a unique starting material for a variety of potentially valuable synthetic transformations[83]. There are very few attempts in the literature reported to the reactivity of vernonia oil, mainly due to the limited availability of this weed in the globe[84]. The reactive sites and the possible reactions which could be carried out to modify the property of vernonia oil and its derivatives is explained in Figure 15.

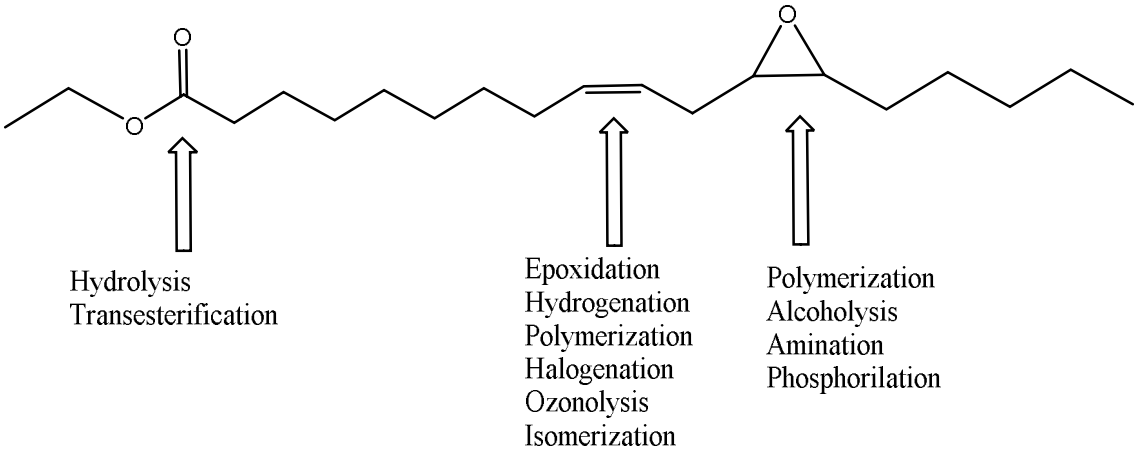

Figure 15. Possible reactive groups in vernonia oil

The chemical properties and the economic importance of vernonia oil could be improved by functionalizing on these reactive sites. Among this epoxidation of the carbon-carbon double bond of vernonia oil could enhance its reactivity for polymer synthesis, which have different applications.

1.3.2. Epoxidation methods of unsaturated organic compounds and their application

Epoxidized vegetable oils (EVOs) have drawn much attention in recent years in the chemical industry since they are environmentally friendly, biodegradable, renewable, readily available and non-toxic. The well-known methods used for epoxidation of the unsaturated carbon of plant oils and their derivatives are: homogeneous catalytic epoxidation (conventional epoxidation method); chemoenzymatic epoxidation; epoxidation in the presence of polyoxometalates; and heterogeneous catalytic epoxidation (in the presence of ion-exchange resins or transition metal incorporated porous silicates like titanium-silicate catalysts)[85, 86].

In conventional epoxidation method, homogeneous catalytic systems such as strong inorganic acids like H_2SO_4 are predominantly used for the generation of peracids. This epoxidation method has several drawbacks such as difficulty of separating this catalyst from the reaction products, low selectivity of epoxide groups due to ring opening reaction facilitated under acidic conditions, the presence of much wastes and the toxicity of this catalysts to the environment and the corrosion problem of the reactor under acidic condition. It is important to emphasize that the reaction is highly exothermic ($\Delta H = -55$ kcal·mol^{-1} for each carbon–carbon double bond). This can cause a risk, especially in the presence of peracids and hydrogen peroxide in the reaction mixture.

Another alternative epoxidation method is using lipases as a catalyst: chemoenzymatic epoxidation method gained much interest as the use of lipases in the epoxidation of fatty acid compounds is characterized by high chemo-, regio-, and stereoselectivity and the ring opening reaction is highly minimized[87]. Lipases can also catalyze vegetable oil transesterification and hydrolysis. As a result of these side reactions, the epoxy product is a mixture of epoxidized mono-, di- and triglycerides, epoxidized free fatty acids and FAMEs, and glycerol. However, lipases show low catalytic activity in the epoxidation of triglycerides due to the narrow and deeply located active sites of the enzyme. This causes a steric hindrance with the interaction of the catalytic center and the large molecule of the substrate. In addition to this problem, the application of enzymes in a large scale process is limited because this method uses large amount of solvents; high cost of enzymes; the rapid deactivation of enzymes under certain conditions like high temperature and high concentration of organic solvents[10, 88].

To minimize the drawbacks of conventional epoxidation method alternative epoxidation methods have been designed by using environmental friendly catalysts[7, 89]. Polyoxometalates which are a class of anionic metal-oxide clusters based on molybdenum (VI), tungsten (VI) and/or vanadium (V) transition metal ion complexes, used as catalysts for the selective epoxidation of vegetable oils. These type of catalysts have good catalytic performance (high epoxide selectivity) under mild reaction conditions. However, the peroxopolyoxometalates stability and their separation and reuse are actual problems, which restrict wide practical applications of these catalysts for the liquid-phase epoxidation of vegetable oils with aqueous H_2O_2. To solve this problem, the immobilization of these complexes onto the surface of an inorganic solid support or polymer support is mostly used.

The use of heterogeneous catalysts is one of the most attractive choices, which could cope with most of the above mentioned drawbacks of homogeneous catalysts[10]. Epoxidation of vegetable oils by using such type of catalysts are more environmentally friendly routes. Ti-based silica materials like TS-1[13], Ti-zeolites[90], Ti-SiO_2[91] and Ti-MCM-41[92] are commonly used as heterogeneous catalysts for the epoxidation of triglyceride oils and their derivatives. The catalytic activity of such type of materials are affected by their surface area, pore diameter, particle morphology[93], and the surface chemistry like surface acidity and hydrophobicity[94]. The bigger pore diameter of Ti-based materials allow for the better diffusion of triglyceride molecule. When a liquid phase epoxidation reaction is carried out by using heterogeneous catalysts, several interactions between the catalyst and the reagents must be taken into account. These possible interactions could be the hydrophobic/hydrophilic relation between reactants (usually hydrophobic alkenes) and solid catalysts (mostly hydrophilic when inorganic catalysts used as a supports), between

catalysts and solvents (usually polar solvents, which are in competition with substrates for adsorption onto the catalyst surface); between oxidants (polar oxygen-rich compounds) and catalysts; between catalysts and oxidized products or by-products (more hydrophilic than the reactants they are derived from and hence in competition with them for the approach to the surface catalyst)[95].

The application of solid catalysts in both liquid and vapour phase reactions gives rise to the heterogeneous system with several advantages from many points of view. The mesostructured metallosilicate catalysts have attracted much attention because of their better catalytic activity compared to microporous zeolites for various reaction of bulky organic groups. The catalytic activity of heterogeneous catalysts strongly depend on the textural/structural parameters, pore diameters and defect holes. In recent years transition metal containing SBA-15 catalysts have gained considerable interest for the selective oxidation of bulky olefinic compounds.

The surface chemistry of Ti-containing SBA-15 materials play an important role in determining catalyst activity and selectivity of surface bound active sites. To overcome the issue of poor catalytic performance of mesoporous SBA-15 several researchers have studied the surface modification of the catalyst with a variety of reagents and significant improvements in activity have been observed.

The catalytic properties of most of the molecular sieves depend on the presence of active sites in their frameworks. Therefore, the incorporation of transition metals in SBA-15 is of great interest in oxidation of large molecules which cannot diffuse in the pores of microporous materials. A good accessibility of reactant to the active sites and rapid departure of the desired products could be possible with anchoring of metal oxide species

onto the inner walls of the mesopores. Among oxidation reactions, production of epoxides is of growing interest in the chemical and petrochemical industries because these compounds are highly reactive[96] and can serve as organic intermediates in pharmaceutical synthesis or as monomers in the production of various functional polymers (Figure 16). For example, polyols for polyurethane can be prepared by a ring opening reaction of epoxy groups to form alcohols. Acrylated epoxidized soybean oil (AESO) is another important functionalization of epoxidized vegetable oil through an epoxy ring opening with acrylic acid[97]. The AESO can be blended with other reactive diluent comonomers such as styrene and then cured by a free radical or cationic initiated polymerization[98]. The formed thermoset has found application as sheet molding compound with mechanical properties comparable to commercially available unsaturated polyester and vinyl ester resins. Direct polymerization of epoxidized vegetable oils to prepare epoxy thermoset polymers has been conducted since 1950s; however, epoxidized vegetable oils have received only limited success so far as an epoxy monomer because of the low reactivity of internal epoxy with common nucleophilic curing agents, such as polyamines and anhydrides. Moreover, the inherently aliphatic nature and residual, saturated fatty acid component in vegetable oil feedstocks lead to less tightly crosslinking structures and polymeric materials that lack necessary rigidity and strengths required for structural applications. Epoxidized vegetable oil are, therefore, mostly used as secondary plasticizers or stabilizers for poly (vinyl chloride) or as reactive diluents for oil-based coatings with lower strength requirement.

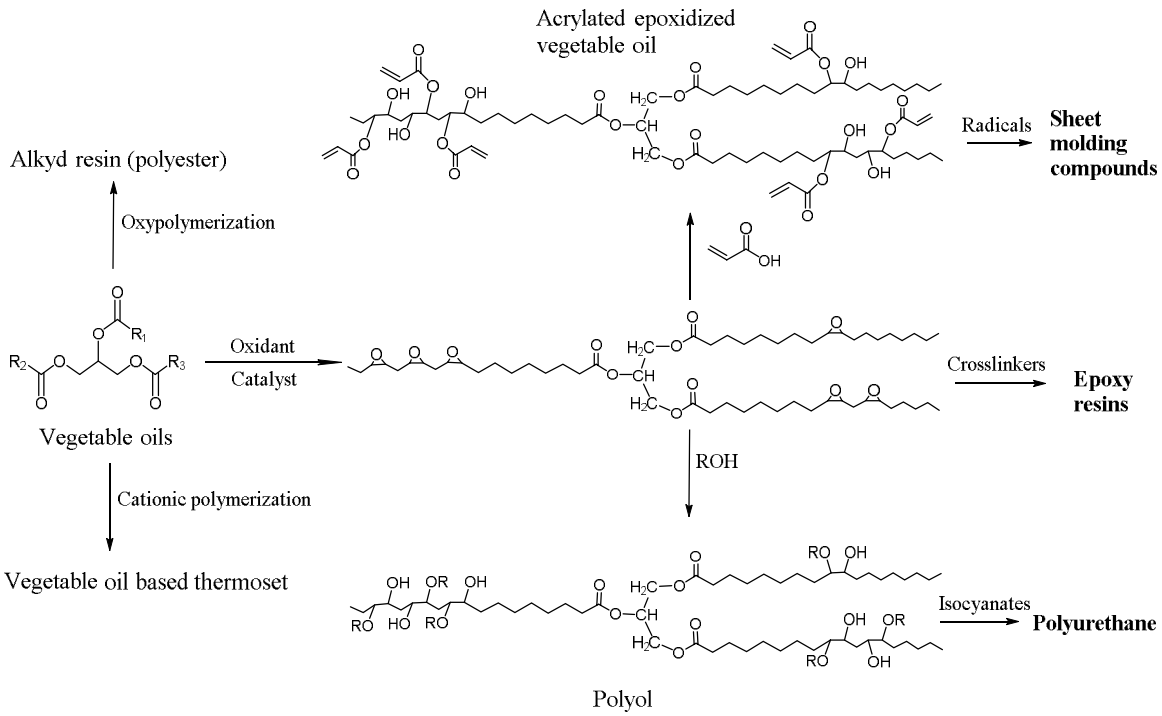

Figure 16. General routes for synthesis of vegetable oil-based polymers

As we have seen in Figure 16, production of polyurethanes by using this method is not environmentally friendly due to the toxicity of isocyanate. As a result, environmentally friendly method of production of polyurethane from epoxidized vegetable oils has been investigated by different scholars. Although several methods for producing non-isocyanate polyurethanes are reported in the literature, the only method directly applicable to triacylglycerol molecules is the ring opening reaction of 5-membered cyclic carbonates with amines. Cyclic carbonates are attractive green intermediates that are non-toxic, biodegradable and can easily be prepared by coupling carbon dioxide with epoxy fatty esters (Figure17). Fatty acid ester carbonates have the physical and chemical properties useful for preparing different valuable chemicals for many applications[99]. The main benefits of the conversion of epoxidized oils into cyclic carbonates are: preparation of

novel materials from renewable resources, and recycling and exploiting of carbon dioxide into the value chain. The coupling reaction of epoxides with CO_2 using tetra-n-butylammonium bromide ($[Bu_4N]Br$) as a catalyst is an intensively studied field of research, these materials have potential uses as industrial lubricants or fuel additives. Shorter chain linear carbonates are useful as emollients, and longer chain carbonates have been used as lubricants and fuel additives. The carbonated ring of the fatty esters can easily be opened by a variety of nucleophiles to produce phthalate-free bio-plasticizers, non-isocyanate polyurethane, biolubricants, adhesives, and many other value-added products[100, 101]. Polyurethanes are the significant class of polymeric materials which could be used in a wide range of applications e.g. thermal insulation for building and fridges, bed mattresses and pillows, automotive seats, shoe soles, fibers for textiles, scaffolds for tissue engineering, implants etc.[102, 103].

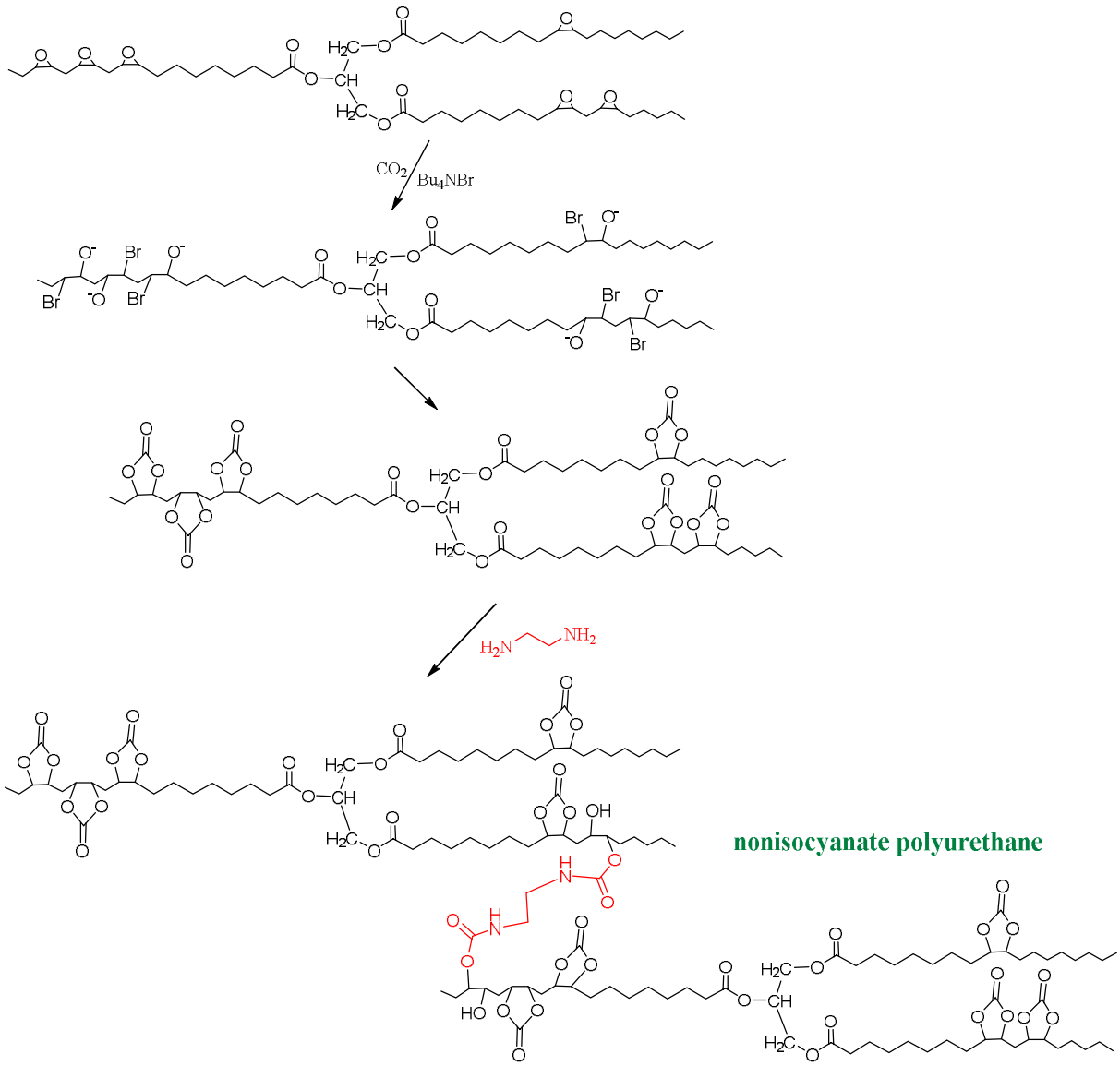

Figure 17. Carbonation of epoxy fatty esters and synthesis of isocyanate free polyurethane[102]

1.4. Motivation of the study

The availability of *vernonia galamensis* weed in Ethiopia, which is rich in naturally epoxidized vernonia oil and the need of modification of its chemical and physical property to use as a raw material in industry for the synthesis of different products is the main

motivation of this PhD work. The main advantage of using *vernonia galamensis* as the principal raw material is that it is a weed, not competing with edible crops. We need to modify the chemical properties of vernonia oil in a green approach. Heterogeneous catalysis is a sustainable way to tackle this objective, by using Ti-containing ordered mesoporous materials with optimum catalysts for this purpose. Hence our research objectives are designed and set based on the research gap observed in the area of heterogeneous catalysis of bulky molecules in the industry. Moreover, this work could be taken as part of our technology transfer approach to do research since this work was closely followed by a Spanish company, BETAQUIMICA, and potential investors in Ethiopia.

1.5. Significance of the study

The significance of this research can be seen from different perspectives.

- Development of new catalysts is used as a knowledge input to the scientific community
- Provide a waste minimization and green method of epoxidation of vegetable oils by using low cost materials.
- Provide a means to exploit and manage local resources.
- Provide a new potential industrial oil seed crop, *Vernonia galamensis* seed oil, for production of bioplastics, lubricants, coatings, and other products.
- Serve as a starting material for further research studies on the application of *Vernonia galamensis* oil for other potential purpose.
- Generally, this research work will contribute to expand the industrial application of non-edible seed oils, such as vernonia oil, to produce biodegradable and environmentally friendly products.

1.6. Objectives of the Study

1.6.1. General Objective

The main objective of this research is to design, synthesize and characterize Ti-containing ordered mesoporous materials for epoxidation of vernonia oil. The synthesis of materials with large pore, short channel path length and hydrophobic pore surface is the main objective of this thesis.

1.6.2. Specific Objectives

- Optimization of the synthesis parameters of pure silica ordered mesoporous materials, SBA-15, with large pore size and short diffusion path.
- Optimization of the synthesis parameters of periodic mesoporous organosilica, PMO, with large pore size and short diffusion path.
- Incorporation of titanium in pure silica SBA-15 materials
- Incorporation of titanium in organosilica PMO materials
- Catalytic test for Ti-containing SBA-15 and PMO materials
- Application of the optimum catalysts in epoxidation of vernonia oil

1.7. Organization of the thesis

This thesis consists of five chapters. Chapter one presents a general introduction of ordered mesoporous materials, description of the intended SBA-15 and PMO, description of Ti-containing SBA-15 and PMO materials, description the renewable resources especially vernonia galamensis, motivation of the study, aims and objectives of the thesis. Chapter two contains information on all the characterization techniques used in the work. Chapter three presents the detailed studies carried out on the systematic synthesis of pure silica

SBA-15 and hybrid organic-inorganic PMO materials. The methods of Ti incorporation in both types of materials through co-condensation and grafting, are explained in detail in this chapter. In Chapter four, the characterization results of the synthetic products are exhaustively presented and discussed. In Chapter five, we report the catalytic application of the synthesized Ti-containing materials for epoxidation of cyclohexene and vernonia oil. This chapter presents the application test methods and the production of new epoxide groups using the synthesized Ti-containing materials as catalysts.

CHAPTER TWO

2. CHARACTERIZATION TECHNIQUES

In this chapter, different techniques used in this study are briefly described. The techniques used are: Powder X-ray diffraction (XRD), N_2 adsorption/ desorption isotherm, Inductively Coupled Plasma Optical Emission Spectroscopy (ICP-OES), Diffusion Reflectance UV-Vis Spectroscopy, Scanning Electron Microscopy (SEM), Transmission Electron Microscopy (TEM) and Thermogravimetric Analysis (TGA).

2.1. Powder X-Ray Diffraction (XRD)

X ray diffraction (XRD) involves focusing beams of X-rays (Figure 18), which scatters in a constructive manner from lattices in the sample forming diffraction patterns.

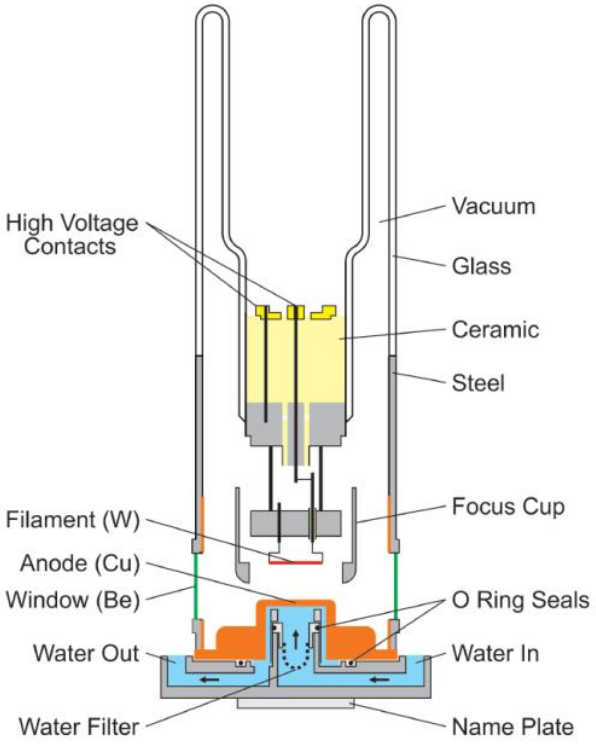

Figure 18. Schematic diagram of X-ray tube with key components[104]

At certain angles, scattered X-rays are combined constructively and are measured as a function of diffraction angle (2θ)[105]. The structural information can be obtained using the Bragg equation (2d sin θ = nλ) (Figure 19). The diffraction patterns formed can be used as a "fingerprint" for the crystal lattices found in the material. This allows for the determination of the crystalline phase, quantitative composition of multi-component systems, lattice parameters, and crystal size.

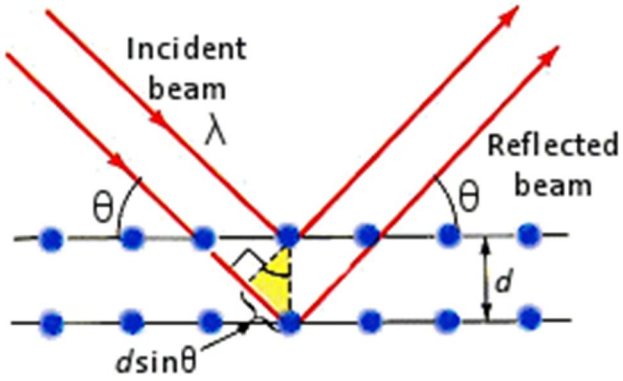

Figure 19. Diffraction of X-rays from crystals

Powder X-ray diffraction is the main characterization technique used in identifying the mesoscopic order of mesoporous materials during synthesis and modification stages[106]. SBA-15 has a hexagonally ordered pore structure. The unit cell size, *a*, can be calculated from the first Bragg peak position. The relationship of unit cell dimension (a_0) and interplanar d-spacing for hexagonally arranged ordered mesoporous materials is: $a_0 = (2/\sqrt{3})\, d_{100}$.

Therefore, to study the effect of different synthesis conditions such as synthesis with expanders, synthesis with different type and content of titanium source, varying the concentration of acid and gelling temperature and calcination on the structural pores arrangement of SBA-15 and PMO materials, XRD patterns were collected with a X´Pert

Pro PANalytical diffractometer (CuK_α radiation = 0.15406 nm with Ni filter). The measurements were made at room temperature with the accelerating voltage of 45 kV and applied current of 40 mA. It was operated in continuous scan mode, in the range 4.00037308^o – 89.99188826^o and the obtained peaks were analyzed using X´Pert HighScore Plus software. The diffraction pattern is plotted within the XRD machine by generating a scan with continuous scanning mode for the intensity of peak (I_{rel}) as the Y-axis versus (2θ) as the X-axis.

2.2. N_2 adsorption/desorption isotherms

According to IUPAC recommendation in 1985[107] and updated very recently in 2015[108], porous materials can be classified as micro-, meso- and macroporus materials depending on the pore size of the porous material. Gas adsorption measurements are used to determine the surface area and pore size of the different solid materials[107, 108]. When gases such as nitrogen are adsorbed on solid materials, different isotherm types are obtained as shown in Figure 20.

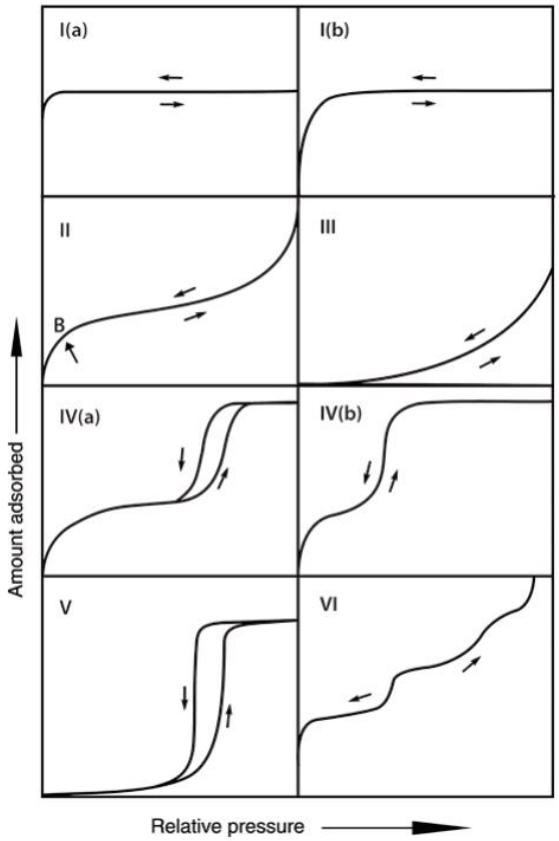

Figure 20. Classification of physisorption isotherms

Type I isotherms are given by microporous solids like molecular sieve zeolites having relatively small external surfaces. Type I(a) isotherms are given by microporous materials having mainly narrow micropores (of width < ~ 1 nm); Type I(b) isotherms are found with materials having pore size distributions over a broader range including wider micropores and possibly narrow mesopores (< ~ 2.5 nm). Type II isotherms are given by the physisorption of most gases on nonporous or macroporous adsorbents. The shape is the result of unrestricted monolayer-multilayer adsorption up to high p/p^{o}. In the case of a Type III isotherm, there is no Point B and therefore no identifiable monolayer formation; the adsorbent-adsorbate interactions are now relatively weak and the adsorbed molecules are clustered around the most favorable sites on the surface of a nonporous or macroporous

solid. Type IV isotherms are given by mesoporous adsorbents like mesoporous molecular sieves. In the case of a Type IV (a) isotherm, capillary condensation is accompanied by hysteresis. This occurs when the pore width exceeds a certain critical width, which is dependent on the adsorption system and temperature (e.g., for nitrogen adsorption in cylindrical pores at 77 K, hysteresis starts to occur for pores wider than ~ 4 nm). With adsorbents having mesopores of smaller width, completely reversible Type IV (b) isotherms are observed. In principle, Type IV (b) isotherms are also given by conical and cylindrical mesopores that are closed at the narrowed end. In the low p/p^o range, the Type V isotherm shape is very similar to that of Type III and this can be attributed to relatively weak adsorbent–adsorbate interactions. At higher p/p^o, molecular clustering is followed by pore filling. For instance, Type V isotherms are observed for water adsorption on hydrophobic microporous and mesoporous adsorbents. Type VI isotherm is representative of layer-by-layer adsorption on a highly uniform nonporous surface. The step-height now represents the capacity for each adsorbed layer, while the sharpness of the step is dependent on the system and the temperature. Amongst the best examples of Type VI isotherms are those obtained with argon or krypton at low temperature on graphitized carbon blacks.

Many different shapes of hysteresis loops have been reported, but the main types are shown in Figure 21. Types H1, H2 (a), H3 and H4 were identified in the original IUPAC classification of 1985, which is also updated with more recent findings in 2015. Each of these six characteristic types are fairly closely related to particular features of the pore structure and underlying adsorption mechanism.

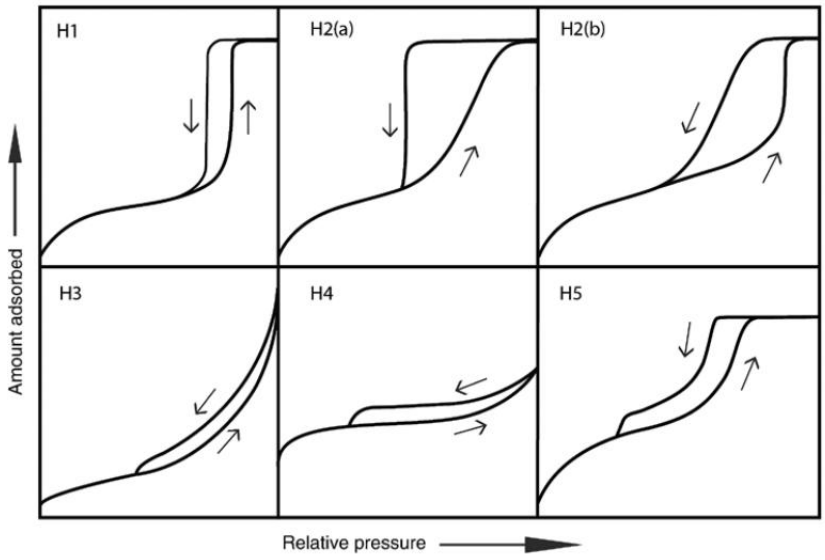

Figure 21. Classification of hysteresis loops

Ordered mesoporous materials with uniform distributed cylindrical pores showed the H1 type of hysteresis loop having steep parallel adsorption and desorption isotherms. At these steps all pores are filled (adsorption) and emptied (desorption). Hysteresis loops of Type H2 are given by more complex pore structures in which network effects are important. The very steep desorption branch, which is a characteristic feature of H2 (a) loops, can be attributed either to pore-blocking/percolation in a narrow range of pore necks or to cavitation-induced evaporation. H2 (a) loops are for instance given by many silica gels as well as some ordered mesoporous materials (e.g., SBA-16 and KIT-5 silicas). The Type H2 (b) loop is also associated with pore blocking, but the size distribution of neck widths is now much larger. Examples of this type of hysteresis loops have been observed with mesocellular silica foams and certain mesoporous ordered silicas after hydrothermal treatment.

There are two distinctive features of the Type H3 loop: (i) the adsorption branch resembles a Type II isotherm (ii) the lower limit of the desorption branch is normally located at the

cavitation-induced p/p_0. Loops of this type are given by non-rigid aggregates of plate-like particles (e.g., certain clays) but also if the pore network consists of macropores which are not completely filled with pore condensate.

The H4 loop is somewhat similar, but the adsorption branch is now a composite of Types I and II, the more pronounced uptake at low p/p_0 being associated with the filling of micropores. H4 loops are often found with aggregated crystals of zeolites, some mesoporous zeolites, and micro-mesoporous carbons.

Although the Type H5 loop is unusual, it has a distinctive form associated with certain pore structures containing both open and partially blocked mesopores (e.g., plugged hexagonal templated silicas). As already indicated, the common feature of H3, H4 and H5 loops is the sharp step-down of the desorption branch. Generally, this is located in a narrow range of p/p_0 for the particular adsorptive and temperature (e.g., at $p/p_0 \sim 0.4 – 0.5$ for nitrogen at temperatures of 77 K).

This technique is also used for evaluating the surface area, pore size, pore volume and pore size distribution of porous solid materials. In this technique, the amount of gas adsorbed by a solid is measured, which is in turn is directly related to the porous properties and pore structure of the material. The volume of gas adsorbed by the solid is measured over a wide range of relative pressures, and a plot of the volume adsorbed with varying relative pressure (p/p^o) is called the adsorption isotherm. N_2 adsorption isotherm at sub atmospheric pressures and -196 ^oC is routinely used for determining pore information and pore size distributions in microporous, mesoporous and macroporous range. Surface area is

determined from the Brunauer-Emmett-Teller (BET) equation and pore size from Barrett-Joyner-Halenda (BJH) computational model.

In this work, in order to investigate textural properties of pure as well as titanium modified SBA-15 and PMO type of ordered mesoporous materials, data of N_2 adsorption-desorption were obtained which were used for developing N_2 sorption isotherms and calculate textural properties like S_{BET} and BJH pore size and pore volume. The isotherms were measured based on the IUPAC 1985 recommendations[107] in a Micromeritics ASAP 2420 physisorption analyzer and the samples were degassed at 350 ^oC for 16 h prior to the measurement. The obtained data were analyzed using Micro Active Version 4.02 software. The specific surface area, S_{BET}, was calculated from nitrogen adsorption data in the relative pressure range from 0.04 to 0.2 using the BET (Brunauer-Emmett-Teller) method. The total pore volume, V_p, was determined from the amount of nitrogen adsorbed at a relative pressure of 0.97. Pore size distributions were determined from the adsorption branch of the N_2 isotherms using the BJH (Barrett-Joyner Halenda) model with cylindrical geometry of the pores. The BJH pore diameter, D_p *BJH*, is defined as the position of the maximum of the pore size distribution.

2.3. Diffuse Reflectance UV-vis Spectroscopy

When a material is irradiated with electromagnetic radiation, part of energy is absorbed by the atoms and molecules of the material and, as a consequence, they pass from a state of lower or fundamental energy to some excited state. For that absorption occurs, the energy of the photons must be equal to the difference of energy between the fundamental state and the excited state, so in a beam polychromatic only part of the radiation is absorbed and the rest is transmitted. The UV-visible radiation absorption produces electronic transitions, in

addition to vibrational and rotational changes. Therefore, given the large number of sub-levels involved with such nearby energies, the UV-visible absorption spectrum of a compound results in a broad band.

In general absorption spectrum is usually due to three types of transitions:

- Transitions produced by electrons of molecular orbitals σ and π or non-binding atomic orbitals n.
- Transitions produced by electrons d and f. It is the case of the metals of transition and lanthanides and actinides. In transition metals, the radiation absorption involves the passage of an electron from a low d orbital energy to another of greater energy. These electronic jumps are the ones that they call d-d transitions and are responsible for the color of the compounds. These transitions take place in the visible region of the spectrum.
- Transitions produced by charge-transfer electrons. They are in the UV region of the spectrum and, generally, are due to the transition of electrons from the bonding to unoccupied antibonding orbitals of the metal ion, though, when metals in a low oxidation state combined with high-affinity ligands electronic charge transfer occurs from a localized orbital on the metal to an orbital of the ligand (MLCT). Ligand to metal charge transfer (LMCT) transitions is common for coordination compounds having ligands with relatively high-energy lone pairs and metals with high oxidation state (having low-lying empty orbitals). The extinction coefficients are much higher than those corresponding to d-d transitions, so bands are more intense.

UV–vis diffuse reflectance spectroscopy (DRS) is generally used as a simple means to predict or verify the coordination environment around a titanium center in the

titanosilicates composite materials based on light reflection properties of the sample under light excitation from the 200 – 800 nm range. Surface coordinations are revealed very clearly by DRS in the case of transition metal ions exchanged into ordered mesoporous silicas, since a very high proportion of the cations can be located on the walls of the channels[109, 110]. It is usually used to obtain spectra of powders with minimum sample preparation.

When a beam of radiation strikes a body, it can be transmitted, reflected, dispersed or absorbed producing fluorescence. In the UV-visible spectroscopy for the study of solids, the phenomenon of interest is the reflection. Therefore, the technique is used when one wants to study a powder sample is diffuse reflectance. The resulting spectrum is obtained as a percentage of reflection (% R) versus wavelength. However, this spectrum does not save direct relationship between the intensity of the band and the concentration, so it is applied with a correction to linearize the results, which is the transformation of Kubelka-Munk, expressed according to equation 1. The most often used theory to describe and analyze diffuse reflectance spectra is the Kubelka-Munk theory. Most molecular spectroscopic software can convert spectra to Kubelka-Munk units automatically.

$$F(R) = \frac{(1-R_\infty)^2}{2R_\infty} \approx c \qquad (1)$$

Where F (R) or remission function is the result of a conversion of the spectrum to a similar format to absorption, which can be correlated with concentration *c* of absorbing species. R∞ is the relationship between the reflectance of the sample and that of the reference, measured at an infinite penetration distance.

Our titanium containing SBA-15 and PMO materials were characterized by using UV–visible diffuse reflectance spectra registered on a Cary 5000 Varian spectrophotometer equipped with an integrating sphere and the obtained data were converted to corresponding spectra expressed according to Kubelka–Munk function, F(R) (equation 1) and plotted against wavelength.

2.4. Inductively Coupled Plasma Optical Emission Spectroscopy (ICP-OES)

Inductively coupled plasma optical emission spectroscopy (ICP-OES) is a powerful analytical technique for the determination the bulk chemical composition of the samples[111]. It is a type of emission spectroscopy that uses the inductively coupled plasma to produce excited atoms and ions that emit electromagnetic radiation at wavelengths characteristic of a particular element. It is a flame technique with a flame temperature in a range from 6000 to 10000 K. With this technique, liquid samples are injected into a radiofrequency (RF)-induced argon plasma using one of a variety of nebulizers or sample introduction techniques. The sample mist reaching the plasma is quickly dried, vaporized, and energized through collision excitation at high temperature. The atomic emission emanating from the plasma is viewed, collected with a lens or mirror, and imaged onto the entrance slit of a wavelength selection device[112]. In this study, the titanium content in the final solid products was determined by inductively coupled plasma optical emission spectroscopy (ICP-OES) Optima 3300 DV Perkin Elmer instrument. Calcined samples were previously dissolved and digested in strong acids ($HF/HNO_3/HClO_4$). The resulting solutions were diluted and were ready for the ICP-OES measurements. Following the filtration process, the samples and standards were quantitatively transferred to volumetric flasks and then introduced into the ICP plasma. Initially, the range of standards prepared were run on the ICP to generate

a typical calibration curve. The sample solution was then analyzed and the emitted radiation was focused into the spectrometer. The emission signal was directly converted into concentration by using the calibration curve in the ICP computer with an analytical error of ± (0.01-0.05).

2.5. Scanning Electron Microscopy (SEM)

Scanning electron microscopy (SEM) is one of the most versatile instruments available for the examination of the morphology of solid materials including ordered mesoporous materials. The configuration of a typical SEM shows that it is made up of an electron gun situated on the top of the column which generates an electron with energy level in the region of 0.1 - 30 eV (Figure 22).

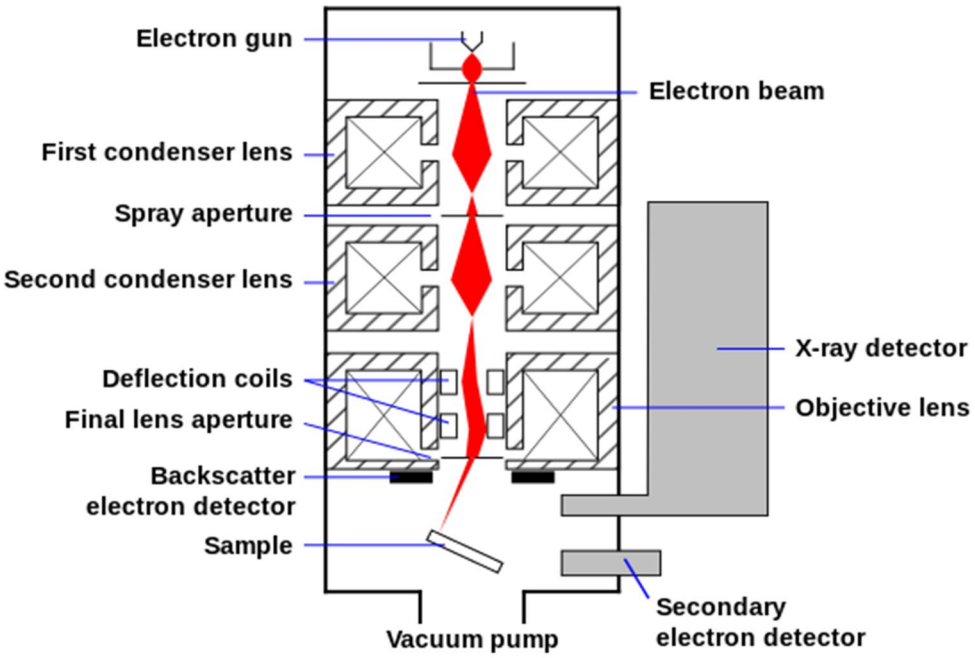

Figure 22. Schematic diagram of a scanning electron microscope[113]

A high vacuum is usually provided to aid electron transport without interference or scattering by air. An electron beam scanning coil and signal detection system are also

needed for the image processing of the sample surface. SEM works under the principle of interaction between the specimen and the electron beam producing a signal from secondary electrons and backscattered electrons which can be used to produce images. Secondary electrons are electrons produced when the incident electron beam collides with a sample atom electron and knock it out of its shell. It is weak in energy (nearly 100 volts). Backscattered electrons are electrons formed when the incident electron beam collides with a nucleus of a sample atom and it bounces back out of the sample as a backscattered electron. These electrons have high energies and because a sample with a higher density will create more of them, they are used to form backscattered electron images, which generally can discern the difference in sample densities[114].

The morphology analysis of the synthesized pure and titanium incorporated SBA-15 and PMO types of ordered mesoporous materials were carried out by using a FE-SEM FEI Nova Nanosem 230 scanning electron microscope with the VCD detector in high vacuum. The output voltage from the electrons gun is 3000 V and the actual voltage reaching the sample is 2000 V. With this detector the signals were collected from both secondary and backscattered electrons simultaneously. The samples were coated with chromium to enhance resolution.

2.6. Transmission Electron Microscopy (TEM)

As it is shown on Figure 23 transmission electron microscopy (TEM) is a microscopic technique in which a beam of electrons is transmitted through an ultra-thin specimen, interacting with the specimen as it passes through it[115]. TEM functions by generating a primary electron beam of high energy and high intensity that passes through a condenser to produce parallel beams that irradiate the sample. Magnified images of the sample are

formed by combining the transmitted electrons using an electromagnetic objective lens. TEM is primarily used to give information on topography and internal structure of nanomaterials. The topographic information obtained by TEM in the vicinity of atomic resolution can be utilized for structural characterization and identification of various phases of mesoporous materials, viz. hexagonal, cubic or lamellar[116, 117]. TEM also provides an information about the distribution of heteroatoms onto the support material. In transition metal incorporation, the distribution of the metal onto the support material needs to be visualized as it is an important parameter related to its catalytic activity. Thus, it has been developed into indispensable tool for scientists for characterization of transition metal incorporated micro and mesostructured materials.

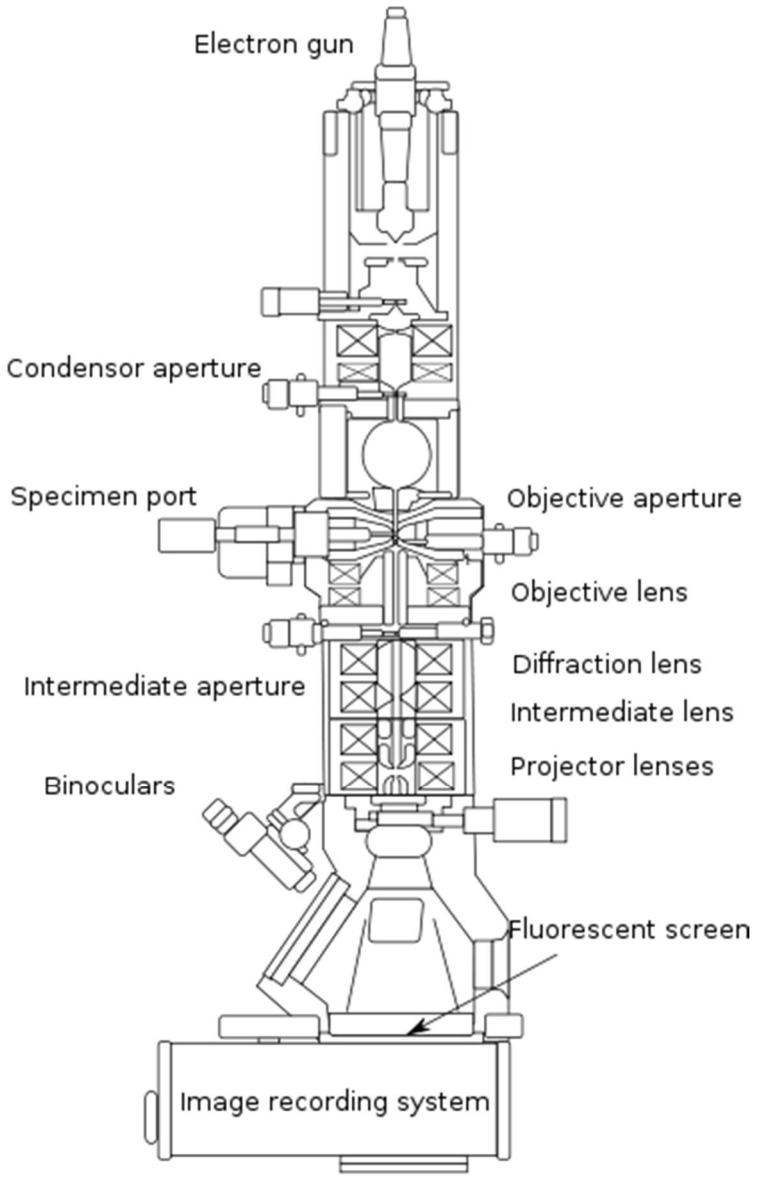

Figure 23**.** Schematic diagram of transmission electron microscope

TEM micrographs were taken using a JEOL 2100 electron microscope operating at 200 kV. The samples for TEM analysis were prepared by suspending a small amount of solid in ethanol. A drop of this suspension was then dispersed onto a holey carbon film on a copper grid, followed by drying at room temperature.

2.7. Thermogravimetric Analysis (TGA)

Thermogravimetric analysis (TGA) is the method in which the effect of heat on the mass of a sample with time is studied to obtain quantitative information. It is an analytical technique used to determine a material's thermal stability and its fraction of volatile components by monitoring the weight change that occurs as a specimen is heated[118]. The measurement is normally carried out in air or in an inert atmosphere, such as helium or argon, and the weight is recorded as a function of increasing temperature. In this particular study, the thermal stability analysis of the as made as well as after surfactant removal was carried out in air with a Perkin-Elmer TGA 7 instrument in the temperature range of 30-900 ^{o}C and at a heating rate of 20 ^{o}C/min by taking sample of 1 to 4 mg weight.

CHAPTER THREE

3. MATERIALS AND METHODS

In this part of the study the necessary reagents and the methods of synthesis of the material are explained in detail. The synthesis methods of ordered mesoporous materials, which have different pore sizes and particle morphologies, the strategy to control surface hydrophobicity and the method of Ti (IV) incorporation in the framework/channel of the ordered mesoporous materials is explained in detail.

3.1. Materials/Reagents

The reagents which are used for the synthesis of pure and Ti-incorporated materials in this study are: Triblock co-polymer poly(ethylene oxide)-poly(propylene oxide)-poly(ethylene oxide) Pluronic P123 ($PEO_{20}PPO_{70}PEO_{20}$), (Aldrich, USA) and Pluronic P104 ($PEO_{27}PPO_{61}PEO_{27}$) (BASF, USA), were used as structure directing agents. Tetraethoxysilane (TEOS) (Merck, USA) and Tetramethoxysilane (TMOS) (Alfa Aesar, Germany). Ammonium fluoride (NH_4F), 1, 3, 5-triisopropylbenzene (TIPB) and 1, 3, 5-trimethylbenzene (TMB) (Alfa Aesar, Germany), 1,2-bis(trimethoxysilyl)ethane (BTMSE, 96%, Aldrich) and 1,2-bis-(triethoxysilyl)ethane (BTESE, 97%, Merck, USA) have been used as a source of organosilica group for PMOs synthesis, and titanocene dichloride (Cp_2TiCl_2) (Sigma- Aldrich, USA) and Ti (IV) isopropoxide (TIP, Alfa Aesar) as Ti source.

3.2. Synthesis of SBA-15

The preliminary activity of this study was optimizing the synthesis conditions of mesostructured supports. The synthesis condition of pure silica SBA-15 with different

particle morphology and different pore size was optimized by varying the surfactant, concentration of acid, temperature and micelle expanders. Therefore, the material with standard pore size and long channel conventional fiber like particle morphology (SBA-L) and standard pore size and short channel plate-like particle morphology (SBA-S) were synthesized by using Pluronic P123 and P104 as structure-directing agents. Large pore size materials with long channel (E-SBA-L) and with short channel (E-SBA-S) were synthesized by using TIPB as a swelling agent and the above mentioned structure-directing agents. Very large pore size and less ordered materials were synthesized by using TMB as a pore expander instead of TIPB; such materials were labelled as "M" instead of "E". The synthesis methods of pure silica materials with different structure-directing agents and swelling agents are explained in detail in the following sub-sections.

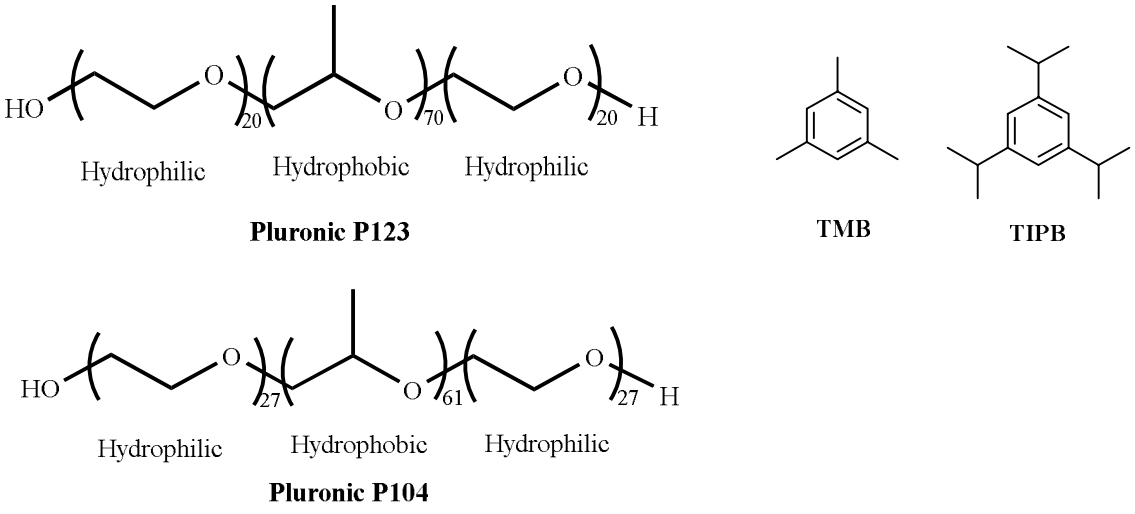

Figure 24. The structure of the selected reagents used for the synthesis of SBA-15 and PMO materials

3.2.1. Synthesis of SBA-15 with P123

Conventional synthesis of pure silica SBA-15 was carried out using Pluronic P123 ($(EO)_{20}(PO)_{70}(EO)_{20}$) as a surfactant according to the reported literature[15, 119] and with tetraethylorthosilicate (TEOS) as the silica source. Pluronic P123 (4 g (0.69 mmol)) was dissolved in 125 mL of 1.9 M aqueous HCl solution. The mixture was stirred at room temperature in a closed Pyrex container until a homogenous clear solution was obtained. Then, the solution was heated at 40 °C for 1 h to homogenize the temperature. TEOS (9.25 mL (41.42 mmol)) was then added to the solution and the resulting mixture was vigorously stirred at 40 °C for 24 h. The final molar composition of the synthesis gel was 1 TEOS: 0.017 P123: 5.73 HCl: 158 H_2O. Subsequently, the container was transferred to an oven and kept at 100 °C for 24 h under static conditions. The resultant product was filtered, washed thoroughly with distilled water and air-dried at room temperature overnight. Finally, the template was removed by calcination at 550 °C for 5 h in air (heating ramp rate: 2 °C/min). This material was labelled as SBA-L.

3.2.2. Synthesis of SBA-15 with P104

Pure silica SBA-15 aiming at plate-like particle morphology with short channels was synthesized using Pluronic P104 ($(EO)_{27}(PO)_{61}(EO)_{27}$) as a structure directing agent and with tetramethylorthosilicate (TMOS) as the silica source. This material has been prepared according to the method reported by Linton *et al*[41]. Pluronic P104 (2.5 g (0.423 mmol)) was dissolved in 97.5 mL of 1.6 M aqueous HCl solution. The mixture was stirred at room temperature in a closed Pyrex container until a homogenous clear solution was obtained. Then, the solution was heated at 55 °C for 1 h to homogenize the temperature. TMOS (3.69 mL (24.79 mmol)) was then added to the solution and the resulting mixture was vigorously

stirred at 55 °C for 24 h. The final molar composition of the synthesis gel was 1 TMOS: 0.017 P104: 5.25 HCl: 206 H_2O. Subsequently, the container was transferred to an oven and kept at 80 °C for 24 h under static conditions. The resultant product was filtered, washed thoroughly with ethanol and air-dried at room temperature overnight. Finally, the surfactant template was removed by calcination at 550 °C for 5 h in air (heating ramp rate: 2 °C/min). This material was labelled as SBA-S.

3.3. Synthesis of SBA-15 with expanders

Pore diameter of the ordered mesoporous materials is one of the key factors for the diffusion of bulk molecules and the accessibility of the active sites. Therefore, to increase the pore size of SBA-15 materials the synthesis method was optimized with organic groups micelle expanders such as 1, 3, 5-triisopropylbenzene (TIPB) and 1, 3, 5-trimethylbenzene (TMB). The procedure was based on previously reported method[28, 119, 120] with some necessary modification. These materials were synthesized at relatively mild acidic conditions with the addition of small amount of NH_4F. NH_4F is a well-known catalyst for the hydrolysis and polymerization of silica species and has been used in the synthesis of purely siliceous mesoporous materials under various conditions[121]. The synthesis method of large pore size SBA-15 was explained in detail in the following subsections by varying the type of surfactant and micelle expander.

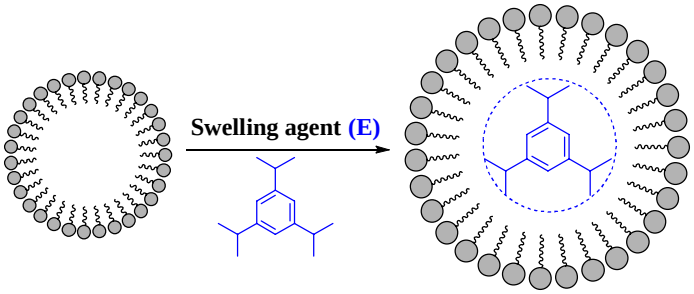

Figure 25. The role of pore expanders during the synthesis of large pore size OMM

3.3.1. Synthesis of SBA-15 with P123

3.3.1.1. Synthesis of SBA-15, P123 with TIPB

Pluronic P123 (2.4 g (0.413 mmol)) and NH_4F (0.027 g (0.729 mmol)) were dissolved in 84.0 mL of 1.30 M aqueous HCl solution at room temperature in a closed Pyrex container, using a magnetic stirrer. Then, the container was transferred to an incubator at 15 °C and the solution was gently stirred for 1 hour to allow for temperature equilibration. Then, the micelle expander TIPB (1.2 mL (4.96 mmol)) was added and mixed for 0.5 h. A calculated amount of TEOS (5.5 mL (24.63 mmol)) was added in under vigorous stirring. The final molar composition of the synthesis gel was 1 TEOS: 0.017 P123: 0.2 TIPB: 0.03 NH_4F: 4.43 HCl: 182 H_2O. The white gel obtained was vigorously stirred for 24 h at 15 °C and subsequently heated at 100 °C in the closed container under static conditions for 48 h. The mixture was then filtered and the solid product was washed with ethanol and dried at room temperature. Finally, the sample was calcined in a furnace for 5 h at 550 °C (heating ramp rate: 2 °C/min). This material was labelled as E-SBA-L-15. To study the effect of gelling temperature on the pore arrangement and textural properties this procedure was repeated by using the gelling temperature is 20 ^oC instead of 15 ^oC during the synthesis. This material is denoted as E-SBA-L-20.

3.3.1.2. Synthesis of SBA-15, P123 with TMB

The above procedure was repeated by changing only the pore expander to study the effect of type of swelling agent on arrangement of pores and other textural properties of the final material. Pluronic P123 (2.4 g (0.413 mmol)) and NH_4F (0.027 g (0.729 mmol)) were dissolved in 84.0 mL of 1.30 M aqueous HCl solution at room temperature in a closed Pyrex container with stirring. Then, the container was transferred to an incubator at 15 °C

and the solution was gently stirred for 1 h. The micelle expander TMB (0.69 mL (4.96 mmol)) was added and mixed for 0.5 h. A calculated amount of TEOS (5.5 mL (24.63 mmol)) was added in under vigorous stirring. The final molar composition of the synthesis gel was 1 TEOS: 0.017 P123: 0.2 TMB: 0.03 NH_4F: 4.43 HCl: 182 H_2O. The white gel obtained was vigorously stirred for 24 h at 15 °C and subsequently heated at 100 °C in the closed container under static conditions for 48 h. The mixture was then filtered and the solid product was washed with ethanol and dried at room temperature. Finally, the sample was calcined in a furnace for 5 h at 550 °C (heating ramp rate: 2 °C/min). This material was named as M-SBA-L.

3.3.2. Synthesis of SBA-15 with P104

Controlling of the pore size and channel length of the material without losing its structure may improve the diffusion of bulk molecules through the channels and the accessibility of the active sites. Therefore, in this study large pore size and short channel materials also synthesized using Pluronic P104 as a structure-directing agent and the above mentioned swelling agents as pore expanders. The detail optimized synthesis condition is explained in the following subsections:

3.3.2.1. Synthesis of SBA-15, P104 with TIPB

Pluronic P104 (1.55 g (0.263 mmol)) and NH_4F (0.016 g (0.432 mmol)) were dissolved in 65.0 mL of 1.1 M aqueous HCl solution at room temperature in a closed Pyrex container with stirring. The container was transferred to an incubator of 15 °C and the solution gently stirred for 1 hour. Then, the micelle expander TIPB (0.8 mL (3.3 mmol)) was added and mixed for 0.5 h. Then a calculated amount of TMOS (2.2 mL (14.78 mmol)) was added in under vigorous stirring. The final molar composition of the synthesis gel was 1 TMOS:

0.017 P104: 0.2 TIPB: 0.03 NH_4F: 4.84 HCl: 236 H_2O. The white gel obtained was vigorously stirred for 24 h at 15 °C and subsequently heated at 80 °C in the closed container under static conditions for 48 h. The mixture was then filtered and the solid product was washed with ethanol and dried at room temperature. Finally, the sample was calcined in a furnace for 5 h at 550 °C (heating ramp rate: 2 °C/min). This material was labelled as E-SBA-S-15. To study the effect of gelling temperature on the pore arrangement and textural properties of the material this procedure was repeated using the gelling temperature of 20 ^oC instead of 15 ^oC. This material is denoted as E-SBA-S-20.

3.3.2.2. Synthesis of SBA-15, P104 with TMB

Here TMB used as pore expander instead of TIPB in order to study the effect of type of swelling agents on the pore arrangement and the textural properties of the final material when Pluronic P104 is used as a structure-directing agent. Pluronic P104 (1.55 g (0.263 mmol)) and NH_4F (0.016 g (0.432 mmol)) were dissolved in 65.0 mL of 1.1 M aqueous HCl solution at room temperature in a closed Pyrex container with stirring. The container was transferred to an incubator of 15 °C and the solution gently stirred for 1 hour. The micelle expander TMB (0.46 mL (3.3 mmol)) was added and mixed for 0.5 h. Then, TMOS (2.2 mL (14.78 mmol)) was added in under vigorous stirring. The final molar composition of the synthesis gel was 1 TMOS: 0.017 P104: 0.2 TMB: 0.03 NH_4F: 4.84 HCl: 236 H_2O. The white gel obtained was vigorously stirred for 24 h at 15 °C and subsequently heated at 80 °C in the closed container under static conditions for 48 h. The mixture was then filtered and the solid product was washed with ethanol and dried at room temperature. Finally, the sample was calcined in a furnace for 5 h at 550 °C (heating ramp rate: 2 °C/min). This material was labelled as M-SBA-S.

3.4. Grafting of selected SBA-15 with titanocene dichloride

Among the synthesized pure silica ordered mesoporous materials the ones which have high degree of ordering and optimum textural properties were selected for grafting with titanocene dichloride. Ti was incorporated via grafting of Cl_2TiCp_2 allowing higher loadings of Ti (IV) in the final solids. For grafting, calcined pure silica SBA-L and E-SBA-L synthesized as indicated above were employed. The final samples were labelled TiG for "grafted" (TiG-SBA-15). 1 g of the vacuum dried mesoporous support was loaded into a two necked flask and degassed at 120 ºC under vacuum for 12 h and then dispersed in a solution containing 0.274 g of Cp_2TiCl_2 in 100 mL of toluene. The mixture was refluxed under N_2 for 24 h[122]. The suspension was filtered and washed with ethanol and air dried at room temperature. Then, Ti(IV) active centers were obtained after calcination at 350 ºC for 5 h.

3.5. Synthesis of PMO

Controlling the surface hydrophobicity of the ordered mesoporous materials is another important factor to improve the rate of adsorption and diffusion of organic molecules. Therefore, in this study both long and short channel ethylene-bridged periodic mesoporous organosilica were synthesized as previously reported[59, 66, 123] with some modifications. The synthesis condition of PMO materials were carried out at milder acidic conditions than that of similar SBA-15 materials. This is because of the organosilica precursors hydrolyze and condense faster than silica precursors due to the inductive effect of the ethylene bridges. During the synthesis of PMO materials, we used inorganic salts to improve the degree of ordering of the material, inorganic salts used to dehydrate water on the wall of the micelle and the micelle becomes more hydrophobic this is a good condition for the condensation

of organosilica group on the wall of the micelle. The detail synthesis condition is explained in the following sub-sections:

3.5.1. Synthesis of PMO with P123

Pluronic P123 (3.19 g (0.55 mmol)) was dissolved at room temperature in 126.84 mL of 0.174 M HCl aqueous solution in a flask with stirring. Once the surfactant was dissolved, potassium chloride (9.38 g (125.8 mmol)) was added and dissolved in the solution. Both, the low acid concentration and the presence of inorganic salts play an important role in the formation of highly ordered materials. When the resulting solution was homogenized, it was heated in the thermostated oil bath to a constant temperature of 40 °C. Then, 1, 2-bis (triethoxysilyl) ethane (5.83 mL (15.75 mmol)), was added at once with rapid stirring. The final molar composition of the synthesis gel was 1 BTESE: 0.035 P123: 8 KCl: 1.39 HCl: 445 H_2O. The resulting mixture was stirred at 40 °C for 24 h and then aged at 100 °C under static conditions for 24 h. Subsequently, the solid product was recovered by filtration, washed with ethanol and dried at room temperature for 24 h. The surfactant was removed from the material either by solvent extraction: two successive reflux extractions in ethanol/HCl (1.5 g of as made PMO in a solution made with 20 mL of 35 wt% HCl and 205 mL of ethanol) for 24 h. The resulting solid was recovered by filtration, washed with ethanol and dried in air. Or by calcination in a furnace for 5 h at 350 °C (heating ramp rate: 2 °C/min). This material was labelled as PMO-L. The effective method for complete surfactant removal was verified by thermogravimetric analysis (TGA).

3.5.2. Synthesis of PMO with P104

As we have explained during the synthesis of pure silica SBA-15 materials, controlling the particle morphology of the material is one of the important factors to improve the

accessibility of the active sites as well as diffusion problem of the reagents. Ethylene-bridged periodic mesoporous organosilica (PMO) with short channels and hexagonal particle morphology was synthesized using Pluronic P104 as a structure-directing agent. Pluronic P104 (3.25 g (0.55 mmol)) was dissolved at room temperature in 126.84 mL of 0.174 M HCl aqueous solution in a flask with stirring. Once the surfactant was dissolved, potassium chloride (9.38 g (125.8 mmol)) was added and dissolved in the solution. When the resulting solution was homogenized, it was heated in the thermostated bath to a constant temperature of 40 °C. Then, 1, 2-bis (triethoxysilyl) ethane (5.83 mL (15.75 mmol)) was added with rapid stirring. The final molar composition of the synthesis gel was 1 BTESE: 0.035 P104: 8 KCl: 1.39 HCl: 445 H_2O. The resulting mixture was stirred at 40 °C for 24 h and then aged at 80 °C under static conditions for 24 h. Subsequently, the solid product was recovered by filtration, washed with ethanol and dried at room temperature for 24 h. The surfactant was removed either by solvent extraction or calcination as we have explained in detail in the above procedure. This material was labelled as PMO-S.

3.6. Synthesis of PMO with expander

The synthesis condition of the large pore size PMO materials was optimized by modifying the synthesis condition. The synthesis was carried out by using both types of surfactants with varying the swelling agents. The detailed synthesis condition is explained in the following sub-section.

3.6.1. Synthesis of PMO with P123

3.6.1.1. Synthesis of PMO, P123 with TIPB

Pluronic P123 (1.914 g (0.33 mmol)) and NH_4F (0.01 g (0.27 mmol)) were dissolved at room temperature in 85.24 mL of 0.12 M aqueous HCl solution in a flask with stirring.

Once the surfactant was dissolved, 5.63 g KCl was added. When the resulting solution was homogenized, it was transferred into an incubator to a constant temperature of 15 °C. TIPB (0.96 mL (3.96 mmol)) was added and stirred for 0.5 h before adding an organosilica source 1,2-bis(trimethoxysilyl)ethane (2.36 mL (9.36 mmol)). The final molar composition of the synthesis gel was 1 BTMSE: 0.035 P123: 0.4 TIPB: 8 KCl: 0.03 NH_4F: 1.09 HCl: 504 H_2O. The resulting mixture (white gel obtained) was stirred at 15 °C for 24 h and then aged at 100 °C under static conditions for 48 h. Subsequently, the solid product was recovered by filtration, washed with ethanol and dried at room temperature. The surfactant was removed from the material either by solvent extraction: two successive reflux extractions in ethanol/HCl (1.5 g of as made PMO in a solution made with 20 mL of 35 wt% HCl and 205 mL of ethanol) for 24 h. The resulting solid was recovered by filtration, washed with ethanol and dried in air or by calcination in a furnace for 5 h at 350 °C (heating ramp rate: 2 °C/min). This material was labeled as E-PMO-L.

3.6.1.2. Synthesis of PMO, P123 with TMB

Large pore size PMO materials were also synthesized by using Pluronic P104 as pore expander in order to study the effect of type of swelling agent on the structure and textural properties of the final material. Pluronic P123 (1.914 g (0.33 mmol)) of surfactant and NH_4F (0.01 g (0.27 mmol)) were dissolved at room temperature in 85.24 mL of 0.12 M aqueous HCl solution in a flask with stirring. Once the surfactant was dissolved, KCl (5.63 g (75.52 mmol)) was added. When the resulting solution was homogenized, it was transferred into bath to a constant temperature of 15 °C. Then, TMB (0.55 mL (3.95 mmol)) was added and stirred for 0.5 h before adding 1,2-bis (trimethoxysilyl) ethane (2.36 mL (9.36 mmol)). The final molar composition of the synthesis gel was 1 BTMSE: 0.035 P123:

0.4 TIPB: 8 KCl: 0.03 NH_4F: 1.09 HCl: 504 H_2O. The resulting mixture (white gel obtained) was vigorously stirred at 15 ℃ for 24 h and then aged at 100 ℃ under static conditions for 48 h. Subsequently, the solid product was recovered by filtration, washed with ethanol and dried at room temperature for 24 h. The surfactant was removed from the material either by solvent extraction or calcination as we have explained in the above procedure. This material was labeled as M-PMO-L.

3.6.2. Synthesis of PMO by using P104

The pore size of short channel PMO materials also increased by using Pluronic P104 as a structure directing agent by varying the type of swelling agents. The detailed optimized synthesis condition was explained in the following sub-sections.

3.6.2.1. Synthesis of PMO, P104 with TIPB

Pluronic P104(1.95 g(0.33 mmol)) and NH_4F (0.01 g (0.27 mmol)) were dissolved at room temperature in 85.24 mL of 0.12 M aqueous HCl solution in a flask with slow stirring. Once the surfactant was dissolved, KCl (5.63 g (75.52 mmol) was added. When the resulting solution was homogenized, it was transferred into an incubator to a constant temperature of 15 °C. Then, TIPB (0.96 mL (3.96 mmol)) was added and stirred for 0.5 h before adding 1,2-bis(trimethoxysilyl)ethane (2.36 mL (9.36 mmol)). The final molar composition of the synthesis gel was 1 BTMSE: 0.035 P104: 0.4 TIPB: 8 KCl: 0.03 NH_4F: 1.09 HCl: 504 H_2O. The resulting mixture was stirred at 15 °C for 24 h and then aged at 80 °C under static conditions for 48 h. Subsequently, the solid product was recovered by filtration, washed with ethanol and dried at room temperature. The surfactant was removed from the material either by solvent extraction or calcination and this material was labeled as E-PMO-S.

3.6.2.2. Synthesis of PMO, P104 with TMB

Pluronic P104(1.95 g (0.33 mmol)) and NH_4F (0.01 g (0.27 mmol)) were dissolved at room temperature in 85.24 mL of 0.12 M aqueous HCl solution in a flask with stirring. Once the surfactant was dissolved, KCl (5.63 g (75.52 mmol)) was added. When the resulting solution was homogenized, it was transferred into bath to a constant temperature of 15 °C. TMB (0.55 mL (3.95 mmol)) was added and stirred for 0.5 h before adding 1, 2 bis(trimethoxysilyl)ethane (2.36 mL (9.36 mmol)). The final molar composition of the synthesis gel was 1 BTMSE: 0.035 P104: 0.4 TMB: 8 KCl: 0.03 NH_4F: 1.09 HCl: 504 H_2O. The resulting mixture was vigorously stirred at 15 °C for 24 h and then aged at 80 °C under static conditions for 48 h. Subsequently, the solid product was recovered by filtration, washed with ethanol and dried at room temperature for 24 h. The surfactant was removed from the material either by solvent extraction or calcination and this material was labeled as M-PMO-S.

3.7. Grafting of PMO materials with titanocene dichloride

The PMO materials which have better degree of ordering and textural properties were selected for grafting of Ti (IV) active sites. Therefore, PMO-L and E-PMO-L materials were grafted with titanocene dichloride. The final samples were labelled TiG for “grafted” (TiG-PMO). 1 g of the vacuum dried mesoporous support was loaded into a two necked flask and degassed at 120 ºC under vacuum for 12 h and then dispersed in a solution containing 0.14 g of Cp_2TiCl_2 in 100 mL of toluene. The mixture was refluxed under N_2 for 24 h[122]. The suspension was filtered and washed with ethanol and air dried at room temperature. Then, Ti(IV) active centers were obtained after calcination at 350 ºC for 5 h.

3.8. Direct synthesis of Ti-SBA-15

Titanium was also incorporated by co-condensation method to improve the stability and the distribution of active sites. In this study, we report on a new approach to synthesize large pore titanium containing SBA-15 and PMO materials by using titanium isopropoxide and titanocene dichloride as titanium sources. Ti-substituted SBA-15 materials have been successfully synthesized by a direct synthesis method through the fluoride-accelerating hydrolysis of TEOS in the mild acidic condition. Our synthesis methods were developed from previously reported method by Zhang *et al*[53] and Melero, *et al*[23] with some modifications.

3.8.1. Direct synthesis of Ti-SBA-15 with P123

Ti-incorporated pure silica SBA-15 with conventional fibrous particle morphology was synthesized by using Pluronic P123 as structure-directing agent and with tetramethylorthosilicate (TMOS) as the silica source and titanium (IV) isopropoxide (TIP) and titanocene dichloride as a titanium source.

3.8.1.1. Synthesis of Ti-SBA-15 with TIP (titanium (IV) isopropoxide)

Pluronic P123 (2 g (0.344 mmol)) and NH_4F (0.027 g (0.729 mmol)) were dissolved in 75 mL of 0.1 M aqueous HCl solution in the Pyrex container. The container was transferred to an incubator of 40 °C and stirred for an hour to homogenize the temperature. A mixture of 3.42 mL of TMOS and TIP (0.073 mL (0.246 mmol)) was added under vigorous stirring and stirring was continued for about 24 h. The final molar composition of the synthesis gel was 1 TMOS: 0.015 P123: 0.01 TIP: 0.03 NH_4F: 0.32 HCl: 180 H_2O. The container was transferred to an oven and kept at 60 °C for 48 h under static conditions. The resultant product was filtered, washed and air-dried at room temperature overnight. Finally, the

surfactant was removed by calcination at 350 °C for 5 h in air (heating temp: 2 °C/min). This material was labeled as Ti-i-SBA-L.

3.8.1.2. Synthesis of Ti-SBA-15 with titanocene dichloride

Ti is also incorporated by using titanocene dichloride as a titanium source with different Ti/Si ratios 0.01, 0.05 and 0.1). Pluronic P123 (2 g (0.344 mmol)) and NH_4F (0.027 g (0.728 mmol)) were dissolved in 75 mL of 0.1 M HCl in three different Pyrex containers and the containers were labelled as 1, 5 and 10. The solution was then heated up to 40 ^oC before adding an appropriate amount of the titanium precursor. Prior to the addition of silicon precursors, calculated amount of titanocene dichloride 0.0573 g (0.203 mmol), 0.275 g (1.1 mmol) & 0.53 g (2.12 mmol) were added in containers 1, 5 and 10, respectively and pre-hydrolyzed for 3 h in order to increase its incorporation efficiency. Afterwards, calculated amounts of TMOS 3.5 g (23 mmol), 3.36 g (22.07 mmol) & 3.2 g (21 mmol) were added in the containers 1, 5 and 10, respectively under vigorous stirring. All the three containers have the same molar composition of reagents except their Si/Ti ratio. Then, the resultant mixture was stirred at 40 ^oC for 24 h and hydrothermally aged at 60 ^oC under static conditions for 48 h. The solid product was recovered by filtration, washed with ethanol and air-dried overnight. Finally, the surfactant was removed by calcination at 350 °C for 5 h in air (heating ramp rate: 2 °C/min). This material was labelled as Ti-SBA-Ln (n=1, 5 & 10).

3.8.2. Direct synthesis of Ti-SBA-15 with P104

Controlling the particle morphology may improve the accessibility of Ti active sites. Due to this reason, the method of controlling the particle morphology of ordered mesoporous

materials during incorporation of titanium was designed. Here we used Pluronic P104 as a structure-directing agent by varying the Ti source and its composition in the synthesis gel.

3.8.2.1. Synthesis of Ti-SBA-15 with TIP (titanium (IV) isopropoxide)

Pluronic P104 (2.04 g (0.345 mmol)) and NH_4F (0.027 g (0.729 mmol)) were dissolved in 75 mL of 0.1 M aqueous HCl solution. The resultant mixture was heated to 40 °C before adding the silicon and titanium source. Then, the mixture of TMOS (3.42 mL (22. 99 mmol)) and TIP (0.07 mL (0.246 mmol)) was added under vigorous stirring and stirring was continued for about 24 h. The final molar composition of the synthesis gel was 1 TMOS: 0.015 P104: 0.01 TIP: 0.03 NH_4F: 0.32 HCl: 180 H_2O. Then, the container was transferred to an oven and kept at 60 °C for 48 h under static conditions. The resultant product was filtered, washed and air-dried at room temperature overnight. Finally, the surfactant was removed by calcination at 350 °C for 5 h in air (heating temp: 2 °C/min). This material was labeled as Ti-i-SBA-S.

3.8.2.2. Synthesis of Ti-SBA-15 with titanocene dichloride

Ti also incorporated by using Pluronic P104 as a structure-directing agent and titanocene dichloride as a titanium source with different Ti/Si ratios (0.01, 0.05 and 0.1). Pluronic P104 (2.04 g (0.345 mmol)) and NH_4F (0.027 g (0.729 mmol)) were dissolved in 75 mL of 0.1 M HCl in three different Pyrex containers and the containers was labelled as 1, 5 & 10. The containers were transferred to an incubator of 40 ^oC and stirred for an hour before adding calculated amount of the titanium precursor. Prior to the addition of silicon precursors, calculated amount of titanocene dichloride 0.0573 g (0.203 mmol), 0.275 g (1.1 mmol) & 0.53 g (2.12 mmol) were added in containers 1, 5 & 10 respectively and prehydrolyzed for 3 h. Then, calculated amounts of TMOS, i.e. 3.5 g (23 mmol), 3.36 g

(22.07 mmol) & 3.2 g (21 mmol) were added into the containers 1, 5 & 10 respectively under vigorous stirring. All the containers have the same molar composition of reagents except their Si/Ti ratio. Then, the resultant mixture was stirred at 40 ^{o}C for 24 h and hydrothermally aged at 60 ^{o}C under static conditions for 48 h. The solid product was recovered by filtration, washed with ethanol and air-dried overnight. Finally, the surfactant was removed by calcination at 350 °C for 5 h in air (heating ramp rate: 2 °C/min). This material was labelled as Ti-SBA-Sn (n=1, 5 & 10).

3.9. Direct synthesis of Ti-SBA-15 with TIPB as expander

In order to improve the diffusion of reagents and the accessibility of Ti active sites, the method was designed in this part of synthesis of ordered mesoporous materials for simultaneous pore expansion and Ti incorporation. Like the previous synthesis methods we varied the surfactant, titanium source and the Ti/Si ratio of the synthesis gel. The detail synthesis method was explained in the following subsections:

3.9.1. Synthesis of Ti-SBA-15, TIPB with P123

Ti incorporation and pore expansion was takes place by using Pluronic P123 and TIPB as structure directing agent and pore expander respectively, by varying the Ti source and Ti/Si ratio of the synthesis gel as it is explained in detail in the following way:

3.9.1.1. Using TIP (titanium (IV) isopropoxide)

Pluronic P123 (2.4 g (0.413 mmol)) and NH_4F (0.027 g (0.729 mmol)) were dissolved in 65.0 mL of 1.1 M aqueous HCl solution at room temperature in a closed Pyrex container with stirring. The container was transferred to an incubator at 15 °C and the solution was gently stirred for 1 hour to allow for temperature equilibration. Then, TIPB micelle expander (1.2 mL (4.96 mmol)) was added and mixed for 0.5 h. Then, a mixture of TMOS

(2.21 g (14.51 mmol) and TIP (0.043 mL (0.145 mmol)) were added under vigorous stirring and the white gel obtained was stirred for 24 h at 15 °C. The final molar composition of the synthesis gel was 1 TMOS: 0.017 P123: 0.01 TIP: 0.03 NH_4F: 0.2 TIPB: 4.95 HCl: 241 H_2O. The container was transferred to an oven and heated at 80 °C for 48 h under static conditions. The mixture was then filtered and the solid product was washed with water and dried at room temperature. Finally, the samples were calcined in a furnace at 350 °C for 5 h (heating ramp rate: 2 °C/min). This material was labelled as Ti-i-E-SBA-L.

3.9.1.2. Using titanocene dichloride

Pluronic P123 (2.4 g (0.413 mmol)) and NH_4F (0.027 g (0.729 mmol)) were dissolved in 65.0 mL of 1.1 M aqueous HCl solution at room temperature in three separate pyrex containers with stirring, the containers were labelled as 1, 5 & 10. Then calculated amounts of Cp_2TiCl_2 (0.04 g (0.16 mmol), 0.174 g (0.7 mmol) and 0.335 g (1.34 mmol)) were added into containers 1, 5 & 10 respectively and prehydrolyzed for 3 h. The containers were transferred to an incubator at 15 °C and the solution was gently stirred for 1 hour to allow for temperature equilibration. Then, TIPB micelle expander (1.2 mL (4.96 mmol)) was added in each container and mixed for 0.5 h. Afterwards, a calculated amount of TMOS (2.21 g (14.51 mmol), 2.13 g (14 mmol) and 2.03 g (13.33 mmol)) were added into containers 1, 5 & 10, respectively under vigorous stirring. The white gel obtained was vigorously stirred for 24 h at 15 °C and subsequently heated in the oven at 80 °C in the closed container under static conditions for 48 h. The mixture was then filtered and the solid product was washed with water and dried at room temperature. Finally, the samples were calcined in a furnace at 350 °C for 5 h (heating ramp rate: 2 °C/min). This material was labelled as Ti-E-SBA-Ln (n=1, 5 & 10).

3.9.2. Direct synthesis of Ti-SBA-15, TIPB with P104

The pore size and particle morphology of ordered mesoporous materials also controlled during Ti-incorporation in order to enhance the diffusion of reagents and accessibility of active sites. The synthesis method of large pore size and short channel Ti-containing materials is explained in the following subsections by using Pluronic P104 as a structure directing agent and by varying the pore expanders, the Ti source and its composition in the synthesis gel.

3.9.2.1. Using TIP (titanium (IV) isopropoxide)

Pluronic P104 (1.5 g (0.254 mmol)) and NH_4F (0.016 g (0.432 mmol)) were dissolved in 65.0 mL of 1.1 M aqueous HCl solution at room temperature in a closed Pyrex container, using a magnetic stirrer. The container was transferred to an incubator at 15 °C and the solution was gently stirred for 1 hour to allow for temperature equilibration. Then, TIPB micelle expander (0.8 mL (3.3 mmol)) was added and mixed for 0.5 h. Then a mixture of TMOS (2.21 g (14.51 mmol) and TIP (0.043 mL (0.145 mmol)) was added under vigorous stirring. The final molar composition of the synthesis gel was 1 TMOS: 0.017 P104: 0.01 TIP: 0.03 NH_4F: 0.2 TIPB: 4.95 HCl: 241 H_2O. The white gel obtained was vigorously stirred for 24 h at 15 °C and subsequently heated in the oven at 80 °C in the closed container under static conditions for 48 h. The mixture was then filtered and the solid product was washed with water and dried at room temperature. Finally, the samples were calcined in a furnace at 350 °C for 5 h (heating ramp rate: 2 °C/min). This material was labelled as Ti-i-E-SBA-S.

3.9.2.2. Using titanocene dichloride

Pluronic P104 (1.5 g (0.254 mmol)) of and NH_4F (0.016 g (0.432 mmol)) were dissolved in 65.0 mL of 1.1 M aqueous HCl solution at room temperature in three separate pyrex containers with stirring, the containers were labelled as 1, 5 & 10. Then calculated amounts of Cp_2TiCl_2 (0.04 g (0.16 mmol), 0.174 g (0.7 mmol) and 0.335 g (1.34 mmol)) were added in the containers 1, 5 & 10 respectively and pre-hydrolyzed for 3 h. The containers were transferred to an incubator at 15 °C and the solution was gently stirred for 1 hour to allow for temperature equilibration. Then, TIPB 0.8 mL (3.3 mmol) was added in each container and mixed for 0.5 h. Then, calculated amounts of TMOS (2.21 g (14.51 mmol), 2.13 g (14 mmol) and 2.03 g (13.33 mmol)) were added in containers 1, 5 & 10, respectively under vigorous stirring. The white gel obtained was stirred for 24 h at 15 °C and subsequently heated in the oven at 80 °C in the closed container under static conditions for 48 h. The mixture was then filtered and the solid product was washed with water and dried at room temperature. Finally, the samples were calcined in a furnace at 350 °C for 5 h (heating ramp rate: 2 °C/min). This material was labelled as Ti-E-SBA-Sn (n=1, 5 & 10).

3.10. Direct synthesis of Ti-PMO

Ti-incorporated PMO materials with high hydrophobic surface was synthesized by using ethane bridged organosilica source. The synthesis was carried out by varying the surfactant, the Ti source and the Ti/Si ratio of the synthesis gel.

3.10.1. Direct synthesis of Ti-PMO with P123

Here Ti-incorporated PMO materials with conventional fibrous like particle morphology and long channel materials were synthesized by using Pluronic P123 as a structure-directing agent and by varying the Ti source and content in the synthesis gel.

3.10.1.1. Using TIP (titanium (IV) isopropoxide)

Pluronic P123 (1.914 g (0.33 mmol)) and NH_4F (0.01 g (0.27 mmol)) were dissolved at room temperature in 85.24 mL of 0.12 M HCl aqueous solution, in a closed container with slow stirring. Once the surfactant was dissolved, KCl (5.63 g (75.52 mmol)) was added, the container was transferred to an incubator at 40 ºC and the mixture kept under gentle stirring for 1 h. Then, a mixture of TIP (0.06 mL (0.211 mmol)) and 1, 2-bis (triethoxysilyl) ethane (3.4 g (9.59 mmol)) was added and continue stirring at 40 °C for 24 h. The final molar composition of the synthesis gel was 1 BTESE: 0.034 P123: 0.02 TIP: 8 KCl: 0.03 NH_4F: 1.07 HCl: 493 H_2O. Finally, the synthesis gel was aged at 80 °C under static conditions for 24 h. Subsequently, the solid product was recovered by filtration, washed with ethanol, dried at room temperature. Finally, the samples were calcined in a furnace at 350 °C for 5 h (heating ramp rate: 2 °C/min). This material was labelled as Ti-i-PMO-L.

3.10.1.2. Using titanocene dichloride

Ti has also been incorporated by using titanocene dichloride as a titanium source with different Ti/Si ratios (0.01, 0.05 and 0.1). Pluronic P123 (1.914 g (0.33 mmol)) and NH_4F (0.01 g (0.27 mmol)) were dissolved in 85.24 mL of 0.1 M HCl in three separate Pyrex containers with stirring, the containers were labelled as 1, 5 & 10. Then, the containers were transferred into an incubator and heated at 40 ºC for 1 hour before adding an appropriate amount of the titanium precursor. Prior to the addition of silica precursors, calculated amount of titanocene dichloride 0.05 g (0.2 mmol), 0.222 g (0.89 mmol) & 0.4 g (1.6 mmol) were added in the containers 1, 5 & 10, respectively and prehydrolyzed for 3 h in order to increase its incorporation efficiency. Afterwards, calculated amount of 1,2-Bis(triethoxysilyl)ethane 3.4 g (9.6 mmol), 3.15 g (8.9 mmol) & 2.9 g (8.2 mmol) were

added in the containers 1, 5 & 10 respectively under vigorous stirring. All the three containers have the same molar composition of reagents except their Si/Ti ratio. Then, the resultant mixture was stirred at 40 ºC for 24 h and hydrothermally aged at 80 ºC under static conditions for 24 h. The solid product was recovered by filtration, washed with ethanol and air-dried overnight. Finally, the surfactant was removed by calcination at 350 °C for 5 h in air (heating ramp rate: 2 °C/min). This material was labelled as Ti-PMO-Ln (n=1, 5 & 10).

3.10.2. Direct synthesis of Ti-PMO with P104

Ti-incorporated short channel and hexagonal particle morphology PMO materials was synthesized in order to improve the accessibility of the active sites and to maintain its surface hydrophobicity. This synthesis method is optimized by using Pluronic P104 as a structure-directing agent and by varying the Ti source and its Ti/Si ratio of the synthesis gel. The detail synthesis procedure is explained in the following subsections:

3.10.2.1. Using TIP (titanium (IV) isopropoxide)

Pluronic P104 (1.95 g (0.33 mmol)) and NH_4F (0.01 g (0.27 mmol)) were dissolved at room temperature in 85.24 mL of 0.12 M HCl aqueous solution, in a closed container with slow stirring. Then, KCl (5.63 g (75.52 mmol)) was added and dissolved, and the container was transferred to an incubator at 40 ºC and the mixture kept under gentle stirring for 1 h. Then, a mixture of TIP (0.06 mL (0.211 mmol) and 1, 2-bistriethoxysilylethane (3.4 g (9.59 mmol)) was added and continue stirring at 40 °C for 24 h. The final molar composition of the synthesis gel was 1 BTESE: 0.034 P104: 0.02 TIP: 8 KCl: 0.03 NH_4F: 1.07 HCl: 493 H_2O. Finally, the synthesis gel was aged at 80 °C under static conditions for 24 h. Subsequently, the solid product was recovered by filtration, washed with ethanol, dried at

room temperature. Finally, the surfactant was removed by calcination at 350 °C for 5 h in air (heating ramp rate: 2 °C/min). This material was labelled as Ti-i-PMO-S.

3.10.2.2. Using titanocene dichloride

Ti has also been incorporated by using titanocene dichloride as a titanium source with different Ti/Si ratios (0.01, 0.05 and 0.1). Pluronic P104 (1.95 g (0.33 mmol)) and NH_4F (0.01 g (0.27 mmol)) were dissolved in 85.24 mL of 0.1 M HCl in three separate Pyrex containers with stirring, and the containers were labeled as 1, 5 & 10. Then, the containers transferred into an incubator and heated at 40 ^oC for 1 hour before adding an appropriate amount of the titanium precursor. Prior to the addition of silicon precursors, calculated amount of titanocene dichloride 0.05 g (0.2 mmol), 0.222 g (0.89 mmol) & 0.4 g (1.6 mmol) were added into the containers 1, 5 & 10 respectively and prehydrolyzed for 3 h. Afterwards, calculated amounts of 1,2-Bis(triethoxysilyl)ethane (3.4 g (9.6 mmol), 3.15 g (8.9 mmol) & 2.9 g (8.2 mmol) were added into the containers 1, 5 & 10 respectively under vigorous stirring. All the three containers have the same molar composition of reagents except their Si/Ti ratio. Then, the resultant mixture was stirred at 40 ^oC for 24 h and hydrothermally aged in the oven at 80 ^oC under static conditions for 24 h. The solid product was recovered by filtration, washed with ethanol and air-dried overnight. Finally, the surfactant was removed by calcination at 350 °C for 5 h in air (heating ramp rate: 2 °C/min). This material was labelled as Ti-PMO-Sn (n=1, 5 & 10).

3.11. Direct synthesis of Ti-PMO with TIPB as expander

Ti-incorporation and pore expansion of the PMO materials also carried out simultaneously in the same scenario of the pure silica materials in order to improve the diffusion of reagents, accessibility of active sites and the adsorption rate of the organic molecules.

During the synthesis, the structure-directing agent and the Ti source and its composition in the synthesis gel also varied. The detail synthesis condition is explained in the following subsections:

3.11.1. Synthesis of Ti-PMO, TIPB with P123

3.11.1.1. Using TIP (titanium (IV) isopropoxide)

Pluronic P123 (1.914 g (0.33 mmol)) and NH_4F (0.01 g (0.27 mmol)) were dissolved at room temperature in 85.24 mL of 0.12 M aqueous HCl solution in a flask with slow stirring. Then, KCl (5.63 g (75.5 mmol)) was added and the resulting solution was homogenized, it was transferred to the incubator with stirring to a constant temperature of 15 °C for 1 hour. Then, TIPB (0.96 mL (3.96 mmol)) was added and mixed for 0.5 h before adding titanium and silica source. Then, a mixture of TIP (0.06 mL (0.2 mmol)) and 1, 2-Bis (trimethoxysilyl) ethane (2.48 g (9.17 mmol) were added into the solution. The final molar composition of the synthesis gel was 1 BTMSE: 0.035 P123: 0.02 TIP: 0.4 TIPB: 8 KCl: 0.03 NH_4F: 1.1 HCl: 514 H_2O. The resulting mixture was vigorously stirred at 15 °C for 24 h and then aged at 80 °C under static conditions for 48 h. Subsequently, the solid product was recovered by filtration, washed with ethanol and dried at room temperature. Finally, the sample was calcined in a furnace at 350 °C for 5h (heating ramp rate: 2 °C/min). This material was labelled as Ti-i-E-PMO-L.

3.11.1.2. Using titanocene dichloride

Pluronic P123 (1.914 g (0.33 mmol)) and NH_4F (0.01 g (0.27 mmol)) were dissolved in 85.24 mL of 0.12 M aqueous HCl solution at room temperature in two separate closed Pyrex containers with stirring, and the containers were labelled as 1 & 5. Then, titanocene dichloride (0.052 g (0.2 mmol)) and (0.21 g (0.84 mmol)) were added into containers 1 &

5 respectively and pre-hydrolyzed for 3 h. Then the containers were transferred to an incubator at 15 °C and the solution was gently stirred for 1 hour to allow for temperature equilibration. Then, TIPB (0.96 mL (3.96 mmol)) was added in each containers and mixed for 0.5 h before adding a calculated amount of 1,2-Bis (trimethoxysilyl)ethane (2.48 g (9.2 mmol)) and 2.3 g (8.5 mmol)) in containers 1 & 5 respectively under vigorous stirring. The white gel obtained was vigorously stirred for 24 h at 15 °C and subsequently heated at 80 °C in the closed container under static conditions for 48 h. The mixture was then filtered and the solid product was washed with water and dried at room temperature. Finally, the samples were calcined in a furnace at 350 °C for 5 h (heating ramp rate: 2 °C/min). These materials were labelled as Ti-E-PMO-Ln (n = 1, 5).

3.11.2. Synthesis of Ti-PMO, TIPB with P104

Ti incorporation and pore expansion was also carried out by using Pluronic P104 as a structure directing agent and TIPB as a pore expander by varying the Ti source and its content in the synthesis gel.

3.11.2.1. Using TIP (titanium (IV) isopropoxide)

Pluronic P104 (1.95 g (0.33 mmol)) and NH_4F (0.01 g (0.27 mmol)) were dissolved at room temperature in 85.24 mL of 0.12 M aqueous HCl solution in the pyrex container with slow stirring. Once the surfactant was dissolved, KCl (5.63 g (75.5 mmol)) was added. When the resulting solution was homogenized, it was transferred to the incubator with stirring to a constant temperature of 15 °C. Then, TIPB (0.96 mL (3.96 mmol)) was added and mixed for 0.5 h before adding titanium and silica source. Then, a mixture of TIP (0.06 mL (0.2 mmol)) and 1, 2-Bis (trimethoxysilyl) ethane (2.48 g (9.17 mmol) were added into the solution. The final molar composition of the synthesis gel was 1 BTMSE: 0.035 P104:

0.02 TIP: 0.4 TIPB: 8 KCl: 0.03 NH_4F: 1.1 HCl: 514 H_2O. The resulting mixture was vigorously stirred at 15 °C for 24 h and then aged at 80 °C under static conditions for 48 h. Subsequently, the solid product was recovered by filtration, washed with ethanol and dried at room temperature. Finally, the sample was calcined in a furnace at 350 °C for 5h (heating ramp rate: 2 °C/min). This material was labelled as Ti-i-E-PMO-S.

3.11.2.2. Using titanocene dichloride

Pluronic P104 (1.95 g (0.33 mmol)) and NH_4F (0.01 g (0.27 mmol)) were dissolved in 85.24 mL of 0.12 M aqueous HCl solution at room temperature in two separate closed Pyrex container with stirring, and the containers was labelled as 1 & 5. Then titanocene dichloride (0.052 g (0.2 mmol)) and (0.21 g (0.84 mmol)) were added in the containers 1 & 5 respectively and pre-hydrolyzed for 3 h. Then the Pyrex containers were transferred to an incubator at 15 °C and the solution was gently stirred for 1 hour to allow for temperature equilibration. Then, TIPB (0.96 mL (3.96 mmol)) was added in each containers and mixed for 0.5 h before adding a calculated amount of 1,2-Bis (trimethoxysilyl)ethane (2.48 g (9.2 mmol)) and 2.3 g (8.5 mmol)) in the containers 1 & 5 respectively under vigorous stirring. The white gel obtained was stirred for 24 h at 15 °C and subsequently heated at 80 °C in the closed container under static conditions for 48 h. The mixture was then filtered and the solid product was washed with water and dried at room temperature. Finally, the samples were calcined in a furnace at 350 °C for 5 h (heating ramp rate: 2 °C/min). These materials were labelled as Ti-E-PMO-Sn (n = 1, 5).

3.12. Reaction set up of cyclohexene oxidation

Cyclohexene oxidation reactions were performed in batch mode using a round bottom flask immersed in a temperature-controlled bath and equipped with a thermometer, a magnetic

stirrer and a reflux condenser provided with a drying tube on the top (Figure 26). All these items were completely dried before the reaction. Circulating water through the condenser is maintained at 5ºC in order to avoid any (selective) evaporation of the chemicals from the reaction mixture[124]. The catalysts were previously activated overnight in the same reaction flask at 120ºC in order to remove any adsorbed water. To evaluate the performance of Ti-containing SBA-15 and Ti-containing PMO materials with different pore size and particle morphology as oxidation catalysts, liquid-phase epoxidation of cyclohexene with tert-butyl hydroperoxide (TBHP, 5.5 M in decane) was carried out in a 50 mL round bottom flask. In a typical run, 12 mmol of a substrate, 13 mmol of TBHP as an oxidant and 0.1 g of a catalyst were mixed in a flask containing 15 g of acetonitrile solvent and 0.1 g toluene as internal standard, this procedure was developed from previously reported literature[12, 125]. The mixture was heated under stirring up to 70ºC and when the reaction temperature was reached, an aliquot was taken as time zero. Successively small aliquots were taken at different reaction times and catalyst particles separated by filtration. Products were separated and analyzed by gas chromatography using a *Varian CP-3380 Gas Chromatograph* equipped with a 15 m length, 0.25 mm internal diameter and 1 µm thickness capillary column (dimethylpolysiloxane) and a flame ionization detector (FID). A blank experiment by using pure SBA-15 material without Ti was performed under the same reaction conditions.

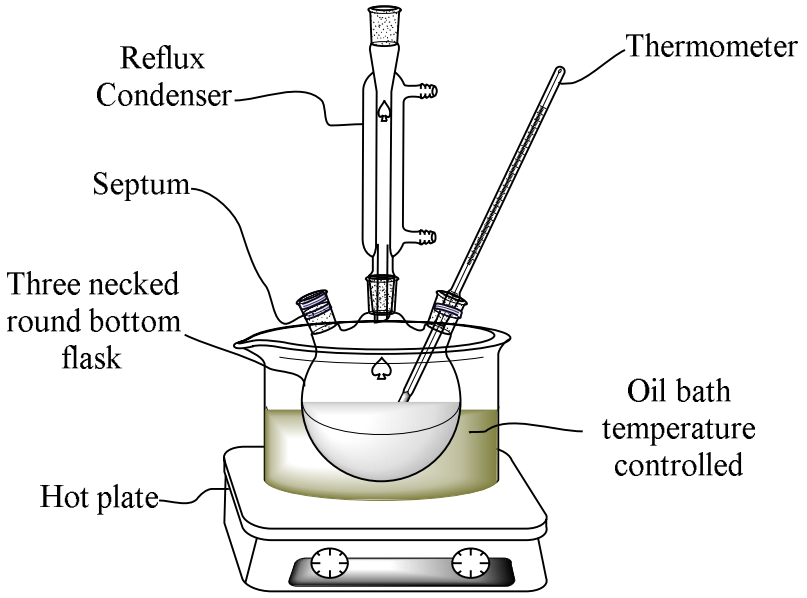

Figure 26. Catalytic set up of cyclohexene epoxidation

3.12.1. Conversion calculations and selectivity to reaction products in epoxidation of cyclohexene

They produce signals proportional to the mass of the product detected. Through the method of integration, the software used allows to determine the area of the signal. In general, experimentally obtained areas must be corrected by corresponding response factors that depend on the nature of the compound detected. The response factors were determined for the reagent and each of the products by the internal standard method, using toluene as such. In this method, the ratio of analyte areas and the internal standard for different standards containing different known concentrations of analyte and the same concentration of the internal standard in all cases. The calibration curve is obtained following equation 1, in which the slope corresponds to the response factor of the calibrated analyte.

$$\frac{A_{analyte}}{A_{internal}} = F * \frac{n_{analyte}}{n_{internal}} \quad (1)$$

Where *A* refers to the areas of the chromatogram peaks, *n* to the number of moles of internal standard and analyte and *F* is the corresponding response factor. The response factors obtained by calibrating with standards are collected. Different known concentrations of 1,2-cyclohexane epoxide, 2-cyclohexenol, 2-cyclohexenone, 1, 2-cyclohexanediol and 2-cyclohexenyl hydroperoxide were analyzed[124]. The reaction conversion is not calculated by the disappearance of the reagent, since this may be overestimated by possible evaporation thereof, but as the sum of yields of the resulting products, as expressed in the equation 2:

$$Conversion(\%) = \sum \frac{n_{product}}{n_{reagent\ t=0}} * 100 \qquad (2)$$

Where $n_{product}$ is the number of moles of each of the products formed throughout the reaction and $n_{reagent\ t\ =\ 0}$ is the number of moles of cyclohexene. The selectivity of the products formed is calculated according to the following expression (equation 3):

$$Selectivity\ (\%) = \frac{Yield_{product}}{conversion} * 100 = \frac{n_{product}/n_{reagent\ t=0}}{\sum(n_{product}/n_{reagent\ t=0})} * 100 \qquad (3)$$

In order to carry out a comparison of the activity by active center in the different catalysts use the Turnover Number (TON) parameter, which calculates by relating the moles of epoxide produced to the moles of center active present in the catalyst studied. In this work the activity per titanium center according to equation 4[12]:

$$TON = \frac{n_{epoxide}}{n_{Ti}} \qquad (4)$$

Where TON is Turnover Number, $n_{epoxide}$ is the number of mole of epoxide produced, ^{n}Ti the number of moles of titanium present in the solid catalyst, whose chemical composition is determined by chemical analysis of ICP.

CHAPTER FOUR

4. RESULTS AND DISCUSSION

4.1. Pure silica SBA-15 and PMO materials

In this study we have initially optimized the synthesis conditions of pure silica SBA-15. In a first step, the nature of the surfactant is varied in order to modify the particle morphology from fiber like to plate like. Secondly, two pore expanding agents are tested aiming to obtain large pore size (larger than 8 nm). The labeling of the samples is described in Figure 27. Later on, the same approach will be discussed for PMO, Figure 39. The complete characterization results and discussion of both pure silica SBA-15 and hybrid organosilica PMO materials are given in the following sections.

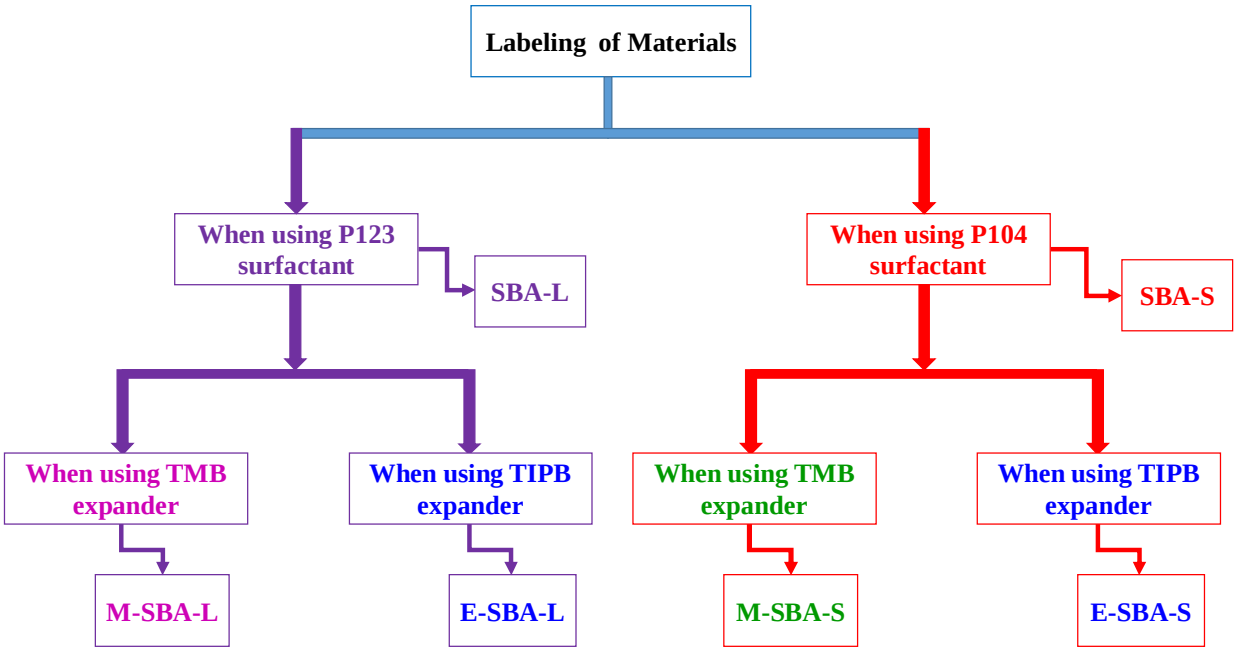

Figure 27. Scheme with SBA-15 samples labeling

4.1.1. Characterization results and discussion on pure silica SBA-15 materials

The synthesized SBA-15 materials using two different types of nonionic surfactants, namely Pluronic P123 and P104 which have the general formula $EO_{20}PO_{70}EO_{20}$ and $EO_{27}PO_{61}EO_{27}$, respectively. Ethylene oxide (EO) sections of both surfactants are responsible for the interaction with the silica source, which in very strong acidic media become highly depolymerized and protonated interacting by H-bonds with the protonated polyethylene oxide (PEO) groups of the surfactants. On the other hand, polypropylene oxide (PPO) units are responsible for the hydrophobic core of the micelles. The obtained samples were characterized by low angle powder X-ray diffraction to evaluate their pore arrangements; N_2 adsorption/desorption isotherms, to obtain the textural properties; transmission electron microscopy, to evaluate the internal structure of the particles and channel length, TGA to confirm the complete removal of the structure-directing agents after calcination and to evaluate the thermal stability of the material and finally by scanning electron microscopy to confirm the particle morphology of the material.

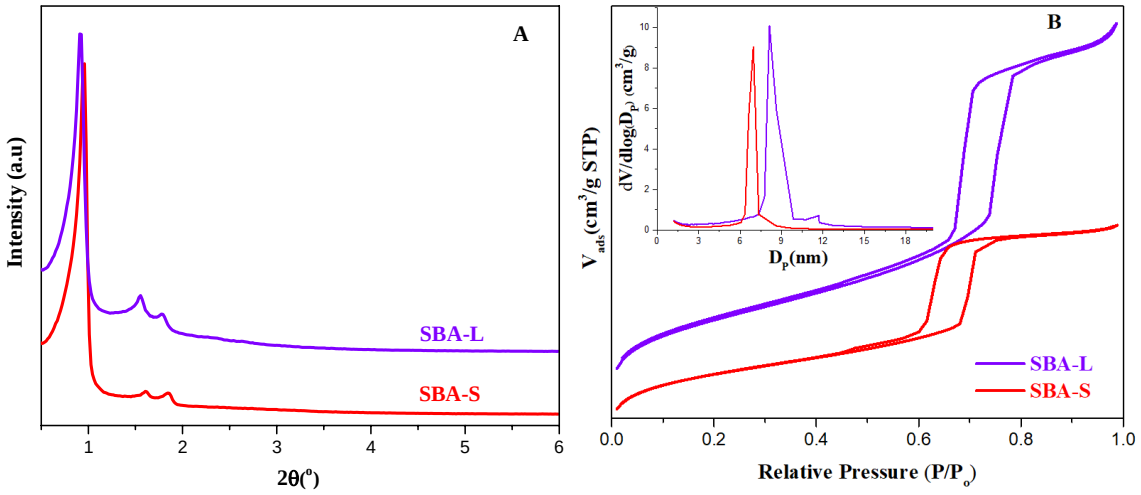

Figure 28. Low angle XRD pattern (A) and N_2 adsorption-desorption isotherms (B) of the calcined SBA-L and SBA-S types of materials

Figure 28 (A) shows the low angle X-ray diffraction patterns at 2Θ between 0.5 and 6 for the synthesized SBA-L and SBA-S materials. Both SBA-L and SBA-S materials show a typical XRD pattern of an ordered hexagonal network arrangement of mesopores. The presence of one very intense diffraction peaks (100) and two weak peaks (110) and (200) in both types of materials characterize a well-defined 2D hexagonal symmetry mesoporous structure with excellent uniformity. The ideal models for these structures are hexagonally close packed cylindrical pore channels belonging to the *P6mm* space group. Both materials, SBA-L and SBA-S, have roughly similar unit cell dimensions (Figure 28 (A) and Table 4). The unit cell dimensions of the calcined samples are smaller than their corresponding uncalcined samples, this is due to the contraction of the unit cell in the calcination process (dehydroxilation of surface hydroxyl groups) (Table 4).

The N_2 adsorption-desorption isotherms of the calcined SBA-15 type of materials are shown in Figure 28 (B) and their textural properties are summarized in Table 4. The adsorption isotherm of both materials, SBA-L and SBA-S, exhibit the classic type IV adsorption isotherms, according to the IUPAC classification[108], with an H1-type hysteresis loop which is characteristic of mesoporous materials with uniformly distributed cylindrical channels. The adsorption and desorption branches are located at high relative pressure (P/P_0 between 0.5 – 0.8) characteristic of mesoporous materials. The isotherm of SBA-L material is shifted slightly toward the higher P/P_0, which suggests an increase of the pore size. This pore size difference is also confirmed by BJH pore size distribution (Figure 28 (B), inset), the pore size of SBA-L and SBA-S materials are 8.6 and 7.2 nm, respectively. The BJH pore size distribution (Figure 28 (B), inset) also confirmed that both materials have a relatively narrow pore size distribution. The pore size, surface area and pore volume of

SBA-L material is slightly higher than SBA-S material. This may be due to the presence of relatively higher hydrophobic PPO groups in the P123 surfactant. The pore wall thickness of SBA-S material is slightly higher than the SBA-L material (Table 4), this may be due to the presence of relatively higher hydrophilic PEO group in the P104 surfactant as the hydrophilic PEO part of the surfactant can easily interact with the hydrolyzed silica source. As a result, the silica source condensed and polymerized on the PEO part of the surfactant to create the pore wall of the final material. Previous studies also confirm that the hydrophobic PPO group of the surfactant is responsible for the formation of mesopores of the final material, although part of the PEO surfactant which is near to the PPO part may also participate for the formation of mesopore depending on the reaction condition and the calcination temperature. On the other hand, the majority of PEO chains insert into silicate frameworks which generate micropores in the pore wall after the removal of the template[31, 126]. Furthermore, the difference of the synthesis condition also may affect their textural properties.

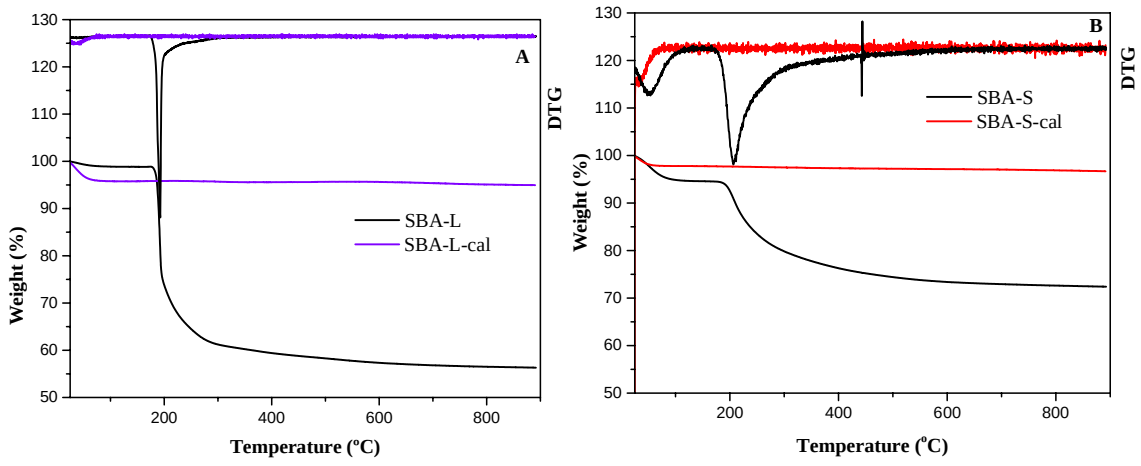

Figure 29. TGA profiles of SBA-L (A) and SBA-S (B) materials before and after removing the surfactant

Table 3. The weight loss in different temperature ranges for pure silica SBA-15 materials

Catalyst	Weight loss (%) in different temperature ranges		
	< 150°C	150 – 350°C	>350°C
SBA-L	1.17	38.61	3.9
SBA-L-cal	4.22	0.21	0.63
SBA-S	5.41	16.8	5.41
SBA-S-cal	2.25	0.37	0.67

In order to create porosity in the synthesized materials, the surfactant must be removed at the end of the synthesis through calcination or other method such as solvent extraction method. Figure 29 (A & B) and Table 3 shows that the complete removal of the surfactants by calcination is possible without affecting the structure of the material. In both types of materials before and after calcinations, the weight loss below 150 °C is too small. This weight loss is due to the loss of water physically adsorbed inside of the pore of the mesoporous materials or the loss of ethanol residues that remained during the washing step. The weight loss at 150 °C of the calcined SBA-L material (SBA-L-cal) is higher than the noncalcined one (SBA-L). This is due to the increase of porosity of the material after calcination responsible for the adsorption of high amount of water from the environment on its hydrophilic surface. However, in the SBA-S material the weight loss at 150 °C is lower after calcination when compared to the noncalcined SBA-S material, this may be due to the presence of ethanol residues that remained during the washing step responsible for this weight loss. As it is shown in Figure 29 (A and B) in both as synthesized SBA-L and SBA-S materials the sharp weight loss between 150 to 350 °C is due to the removal of

the surfactants. When we compare the amount surfactants removed in the temperature range of 150 to 350 ^{o}C, SBA-L is higher than the SBA-S one. This significant weight loss difference between the two materials is due to the difference of solvents used in the washing step. SBA-S was washed with ethanol which is less polar than water and more efficient to dissolve organic substances, the PPO group of the micelle and unreacted surfactants, during the washing step. Both calcined materials showed a very low weight loss in the temperature range of 150 to 350 ^{o}C, which indicates that the surfactant have been efficiently removed during the calcination process. The small weight loss in both SBA-L and SBA-S above 350 ^{o}C is due to the dehydroxylation of surface silanol groups and removal of part of the surfactant in the pore wall of the material which is responsible for the creation of micropores. The slightly higher weight loss in the SBA-S than SBA-L material above 350 ^{o}C is due to the presence of slightly higher poly(ethylene)glycol (PEO) group in the P104 surfactant. PEO is responsible for the synthesis of the pore wall of the material, therefore if there is high amount PEO group in the pore wall the weight loss at high temperature increases and the micropore volume of the final material also increases. The very low weight loss above 350 ^{o}C of the calcined materials of both types confirms all the PEO groups are removed during the calcination process, this weight loss may be due to the dehydroxylation of surface hydroxyl groups.

The internal structures of the calcined SBA-L and SBA-S materials were further characterized by TEM in order to check the channels lengths and the accessibility and arrangement of pore mouths. Figure 30 shows the TEM images of SBA-L (A and B) and SBA-S (C and D) materials perpendicular and along the plane. The channels and the accessibility of the pore mouths are clearly observed in both SBA-L and SBA-S materials.

From TEM the channel length of SBA-L is in the order of microns while SBA-S material is around 400 nm. This confirms that P104 surfactant is suitable to synthesize materials with short diffusion pathlengths.

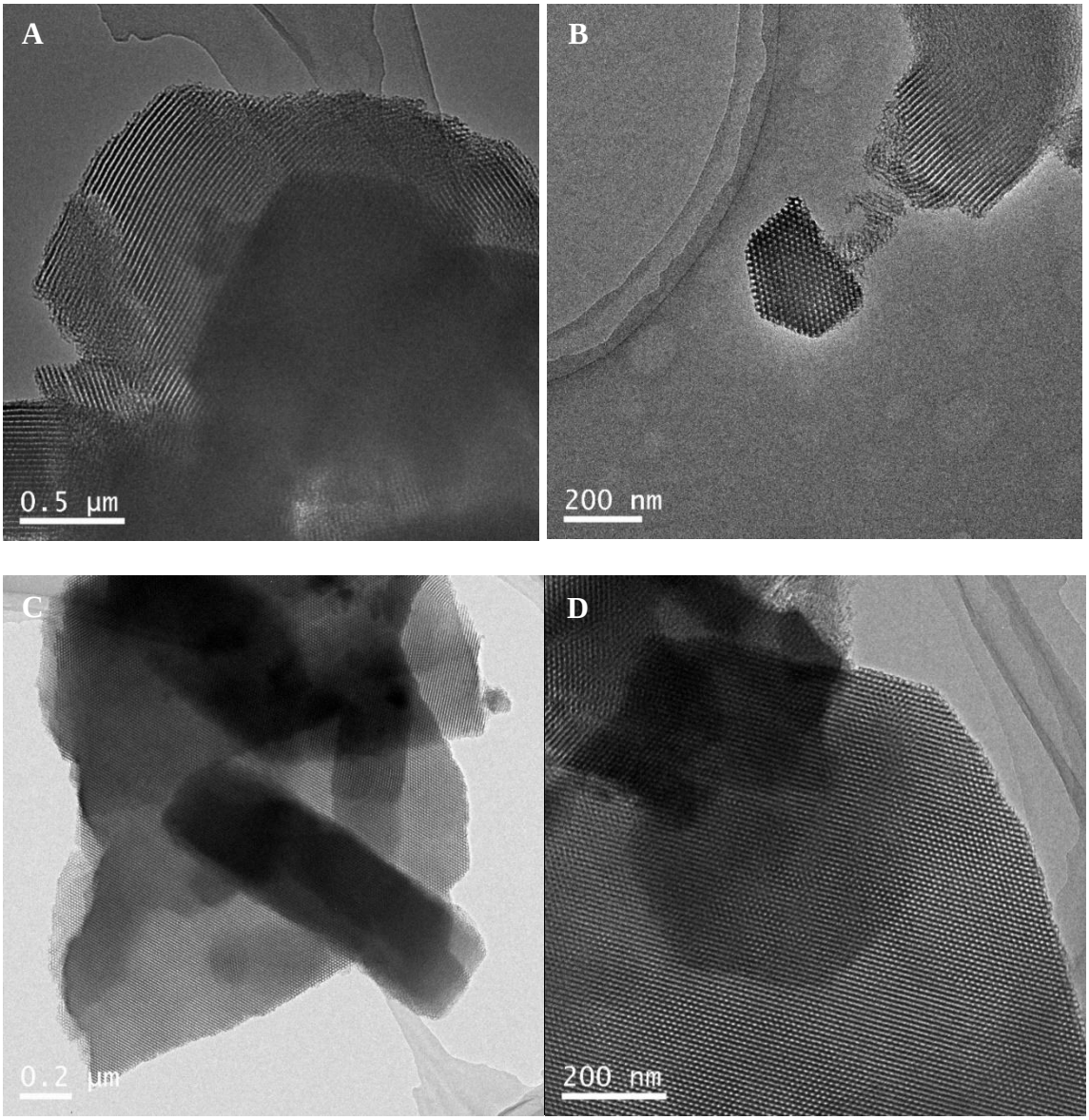

Figure 30. TEM images of SBA-L (A) perpendicular to the plane and (B) along the plane and SBA-S material (C) perpendicular to the plane and (D) along the plane

Finally, the particle morphology of both SBA-L and SBA-S materials was characterized by using scanning electron microscopy to confirm whether our objective is achieved or not. As shown in Figure 31 SBA-L, the material is composed of fiber-like particle morphologies and SBA-S material is composed of plates-like particle morphology, which have an average particle size of 330 nm. In summary, both surfactants provide high quality materials, P123 gives materials with fiber-like morphology which may have diffusion problems of bulky molecules, while P104 offers materials with short diffusion paths and plates-like particle morphology.

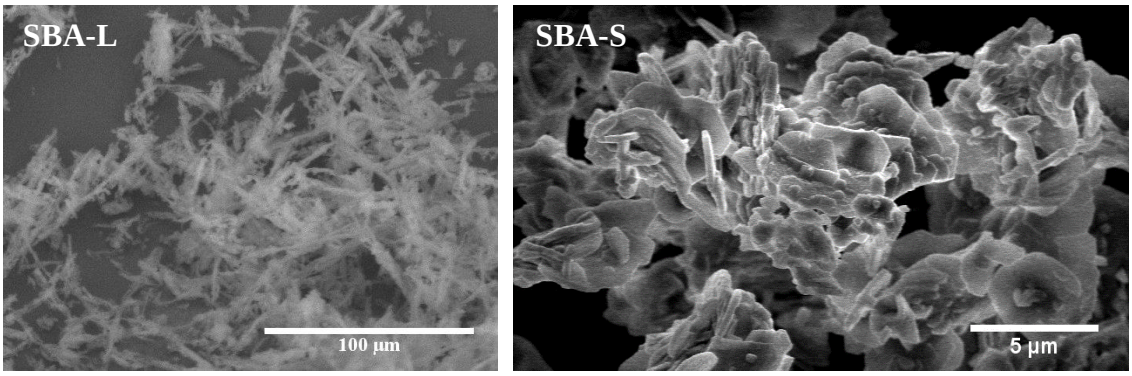

Figure 31. SEM images of the SBA-L and SBA-S materials

In order to facilitate the diffusion of the vernonia oil molecules we tried to prepare materials with larger pore diameter than SBA-L (8.6 nm) and SBA-S (7.2 nm). Several experimental works were made and characterized by the above mentioned techniques. As shown in Figure 27, first we tried to expand the pore size of both types of materials (M-SBA-L and M-SBA-S) by using 1, 3, 5-trimethylbenzene (TMB) as a pore expander. Both materials were characterized by X-ray diffraction in order to check their pore structure. Figure 32 (A & B) shows the low angle X-ray diffraction patterns at 2Ɵ between 0.5 and 6 for the synthesized mesoporous silica materials with and without pore expanders for comparison purpose.

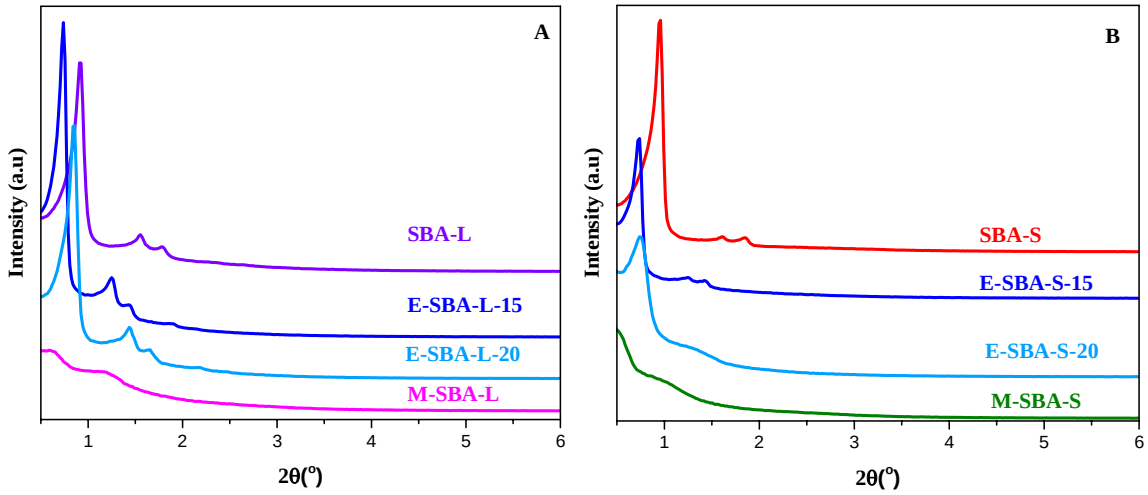

Figure 32. Low angle XRD pattern of the calcined SBA-L (A) and SBA-S (B) types of materials which are synthesized with and without pore expander

All XRD peaks of both M-SBA-L and M-SBA-S materials disappear, suggesting that the addition of 1, 3, 5-trimethylbenzene (TMB) gives rise to lose the hexagonal arrangement of pores. This may be due to uncontrolled swelling of the triblock copolymers by the swelling agent that causes disruption of the honeycomb nodes of the traditional SBA-15 material. This may produce less ordered mesocellular foam material with a wider pore size[127]. To prove this idea the material was characterized by N_2 adsorption-desorption isotherm (Figure 33). The N_2 adsorption-desorption isotherm and BJH pore size distribution of the parent materials SBA-L and SBA-S was drawn together with M-SBA-L and M-SBA-S respectively for comparison purpose. The isotherm of samples M-SBA-L and M-SBA-S, resemble Type IV isotherms, exhibiting a wider hysteresis located at higher values of P/P_0, probably due to the increase of the interparticle voids, which leads to the process of capillary condensation and evaporation that occurs in a shorter interval of relative pressures. It is also a type of H2 (b) hysteresis loop which is associated with materials with non-uniform pore size distribution. This is commonly observed in

mesocellular silica foams. The BJH pore size distribution of these samples shows a considerably broader range of pore sizes. From this result we can say that the material loses its hexagonal structure when using TMB as pore expanders. TEM images (Figure 34) of samples prepared with TMB are disordered both with P123 (L) and P104 (S) surfactant, probably due to the disturbing of the micelle formation. Figure 34 shows that materials M-SBA-L and M-SBA-S possess the ringed multi-lamellar silica vesicles due to formation of mesocellular foams. This idea is supported by previously reported papers which showed that hexagonal structure of the material can be transited to mesocellular foam structure during pore expansion[128, 129]. Therefore, as shown in Figure 27 we tried to expand the pore size of both types of materials by using another type of pore expander, 1, 3, 5-triisopropylbenzene (TIPB), which has relatively large size and more hydrophobic group. This characteristic may help the expander to selectively interact with the core of the micelle.

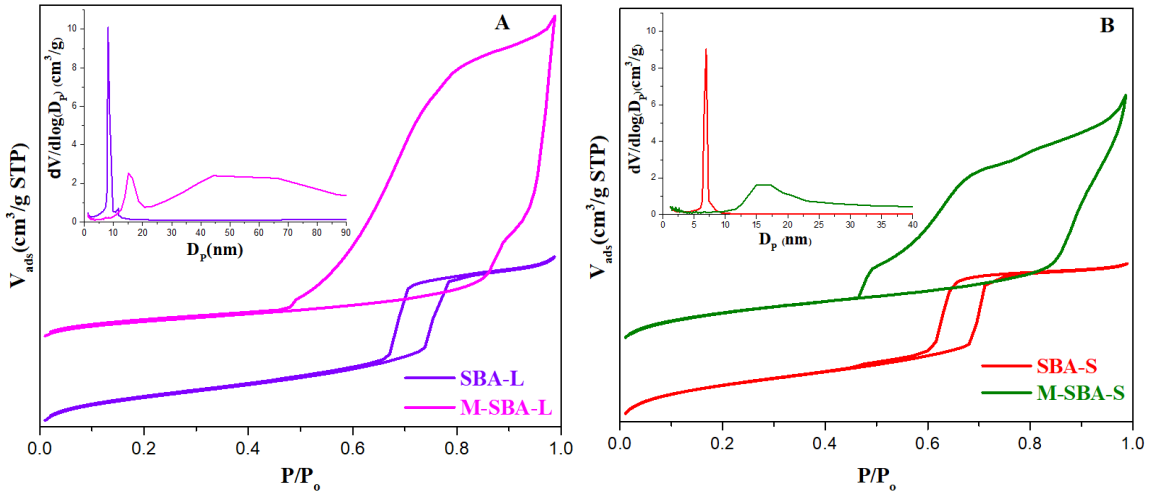

Figure 33. N_2 adsorption-desorption isotherms and BJH pore size distributions (inset) of (A) calcined SBA-L and M-SBA-L and (B) calcined SBA-S and M-SBA-S materials

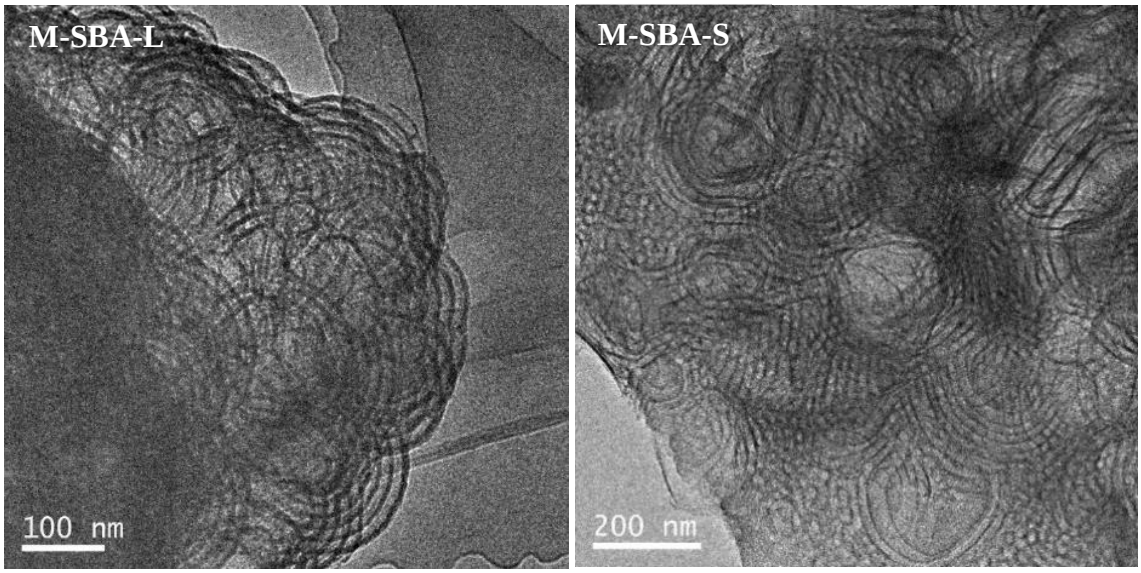

Figure 34. TEM images of M-SBA-L and M-SBA-S materials

As shown in Figure 32, when using TIPB as a pore expander the E-SBA-L-20 material retains its hexagonal symmetry (the three XRD peaks are well resolved) and E-SBA-S-20 seems moderately ordered (partially losing its pore arrangement, the two weak XRD peaks disappear). As a result, the gelling temperature was lowered from 20 to 15 ^{o}C in order to improve the capacity of TIPB to penetrate into the hydrophobic micelle cores that causes pore expansion and improve its degree of ordering. It can be seen that both E-SBA-L-15 and E-SBA-S-15 materials (Figure 32) exhibit XRD patterns with one very intense diffraction peak (100) and two weak peaks (110) and (200), which are characteristic of 2-dimensional hexagonal (*P6mm*) structure with excellent uniformity. When using P123 as a structure-directing agent the hexagonal symmetry of the material at both gelling temperatures is maintained. However, the XRD peaks are shifted towards the lower 2Θ when the gelling temperature is lowered from 20 ^{o}C, E-SBA-L-20, to 15 ^{o}C, E-SBA-L-15, due to the increase of the pore size as it is also confirmed by N_2 adsorption-desorption isotherm. This may be that at lower gelling temperature larger number of TIPB molecules

penetrate into the hydrophobic micelle cores causing pore expansion. The three XRD peaks of the E-SBA-L-15 and E-SBA-S-15 materials were shifted towards the lower 2Θ value (larger a_o) when compared to their SBA-L and SBA-S parent materials. This confirms that 1, 3, 5-triisopropylbenzene (TIPB) increases the unit cell dimension of SBA-L and SBA-S very well without affecting the pore arrangement of the material. These materials were characterized by N_2 adsorption-desorption isotherm in order to confirm the pore size difference with the parent material.

The N_2 adsorption-desorption isotherms of the calcined E-SBA-L-15 and E-SBA-S-15 materials are given in Figure 35 (A & B) and their textural properties are summarized in Table 4. Both materials exhibit the classic type IV adsorption isotherms, according to the IUPAC classification[108], with an H1-type hysteresis loop which is characteristic of mesoporous materials with cylindrical channels. The adsorption and desorption branches of these materials are located at higher relative pressure and the hysteresis loop shifted slightly towards higher relative pressure (P/P_o= 0.9) when compared to their parent one, which suggests an increase of the pore size. The mesopore size distribution obtained by BJH (Figure 35 (A and B), inset) for both E-SBA-L-15 and E-SBA-S-15 materials have a relatively narrow pore size distribution and the efficiency of the incorporation of TIPB as a swelling agent indicates the increasing of the pore diameter without affecting its hexagonal symmetry. However, the lack of sharpness and presence of two distinctive steps in the desorption branch of the isotherm of E-SBA-S-15 indicates the presence of partial blockage of some mesopores or presence of bottlenecks.

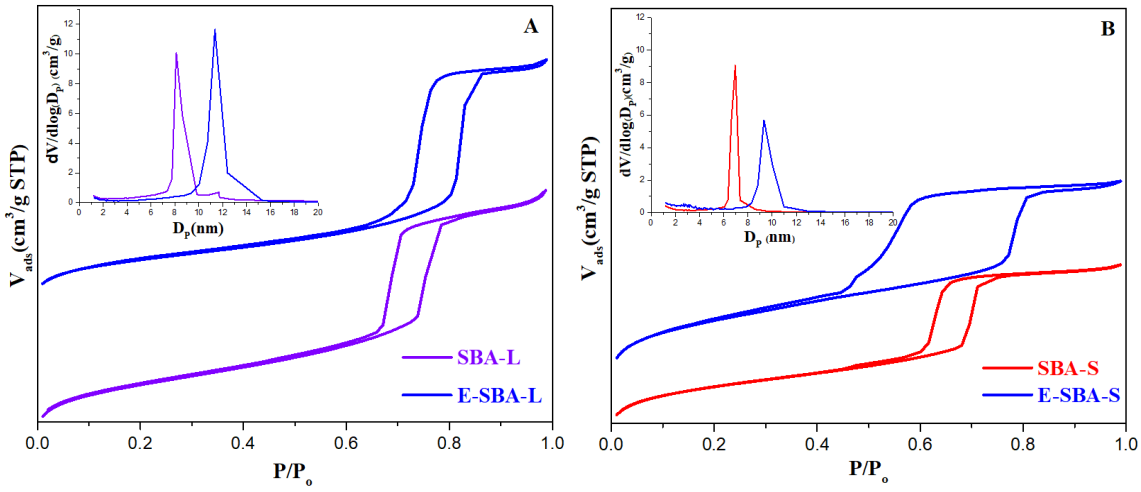

Figure 35. N_2 adsorption-desorption isotherms and BJH pore size distributions (inset) of (A) E-SBA-L-15 and (B) E-SBA-S-15 materials

Table 4. Structural parameters of pure silica (SBA-15) materials

Sample	ao (nm)[a]	ao (nm)[b]	S_{BET} (m^2g^{-1})	V (cm^3g^{-1})	V_m (cm^3g^{-1})	d_{BJH} (nm)	t (nm)
SBA-L	11.6	11	707	1.09	0.044	8.6	2.4
M-SBA-L	-	-	454	1.7	0.039	16.4	-
E-SBA-L-20	12.6	11.9	527	1.08	0.013	11	0.9
E-SBA-L-15	14.3	13.7	505	1.04	0.025	12	1.7
SBA-S	11.9	10.8	543	0.65	0.069	7.2	3.4
M-SBA-S	-	-	452	0.84	0.044	18	-
E-SBA-S-20	13.7	12.6	494	0.72	0.025	9.0	3.6
E-SBA-S-15	14.5	13.7	674	0.76	0.054	10	3.7

Unit cell parameter, ao, of [a] non-calcined and [b] calcined, samples. ao was determined from the interplanar spacings of the (100) planes using the formula of $ao = 2d_{100}/\sqrt{3}$, in which $d_{100} = 1.5406/2\sin\theta$ where θ is the scanning diffraction angle corresponding to peak (100). The pore size, d_{BJH}, was obtained from the maxima of the pore size distribution curve calculated by the Barrett-Joyner-Halenda (BJH) algorithm using the adsorption branch. Pore wall thickness, t, was assessed by subtracting d_{BJH} from ao. The BET surface area, S_{BET}, was calculated using adsorption data in a relative pressure range $P/p_0 = 0.05$-0.24. The total pore volumes, V, and micropore volumes, V_m, were estimated from the adsorbed amounts at a relative pressure of about 0.99.

Large pore size materials, E-SBA-L-15 and E-SBA-S-15, were further characterized by TGA, TEM and SEM characterization techniques.

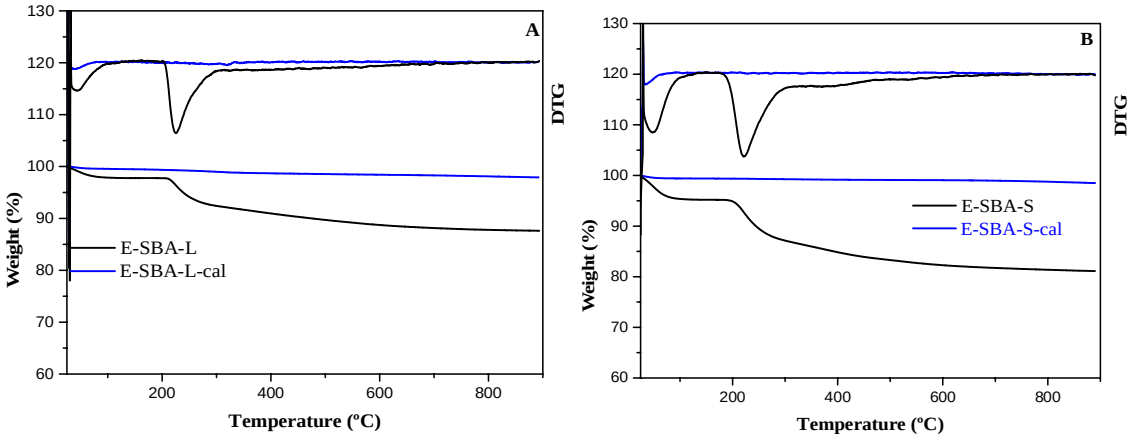

Figure 36. TGA profiles of E-SBA-L-15 and E-SBA-S-15 materials before and after calcination

Table 5. The weight loss in different temperature ranges for large pore size pure silica SBA-15 materials

Catalyst	Weight loss (%) in different temperature ranges		
	< 150 °C	150 – 350 °C	>350 °C
E-SBA-L-15	2.24	6.1	4.01
E-SBA-L-15-cal	0.53	0.69	0.86
E-SBA-S-15	4.81	9.23	4.83
E-SBA-S-15-cal	0.61	0.19	0.68

Figure 36 (A and B) and Table 5 shows the weight loss profile of E-SBA-L-15 and E-SBA-S-15 materials before and after calcination. Small weight loss below 150 °C in both E-SBA-L-15 and E-SBA-S-15 is due to the loss of water physically adsorbed inside of the

pore of the mesoporous materials and ethanol residues remained during the washing step. As a result, the amount of surfactant remained with the material after the washing step is very low. The weight loss in the temperature range of 150 to 350 ^{o}C is due to the removal of the surfactants. Further weight loss above 350 ^{o}C for non-calcined materials is due to the loss of the surfactants, from the pore walls of the materials and due to the dehydroxylation of the surface hydroxyl groups. In both temperature ranges the weight loss in E-SBA-S-15 is slightly higher than E-SBA-L-15 indicating that the surfactant P104 is relatively hard to remove from the material, due to the presence of higher PEO groups which is responsible for pore wall formation needs high temperature to remove it and to create micropores in the pore wall. This TGA profile also proves that the surfactants are completely removed in both E-SBA-L-15 and E-SBA-S-15 materials in the calcination process.

The particle morphology of both E-SBA-L-15 and E-SBA-S-15 materials were analyzed by SEM images (Figure 37). In these cases, the morphology is not clear, as both look like fibers but the fibers of E-SBA-S-15 material look like being formed by aggregates. The particle morphology E-SBA-S-15 is affected by the addition of the expander probably due to the different particle growth mechanism. The addition of TIPB as a swelling agent in the synthetic procedure of E-SBA-L-15 maintains the morphology of the fiber-like particle with increased particle diameter. To get a clear information about the channel pathlength and the pore arrangement of both materials were further analyzed by TEM.

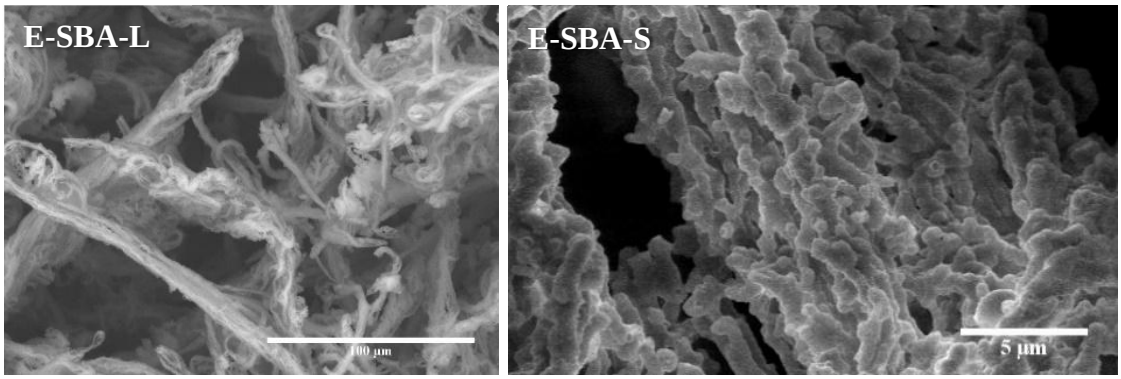

Figure 37. SEM images of the E-SBA-L and E-SBA-S materials

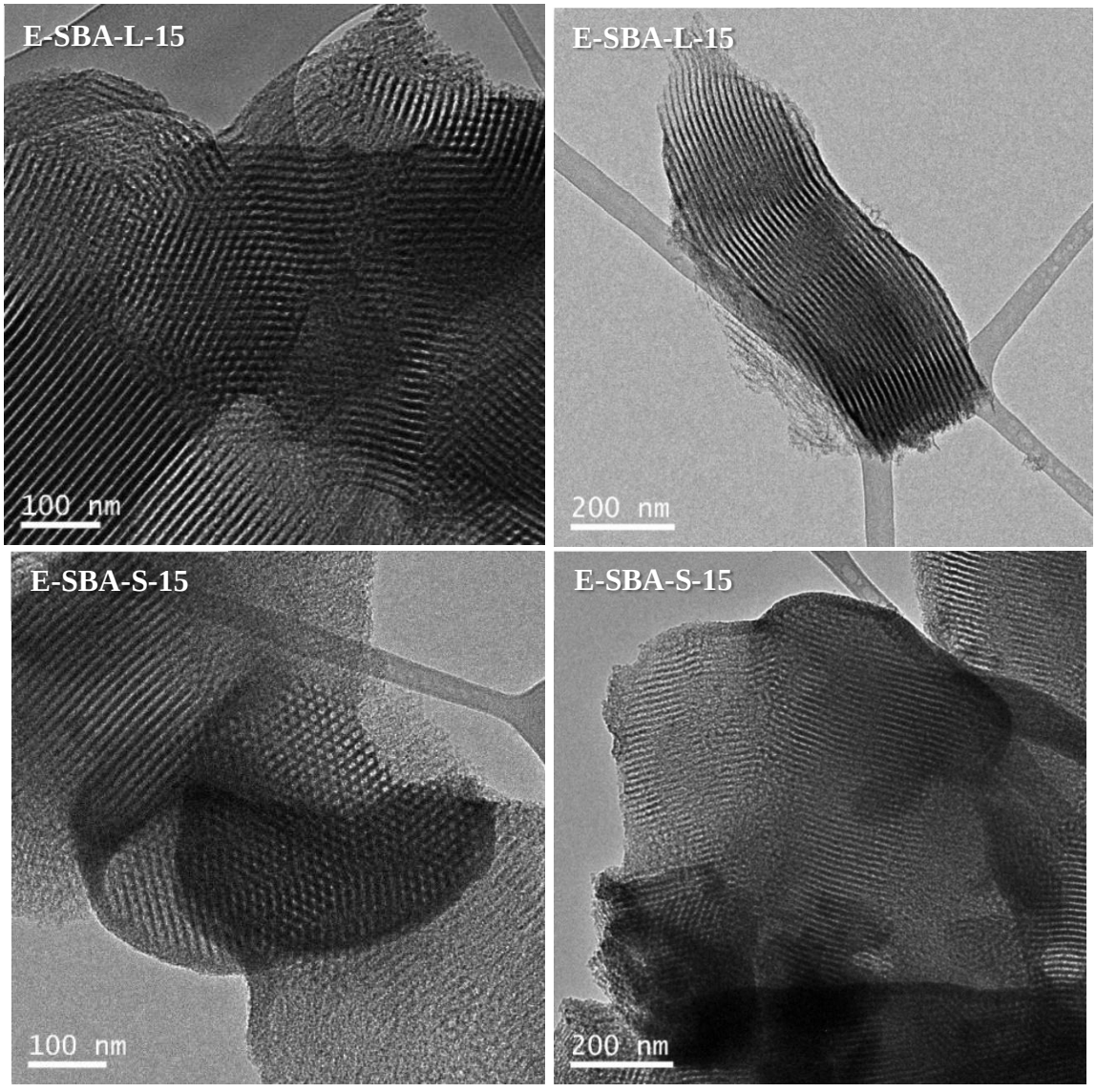

Figure 38. TEM images of E-SBA-L and E-SBA-S materials.

Figure 38 shows the TEM images of both E-SBA-L-15 and E-SBA-S-15 depicting the well-ordered mesoporous structures in both materials. The presence of very thick layers surrounding the outer surface of the particles in E-SBA-S-15 materials explains the presence of partially blocked pore mouths (lack of pore openings). This pore blockage problem is not observed in E-SBA-L-15 materials, the channels and the pore mouths are accessible. Furthermore, the TEM of E-SBA-L-15 material also shows that the channel length of this material is around 850 nm. This value is almost half of the channel length of the parent SBA-L (~ 1500 nm). This proves that the diffusion path length of the E-SBA-L-15 material is become short, due to the presence of TIPB. This may be due to the presence of TIPB droplets in the synthesis solution that may facilitate the nucleation formation and particle growth to produce materials with short path length. In general the short diffusion paths in E-SBA-L-15 and the presence of outer thick layer in E-SBA-S-15 from TEM we can conclude that E-SBA-L-15 is the optimum material.

4.1.2. Characterization results and discussion on hybrid organosilica PMO materials

Attempts were made to improve the pore surface to enhance the adsorption of vernonia oil during the catalytic process by using organosilica precursors. At the same time, we tried to synthesize PMO with short channels morphology by varying surfactants P123 and P104 to facilitate diffusion of vernonia oil in the channels. Given the large size of vernonia oil, large pore size would be required. Thus, we tried to optimize the synthesis of PMO using TMB and TIPB as a pore expander as sown in Figure 39.

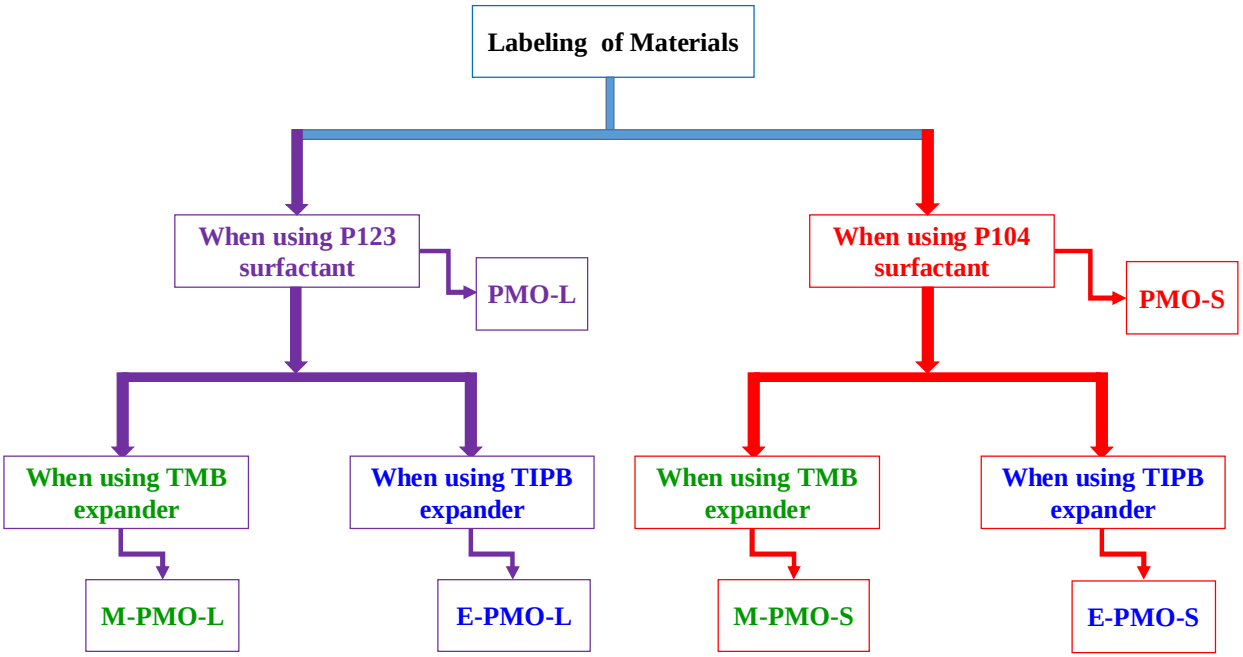

Figure 39. Scheme with PMO samples labeling

Figure 40 (A) shows the low angle X-ray diffraction patterns of PMO-L and PMO-S materials, the presence of one very intense peak (100) and two weak peaks (110) and (200) in both materials, indicating that both are ordered materials in the hexagonal network arrangement of mesopores belonging to *P6mm* space group.

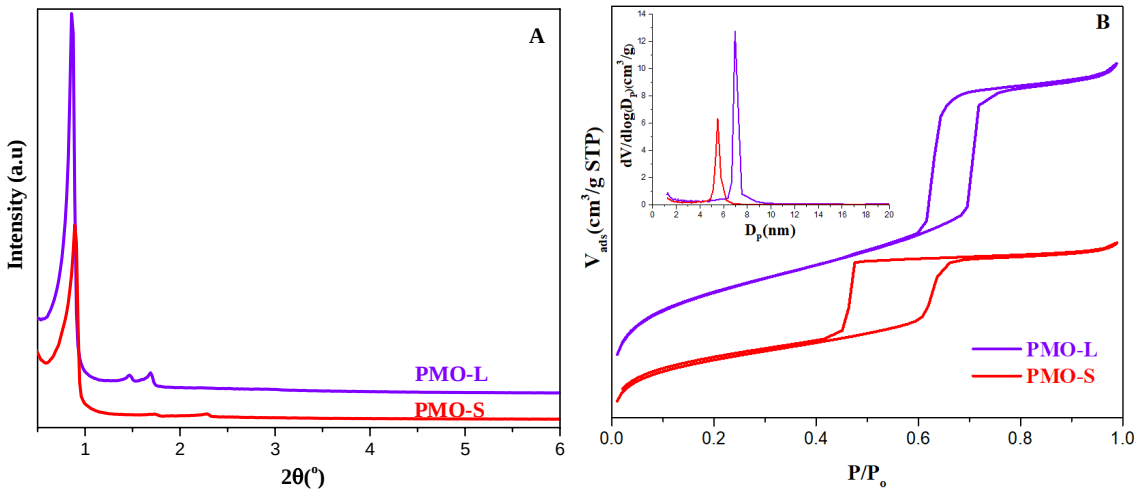

Figure 40. Low angle XRD pattern (A) and N_2 adsorption-desorption isotherms (B) of the calcined PMO-L (P123) and PMO-S (P104) types of materials

The high intensity of the three XRD peaks in PMO-L material indicate that the degree of ordering is better in the presence of P123, although both of them adopt hexagonal structure. Both materials have almost the same unit cell dimensions (Table 8). These materials were characterized by N_2 adsorption/desorption isotherms to compare their textural properties, i.e. surface area, pore diameter, pore volume, and pore wall thickness. Figure 40 (B) shows N_2 adsorption–desorption isotherms and the corresponding pore size distributions calculated by the BJH method for the calcined hybrid organosilica materials. The isotherms of both materials are type IV, with H1 type hysteresis loop at high relative pressure, which is characteristic of mesoporous materials with uniform size cylindrical pores. This fact is also confirmed by the BJH pore size distribution as shown in Figure 40 (B, inset). However, the desorption curve of the PMO-S (P104) is not as sharp as PMO-L (P123). It seems that there is the delay of diffusion. This may be due to the presence of partially blocked pores or the presence of bottlenecks. The BJH pore size distribution (Figure 40 (B), inset) also shows that the average pore diameter of the PMO-L material is relatively larger than the

PMO-S one, since PMO-L was synthesized by using the P123 surfactant which has a relatively more hydrophobic PPO group, responsible for the formation of the core of the micelle which becomes the pore diameter at the end. As a result, PMO-L has larger pore diameter, surface area and pore volume (Table 8). On the other hand, PMO-S material has a larger pore wall thickness, because this material was synthesized by using the P104 surfactant which has a relatively more hydrophilic PEO group, responsible for the formation of pore wall which becomes micropores in the pore wall after its removal through calcination[126].

The removal of the surfactants and interpretation of the TGA profiles of PMO materials is not as easy as the SBA-15 type of materials. This is due to the presence of two types of organic groups in the final material, the framework ethane (-CH_2CH_2-) group which is needed to maintain the structure and the hydrophobicity of the material, and the surfactant organic group which fills the pore of the final material and should be removed to make the material porous. To create porosity in PMO type of materials the surfactant should be removed from the final material without affecting the framework organic group (-CH_2CH_2-). In our study we tried to remove the surfactants by using the conventional solvent extraction (acidified ethanol solution) and by calcination at a relatively low temperature (350 ^oC for 5 h) to compare which one is an optimum method to remove the surfactant. The TGA profile of PMO-L and PMO-S before and after surfactant removal is given in Figure 41 (A and B).

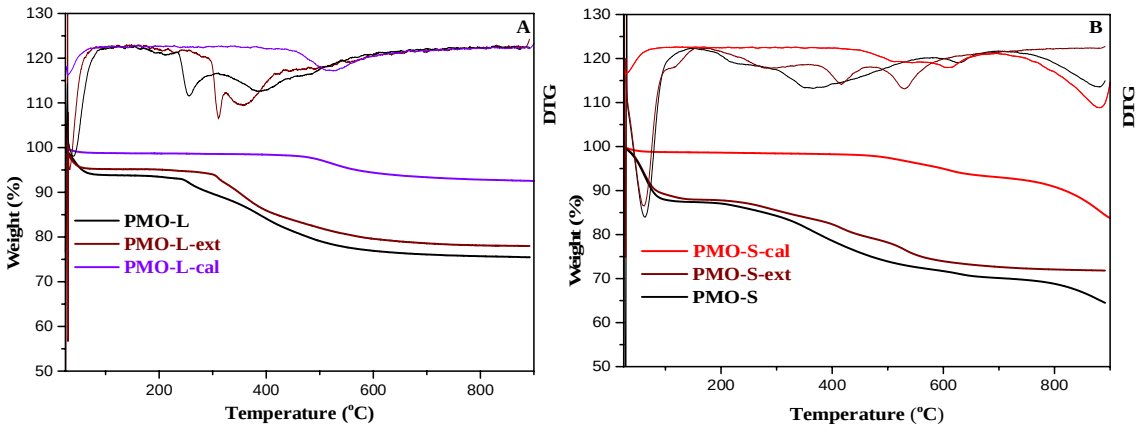

Figure 41. TGA profiles of (A) as synthesized PMO-L, surfactant extracted PMO-L (PMO-L-ext) and calcined PMO-L (PMO-L-cal); and (B) as synthesized PMO-S, surfactant extracted PMO-S (PMO-S-ext) and calcined PMO-S (PMO-S-cal) materials

Table 6.The weight loss in different temperature ranges for PMO materials

Catalyst	Weight loss (%) in different temperature ranges			
	< 150 °C	150 – 425 °C	425 – 700 °C	>700 °C
PMO-L	6.25	11.18	6.48	0.61
PMO-L-ext	4.83	10.45	6.13	0.59
PMO-L-cal	1.29	0.39	4.96	0.79
PMO-S	12.61	10.22	7.05	5.55
PMO-S-ext	12.03	6.99	8.34	0.81
PMO-S-cal	1.32	0.51	5.15	8.84

In Figure 41 (A and B) and Table 6, the small weight loss below 150 °C is due to the removal of physically adsorbed water or ethanol residues that remained in the washing step. As it is shown in Figure 41, the main weight loss in the non-calcined samples is in the

temperature range of 150 – 425 ^{o}C of all samples is due to the removal of the surfactant. Large weight loss from samples of PMO-L, PMO-L-ext, PMO-S and PMO-S-ext and the lowest weight loss from samples PMO-L-cal and PMO-S-cal, prove that calcination is a more efficient method to remove surfactants, very small amount of surfactants are removed by ethanol extraction. The weight loss in the temperature range of 425 – 700 ^{o}C of all samples is due to the removal of framework ethane (-CH_2CH_2-) group. The non-calcined samples show relatively higher weight losses in this temperature range than the calcined ones, probably due to the loss of part of surfactants residue on the wall of the silica together with the ethane group. All samples have roughly similar weight losses in this temperature range, i.e. calcination doesn't affect the framework ethane group. Finally, the very small weight loss above 700 ^{o}C of "L" types of samples is due to the dehydroxylation of surface silanol groups. The significant weight loss of "S" types of materials above 700 ^{o}C may be attributed to the decomposition of organic groups from its very thick pore wall and the dehydroxylation of surface hydroxyl groups. In general from the TGA profile in Figure 41 we can summarize that calcination at 350 ^{o}C for 5 h is effectively removing the surfactant without affecting the framework ethane (-CH_2-CH_2-) group.

The desired effect of morphology modification was observed by scanning electron microscopy. SEM images of PMO-L and PMO-S are shown in Figure 42. The structure of PMO-L synthesized with P123 produces particles is a conventional very long fiber-like morphology (Figure 42). Materials with such type of particle morphology have limited application in catalysis due to the diffusion limitation of bulky molecules (e.g. vernonia oil) in the channels and limited accessibility of the active sites of the material. As a result,

the material (PMO-S) synthesized by using Pluronic P104 has short channel platelets hexagonal particle morphology as shown in Figure 42, right side.

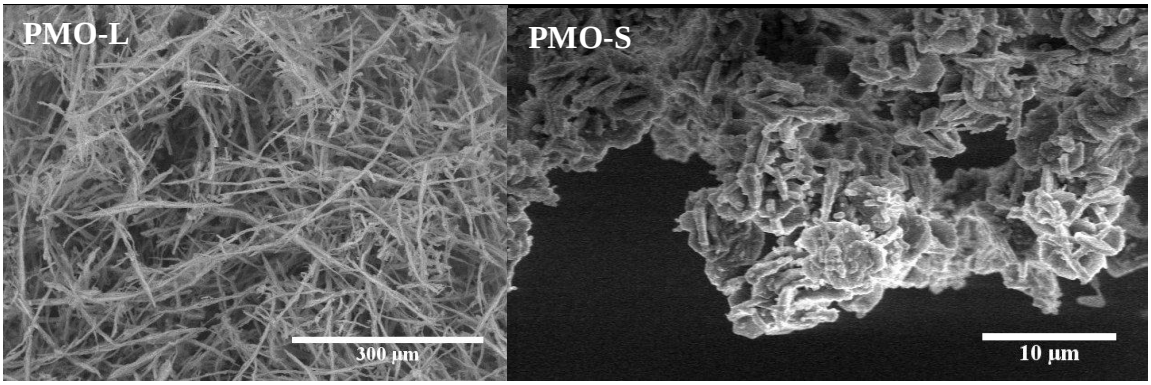

Figure 42. SEM images of the PMO-L and PMO-S materials

Therefore, from SEM we can conclude that the particle morphologies of PMO materials can be controlled by using Pluronic P104 as a surfactant, and particle dimension of 3.2 µm diameter by 550 nm length is obtained. This channel dimension is roughly similar with the SBA-S material which has been synthesized by using the same type of surfactant but different type of silica source. This indicates that Pluronic P104 is a suitable surfactant to synthesize platelets particles of both types (pure silica SBA as well as organosilica PMO).

The channel length and the accessibility of pore mouths of both materials were characterized by transmission electron microscopy (TEM) (Figure 43). The internal structure of PMO types of materials can be supported by TEM, perpendicular and parallel to the plane to observe the alignment of channels and pore mouths, respectively.

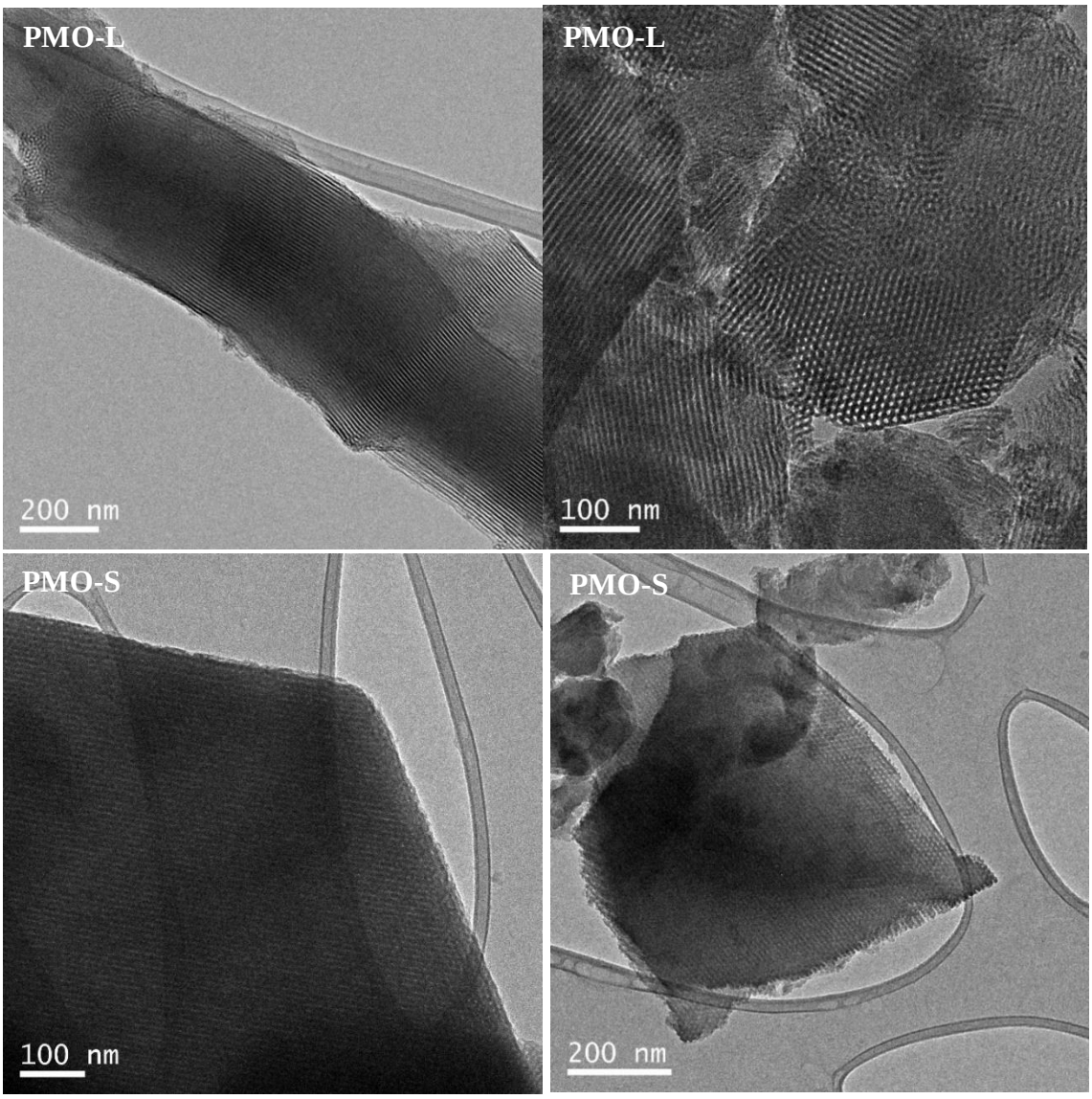

Figure 43. TEM images of PMO-L and PMO-S materials

TEM images of both samples, PMO-L & PMO-S, (Figure 43) show the arrangements of parallel channels and pore mouths. It is also observed that the channel length of PMO-S is short (~ 700 nm) and very thick pore wall. This result also proved that the channel length of PMO material becomes short when using Pluronic P104 surfactant. Although the channel length of PMO-S is shorter than PMO-L, its pore size (< 6 nm) is too narrow for the application aimed in this work, which is the catalytic conversion of vernonia oil. There

may be diffusion problem of bulky vernonia oil and epoxidized vernonia oil molecules in the long channel PMO-L and in the narrow pore sized PMO-S materials.

Different attempts were made to synthesize large pore size PMO materials and characterize by the above mentioned characterization techniques. As shown in Figure 39, first we tried to expand the pore size of the materials of both types by using 1, 3, 5-trimethylbenzene (TMB) as a pore expander (M-PMO-L and M-PMO-S), by varying the gelling temperature and only the best result at 15 ^{o}C gelling temperature is reported here. The materials were characterized by X-ray diffraction to evaluate their pore structure.

Figure 44 (A & B) show the low angle X-ray diffraction patterns at 2Ɵ between 0.5 and 6 for PMO materials which have been synthesized with both types of pore expanders (TMB and TIPB). The XRD patterns of the materials which have been synthesized without pore expanders (PMO-L and PMO-S) are drawn together for comparison purpose.

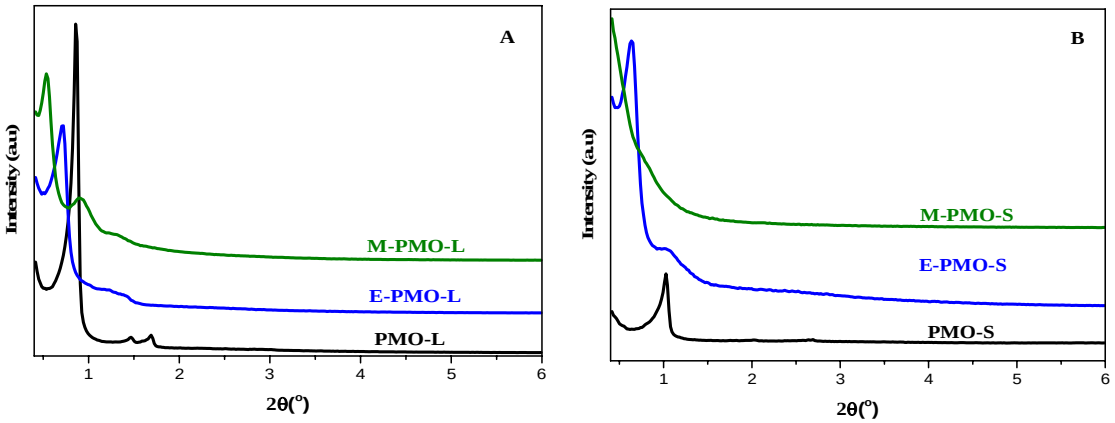

Figure 44. Low angle XRD patterns of PMO synthesized with P123 (A) and P104 (B) type of materials synthesized with TMB (M-PMO-L and M-PMO-S) and TIPB (E-PMO-L and E-PMO-S) pore expanders. Parent materials without expander are plotted in black

The presence of three weak XRD peaks in M-PMO-L material (100), (110) and (200) planes indicates that it is a moderately ordered hexagonally arranged mesopores structure. The three XRD peaks of M-PMO-L are shifted towards the lower 2θ due to the increase of the unit cell dimension. But there is no XRD peak observed in M-PMO-S sample, all the three XRD peaks of the parent material disappear. This indicates that the M-PMO-S material completely loses its structure. To prove this, both materials were characterized by N_2 adsorption-desorption isotherm and TEM.

Figure 45 (A and B) shows the N_2 adsorption-desorption isotherms of the M-PMO-L and M-PMO-S materials. The isotherms of both M-PMO-L and M-PMO-S shows type IV isotherm due to their mesoporosity and the shape of their hysteresis loop is different from their parent materials due to the difference of their pore size uniformity. The hysteresis loops of both samples M-PMO-L and M-PMO-S looks like H2 type which is a type of mesoporous material with non-uniform pore size distribution.

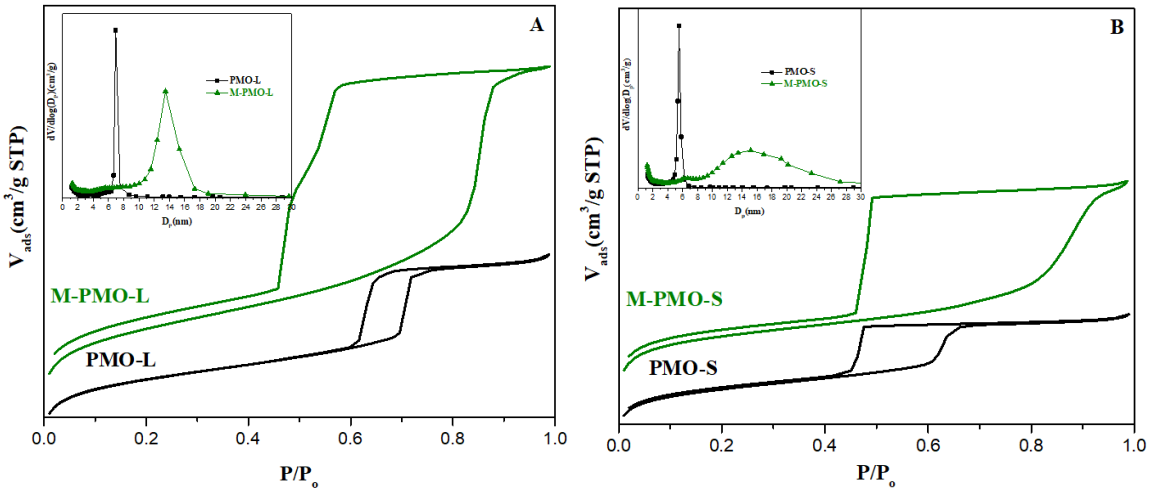

Figure 45. N_2 adsorption-desorption isotherms and BJH pore size distributions (inset) for (A) M-PMO-L and (B) M-PMO-S materials, the parents of both materials drawn together for comparison and plotted in black

This is clearly observed on the desorption branch of the isotherm of both materials, the curve is not sharp due to the partial blockage or the presence of bottlenecks causing delay of diffusion. This fact is also confirmed by the BJH pore size distribution which is given in Figure 45 (inset). This property is significant in M-PMO-S material (very broad pore size distribution indicates non-uniform pore diameter). This is also apparent in the pore size distribution that evidences the presence of secondary mesoporosity, with a relatively broad pore size distribution above 15 nm, which can be attributed to interparticle spaces. As it is shown in the BJH pore size distribution, the average pore size of both materials significantly increases as compared to their parent materials (PMO-L and PMO-S) (Table 8). Furthermore, M-PMO-L has relatively narrow pore size distribution when compared to the M-PMO-S material, i.e. M-PMO-L is relatively more ordered. To prove this both materials were characterized by TEM.

Figure 46 shows the TEM images of both M-PMO-L and M-PMO-S materials. Moderately ordered M-PMO-L material was obtained in the presence of P123 with TMB. However, the micelles become globular rather than cylindrical leading to a mesocellular foam type of material. In this case, the accessibility to the cages is given by the condensation of the silica source around the connecting globular micelles. In the end, the materials have limited accessibility.

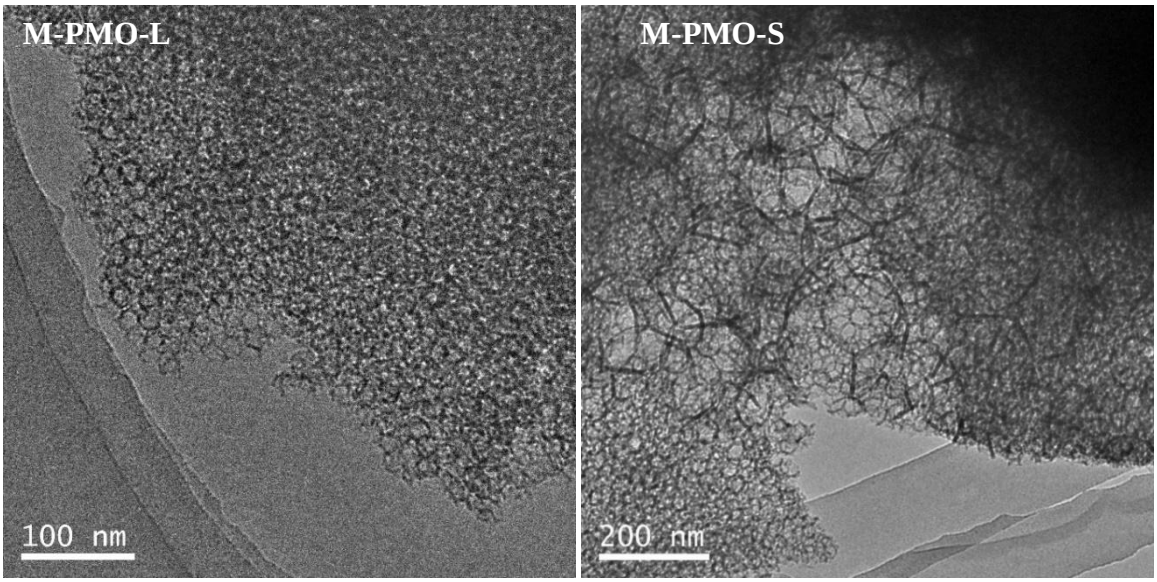

Figure 46. TEM images of large pore size M-PMO-L (left) and M-PMO-S (right) materials

The presence of more vesicles in the M-PMO-S material indicates a different growth mechanism in this case. In the TEM image of Figure 46 (right), it can be observed that in this case, the globular micelles are mixed with large vesicles leading to a highly disordered material with a broad pore size distribution. These vesicles were observed as well in the synthesis of SBA-15 with TMB, meaning that the aggregation of TMB with P104 is not as uniform as TMB with P123. However, the hydrophobic silica source in this case is somehow helping in the self assembling process with P123. This indicates that M-PMO-L material is more ordered and has better accessible pore mouths than M-PMO-S. This may be due to the presence of better hydrophobic interaction between the core of micelle in Pluronic P123 and the organosilica source 1, 2-bis (trimethoxysilyl) ethane (BTMSE) that helps 1, 3, 5-trimethylbenzene (TMB) to selectively interact to the core of the micelle. This causes pore expansion while slightly maintaining the structure of the material. However, there is no observable channel in both materials because they are less ordered. To improve the degree of ordering of both types of materials we used relatively large size and more

hydrophobic 1, 3, 5-triisopropylbenzene (TIPB) as micelle expander instead of TMB. These materials are labeled as E-PMO-L and E-PMO-S as shown in Figure 39.

Large pore size materials E-PMO-L and E-PMO-S were synthesized and characterized by using the above mentioned characterization techniques. As shown in Figure 44, the presence of one strong peak (100) and two less resolved peaks (110) and (200) of E-PMO-L and E-PMO-S indicates that both materials have moderately ordered hexagonal symmetry arrangement of pores. The main peaks in both materials are shifted towards the lower 2θ which indicates that the unit cell dimension is increased due to the effect of the pore expanders in pore diameter or pore wall thickness. Both materials, E-PMO-L and E-PMO-S, were characterized by TGA to prove the removal of the surfactants followed by N_2 adsorption/desorption isotherm for pore diameter change.

TGA profiles for both E-PMO-L and E-PMO-S materials are shown in Figure 47 (A and B). Here also, we tried to selectively remove the surfactants from the final material by using solvent extraction method with acidified ethanol solution and calcination at 350 ^{o}C for 5 h. As we can see from the TGA curve, there is no significant weight loss difference between the ethanol extracted and the as synthesized materials of both types (E-PMO-L and E-PMO-S). This indicates that ethanol extraction does not effectively remove the surfactants.

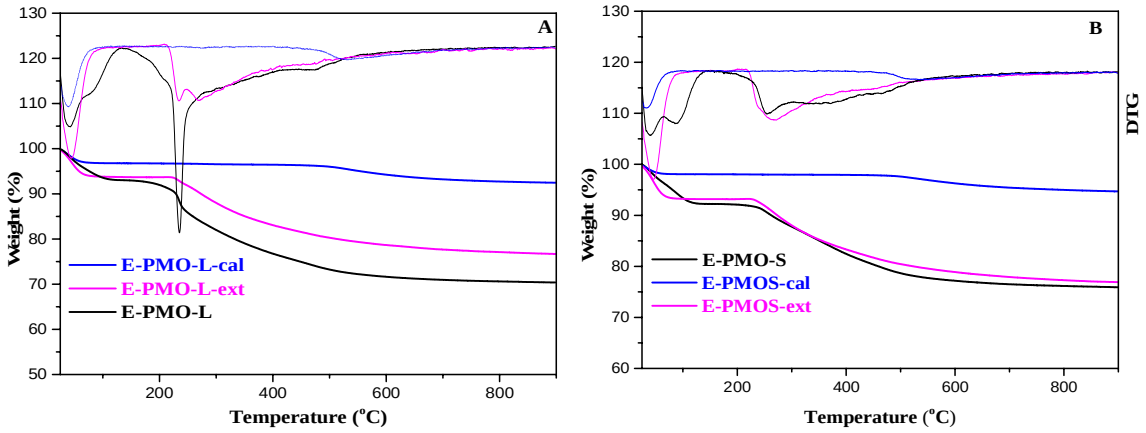

Figure 47. TGA profiles of (A) as synthesized E-PMO-L, surfactant extracted E-PMO-L (E-PMO-L-ext) and calcined E-PMO-L (E-PMO-L-cal); and (B) as synthesized E-PMO-S, surfactant extracted E-PMO-S (E-PMO-S-ext) and calcined E-PMO-S (E-PMO-S-cal) materials

Table 7. The weight loss in different temperature ranges for large pore size PMO materials

Catalyst	Weight loss (%) in different temperature ranges			
	< 150 °C	150 – 425 °C	425 – 700 °C	>700 °C
E-PMO-L	7.04	17.14	4.87	0.55
E-PMO-L-ext	6.30	11.43	4.61	0.93
E-PMO-L-cal	3.23	0.37	3.19	0.71
E-PMO-S	6.83	11.82	4.86	0.54
E-PMO-S-ext	6.33	10.68	4.58	0.94
E-PMO-S-cal	1.95	0.15	2.48	0.67

As shown in Figure 47 (A and B) and Table 7 there is a small weight loss at temperature below 150 °C for all samples. The weight losses of the as made and ethanol extracted samples are relatively higher than the calcined one, because these weight losses are due to

the removal of physically adsorbed water and ethanol residues that remained in the washing step. The weight losses in the temperature range of 150 – 425 ^{o}C for all samples are due to the removal of the surfactant. Although ethanol removes some part of the surfactants, more than half of it remains with the material. However, the weight loss of the calcined samples in this temperature range is very small, because all the surfactants are removed during calcination. Equivalent weight losses in the temperature range of 425 – 700 ^{o}C for all samples, is due to the removal of the framework ethane (-CH_2CH_2-) group. This indicates that the material didn't lose its framework ethane group during the calcination step. The very small weight loss above 700 ^{o}C for all samples may be due to the dehydroxylation of surface hydroxyl groups.

In conclusion, calcination at 350 ^{o}C for 5 h is effectively removing the surfactant in the final material of both types without affecting the framework ethane group. The ethane organic contents in the synthesized PMO materials are below the expected ones if every Si atom in the framework would be linked to one ethane group. This may be due to a fraction of the bis-silylated compound is hydrolyzed in the synthesis medium by breaking C-Si bonds. According to these TGA values, the actual organic content of the framework is really small, and most of it should be formed by SiO_4 units. We also suggest that the given temperature ranges are to show simply the main weight loss contributor i.e. there may be the possibility for the loss of a mixture of different species. Therefore, such type of samples should be characterized by other more accurate techniques to determine the exact carbon content of the samples to know the exact ethane content. It can also be noticed that the hydroxyl content of the PMO materials (weight loss > 700 ^{o}C) and the amount of adsorbed water are much larger than those of calcined SBA-15 materials. However, from these

results we couldn't compare the surface hydrophilicity of the materials, because these materials were synthesized at different time and the calcined materials were stored at room temperature before characterizing by TGA. The water content adsorbed on the surface of the material may also affected by the moisture content of the environment. Therefore, the water content don't necessarily depend on the concentration of surface hydroxyl groups, it also depend on the moisture content of the environment. The SBA-15 materials were calcined at higher temperature (550 ^{o}C) than PMO materials (350 ^{o}C). Thus, it is difficult to compare the concentration of the surface hydroxyl groups in two groups of materials and to conclude the decrement of surface hydroxyl groups due to the effect of $–CH_2CH_2–$ group in PMO. Furthermore, dehydroxylation of surface hydroxyl groups could be takes place above 350 ^{o}C, therefore, we couldn't compare the concentration of surface hydroxyl groups by comparing only the weight loss value given above 700 ^{o}C (these weight loss may not necessarily from only surface hydroxyl groups, could be a mixture of different species).

Figure 48 shows N_2 adsorption–desorption isotherms and the corresponding pore size distributions (inset) calculated by the BJH method for the calcined E-PMO-L and E-PMO-S materials. The isotherm and pore size of parent materials PMO-L and PMO-S are also included for comparison purpose. The isotherms of both types (E-PMO-L and E-PMO-S) are a type IV isotherm due to their mesoporosity and the shape of their hysteresis loop is different from one another due to the difference of their pore size uniformity. The typical isotherm which is obtained in E-PMO-L sample is type IV isotherm with H1 type hysteresis loop indicating uniform pore size distribution. However, the desorption branch of the isotherm exhibits clearly two distinctive steps due to the partial blockage of some

mesopores as it is also confirmed from TEM image discussed below (Figure 49). The hysteresis loops of E-PMO-S material looks like H2 type which is mesoporous materials with non-uniform pore size distribution. This is clearly observed on the desorption branch of the isotherm, the curve is not sharp enough. This may be due to the presence of bottlenecks causing delays the diffusion of reagents. This fact is also confirmed by the BJH pore size distribution.

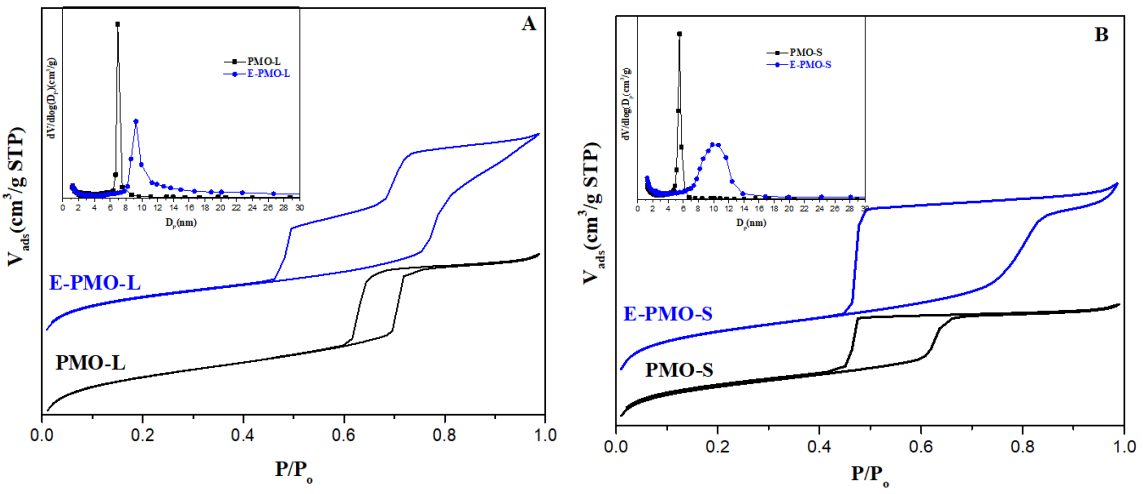

Figure 48. N_2 adsorption-desorption isotherms and BJH pore size distributions (inset) for (A) E-PMO-L and (B) E-PMO-S materials. Parent materials plotted in black for comparison purpose

In the case of samples synthesized with expanders, the nitrogen isotherm shows that, besides the main steep nitrogen uptake at a relative pressure around 0.8, corresponding to the regular mesopore channels, an additional increase of nitrogen adsorption occurs at relative pressures above 0.9. This is also apparent in the pore size distribution that evidences the presence of secondary mesoporosity, with a relatively broad pore size distribution above 15 nm, which can be attributed to interparticle spaces. The average pore diameter of the channels estimated by the BJH method is also reported in Table 8, showing

that the pore size of both E-PMO-L and E-PMO-S increases significantly when compared to their parent materials (PMO-L and PMO-S). Both materials were characterized by TEM to evaluate the degree of ordering, i.e. the arrangement of channels and accessibility of pore mouths.

Table 8. Structural parameters of organosilica (PMO) materials

Sample	d_{100} (nm)	ao (nm)	S_{BET} (m^2g^{-1})	V (cm^3g^{-1})	V_m (cm^3g^{-1})	d_{BJH} (nm)	t (nm)
PMO-L	10.0	11.6	863	0.96	0.12	7.3	4.3
M-PMO-L	16.3	18.8	969	1.6	0.03	14.3	3.7
E-PMO-L	12.1	14	780	1.1	0.11	10	4.0
PMO-S	10.0	11.6	611	0.57	0.11	5.7	5.9
M-PMO-S	-	-	754	0.95	0.15	16	-
E-PMO-S	13.7	15.9	759	0.86	0.15	11	4.9

The unit cell parameter, ao, was determined from the interplanar spacings of the (100) planes using the formula of $a0 = 2d_{100}/\sqrt{3}$, in which $d_{100} = 1.5406/2\sin\theta$ where θ is the scanning diffraction angle corresponding to peak (100). The pore size, d_{BJH}, was obtained from the maxima of the pore size distribution curve calculated by the Barrett-Joyner-Halenda (BJH) algorithm using adsorption branch. Pore wall thickness, t, was assessed by subtracting d_{BJH} from a. The BET surface area, S_{BET}, was calculated using adsorption data in a relatively pressure range $P/p_0 = 0.05$-0.24. The total pore volumes, V, and micropore volume, V_m, were estimated from the adsorbed amounts at a relative pressure of about 0.99.

TEM images of both materials (E-PMO-L and E-PMO-S) are shown in Figure 49, the alignment of channels for E-PMO-L material is observed. However, there is partial blockage of pores due to the formation of some vesicles which was previously observed by the desorption curve of N_2 isotherm (Figure 48 (A)). This result proved that E-PMO-L is ordered, we have successfully increased the pore size, but the presence of some vesicles may hinder its potential applicability in catalysis. On the other hand, the accessibility of pore mouths for E-PMO-S material was observed, but there is no observable channel

alignment in this material, indicating that E-PMO-S is a moderately ordered material. Nevertheless, the pore size seems to be homogeneous in the size of 11 nm, indicating that TIPB seems the better pore expander whether with P123 or P104 surfactants

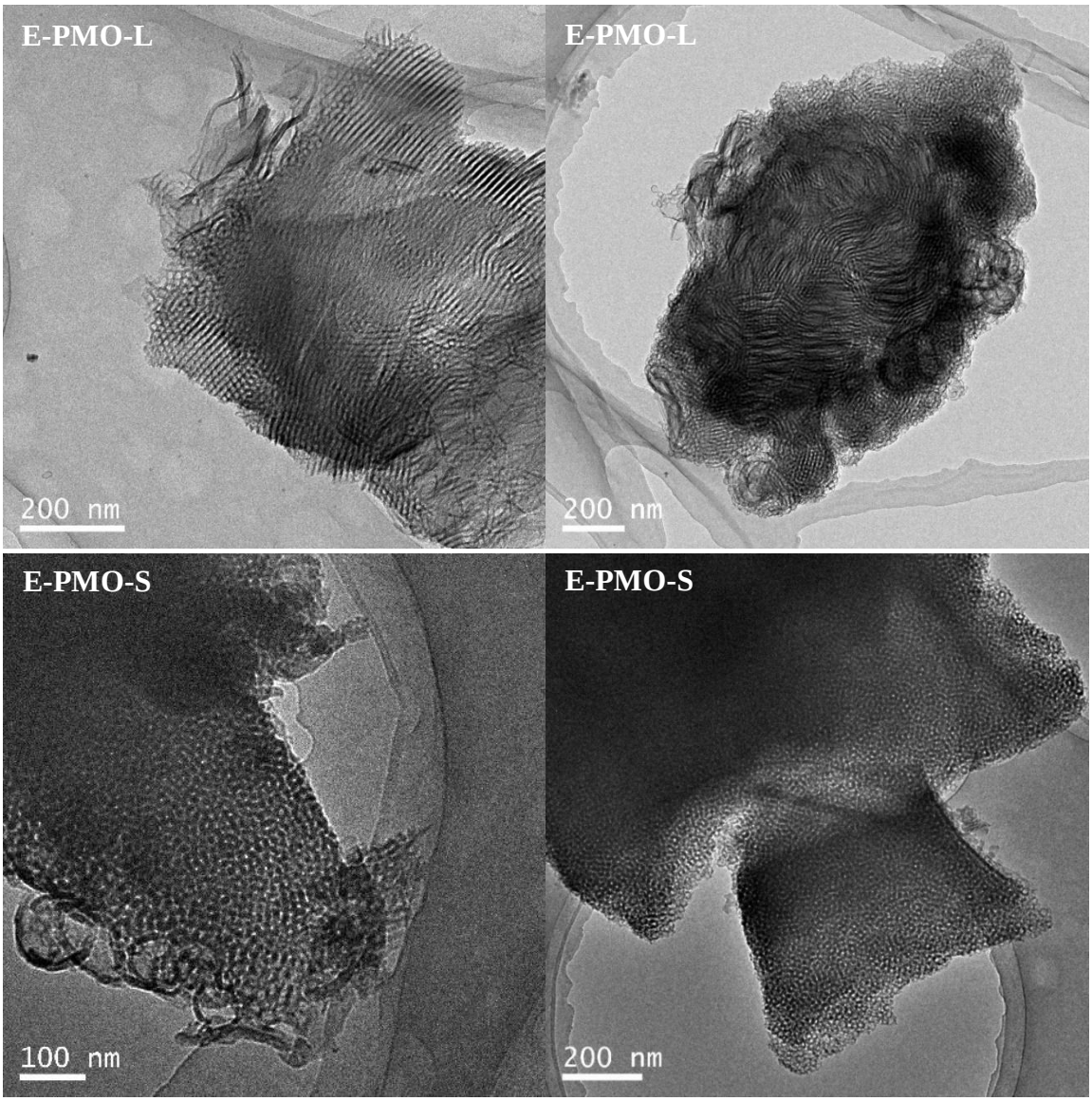

Figure 49. TEM images of large pore size E-PMO-L and E-PMO-S materials

Finally, both materials were characterized by SEM to evaluate their particle morphology. The particle morphology of E-PMO-L and E-PMO-S materials are given in Figure 50 which were synthesized in the presence of TIPB micelle expander. The particle

morphology of these materials is different from their corresponding parent materials, which produces materials with bean-shaped small particles. The presence of expander has led to the loss of the conventional fiber-like and plate-like particle morphology, commonly observed in ordered mesoporous materials. Beyond expanding of the pore size, TIPB also affects the particle morphology of the materials. This may be due to the presence of some droplets of TIPB in the synthesis solution limiting particle growth.

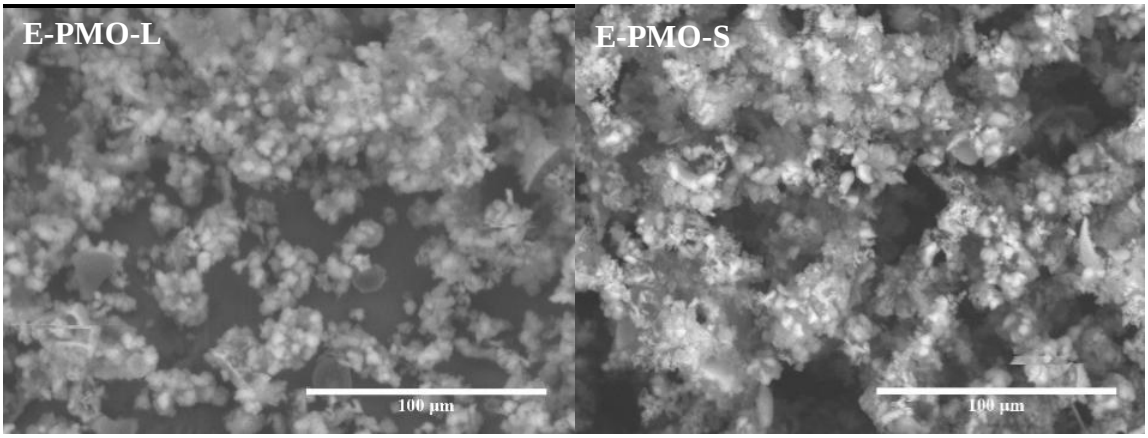

Figure 50. SEM images of E-PMO-L and E-PMO-S materials

Summary

- ✓ SBA-15 material with high degree of ordering, average pore diameter of 7.2 nm and accessible pore mouths with channel length around 400 nm was synthesized by using P104 surfactant (SBA-S).
- ✓ SBA-15 material with high degree of ordering, large pore diameter (12 nm), and accessible pore mouths with channel length of 850 nm was synthesized by using P123 surfactant and TIPB micelle expander at 15 ^{o}C gelling temperature (E-SBA-L-15).

- ✓ PMO material with high degree of ordering, average pore diameter of 5.7 nm, very thick pore wall, accessible pore mouths and platelets particle morphology was synthesized by using P104 surfactant (PMO-S).
- ✓ PMO material with moderately ordered large pore diameter (10 nm) and accessible pore mouths and channel alignment with hydrophobic surface was synthesized by using P123 surfactant, TIPB micelle expander at 15 ^{o}C gelling temperature (E-PMO-L).

In general, Pluronic P123 is an optimum surfactant to synthesize materials of both types (SBA-15 and PMO) with large pore diameter (> 8 nm) and Pluronic P104 is an optimum surfactant to synthesize particles with platelets morphology and short channel length.

4.2.Ti grafted OMMs

Ordered mesoporous materials (OMMs) should be functionalized with active functional groups to catalyze different chemical reactions. Incorporation of transition metals in the framework/channel of ordered mesoporous materials is a commonly known method to improve its surface acidity and catalytic activity. The necessity of Ti incorporation comes from the objective of the thesis, aiming to make derivatives of vernonia oil to increase their market value. Epoxidation of the double bond of vernonia oil will require Ti-based catalysts, which are environmentally friendly and economically feasible materials. We want to epoxidize bulky vernonia oil molecule to increase its reactivity towards the synthesis of polymers and value-added products. Its large molecular weight and hydrophobicity motivated us to optimize for the synthesis of large pore size, short diffusion pathlength and hydrophobic surface Ti-containing ordered mesoporous materials. Ti was

incorporated in the channel/framework of the SBA-15 and PMO materials by grafting and co-condensation methods. The optimum materials among the synthesized silica supports (Chapter 4.1) were selected for Ti grafting to incorporate the Ti active sites on the pore wall surface, in order to improve its accessibility towards the reactants. To improve the dispersion of the active sites titanocene dichloride (Cl_2TiCp_2) was chosen among other Ti-sources, because of its availability and the presence of the Cp group prevents the agglomeration of TiO_2 species. The grafting process requires inert conditions to create a favorable condition for the reaction between the calcined mesoporous material and the Cl_2TiCp_2 material, dissolved in toluene and the grafting process was carried out under inert condition[122]. The final material was calcined at 350 ^oC for 5 h to promote further condensation of Ti species which was found in different systems.

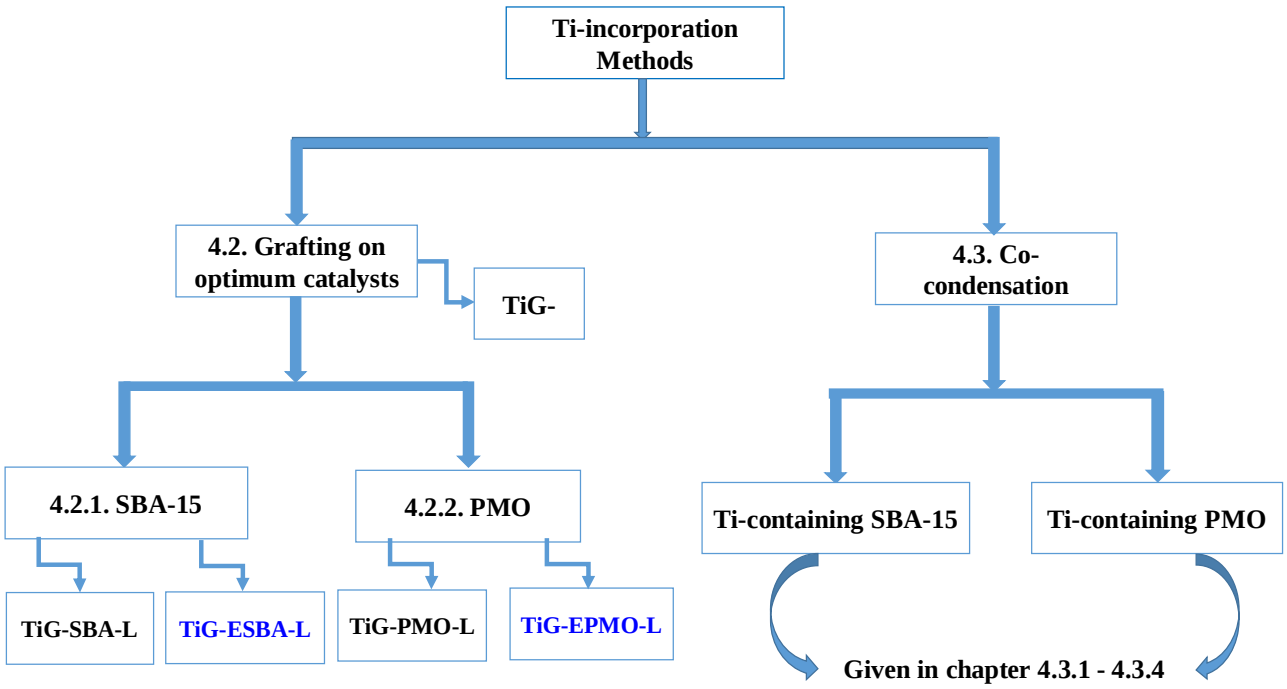

Figure 51. Scheme with Ti-incorporation methods and samples labeling

4.2.1. Ti-grafted SBA-15 materials

Two Ti-grafted SBA-15 materials with different pore diameters were prepared. Hexagonally arranged pure silica SBA-15 materials with fiber-like particles morphology, synthesized without and with micelle expander (SBA-L and E-SBA-L, respectively), were grafted with Cl_2TiCp_2 species and calcined at 350 °C yielding TiG-SBA-L and TiG-ESBA-L samples, with pore diameters of 8.4 nm and 10.5 nm, respectively. The chemical, structural and textural properties of both materials are included in Table 5. As can be observed in the XRD profiles shown in Figure 52 (A), the symmetry and arrangement of pores was not affected by the grafting procedure (the value of the unit cell dimension (a_0) was retained). All the grafted materials have high Ti content (Table 9) with no significant presence of anatase phase according to XRD analysis (Figure 52 (A, inset)). The pore diameter, surface area and pore volume have decreased in all cases from the starting material before grafting yet the isotherms remain those of typical ordered mesoporous materials (Figure 52(B)). The UV-vis spectra of non-calcined Ti-grafted materials show a very broad band from 210 – 400 nm due to presence of Cp groups and Ti-species in different systems. Thus, the electronic transition from Cp or O^{2-} to Ti (IV) ion, which is found in different systems, give very broad absorption band. However, the UV–vis spectra of calcined materials show a band at around 210 nm that extends to 230 nm owing to the presence of isolated Ti(IV) T_d species at 4-coordination stages indicating that the grafting method produces one type of Ti species population (T_d Ti(IV) species) (Figure 52 (C)). A single peak at 210 nm, which can be taken as a clear indication of isolated Ti(IV) in tetrahedrally coordinated sites. The slight shift in band position and the increase in bandwidth point to a distorted tetrahedral environment of the titanium[130]. This indicates

calcination is very important to promote the condensation of Ti-species to produce T_d Ti (IV) active sites. However, in this grafted samples, the Ti active sites might be mainly anchored to the surface of the particles and to the pore openings of the channels instead of incorporated to the channel walls.

Figure 52 (D) shows the TGA profiles of the Ti-grafted SBA-15 materials (TiG-SBA-L and TiG-ESBA-L) before and after calcination. The TGA of the parent materials (calcined pure silica SBA-L and E-SBA-L) drawn together for comparison purposes. The weight losses in the temperature range of 150– 580 ^{o}C for samples TiG-SBA-L (9.14 %) and TiG-ESBA-L (10.06 %) is due to the removal of Cp groups which may incorporate on the surface of the material with Ti species. However, the weight losses in this temperature range of the calcined samples is very low, due to the removal of Cp groups during calcination. The weight losses in the temperature range of 150 – 580 ^{o}C for the calcined samples TiG-SBA-L-cal (1.81 %) and TiG-ESBA-L-cal (1.82 %) this may be due to the dehydroxylation of surface hydroxyl groups. The weight losses above 150 ^{o}C for all calcined materials (parent and Ti-grafted materials) are very low and comparable. This confirms that Cp groups are removed during calcination and this weight loss is due to dehydroxylation of surface hydroxyl groups.

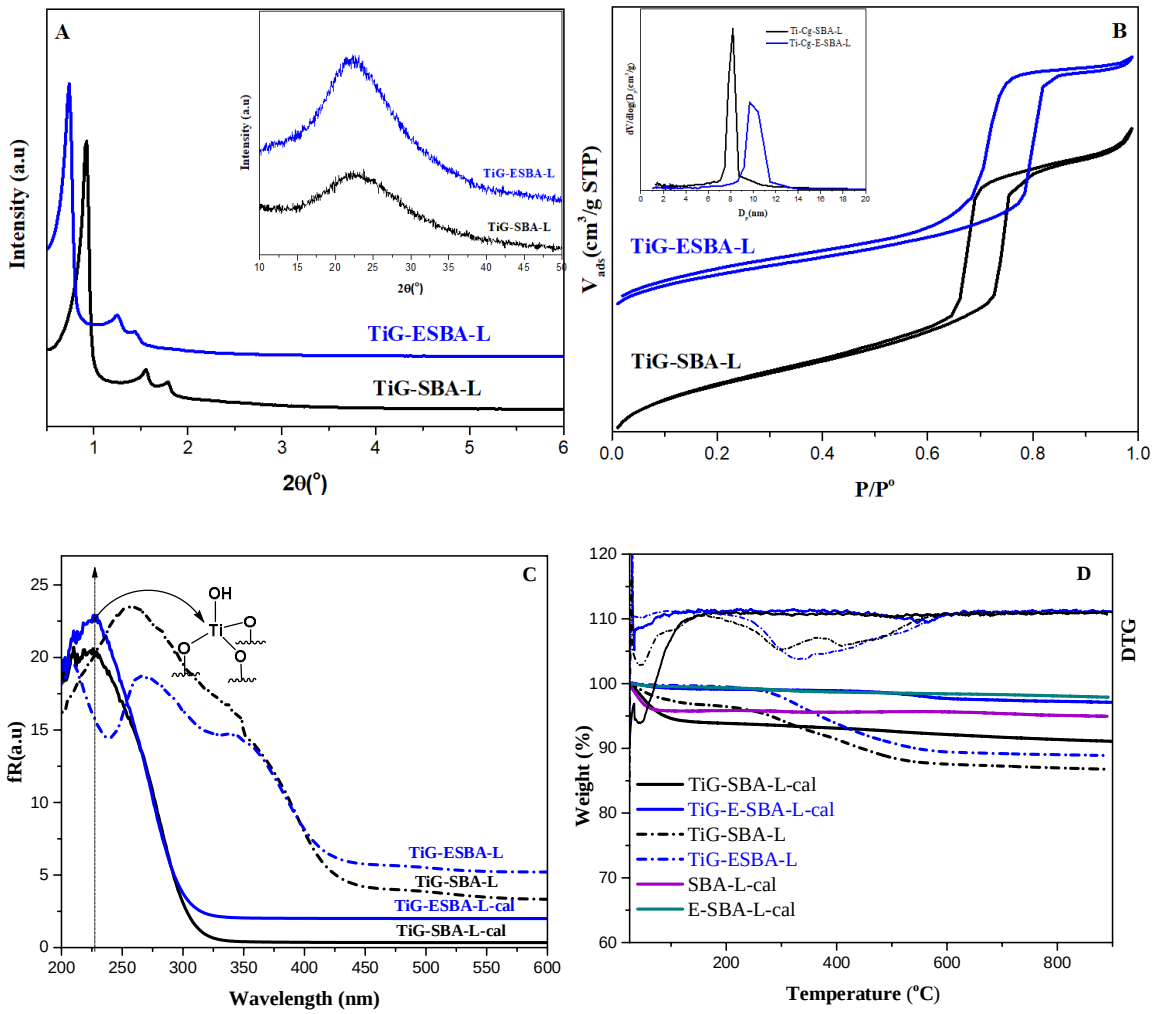

Figure 52. Characterization of Ti-containing SBA-15 samples prepared by grafting of Cl_2TiCp_2. (A) Low angle XRD and high angle XRD (inset), (B) N_2 adsorption-desorption isotherms, (C) UV-vis and (D) TGA plots

Table 9. Structural, chemical and textural properties of the Ti-grafted SBA-15 materials

Catalyst	a_0 (nm)	Pore size (nm)	Pore wall (nm)	Ti (wt %)	Vp (cm^3/g)	S_{BET} (m^2g^{-1})
TiG-SBA-L	11.0	8.4	2.6	4.65	0.98	630
TiG-ESBA-L	13.7	10.5	3.2	3.31	0.75	368

The catalytic performance of both Ti-grafted materials was tested in the epoxidation of cyclohexene to evaluate the activity and potential location of the active sites. The catalytic setup of epoxidation of cyclohexene and the results produced by using Ti-grafted catalysts explained in detail in Chapter 3.12 and chapter 5.1, respectively.

4.2.2. Ti-grafted PMO materials

Another two calcined ethane (-CH_2-CH_2-) bridged PMO materials which have relatively good structural and textural properties were selected for further grafting with titanocene dichloride in order to incorporate Ti active sites on the surface of the material. As compared with pure silica SBA-15 materials, PMO materials have lower number of surface hydroxyl groups which are far apart from each other. Therefore, organically modified PMO with long pore channels (fiber type of particles), synthesized without and with micelle swelling agent (PMO-L and E-PMO-L, respectively) were also grafted obtaining TiG-PMO-L and TiG-EPMO-L materials with pore diameter 7.5 & 10 nm, respectively. As shown in Figure 53 (A) the PMO materials retain their structure after grafting with Cl_2TiCp_2 and calcined at 350 ^oC since the value of unit cell dimension (a_0) was preserved. This indicates the post grafting process as well as the calcination process didn't affect the pore arrangement of the parent materials. Like the pure silica SBA-15 materials, (Figure 53 (A, inset), large angle XRD confirm that there is no formation of anatase clusters on the final material after grafting with Cl_2TiCp_2. As it is shown in Figure 53 (B) the shape of the isotherm is the same as the parent material. The grafting process doesn't affect the textural properties of the material. The UV–vis spectra (Figure 53 (C)) of non-calcined Ti-grafted PMO materials show very broad band from 210 – 400 nm due to the electronic transition from Cp or O^{2-} to Ti (IV) ion, which is found in different environment. However, after calcination there is

an absorption band between 210 – 230 nm due to the presence isolated T_d Ti (IV) species. TiG-PMO-L sample show a band at around 210 nm that extends to 230 nm owing to the presence of isolated Ti (IV) T_d species at 4-coordination stages indicating that the grafting produces uniform type of Ti species. However, TG-EPMO-L show that two absorption peaks at 210 and 260 nm due to presence of T_d and octahedral/ non isolated Ti-O-Ti species respectively. The sharp absorption peak at 210 nm indicates the presence of highly dispersed T_d Ti (IV) species due to the large pore size of this material is taking as an advantage of the parent material. However, the presence of some vesicles in the parent material may hinder the diffusion of reagents as a result there is a formation some saturated octahedral Ti (IV) species or it is a sign of the presence of Ti-O-Ti bonds, i.e., not all the Ti species would be isolated from each other (weak absorption peak at 260 nm). In general, there is also incorporation of high amount of Ti (IV) species on the pore surface of the PMO materials without anatase formation (Table 10). Figure 53 (D) shows the TGA profile of the Ti-grafted PMO materials (TiG-PMO-L and TiG-EPMO-L) before and after calcination. The weight losses in the temperature range of 150 – 480 ^oC for samples TiG-PMO-L (11.52 %) and TiG-EPMO-L (11.58 %) is due to the removal of Cp groups and may be part of surfactants that remained after the extraction step. The weight losses in this temperature range are very low for calcined materials TiG-PMO-L-cal (2.29 %) and TiG-EPMO-L-cal (2.28 %) this probably due to the dehydroxylation of surface hydroxyl groups. The weight losses in the temperature range of 480 – 750 ^oC for samples TiG-PMO-L (7.42 %), TiG-EPMO-L (6.45 %), TiG-PMO-L-cal (6.28 %) and TiG-EPMO-L-cal (6.30 %) is due to the removal of framework ethane ($-CH_2CH_2-$) groups. This result indicates,

calcination promote condensation of Ti species by removing Cp groups without affecting the framework ethane groups.

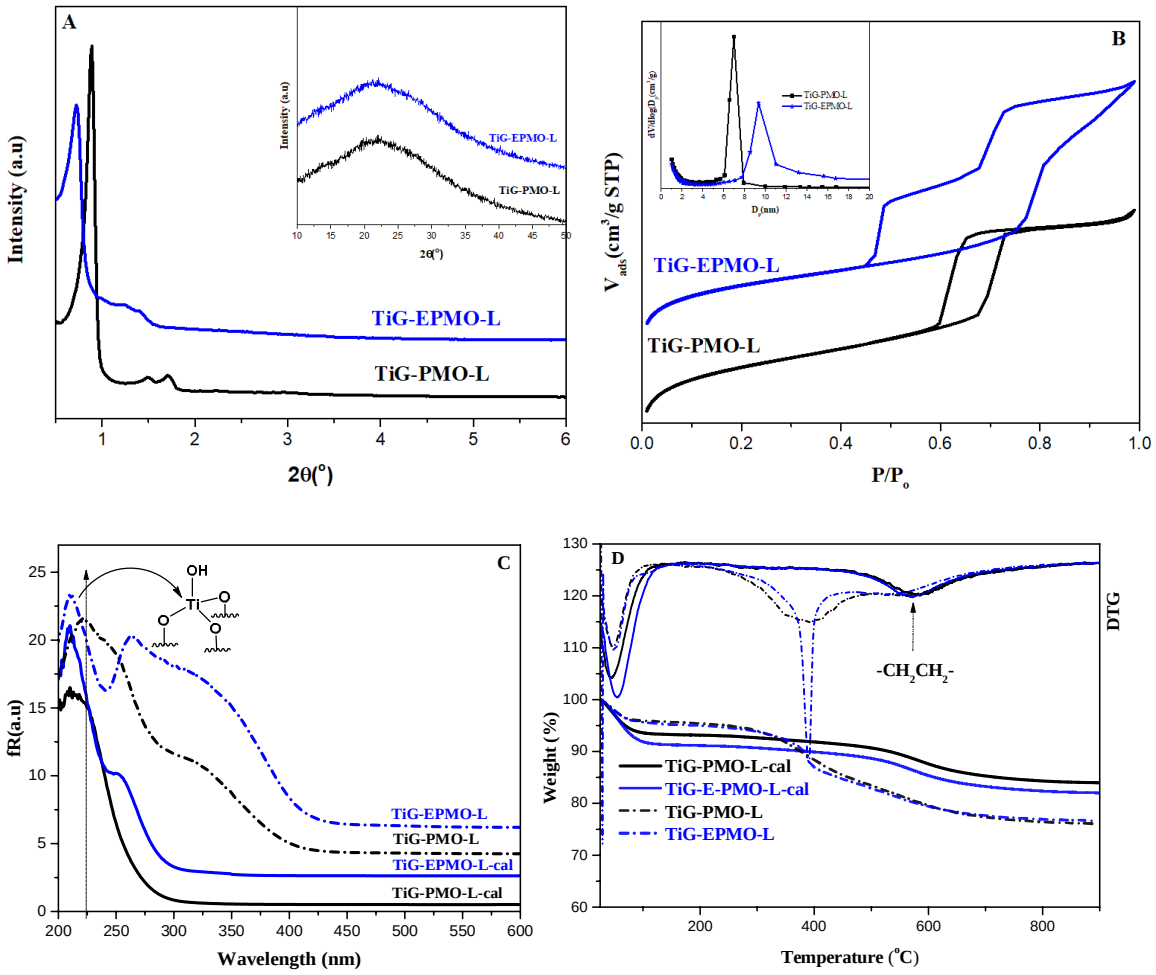

Figure 53. Characterization of Ti-containing PMO materials prepared by grafting of Cl_2TiCp_2. (A) Low angle XRD and high angle XRD (inset), (B) N_2 adsorption-desorption isotherms, (C) UV-vis and (D) TGA plot

Table 10. Structural, chemical and textural properties of the Ti-grafted PMO materials

Catalyst	a_0 (nm)	Pore size (nm)	Pore wall (nm)	Ti (wt %)	Vp (cm^3/g)	S_{BET} (m^2g^{-1})
TiG-PMO-L	11.4	7.5	3.9	1.87	1.01	944
TiG-EPMO-L	14	10	4.2	2.46	1.13	803

The catalytic performance of both materials was tested in the epoxidation of cyclohexene. The catalytic setup of epoxidation reaction and the results obtained by using these catalysts explained in detail in chapter 3.12 and chapter 5.1, respectively.

Summary

Grafting is a good method for incorporation of high amount of T_d Ti (IV) species on the surface of SBA-15 and PMO materials. The structural properties and pore arrangement of the parent materials were not affected by the grafting process, only a slight decrease in the pore diameter, the surface area and the pore volume of the parent materials, due to the presence of functional groups grafted in the process.

4.3. Titanium incorporated into OMMs by co-condensation

The main objective of this chapter is to report the results on the optimized Ti-containing SBA-15 and PMO materials prepared by co-condensation, in one step, to incorporate the Ti-active sites in the framework of the material and to improve its stability. The main characteristics required in the final material of such type will be, good hexagonal structure with a narrow pore size distribution, good accessibility of the pore mouths and active sites, short diffusion path lengths, hydrophobic surface and if possible large pore size (> 8 nm)

while maintaining Ti active species on the pore surface. As it is shown in Figure 54, to obtain an optimum catalyst, initially titanium (IV) isopropoxide was used as a Ti source by following the conventional synthesis of Ti-SBA-15 adapted in mild acidic condition[23, 53] by using both types of non-ionic surfactants (Pluronic P123 and P104). Ti-incorporation and pore expansion has been carried out *in situ* by using Ti (IV) isopropoxide as a titanium source and TIPB as a pore expander for better diffusion of bulky vernonia oil molecule. Additionally, Ti-containing SBA-15 materials were synthesized by using titanocene dichloride as a titanium source by maintaining other synthesis conditions. The maximum Ti-loading on the pore surface was investigated by varying the content of Ti in the synthesis gel. Finally, Ti-containing PMO materials with hydrophobic pore surface were synthesized for better adsorption of vernonia oil next to the active sites and diffusion after the reaction. The results corresponding to Ti-containing PMO materials by using Ti (IV) isopropoxide and titanocene dichloride as a titanium source will be discussed in chapter 4.3.3 and 4.3.4 (Figure 78). The Ti-containing materials of both types which show promising characterization results were selected for catalytic tests for epoxidation of cyclohexene to test the activity of the Ti-active sites. The catalytic setup and the results obtained by using these catalysts explained in detail in chapter 3.12 and chapter 5.1, respectively.

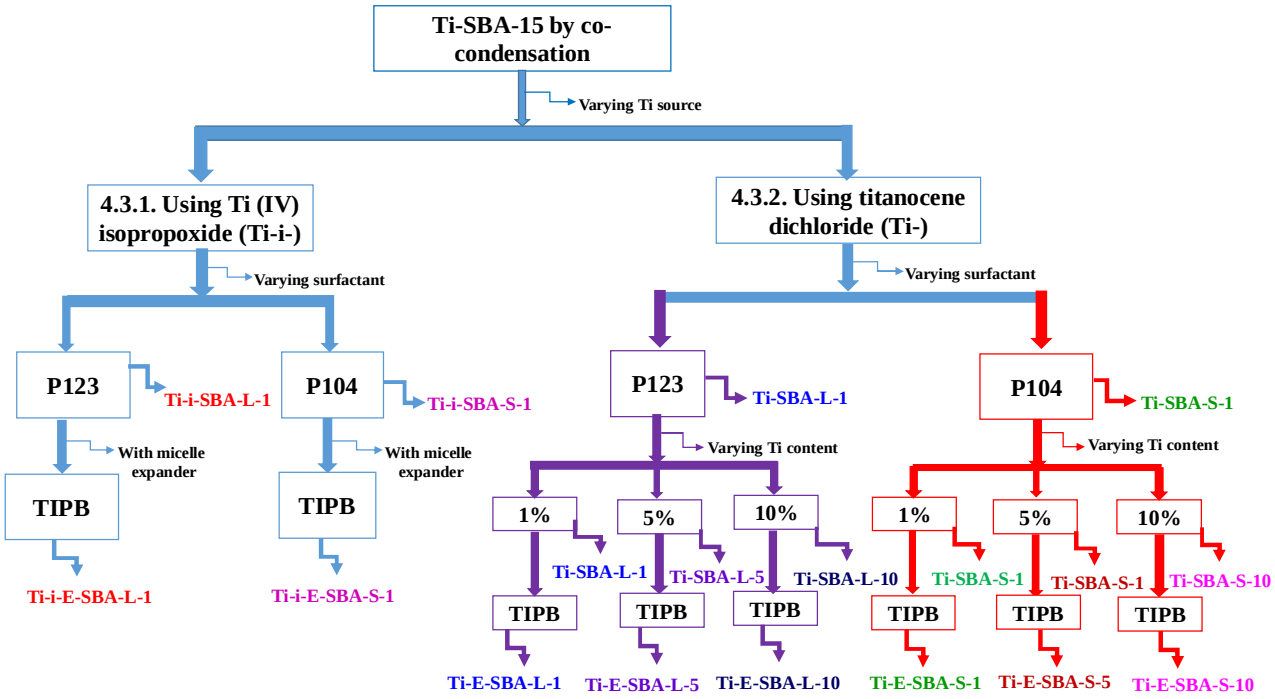

Figure 54. Scheme of labeling of Ti-containing SBA-15 materials synthesized by co-condensation method

4.3.1. Characterization results and discussion on Ti-incorporated SBA-15 materials by using Ti (IV) isopropoxide

The functionalization of SBA-15 type of materials with Ti (IV) species through co-condensation methods has involved several lines of investigations. In this sense, starting from the synthesis method previously described in the literature[53] as a starting material, this was modified for the incorporation of different amount of Ti(IV) active sites, controlling the particle morphology and pore size of the final material. Therefore, the influence of the Ti source precursor, Ti/Si ratio of the synthesis gel and the nature of surfactants used were studied. The synthesized Ti-SBA-15 materials obtained were characterized by X-ray diffraction, N_2 adsorption-desorption, and DRS UV-vis techniques.

Ti-containing SBA-15 materials, Ti-i-SBA-L-1 and Ti-i-SBA-S-1, were prepared by using surfactants Pluronic P123 and P104, respectively. These materials were prepared using Ti/Si ratio of the synthesis gel is 0.01.

Figure 55 (A) shows the X-ray diffraction patterns achieved for the Ti-i-SBA-L-1 and Ti-i-SBA-S-1 materials. In Ti-i-SBA-L-1, all the three XRD peaks (100), (110) and (200) are detected and well resolved. This indicates that the materials show diffraction patterns typical of a mesoscopic *P6mm* structure formed by the hexagonal array of mesopores. However, the two weak XRD peaks (110) and (200) for Ti-i-SBA-S-1 material disappear, indicating that the pore structure of the material is less ordered. This indicates that P123 is better to maintain the pore structure of the SBA-15 during Ti-incorporation, probably due to its more hydrophobic micelle assisting to maintain the structure.

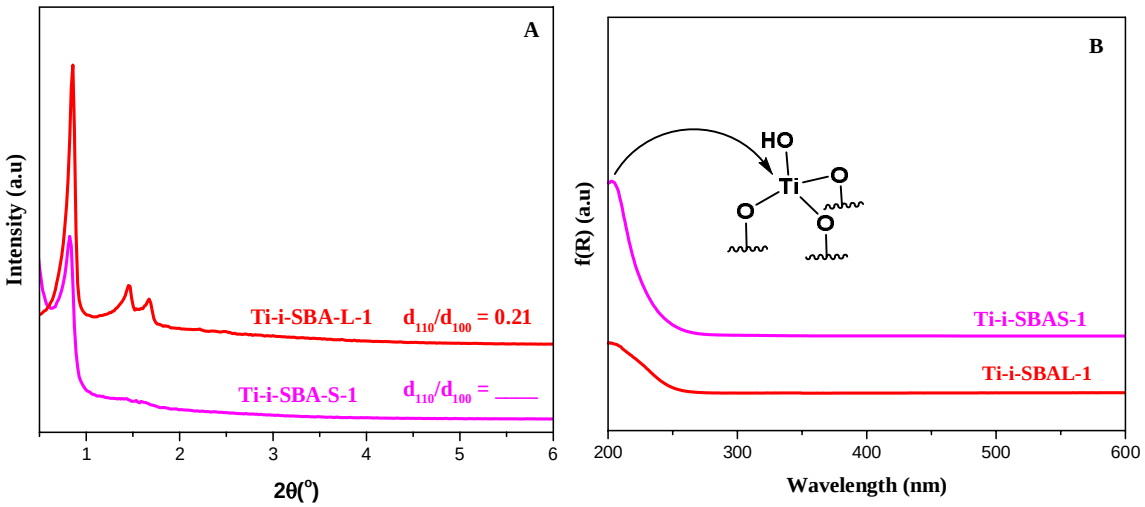

Figure 55. Low angle XRD patterns (A) and DR UV-vis spectra (B) for Ti-i-SBA-L-1 and Ti-i-SBA-S-1 materials

As it is shown in Figure 55 (B) there is a UV-vis band between 200 – 220 nm in both types of materials, due to the electronic transitions occurring in isolated tetrahedrally coordinated

Ti species bonded to oxygen atoms (ligand to metal charge transfer (LMCT)). However, the band for Ti-i-SBA-L1 is broad, probably due to the aggregation of Ti-species during the synthesis of the material. Both spectra show weak absorption intensities in the given wavelength range. This may be due to the presence of small amount Ti (IV) species in the material. Both materials have also been characterized by N_2 adsorption/desorption measurements (Figure 56).

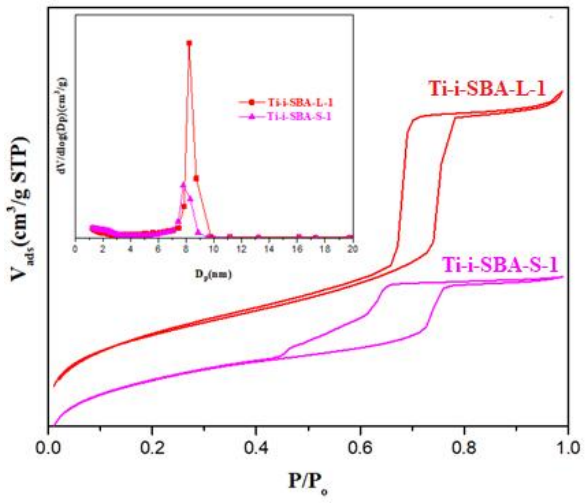

Figure 56. N_2 adsorption-desorption isotherm and BJH pore size distribution (inset) of Ti-i- SBA- L-1 and Ti-i-SBA-S-1 materials

The N_2 adsorption-desorption isotherms of both materials display type IV isotherms, which is the characteristic of ordered mesoporous materials. Ti-i-SBA-L-1 has H1 type hysteresis loops indicating mesoporous materials with homogenous cylindrical pore size distributions. However, Ti-i-SBA-S-1 has H5 type isotherm in which the desorption branch of the isotherm exhibits two distinctive steps due to the presence of both open and partially blocked mesopores. The BJH plots (Figure 56 (inset)) show the very narrow pore size distributions in the Ti-i-SBA-L-1 sample supporting this fact. In general, Ti-i-SBA-L-1

have more uniform pore size distribution, better textural properties (higher surface area, pore volume and pore diameter) than Ti-i-SBA-S-1 materials (Table 11). This is because Ti-i-SBA-L-1 has an ordered hexagonal array pore arrangements as we have discussed in the XRD result.

Expansion of the pore size of materials of both types by using the same titanium source (Ti (IV) isopropoxide), and 1, 3, 5- triisopropylbenzene (TIPB) as the micelle expanders has been carried out.

As it shown in Figure 57 (A), the presence of three well resolved XRD peaks for Ti-i-E-SBA-L-1 sample indicates the hexagonal pore structure of the material is maintained during this synthesis conditions. However, the disappearance of all XRD peaks of Ti-i-E-SBA-S-1 sample, indicates that this material loses its hexagonal pore structure. This may be due to the fast hydrolysis of Ti (IV) isopropoxide disturbs the micelle formation when using P104 surfactant which have relatively larger hydrophilic/hydrophobic block ratio. The DRS UV-vis measurements (Figure 57 (B) show that there are very weak absorption bands observed in both samples between 200 – 220 nm indicating a very small amount of Ti is incorporated in the framework/channel of the material.

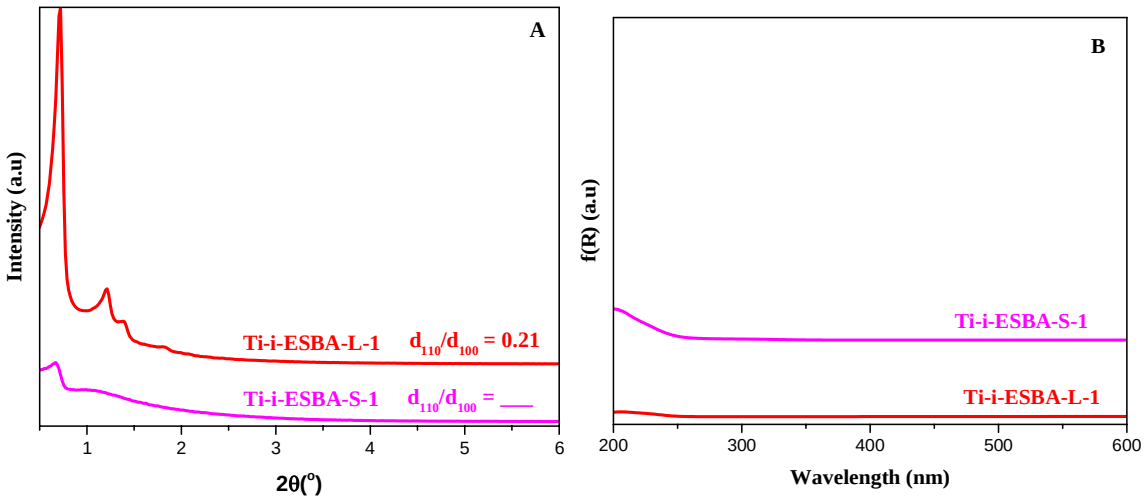

Figure 57. Low angle XRD patterns (A) and DR UV-vis spectra (B) for Ti-i-E-SBA-L-1 and Ti-i-E-SBA-S-1 materials

The textural properties of both materials Ti-i-E-SBA-L-1 and Ti-i-E-SBA-S-1 have been characterized by N_2 adsorption/desorption measurements as shown in Figure 58.

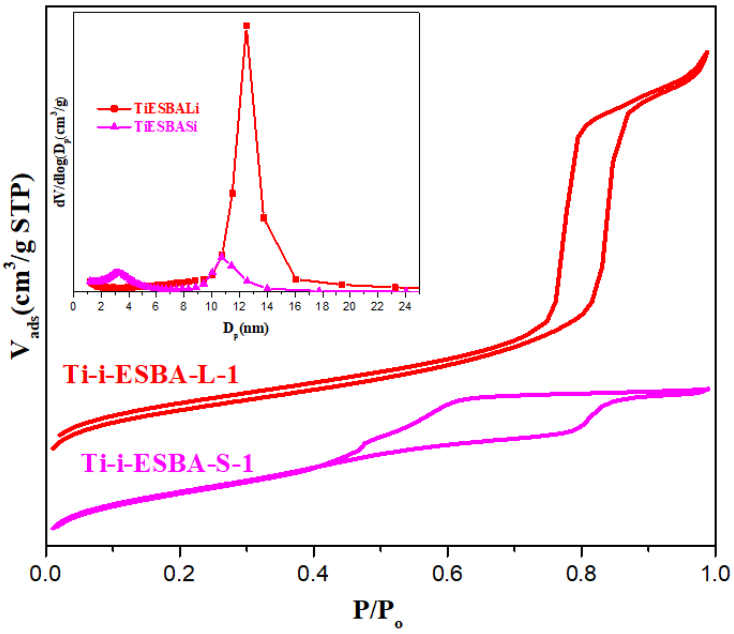

Figure 58. N_2 adsorption-desorption isotherm and BJH pore size distribution (inset) for Ti-i-E-SBA-L-1 and Ti-i-E-SBA-S-1

The isotherm of Ti-i-E-SBA-L-1 shows type IV isotherm, with H1 type hysteresis loops indicating a mesoporous materials with homogenous cylindrical pore size distributions. This fact is also supported by the BJH plot, the very narrow pore size distribution in the material (Figure 58, inset). The unit cell dimension, pore size and pore volume of Ti-i-ESBA-L-1 is higher than the parent Ti-i-SBA-L-1 material, which was synthesized without TIPB, (Table 11). This indicates that when using P123 surfactant and TIPB micelle expander, the pore is expanded without affecting the pore structure, but with very small Ti incorporation. The N_2 adsorption-desorption isotherm of Ti-iE-SBA-S-1 shows type IV isotherm, indicating the mesoporous nature of Ti-i-E-SBA-S-1. It's H4 type hysteresis loop, which is associated with mesoporous materials indicates aggregated crystals, i.e. materials with non-uniform pore size distributions. This fact is also confirmed by the BJH pore size distribution (Figure 58 (inset)).

The overall results obtained by using Pluronic P123 and P104 surfactants, Ti (IV) isopropoxide as a titanium source with and without micelle swelling agent (TIPB) is summarized in Table 11.

From the overall results, we conclude that the final material loses its hexagonal structure when using Pluronic P104 surfactant and Ti (IV) isopropoxide Ti source in the presence as well as absence of TIPB micelle expander in the synthesis solution. Pluronic P123 is better in case of maintaining the hexagonal pore structure under the same synthesis conditions. However, the Ti content in the final material is very low (UV-vis bands intensity is very weak) when using Ti (IV) isopropoxide as a Ti source. As a result, another synthesis method was designed by using a relatively hydrophobic titanocene dichloride as a Ti source, instead of a relatively highly hydrolyzable Ti (IV) isopropoxide.

Table 11. Synthesis conditions and physicochemical properties of Ti-containing SBA-15 materials

Sample	Ti source	$(Ti/Si)_o$[a]	S_{BET} (m^2/g)[b]	V (cm^3/g)[c]	d_{BJH} (nm)[d]	d_{100} (nm)[e]	a_o (nm)[f]	t (nm)[g]
Ti-i-SBA-L-1	TIP	0.01	746	0.98	8.7	10.0	11.6	2.9
Ti-i-SBA-S-1	TIP	0.01	679	0.6	8.1	10.0	11.6	3.5
Ti-i-ESBA-L-1	TIP	0.01	608	1.26	13.2	12.4	14.4	1.2
Ti-i-ESBA-S-1	TIP	0.01	553	0.53	11.2	13.1	15.1	3.9

[a] Initial Ti to Si ratio in the synthesis gel
[b] Specific surface area measured by the BET method
[c] Total pore volume recorded at $P/P_0 = 0.985$
[d] Mean pore size calculated by the BJH method
[e] Interplanar spacing measured by XRD
[f] Unit cell parameter calculated as $a_0 = 2/\sqrt{3}d_{100}$.
[g] Pore wall thickness calculated as $wt = a_0 - D_p$

4.3.2. Characterization results and discussion on Ti-incorporated SBA-15 materials by using titanocene dichloride

In this section, Ti incorporated SBA-15 materials obtained by co-condensation synthesis method using titanocene dichloride as a Ti source, and Pluronic P123 and P104 surfactants with and without TIPB micelle expander is reported and discussed (see also Figure 54). This helps to study the influence of the Ti source precursor, Ti/Si ratio of the synthesis gel and the nature of the surfactants on the property of the final material. The Ti-incorporated SBA-15 materials, which have different particle morphology, different pore size, and different Ti-content in the final material are reported in this section.

To study the effect of the nature of the surfactant used two different materials, i.e. Ti-SBA-L-1 and Ti-SBA-S-1 were synthesized by using Pluronic P123 and P104 surfactants, respectively under the same synthesis conditions. Both materials were prepared using the

Ti/Si ratio of the initial synthesis gel is 0.01 and the materials were characterized by X-ray diffraction, N_2 adsorption-desorption, and DRS UV-vis measurements.

Figure 59 (A) shows the X-ray diffraction patterns for both materials, Ti-SBA-L-1 and Ti-SBA-S-1, which have been synthesized using titanocene dichloride as a Ti source via co-condensation. Both materials show diffraction patterns typical of a mesoscopic *P6mm* structure formed by the hexagonal array of mesochannels. This indicates that the pore structure of the material is maintained in both types during the synthesis conditions involving Cl_2TiCp_2 incorporation. This indicates that titanocene dichloride is better than Ti (IV) isopropoxide in maintaining the pore structure of the material during titanium incorporation. This difference is significantly observed when using Pluronic P104 surfactant (Figure 55 (A) and Figure 59 (A)).

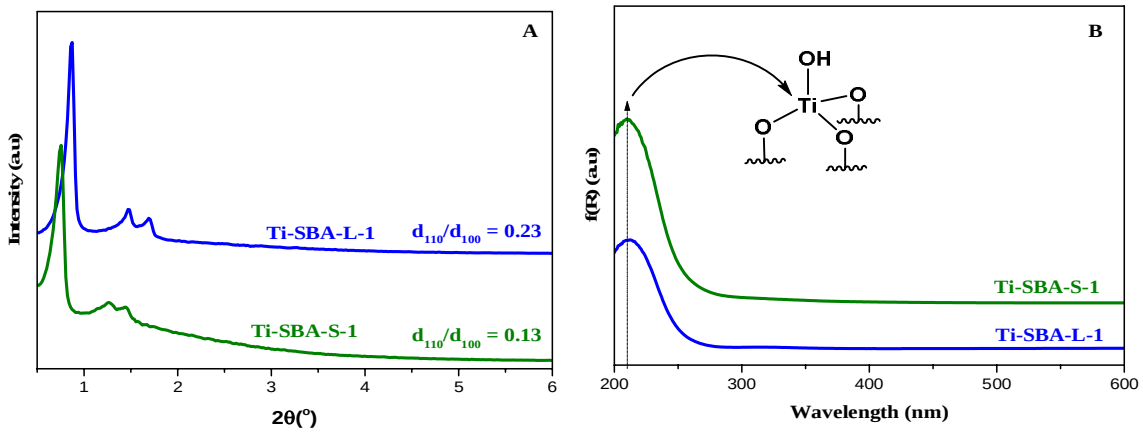

Figure 59. Low angle XRD patterns (A) and DR UV-vis spectra (B) for Ti-SBA-L-1 and Ti-SBA-S-1 materials

The Ti-incorporation was characterized by DRS UV-vis measurements and the results obtained are shown in Figure 59 (B). In both materials there is a sharp UV-vis band at ~ 210 nm, due to the electronic transitions occurring in isolated tetrahedrally coordinated Ti

species bonded to oxygen atoms. Both materials show better absorption band intensities when compared to their corresponding materials which have been synthesized by using Ti (IV) isopropoxide as a Ti source (Figure 55 (B)). This proves when using titanocene dichloride as Ti source there is better Ti (IV) incorporation, i.e. more isolated Ti species, as compared with the ones which have been synthesized using Ti (IV) isopropoxide as a Ti source.

The mesoporosity and textural properties of both materials were characterized by N_2 adsorption-desorption isotherm (Figure 60).

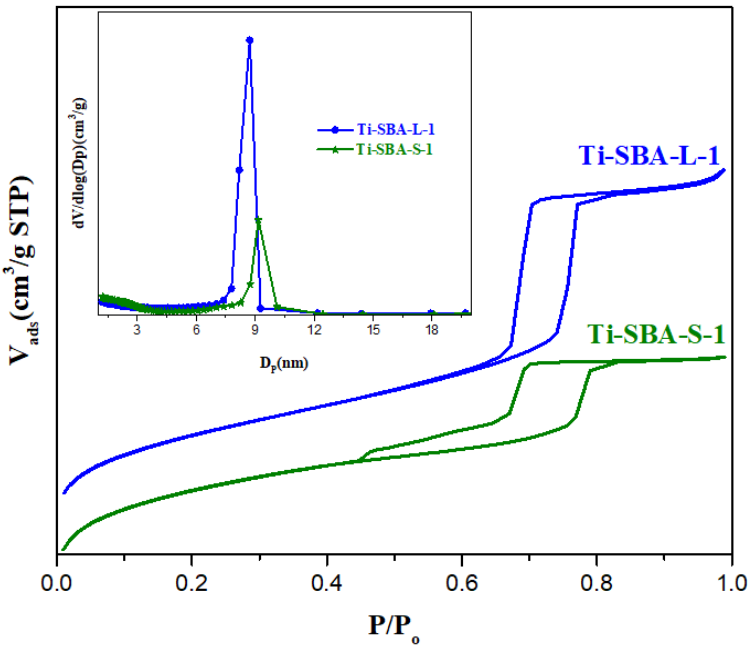

Figure 60. N_2 adsorption-desorption isotherm and BJH pore size distribution (inset) of Ti-SBA-L-1 and Ti-SBA-S-1

The N_2 adsorption-desorption isotherms of both materials display type IV isotherms, which confirm that both are mesoporous materials. The H1 type hysteresis loop of Ti-SBA-L-1 material, indicates a mesoporous material with homogenous cylindrical pore size

distributions (Figure 60). The very narrow pore size distributions for the Ti-SBA-L-1 sample, which is given by BJH plots (Figure 60 (inset)), confirms the pore size uniformity. However, the H5 type hysteresis loop of Ti-SBA-S-1 depicts that desorption branch of the isotherm exhibits two distinctive steps, due to the presence both open and partially blocked mesopores. This is very sharp in the case of Ti-SBA-L-1 because it is more ordered compared to Ti-SBA-S-1. This fact is also supported by BJH pore size distribution (Figure 60 (inset)). Both materials have a large and conventional value of surface area, pore volume and pore diameter (Table 12). From the overall characterization results, we conclude that both materials, Ti-SBA-L-1 and Ti-SBA-S-1, are good in quality, but Ti-SBA-L-1 is more ordered.

Large pore size Ti-containing SBA-15 materials of both types (Ti-E-SBA-L-1 and Ti-E-SBA-S-1) were synthesized by *in situ*, one step, using TIPB pore expander and titanocene dichloride as a Ti source and characterized by the above mentioned characterization methods.

The presence of one intense (100) and two weak (110) and (200) XRD peaks in both materials as shown in Figure 61 (A) indicates that the materials adopt hexagonal arrays of pore arrangements. This means that the materials maintain their parent pore structure. However, the intensities of XRD peaks of Ti-E-SBA-S-1 are weak, due to the partial loss of its structure. Both materials have also been characterized by DRS UV-vis measurements.

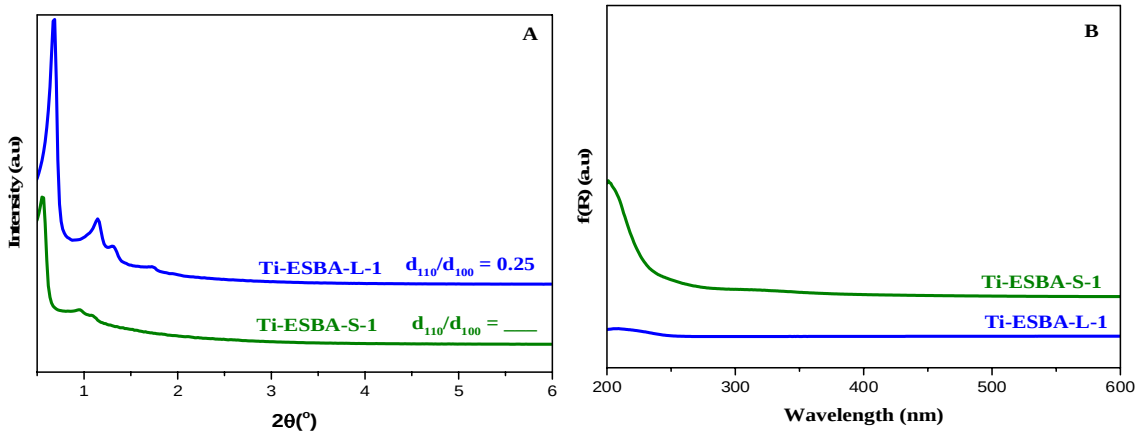

Figure 61. Low angle XRD patterns (A) and DR UV-vis spectra (B) for Ti-E-SBA-L-1 and Ti-E-SBA-S-1 materials

The presence of very weak UV-bands between 200 – 220 nm indicates a very small amount of Ti is incorporated in the material. This indicates that whatever the Ti source used in the case of in situ Ti incorporation and pore size expansion synthesis method, the amount of Ti incorporated in the final material is very low. The textural properties such as surface area, pore volume and pore diameter of both materials Ti-E-SBA-L-1 and Ti-E-SBA-S-1 are characterized by N_2 adsorption/desorption isotherm (Figure 62).

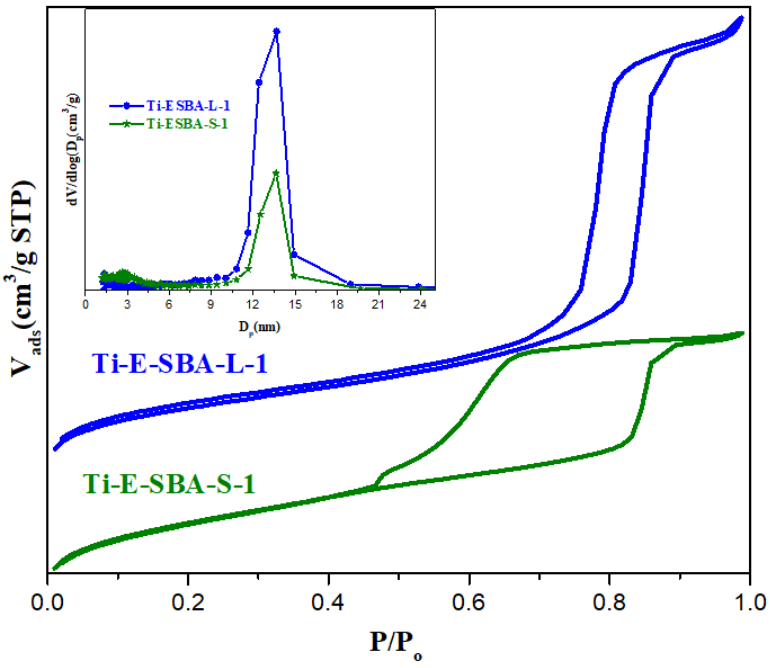

Figure 62. N_2 adsorption-desorption isotherm and BJH pore size distribution (inset) of Ti-containing SBA-15 materials

The N_2 adsorption-desorption isotherms of both materials show a type IV isotherm, which confirms that they are mesoporous materials. Ti-E-SBA-L-1 has H1 type hysteresis loop indicating a mesoporous material with homogenous cylindrical pore size distributions (Figure 62). This is also supported by the BJH pore size distribution plot which is given in Figure 62 (inset), which has narrow pore size distribution. Ti-E-SBA-S-1 material has type H5 hysteresis loop, of the desorption branch of the isotherm exhibits two distinctive steps, due to the presence of both open and partially blocked mesopores. Both materials have a very large average pore diameter (~14 nm) when compared to the parent materials which have pore diameter less than 10 nm. This proves the pore size of the material is expanded due to the interaction of TIPB with the core of the micelle without affecting its pore structure.

In general, the degree of ordering of all materials was calculated and compared by using the ratio between the XRD diffraction intensities of the d_{110} and d_{100} signals as reported in the literature[131]. The material showing the highest ratio of d_{110}/d_{100} is the most ordered material among the tested materials. Ti-containing SBA-15 materials that have been synthesized using titanocene dichloride as a titanium source, have higher d_{110}/d_{100} ratios than those that have been synthesized using Ti (IV) isopropoxide. In other words, titanocene dichloride produces highly ordered mesoporous materials. This may be due to the presence of the cyclopentadienyl ligands which assists the incorporation of Ti (IV) on the framework of the silica material due to the hydrophobic interaction of cyclopentadienyl with the center of the micelle of the surfactant solution. In the case of Ti (IV) isopropoxide, the fast hydrolysis rate of the isopropyl oxide group decreases the amount of Ti incorporated in the framework of the mesoporous material. There is a high probability to agglomeration, disturbing the micelle arrangement. This affects the quality of the material (less ordered material) as well as the Ti content incorporated in the framework/channel of the material. The materials which have been synthesized by using titanocene dichloride as a titanium source have a relatively higher surface area, pore volume, and uniform pore size distribution than their corresponding materials which have been synthesized by using Ti (IV) isopropoxide as a titanium source. From the above results, we conclude that the use of titanocene dichloride instead of titanium (IV) isopropoxide is suitable for the synthesis of Ti-containing mesostructured silica to achieve high titanium loadings and metal dispersion. The hydrophobic nature of the cyclopentadienyl ligands allows deep interactions of the titanocene species with the surfactant micelles so that these act as protecting agents against the strong acidic medium, responsible for the dissociation of the

Ti–O–Si. Additionally, the presence of the highly stable cyclopentadienyl groups prevents the homo-condensation of titanium species to yield titanium oxide domains, allowing a higher dispersion degree of metallic species[23]. Thus, by using titanocene dichloride as a Ti source we tried to increase the population of Ti (IV) active sites in the final material. To achieve this objective, the materials were synthesized by varying the Ti content in the synthesis gel (Ti/Si ratio of 0.01, 0.05 and 0.1).

The use of titanocene dichloride as a source of Ti in the direct synthesis of Ti-SBA-15 gives a highly ordered hexagonal SBA-15 using Pluronic P104 and P123 surfactants. Figure 63 shows the XRD profiles of two sets of samples after calcination at 350 °C to remove the structure-directing agent and the cyclopentadienyl group. Figure 63 (A) shows the profiles of the three samples obtained in the presence of P104 (Ti-SBA-Sn) and Figure 63 (B), those of the three samples prepared using P123 (Ti-SBA-Ln), using n = 1, 5 and 10 mol Ti per 100 mol Si in the synthesis gel, the patterns exhibit a strong 100 diffraction peak at very low angle followed by (110) and (200) weaker peaks in the *P6mm* symmetry characteristic of SBA-15[15]. The unit cell parameters (a_0) obtained from the d_{100} spacing are included in Table 12.

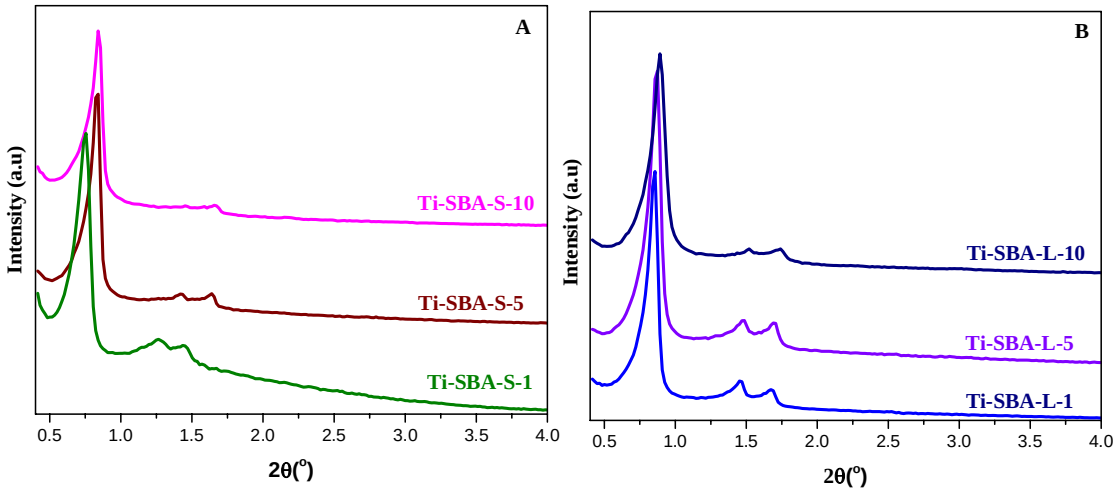

Figure 63. Low-angle X-ray diffraction patters of the samples prepared by co-condensation using three different Ti/Si ratios, (A) in the presence of P104 (Ti-SBA-Sn) and (B) in the presence of P123 (Ti-SBA-Ln)

Table 12. Physicochemical properties of Ti-containing SBA-15 materials with different Ti content, structural and textural parameters

Sample	$(Ti/Si)_o$[a]	Ti (%)[b]	S_{BET} (m^2/g)[c]	V (cm^3/g)[d]	d_{BJH} (nm)[e]	d_{100} (nm)[f]	a_o (nm)[g]	t (nm)[h]
Ti-SBA-L-1	0.01	0.22	869	1.08	8.6	10.3	11.8	3.2
Ti-SBA-L-5	0.05	1.25	849	0.98	8	10	11.6	3.6
Ti-SBA-L-10	0.1	2.97	763	0.83	7.3	9.9	11.4	4.1
Ti-SBA-S-1	0.01	0.26	888	0.76	9.6	11.6	13.4	3.8
Ti-SBA-S-5	0.05	2.83	842	0.93	8	10.5	12.1	4.1
Ti-SBA-S-10	0.1	5.51	731	0.76	7.2	10.5	12.1	4.9

[a] Initial Ti to Si ratio in the synthesis gel
[b] Final Ti content in weight obtained from ICP-OES
[c] Specific surface area measured by the BET method
[d] Total pore volume recorded at $P/P_0 = 0.985$
[e] Mean pore size calculated by the BJH method
[f] Interplanar spacing measured by XRD
[g] Unit cell parameter calculated as $a_0 = 2/\sqrt{3}d_{100}$
[h] Pore wall thickness calculated as $wt = a_0 - D_p$

It can be observed how the nature of the surfactant seems to affect the unit cell size obtaining larger unit cell parameters when P104 is used. The higher ratio of hydrophilic branch of the surfactant seems to provoke the growth of the crystals in the *ab* plane, rather than along the c-direction, the direction of the channels producing thicker pore walls as a consequence of the different crystal growth mechanism[41]. The increase of the Ti/Si ratio of the synthesis gel slightly decreases the unit cell dimension, probably due to the increase of hydrophobic Cp group that may penetrate further with the core of the micelle, resulting in smaller unit cell dimension. The incorporation of more Cp group on the pore wall and its hydrophobic interaction with the core of the micelle results in decreasing the pore diameter and increasing the pore wall thickness (Table 12). This fact is also supported by TGA measurements (Figure 65 (B), when the Ti-content increases, the weight loss due to the surfactants shifted towards the higher temperature region.

The incorporation of Ti in the presence of Pluronic P123 and P104 surfactant is not straightforward due to the hydrophobic nature of the cyclopentadienyl groups[18]. As the content of Cl_2TiCp_2 increases in the synthesis gel, the segregation of Ti takes place, forming anatase separate phases as observed in high angle XRD profiles (Figure 64 (A)). These phases were further observed by SEM and TEM. This phase segregation does not significantly occur in the presence of P123, were no diffraction peaks of anatase were observed at high angle XRD (Figure 64 (B)), only traces of anatase are already visible in the XRD pattern of the Ti-SBA-L-10. This indicating that in this case, the cyclopentadienyl has more affinity for the Pluronic P123 micelle (which has high volume of hydrophobic (PPO) moiety)[23].

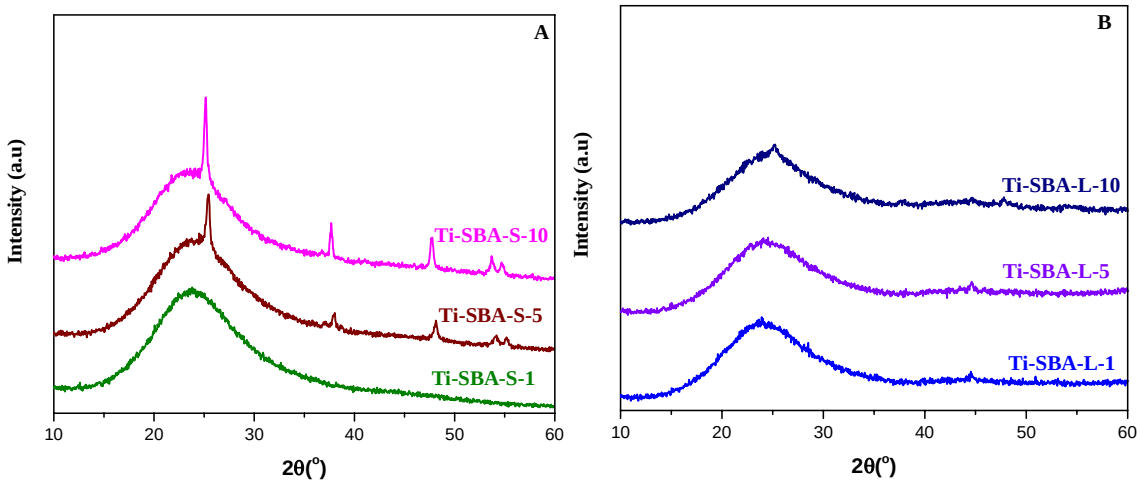

Figure 64. High angle X-ray diffraction patterns of the samples prepared by co-condensation using three ratios of Cp_2TiCl_2: (A) in the presence of P104 (Ti-SBA-Sn) and (B) in the presence of P123 (Ti-SBA-Ln). Sharp diffraction peaks correspond to anatase phase

In order to create porosity and to make Ti active sites accessible, all materials were calcined at 350 °C for 5h. Calcination at this temperature also helps to promote condensation of Ti species incorporated in different systems and to remove the cyclopentadienyl groups and to avoid burial of the Ti species in the pore walls. The calcination process was followed by thermogravimetric analysis (Figure 65 (A and B)). The thermogram shows a sharp weight loss centered at ca. 300 °C in the non-calcined samples, due to the removal of the surfactant molecule. All calcined materials of both types show a significant weight loss below 150 °C due to the removal of physically adsorbed water molecule. Above 400 °C the small weight loss for calcined samples in Figure 65 (A) Ti-SBA-S-1-cal (2.17 %), Ti-SBA-S-5-cal (2.90 %) and Ti-SBA-S-10-cal (3.04 %) and in Figure 65 (B) Ti-SBA-L-1-cal (2.11 %), Ti-SBA-L-5-cal (2.84 %) and Ti-SBA-L-10-cal (2.97 %) may be due to the dehydroxylation of surface hydroxyl groups and Cp that may have remained after calcination. In both types of

materials, when the Ti-content of the final material increases, the weight loss of the materials above 400 ^{o}C also slightly increases, this may be due to the increase of Cp groups.

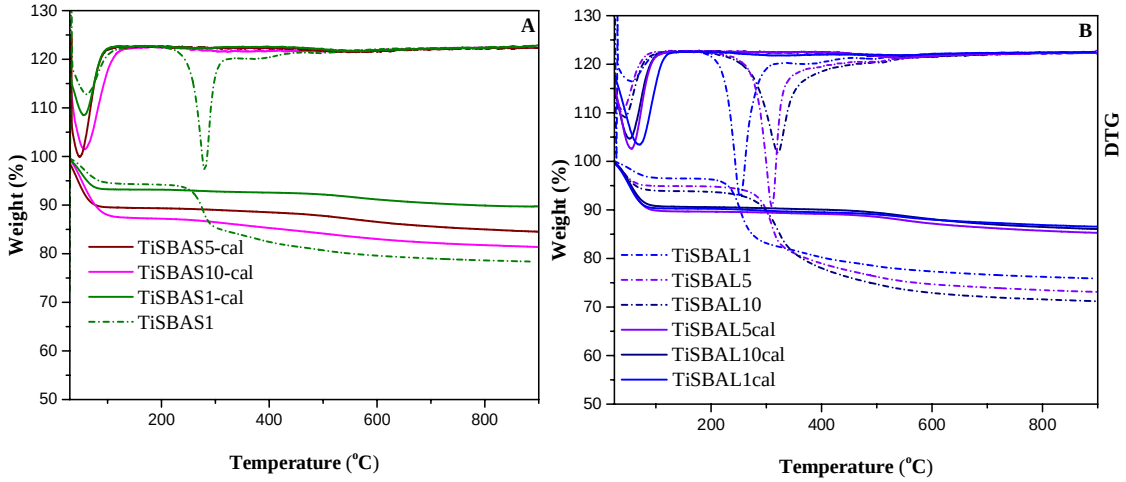

Figure 65. Thermograms of Ti-containing materials before and after calcination (A) Ti-SBA-Sn (B) Ti-SBA-Ln

The N_2 adsorption-desorption isotherms of all materials are type IV and show steeply sloping isotherms and large hysteresis at high relative pressures (Figure 66 (A and B)). All materials which have been synthesized by using Pluronic P123 surfactant (Figure 66 (B) show type H1 hysteresis loop, which is often associated with porous materials consisting of well-defined cylindrical-like pore channels[132]. The small extra step observed in the desorption branch of samples prepared with Pluronic P104 ("S" series), could be due to a possible for the presence of both open and partially blocked mesopores. The narrow pore size distributions in the materials of all types which are given by BJH plots (Figure 66 (inset)) prove the pore size distribution uniformity in the material. The actual pore size, surface area, pore volume and pore wall thickness in each sample is given in Table 12. These values vary upon the purity and degree of the structuring of the samples without a

clear tendency. Large pore size Ti-containing SBA-15 materials with ordered hexagonal pore structures were successfully synthesized.

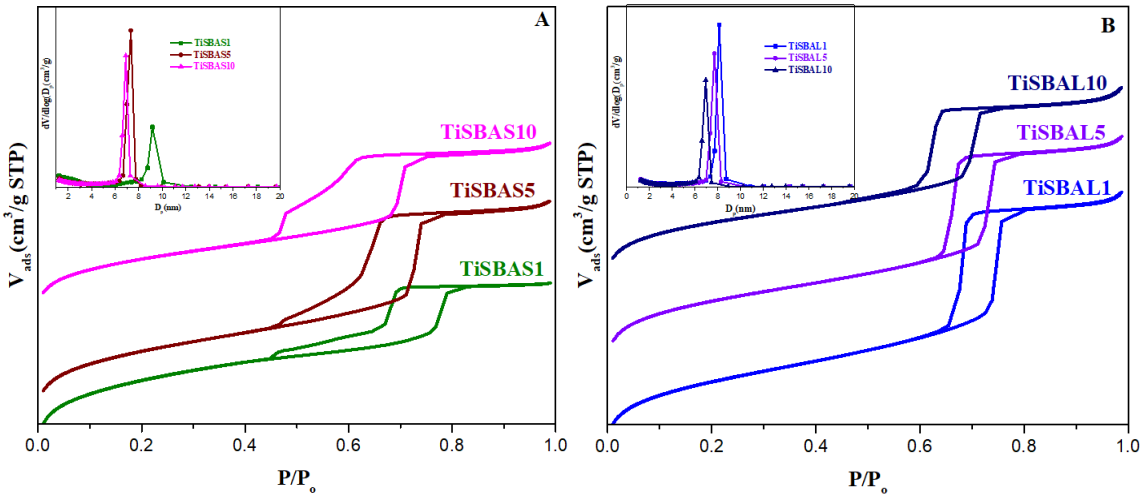

Figure 66. N_2 adsorption-desorption isotherms (A-D) and BJH pore size distribution (inset) of the materials prepared by co-condensation in the presence of (A) P104 (Ti-SBA-Sn) and (B) P123 (Ti-SBA-Ln)

The particle morphology of the catalysts was evaluated systematically by scanning electron microscopy. Figure 67 shows the SEM micrographs of the synthesized Ti-SBA-15 catalysts obtained with different channel lengths. The particle morphology of the materials which have been synthesized by using Pluronic P104 surfactant is highly sensitive towards Ti/Si ratio. The particle morphology of the Ti-SBA-S-1 (Ti/Si ratio of the initial synthesis gel is 0.01) is spherical (Figure 67 (A)). However, samples with a Ti/Si ratio of 0.05 and 0.1 (Ti-SBA-S-5 and Ti-SBA-S-10) are formed by uniform hexagonal plates. Ti-SBA-S-5 shows 2 μm width hexagonal faces, while the thickness of the particles, containing the axis of the channels, is as short as 0.3 μm, corroborating the desired morphology; however, small particles of anatase observed as brighter small spots, more abundant in the case of 10%Ti (Ti-SBA-S-10). Samples prepared using P123 were formed in all cases by fibers,

typical of SBA-15 type of materials (Figure 67 (D-F)). The orientation of the channels within the crystals was corroborated by TEM. Interestingly, the TEM observations revealed that anatase crystals (previously detected by XRD) are systematically formed by oval-shaped mesoporous anatase. Figure 69 (A) shows a typical image of sample Ti-SBA-S-5 with hexagonal arrangement of mesopores, and oval-shaped 200 nm particles (marked with a circle), which at high magnification (Figure 69 (C)) reveals the mesoporosity seen as diffuse lighter contrast areas within the crystalline structure of anatase (indexed in the electron diffraction pattern of the inset). These mesoporous anatase particles are observed in all the samples for which XRD and SEM show phase segregation.

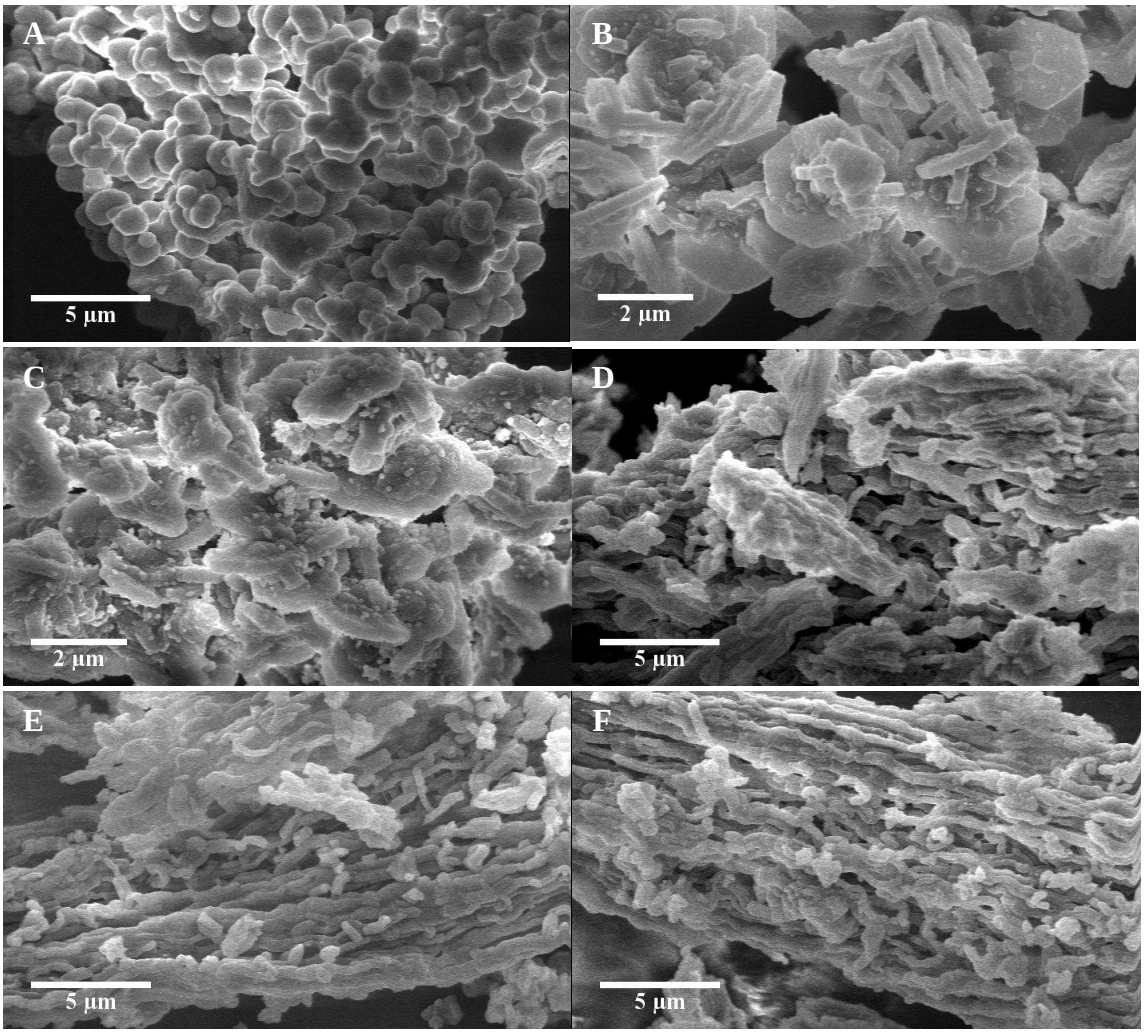

Figure 67. SEM micrographs of Ti-SBA-15 synthesized with different Ti/Si ratio: (A) Ti-SBA-S1, (B) Ti-SBA-S5, (C) Ti-SBA-S10, (D) Ti-SBAL-1, (E) Ti-SBA-L5 and (F) Ti-SBA-L10

Figures 68 & 69 show TEM micrographs of the selected Ti-containing SBA-15 materials produced using different structure-directing agents, different Ti/Si ratio of the synthesis gel. In Figure 68, materials synthesized using Pluronic P123 surfactant have ordered pore structure, ordered cylindrical pores and channels are observed, regardless of the Ti content. Figure 69 shows the materials synthesized using Pluronic P104 surfactant in different Ti/Si ratio, both materials look ordered. However, the degree of order is affected by the Ti/Si

ratio. The pore mouths and channels of the material in which relatively higher content of Ti (Ti/Si = 0.05) is more ordered than the other one which has a lower content of Ti (Ti/Si = 0.01).

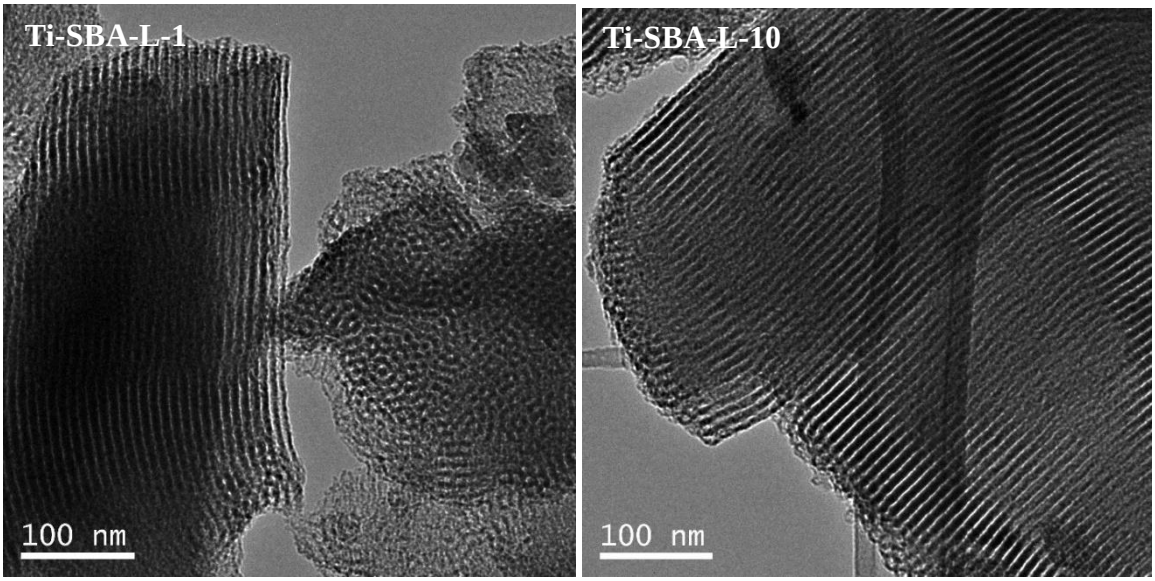

Figure 68. TEM images of Ti-containing SBA-L materials synthesized using P123 surfactant and Ti/Si ratio of synthesis gel 0.01 (left) and 0.1 (right)

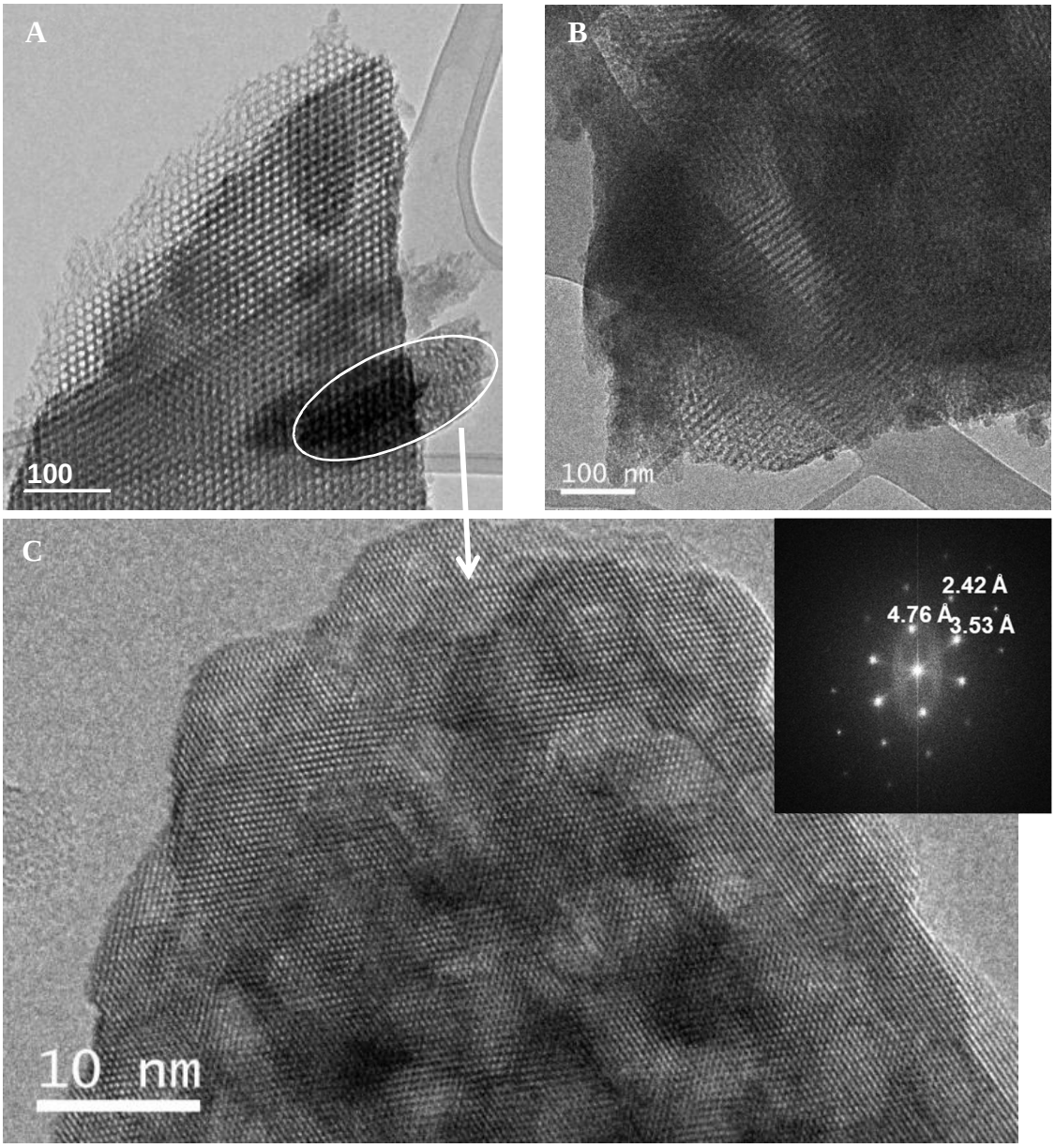

Figure 69. TEM images of Ti-containing SBA-S materials synthesized using P104 surfactant and Ti/Si ratio of synthesis gel 0.05 (A) and 0.01 (B) and high magnification image of the anatase crystals in Ti-SBA-S-5 (C), with the electron diffraction pattern in the inset

The bulk Ti content found in the final material was determined by ICP-OES and the results obtained for each material are given in Table 12. In all cases when the Ti/Si ratio of the synthesis gel is increased, the amount of Ti content in the final material also increases. When we compare the Ti intake capacity of P123 and P104 surfactants, P104 has a high affinity to incorporate a high amount of Ti in the final material. This may be due to the presence of a relatively higher hydrophilic (PEO)/ hydrophobic (PPO) block ratio in the P104 surfactant because PEO is part of the surfactant which interacts with the silicon and titanium species.

Regardless of the presence of anatase, the DR UV–vis spectra of all the samples show a band at 200–220 nm (Figure 70). This absorption band could be assigned to a charge transfer between the oxygen ligands and a central Ti (IV) ion with tetrahedral coordination in isolated species. Figure 70 (A) shows the DR UV–vis of the samples obtained in the materials synthesized using P104 and Figure 70 (B) shows the samples prepared using P123. At low titanium loading, the observed absorption band at 210 nm is very weak. When the Ti loading increases, the intensity of the absorption band in this wavelength range increases due to the incorporation of a high amount of Ti (IV) isolated sites, shifting the band towards $\lambda \geq 230$ nm indicating an extension of the coordination number to 5- or 6- but still for single Ti atom species. The shoulders observed in the curves extending up to 350 nm, showed the presence of TiO_2-like clusters as observed before[133].

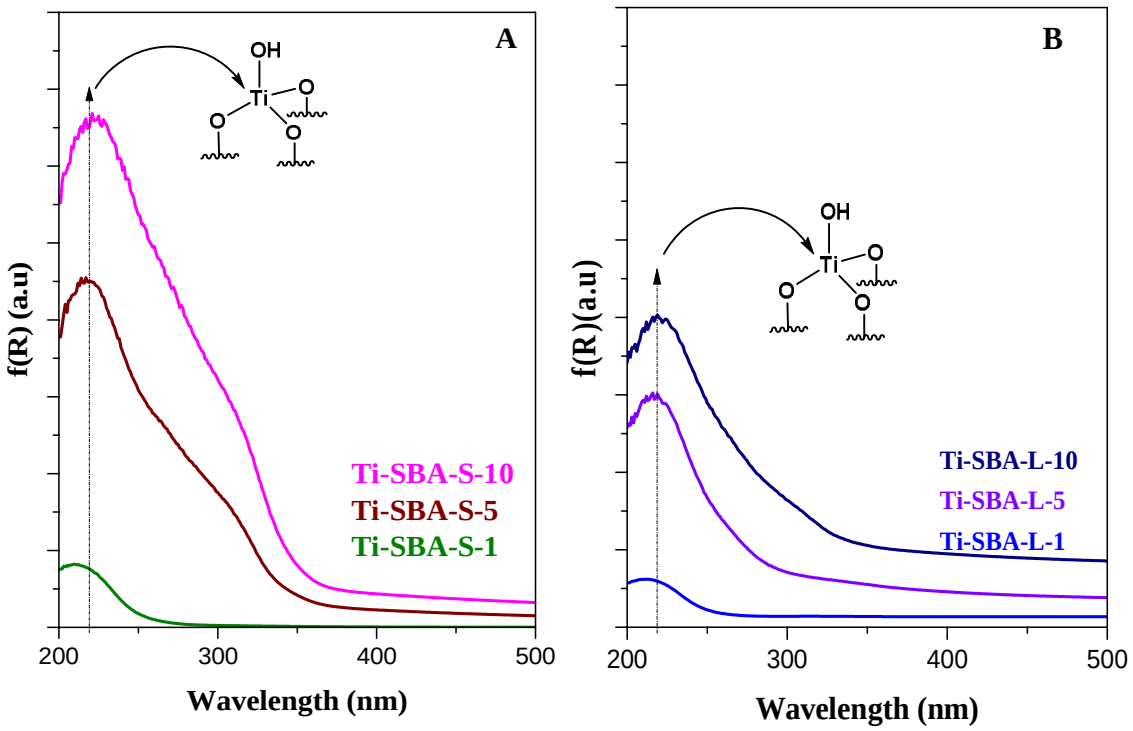

Figure 70. UV-Vis of the samples prepared by co-condensation (A) in the presence of P104 (Ti- SBA-Sn) and (B) in the presence of P123 (Ti-SBA-Ln)

Samples prepared with P104 follow a regular distribution of more isolated Ti (IV) species, probably due to the presence of the cyclopentadienyl ligands that assist the incorporation of titanium on the surface of the material minimizing the agglomeration of titanium clusters due to hydrophobic interaction of cyclopentadienyl with the center of the micelle. In addition to this, the presence of a relatively higher hydrophilic (PEO)/ hydrophobic (PPO) ratio in P104 interacts with a relatively higher amount of Ti species.

When the swelling agent (1, 3, 5-triisopropylbenzene) is added to the synthesis gel (samples labeled with "E": Ti-ESBA-Sn and Ti-ESBA-Ln) (Figure 54), there is an inverse trend for structuring versus Ti incorporation. In all Ti-ESBA-Sn type of materials in Figure 71 (A) the presence of three XRD peaks of (100), (110) and (200) indicates the hexagonal

pore structure is maintained during in situ pore expansion and Ti-incorporation. However, in the case of Ti-ESBA-Ln materials in Figure 71 (B), the XRD peaks become less resolved when the Ti/Si ratio of the synthesis gel increases from 0.01 to 0.1, indicating that the arrangement of pores become less ordered. This is due to the formation of TiO_2 anatase phases on the surface of Ti-ESBA-L-5 and Ti-ESBA-L-10 materials (Figure 72 (B)) decreasing its quality.

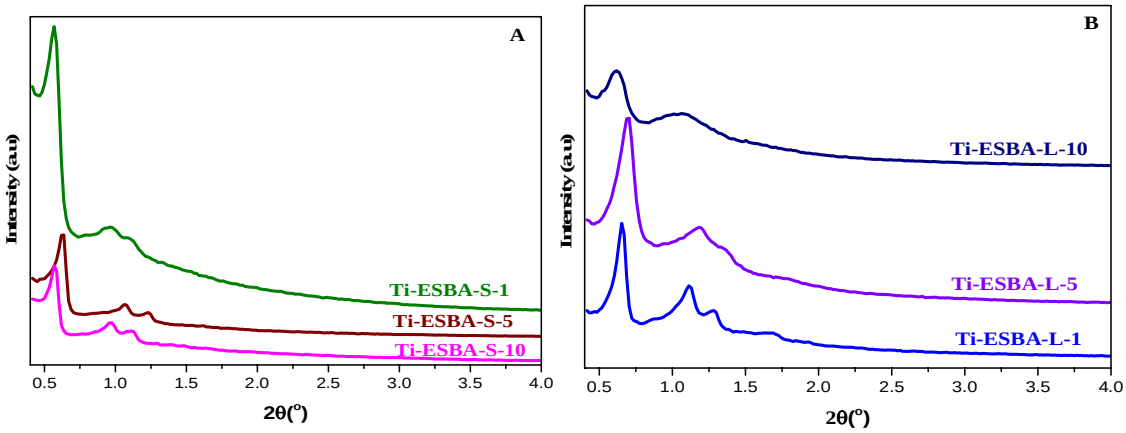

Figure 71. Low-angle X-ray diffraction patterns of the samples prepared by co-condensation using three different Ti/Si ratios, (A) in the presence of P104 with TIPB (Ti-ESBA-Sn) with and (B) in the presence of P123 (Ti-ESBA-Ln) with TIPB

When Pluronic P123 surfactant is used, TIPB together with Cl_2TiCp_2 provoke a segregation of phases leading to high amount of anatase crystals as the Ti content increases (as shown in XRD patterns of Figure 72 (B)), whereas Pluronic P104 incorporates Ti homogeneously into the pore surface as a result of the affinity between the cyclopentadienyl and the core of the micelle (showing no anatase peaks in the XRD patterns plotted in Figure 72 (A)). This trend seems to indicate that the expander not only acts as a micelle swelling agent, but

it seems also to be located at the interface of the wall and the micelles. In the presence of TIPB, the higher incorporation of Ti in the P123 system (see Ti-ESBA-Ln samples in Table 13) results in a poorly ordered SBA-15 hexagonal structure. On the other hand, the successful incorporation of Ti into well-ordered SBA-15 structure using P104 is accompanied by a rather low amount of Ti content in the final material (samples Ti-ESBA-S, Table 13). As can be observed in the XRD profiles of Figure 71, both systems incorporate the swelling agent, leading to a systematic shift of the d_{100} diffraction peak to lower angles due to the larger unit cell parameter.

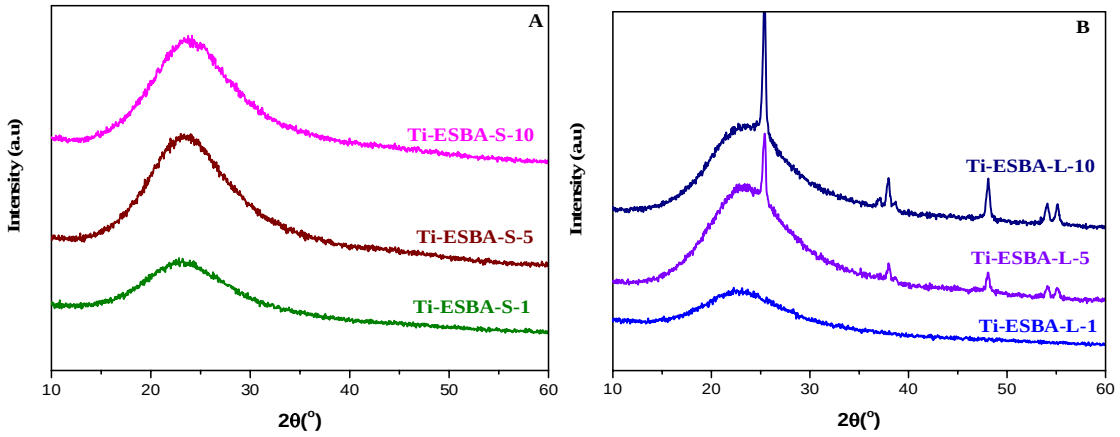

Figure 72. High angle X-ray diffraction patters of the samples prepared by co-condensation using three ratios of Cp_2TiCl_2: (A) in the presence of P104 with TIPB (Ti-ESBA-Sn) and (B) in the presence of P123 with TIPB (Ti-ESBA-Ln). Sharp diffraction peaks correspond to anatase phase

The TGA profiles of all Ti-containing large pore size materials of both types are shown in Figure 73 (A and B). The sharp weight loss around 300 °C for the non-calcined is due to the removal of surfactants. In all calcined materials there is no sharp weight loss around 300 °C indicating that the surfactant molecules are removed during the calcination step.

The weight loss above 400 ºC for calcined materials Ti-ESBA-S-1 (3.27 %), Ti-ESBA-S-5 (2.32 %), Ti-E-SBA-S-10 (3.27 %), Ti-ESBA-L-1 (2.31 %), Ti-ESBA-L-5 (2.09 %) and Ti-ESBA-L-10 (2.31 %) may be due to the dehydroxylation of surface hydroxyl groups and Cp incase remained after calcination.

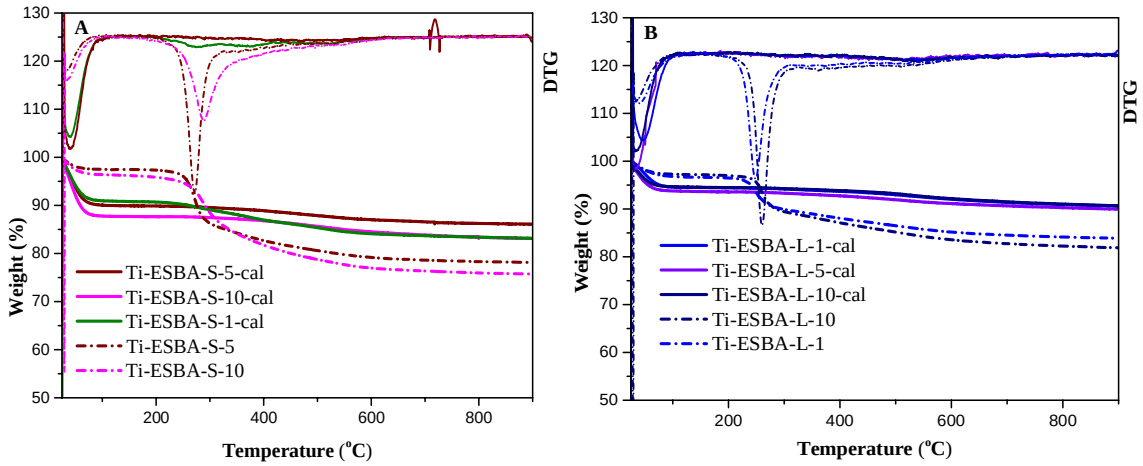

Figure 73. Thermograms of Ti-containing materials after calcination (A) Ti-ESBA-Sn (B) Ti-ESBA-Ln

The N_2 adsorption-desorption isotherms of all materials are type IV and show steeply sloping isotherms and large hysteresis at high relative pressures (Figure 74 (A and B)). This feature is typical of mesoporous materials that have large pore sizes. All materials which have been synthesized by using Pluronic P123 surfactant with TIPB micelle expander (Figure 74 (B) show type H1 hysteresis loop, which is often associated with porous materials consisting of well-defined cylindrical-like pore channels. The small extra step observed in the desorption branch of samples prepared with Pluronic P104 (“S” series), could be due to a possible presence of both open and partially blocked mesopores. The narrow pore size distributions in all materials of both types which are given by BJH plots (Figure 74 (inset)) confirm the pore size distribution uniformity in the material,

characteristics of ordered mesoporous materials. The average pore diameter, surface area, pore volume and pore wall thickness in each sample are given in Table 13. These values vary upon the purity and degree of the structuring of the samples without a clear tendency. The pore diameters of all materials significantly increase on an average value of ~ 5.6 nm (Table 12 & 13), indicating the possibility of *in situ* pore size expansion and Ti-incorporation although a small amount of T_d Ti (IV) species are incorporated.

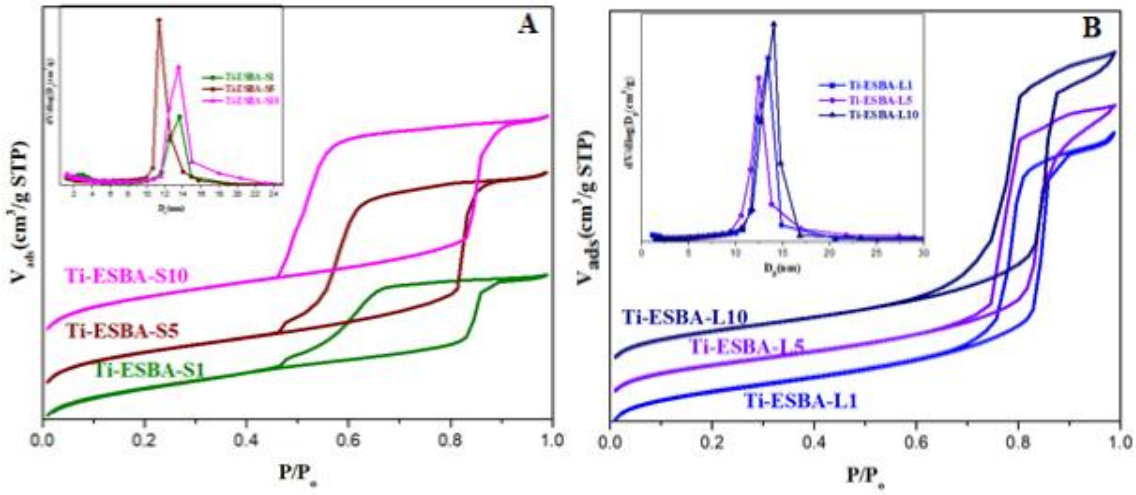

Figure 74. N_2 adsorption-desorption isotherms (A and B) and BJH pore size distribution (inset) of the materials prepared by co-condensation in the presence of (A) P104 with TIPB (Ti-ESBA-Sn) and (B) P123 with TIPB (Ti-ESBA-Ln)

Summary of the physicochemical properties, including the initial and final Ti content and the textural and structural parameters of the calcined large pore size Ti-containing materials are given in Table 13.

Table 13. Physicochemical properties of Ti-containing SBA-15 materials with different Ti content, structural and textural parameters

Sample	$(Ti/Si)_o$[a]	Ti (%)[b]	S_{BET} (m^2/g)[c]	V (cm^3/g)[d]	d_{BJH} (nm)[e]	d_{100} (nm)[f]	a_o (nm)[g]	t (nm)[h]
Ti-E-SBA-L-1	0.01	0.08	556	1.25	14	13.4	15.5	1.5
Ti-E-SBA-L-5	0.05	2.25	589	1.34	13.2	12.4	14.4	1.2
Ti-E-SBA-L-10	0.1	4.72	598	1.41	14.4	14.1	16.3	1.9
Ti-E-SBA-S-1	0.01	0.12	675	0.81	14	14.9	17.2	3.2
Ti-E-SBA-S-5	0.05	0.22	776	1.17	12	13.7	15.9	3.9
Ti-E-SBA-S-10	0.1	0.52	830	1.14	14.3	14.9	17.2	2.9

[a] Initial Ti to Si ratio in the synthesis gel
[b] Final Ti content in weight obtained from ICP-OES
[c] Specific surface area measured by the BET method
[d] Total pore volume recorded at $P/P_0 = 0.985$
[e] Mean pore size calculated by the BJH method
[f] Interplanar spacing measured by XRD
[g] Unit cell parameter calculated as $a_0 = 2/\sqrt{3}d_{100}$
[h] Pore wall thickness calculated as $wt = a_0 - D_p$

Figure 75 shows the characteristic SEM micrographs of the Ti-containing SBA-15 materials produced in the presence of TIPB micelle expander using Pluronic P104 and P123 structure-directing agent and different amounts of Ti/Si ratio of the synthesis gel. Materials synthesized using Pluronic P104, for the lowest Ti/Si ratio (0.01), the material consists of big voids of particles connected and embedded in a foamy structure, Figure 75 (A). The foam disappears when the Ti/Si ratio is increased to 0.05 and 0.1, Figure 75 (B & C), and discrete particles are formed, attached short end to short end. When the synthesis is conducted in the presence of expanders (Ti-ESBA-S-5, Figure 75 (B)), the size of the crystals is much smaller, 0.5 μm particle diameter, having the shape of small cylinders. No phase segregation was observed in samples that have been synthesized with micelle expander (Ti-ESBA-S-5 and Ti-E-SBA-S-10).

On the other hand, materials synthesized using Pluronic P123 with TIPB, for the lowest Ti/Si ratio (0.01) the materials retained their conventional fiber-like morphology (Figure 75 (D)). The fiber-like morphology disappeared when the Ti/Si ratio is increased to 0.05 and 0.1, Figure 75 (E & F), and discrete particles are formed attached short end to short end. This is probably due to the presence of cyclopentadienyl groups with TIPB helps the aggregation of particles and terminates one-dimensional particle growth. The presence of small white spots in samples Ti-ESBA-L-5 and Ti-ESBA-L-10 (Figure 75 (E & F)) confirms the presence of anatase TiO_2 species which was also observed in large-angle XRD measurements (Figure 72 (B)).

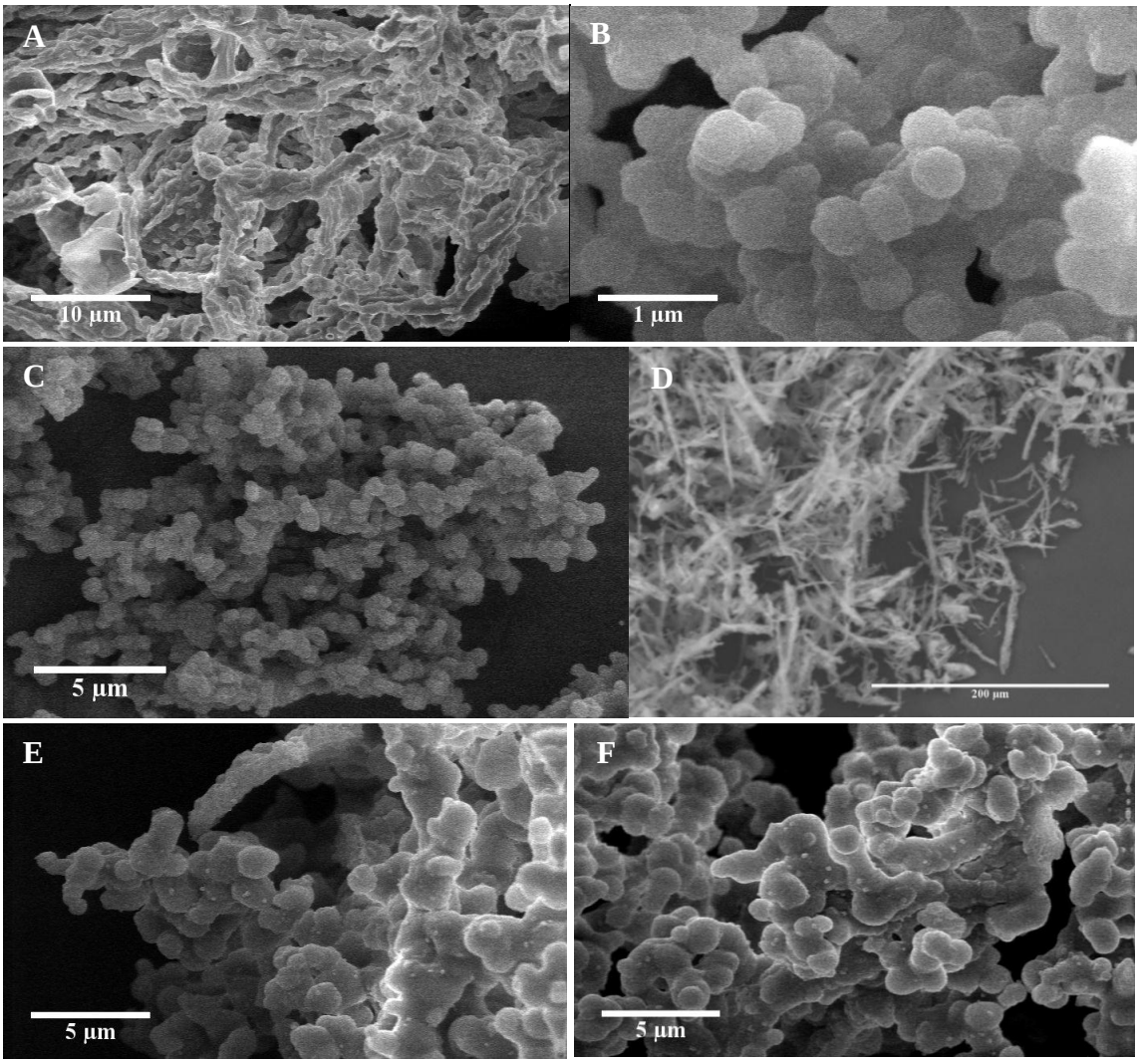

Figure 75. SEM micrographs Ti-SBA-15 synthesized in the presence of micelle expander: (A) Ti-ESBA-S1, (B) Ti-ESBA-S5, (C) Ti-ESBA-S10, (D) Ti-ESBAL-1, (E) Ti-ESBA-L5 and (F) Ti-ESBA-L10

Figure 76 shows TEM micrographs of the selected Ti-containing large pore size SBA-15 materials produced by using Pluronic P104 surfactant in the presence of TIPB micelle expanders and different Ti/Si ratio of the synthesis gel. The accessibility of the pore mouths of Ti-ESBA-S-5 material are clearly observed in the TEM images (Figure 76 (A)). The TEM images for the Ti-ESBA-S-10 material (Figure 76 (B)), which is synthesized by using

the Ti/Si ratio of the synthesis gel 0.1, the pore structure and the accessibility of the pore mouths is maintained.

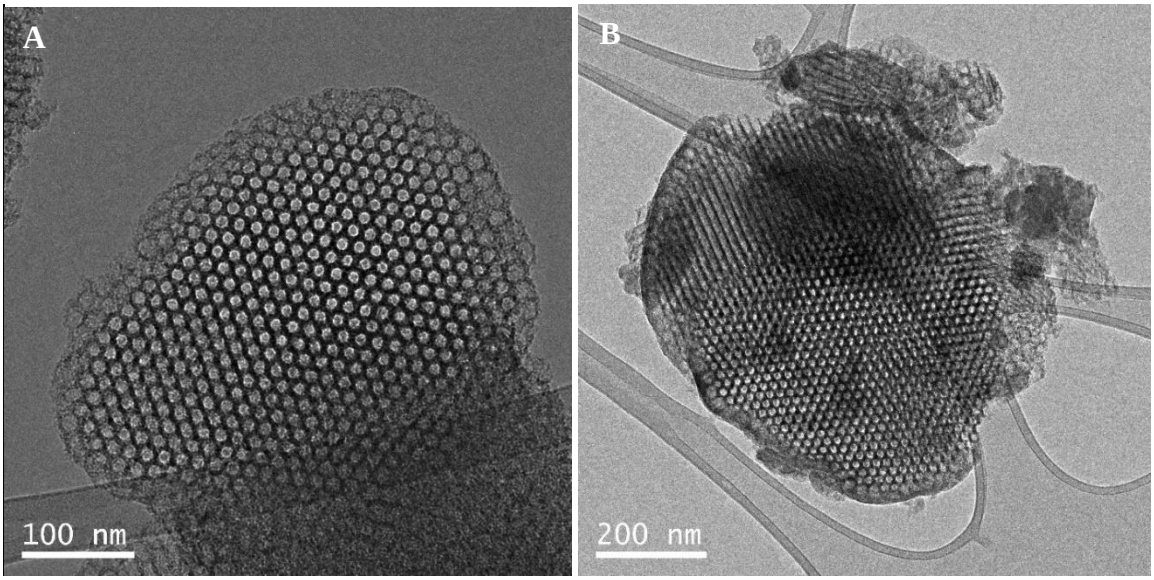

Figure 76. TEM images of selected Ti-containing SBA-S materials synthesized using P104 surfactant with TIPB, Ti-ESBA-S-5 (A) and Ti-ESBA-S-10 (B)

The bulk Ti content found in the final material was determined by ICP-OES and the results obtained for each material are given in Table 13. In both cases when the Ti/Si ratio of the synthesis gel is increased, the amount of Ti content in the final material also increases. When using the P123 surfactant, the amount Ti-content in the final material is higher than P104 (Table 13). However, the absorption peaks in the DR UV-vis spectra show the type of Ti-species present in the final materials synthesized using P123 are highly heterogeneous (Figure 77 (B)), presence of absorption bands in the range of 200 – 340 nm. On the other hand, for materials synthesized by using P104 show only a single intense peak at 210 – 230 nm indicating that the uniformity of Ti-species, T_d Ti (IV) species (Figure 77 (A)). Thus, the presence of TIPB micelle expander affects the amount of T_d Ti-species incorporated in the final material when using P123 or P104 surfactants. The presence of

micelle expander may facilitate nucleation and agglomeration of titanium species in separate phases, i.e. disturbs the incorporation of Ti species in the framework. The anatase formation is also confirmed by a large angle XRD measurements as shown in Figure 72 (B).

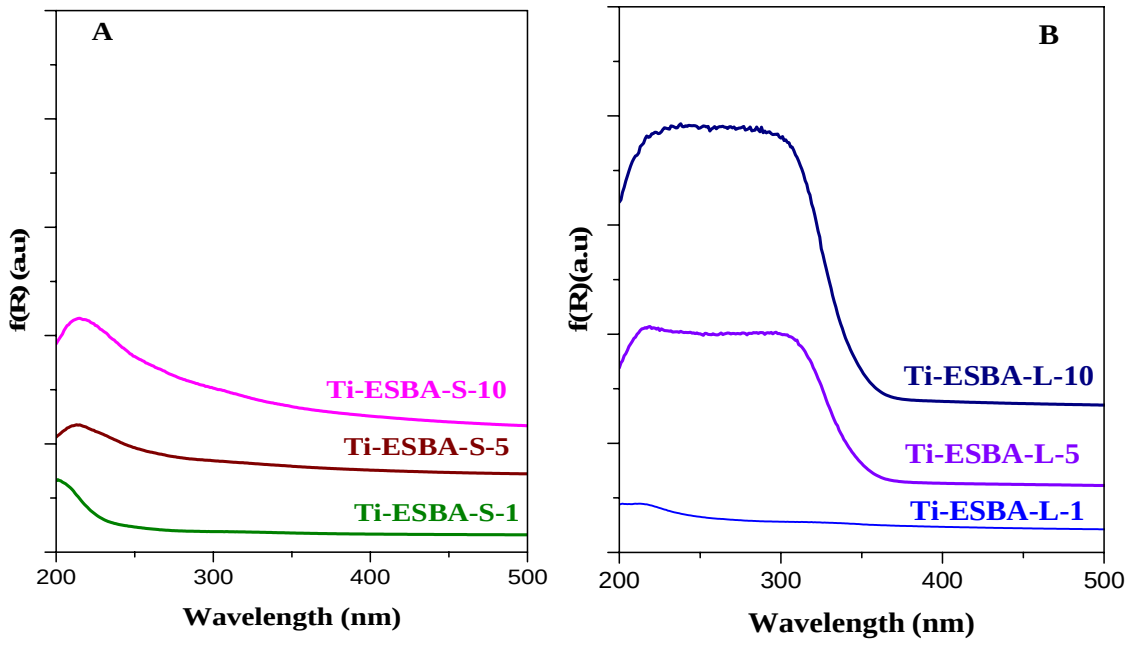

Figure 77. UV-Vis of the samples prepared by co-condensation (A) in the presence of Pluronic P104 with TIPB (Ti-ESBA-Sn) and (B) in the presence of Pluronic P123 (Ti-ESBA- Ln)

Generally, the little amount of Ti incorporated when using the P104 surfactant led to a very weak yet clearly defined 210 – 230 nm band in Ti-ESBA-S5 and Ti-ESBA-S10 due to isolated Ti (IV) species. On the other hand, the use of expander in the presence of P123 allowed incorporating higher amount of Ti (see Table 13) although in a very broad range of coordination stages (210 – 260 nm) and extensive agglomeration (290 – 340 nm) as can be observed by the broad plateau extending from 210 to 340 nm. Although more titanium

is found in the final material of the large pore samples prepared with P123 ("L" series), those catalysts were ignored due to the heterogeneity of the sample in terms of Ti species.

Summary

- ✓ Ti-containing SBA-15 type ordered mesoporous materials with an isolated Ti environment were prepared in a direct synthesis method.
- ✓ Ti-containing SBA-S type of materials with a high content of isolated T_d Ti (IV) species and hexagonal plate-like particle morphology was synthesized by using Pluronic P104 surfactant and the optimum Ti/Si ratio of synthesis gel is 0.05.
- ✓ Ti-containing SBA-L type of materials with isolated T_d Ti (IV) species and with conventional fiber like particle morphology was synthesized by using Pluronic P123 surfactant and Ti/Si ratio of (0.01, 0.05 and 0.1).
- ✓ Ti-containing large pore size (12 and 14.3 nm) SBA-S materials (Ti-ESBA-S-5 and Ti-E-SBA-S-10) with isolated T_d Ti (IV) species was synthesized by using Pluronic P104 surfactant and TIPB micelle expander.
- ✓ Ti content above 2-2.5 wt%, polymeric TiO_2-like species are formed together with isolated Ti species.

4.3.3. Characterization results and discussion on Ti-incorporated PMO materials by using Ti(IV) isopropoxide

The degree of surface hydrophobicity is one of the main factors that could affect the catalytic performance of mesoporous materials during epoxidation reactions. The materials with hydrophobic groups in the framework may have a high adsorption capacity of vernonia oil molecule inside the pore and better diffusion rate of the reactants and the

products. Another advantage of using PMO materials as support has to do with the dispersion of Ti (IV) active sites in the material due to the presence of ethane organic groups between two silicon atoms enhancing the adsorption and therefore the turnover number (TON) of the catalyst. Therefore, the same attempts were tried for a Periodic Mesoporous Organosilica, PMO, aiming to prepare short channels or large pore size in more hydrophobic catalysts in order to enhance adsorption and diffusion of bulky of vernonia oil molecules.

The combined functionalization of ordered mesoporous materials with titanium species as well as organic functionalities through direct synthesis procedures is the aim of this study. Thus, the influence of the type of titanium precursors to the synthesis gel, the Ti/Si ratio of the synthesis gel, the structure-directing agent and presence of micelle expanders on the incorporation of Ti as well as the structure and particle morphology of the final material were studied in this part of the study.

In this section, results corresponding to Ti-containing PMO materials, which have been synthesized by using Ti (IV) isopropoxide as a titanium source and Pluronic P123 and P104 surfactants is reported and discussed. The types of materials synthesized and the scheme of labeling is given in Figure 78.

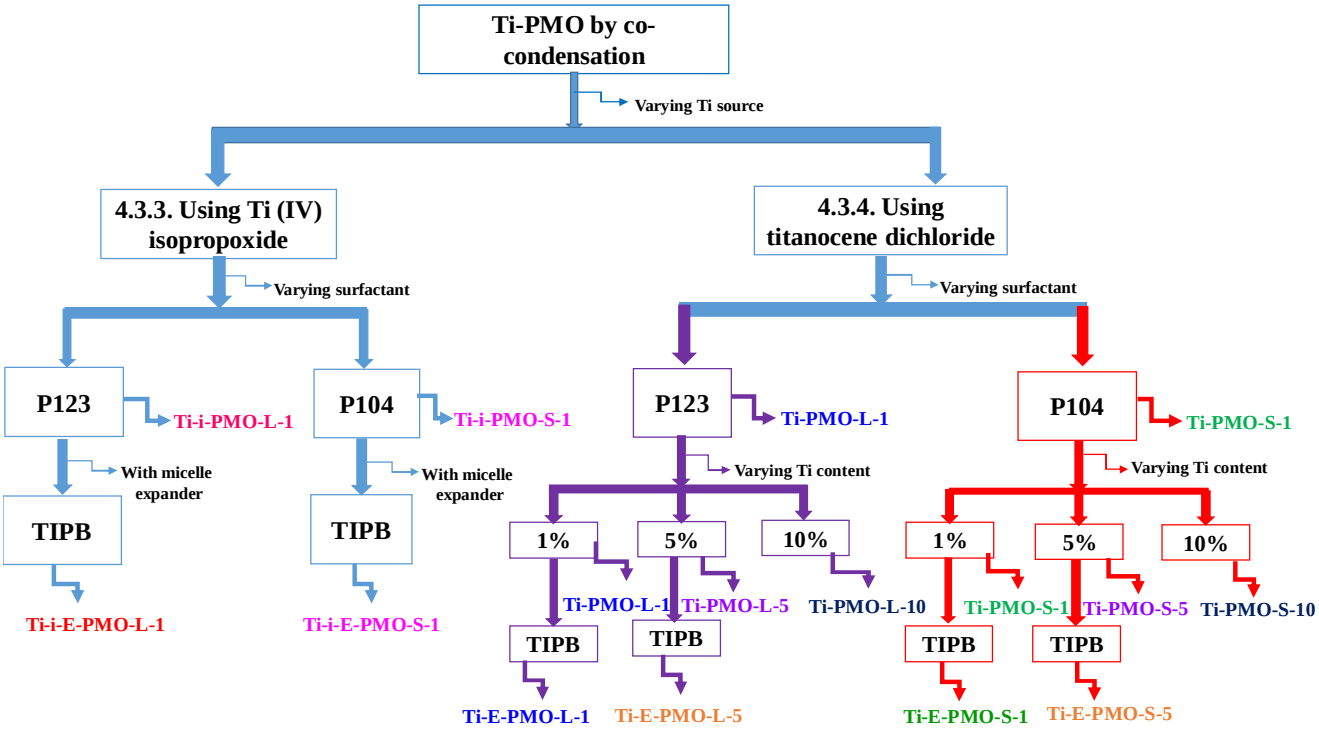

Figure 78. Scheme of labeling of Ti-containing PMO materials synthesized by co-condensation method

To study the effect of surfactant type on the Ti-incorporation capacity when using Ti(IV) isopropoxide as a titanium source and the capacity of maintaining its pore structure, two materials (Ti-i-PMO-L-1 and Ti-i-PMO-S-1) were synthesized and characterized by the above mentioned characterization techniques. These materials were synthesized by using the Ti/Si ratio of the synthesis gel is only 0.01.

The XRD patterns of both materials are shown in Figure 79 (A), both materials have one intense peak (100) and two weak peaks (110) and (200). This is characteristic of ordered mesoporous materials which have hexagonally arranged pore structure. Therefore, these

XRD peaks indicate both materials have hexagonal pore structure in the *P6mm* space group.

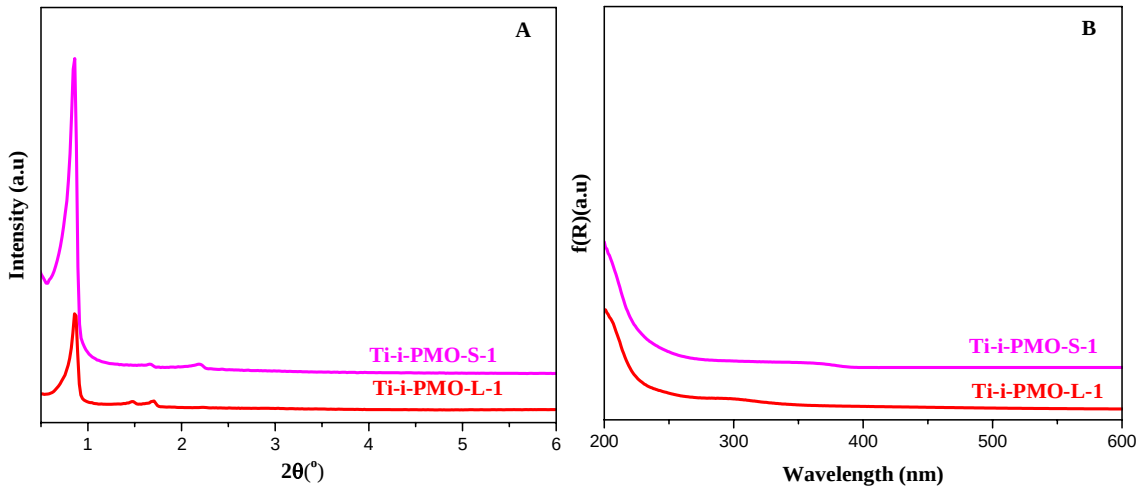

Figure 79. Low angle XRD patterns recorded (A) and DR UV-vis spectra (B) for Ti-containing PMO materials prepared using different Ti source and structure-directing agent

Figure 79 (B) depicts the DR UV-vis spectra recorded for Ti-i-PMO-L-1 and Ti-i-PMO-S-1 materials. Both materials show weak bands, formed by the absorption of UV radiation between 200 – 220 nm, this is due to the electronic transitions occurring in isolated tetrahedrally coordinated titanium species bonded to oxygen atoms. This weak absorption band indicates the presence of a very small amount of Ti in the final material.

The N_2 adsorption/desorption isotherms of Ti-i-PMO-L-1 and Ti-i-PMO-S-1 materials are shown in Figure 80. Both materials display type IV isotherms with H1 type hysteresis loops, indicating a uniformly distributed cylindrical mesopores. The very narrow pore size distributions, calculated by the BJH methods (Figure 80 (inset)), supports this fact.

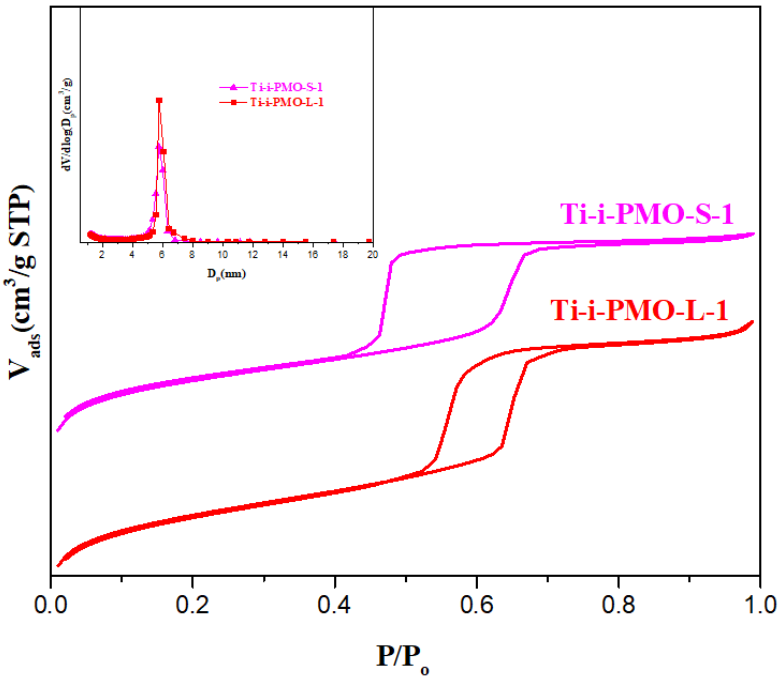

Figure 80. N_2 adsorption-desorption isotherm and BJH pore size distribution (inset) for Ti-i-PMO-L-1 and Ti-i-PMO-S-1 materials

The structural (unit cell dimension) and textural properties (surface area, pore volume, and pore diameter) of both materials are summarized in Table 14. Both Ti-i-PMO-L-1 and Ti-i-PMO-S-1 have roughly similar unit cell dimensions, pore size, and pore volume. The pore diameter of both materials is 6.0 nm, which may not be enough for the diffusion of bulky vernonia oil and its product (epoxidized vernonia oil) in the channel of the material. As a result, we tried to increase the pore diameter of both types of materials by using 1, 3, 5-triisopropylbenzene (TIPB) as micelle expander during the synthesis. The synthesized large pore diameter materials are also characterized by the above mentioned characterization techniques.

The XRD peaks pattern of large pore size PMO materials of both types (Ti-i-EPMO-L-1 and Ti-i-EPMO-S-1) is shown in Figure 81 (A). In both materials only the main XRD peaks

(100) appears, the expected weak peaks of (110) and (200) are not well resolved. This is a typical feature for hexagonal pore structure mesoporous materials with less degree of ordering. This indicates the pore structure is affected by the micelle expander during pore expansion. In both materials, the main XRD peaks (100) are slightly shifted towards the lower 2θ value when compared to their parent materials (Ti-i-PMO-L-1 and Ti-i-PMO-S-1) due to the increase of the unit cell dimension.

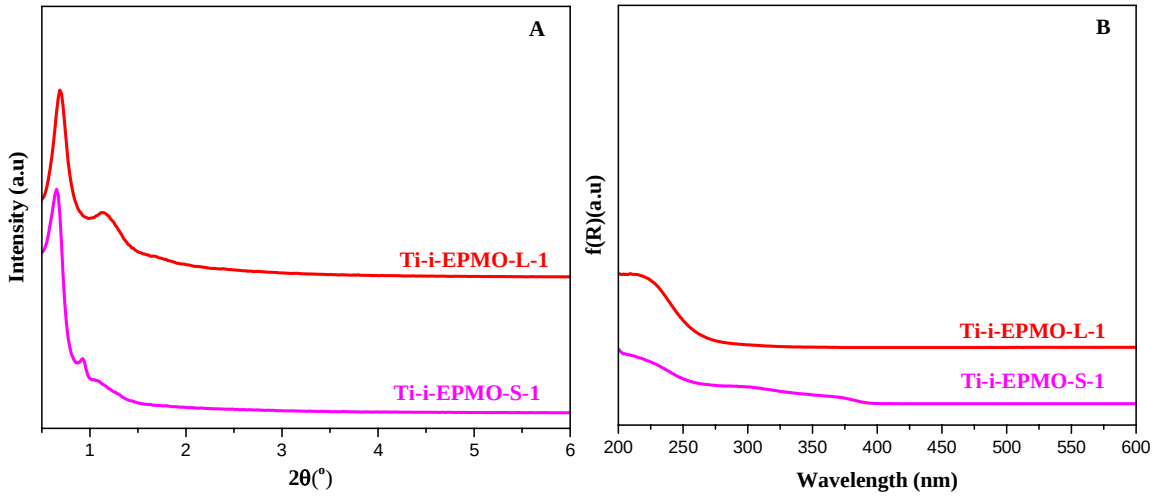

Figure 81. Low angle XRD patterns recorded (A) and DR UV-vis spectra (B) for Ti-i-E-PMO-L-1 and Ti-i-E-PMO-S-1 materials

Figure 81 (B) shows the DR UV-vis spectra recorded for the Ti-i-E-PMO-L-1 and Ti-i-E-PMO-S-1 materials. Both materials display a weak band, formed by the absorption of UV radiation between 210 – 230 nm, this is due to the electronic transitions occurring in isolated tetrahedrally coordinated titanium species bonded to oxygen atoms. This weak absorption band indicates only small amount of T_d Ti (IV)-species is found in the final material of both types. The textural properties of both types of materials is also characterized by N_2 adsorption-desorption isotherms (Figure 82).

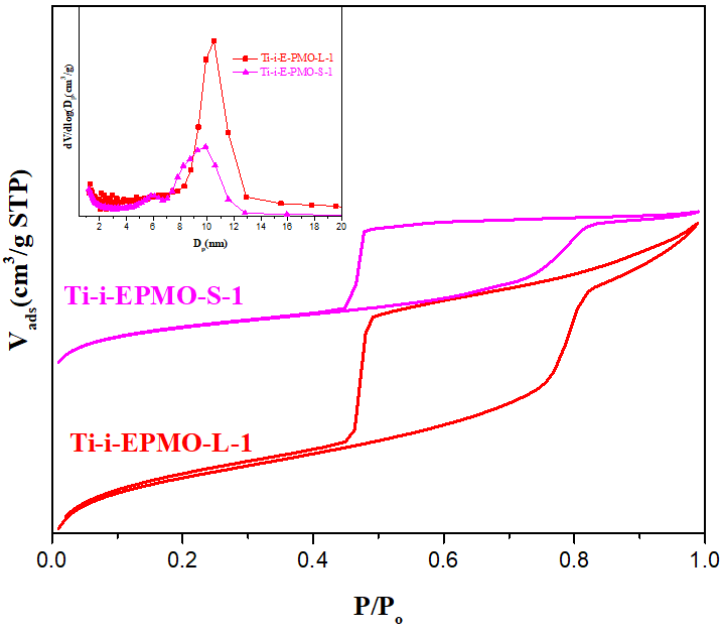

Figure 82. N_2 adsorption-desorption isotherms and BJH pore size distribution (inset) of Ti-i-E-PMO-L-1 and Ti-i-E-PMO-S-1 materials

N_2 adsorption/desorption isotherms of both Ti-i-E-PMO-L-1 and Ti-i-E-PMO-S-1 materials are of type IV with H2 (a) hysteresis loops, indicating the presence of partially blocked mesopores or bottlenecks. Both materials have a wider hysteresis loops due to the increase of the pore diameter of the material. This is also supported by the BJH pore size distribution, which is shifted towards the larger pore diameter range. The isotherms of the desorption curve are not sharp enough, delaying diffusion of reagents due to the presence of bottlenecks or pore blockages. Ti-i-EPMO-L-1 has relatively narrow pore size distribution than Ti-i-EPMO-S-1 material, i.e. Ti-i-EPMO-L-1 has a relatively more ordered pore structure. The structural and textural parameters of all Ti-containing PMO materials synthesized by using Pluronic P123 and P104 surfactants and Ti (IV) isopropoxide as Ti source with and without micelle expander is summarized in Table 10. The unit cell dimensions and pore diameters of both Ti-i-EPMO-L-1 and Ti-i-EPMO-S-1

materials increase by an average value of 4 nm when compared to their parent materials (Ti-i-PMO-L-1 and Ti-i-PMO-S-1). The surface area and pore volume of Ti-i-EPMO-L-1 are higher than Ti-i-EPMO-S because it is better in mesopores arrangement and pore size uniformity.

Table 14. Structural and textural properties of the Ti-containing PMO materials

Catalyst	Unit cell dimension (nm)	Pore size (nm)	Pore wall (nm)	Pore volume (cm^3/g)	S_{BET} (m^2g^{-1})
Ti-i-PMO-L-1	10.4	6.0	4.4	0.56	488
Ti-i-EPMO-L-1	14.7	10.1	4.6	1.29	884
Ti-i-PMO-S-1	11.8	6.0	5.8	0.52	542
Ti-i-EPMO-S-1	15.5	10.0	5.5	0.73	688

In summary, the amount of Ti incorporated in all materials of the final material is very small. As a result, we tried to synthesize the same types of materials under the same conditions by using titanocene dichloride, which is relatively more hydrophobic and has a low rate of hydrolysis, instead of Ti (IV) isopropoxide. The obtained characterization results are reported and discussed in the next sections.

4.3.4. Characterization results and discussion on Ti-incorporated PMO materials by using titanocene dichloride

The materials which have been synthesized by using titanocene dichloride and the sample name labeling is shown in Figure 78. Initially two materials were synthesized to study the

pore structure maintaining and Ti intake capacity of the two surfactants (Pluronic P123 and P104) when using titanocene dichloride as a silica source. As shown in Figure 83 (A) from the XRD result, the presence of one strong peak (100) and two weak peaks (110) and (200) indicate that both materials retain their hexagonal pore arrangement.

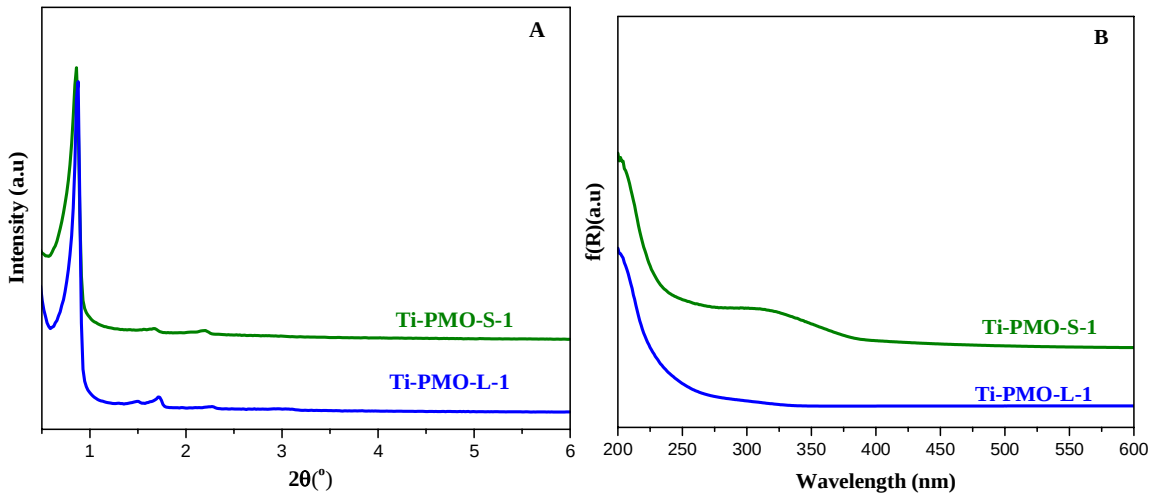

Figure 83. Low angle XRD patterns recorded (A) and DR UV-vis spectra (B) for Ti-containing PMO materials prepared using different Ti source and structure-directing agent

Figure 83 (B) depicts the DR UV spectra recorded for the Ti-PMO-L-1 and Ti-PMO-S-1 materials. Both materials show a weak band, formed by the absorption of UV-vis radiation between 200 – 220 nm, this is due to the electronic transitions occurring in isolated tetrahedrally coordinated titanium species bonded to oxygen atoms. This weak absorption band indicates the presence of a small amount of Ti in the final material. The broad band at 320 nm for Ti-PMO-S-1 sample is probably due to the electronic transition from Cp, which remains intact with the Ti (IV) active sites after surfactant removal, to Ti (IV) ion.

Table 15. The weight loss in different temperature ranges for Ti-containing PMO materials

Catalyst	Weight loss (%) in different temperature ranges			
	< 150 ^{o}C	150 – 450 ^{o}C	450 – 750 ^{o}C	>750 ^{o}C
Ti-PMO-L-1	3.11	7.78	7.93	1.02
Ti-PMO-L-1-cal	0.27	0.37	8.49	3.82
Ti-PMO-S-1	12.68	11.85	7.76	0.45
Ti-PMO-S-1-cal	7.32	1.57	7.51	0.47

The removal of the surfactant molecules and the thermal stabilities of both types of materials (Ti-PMO-L-1 and Ti-PMO-S-1) before and after calcination are given in Figure 84 (A) and Table 15. The weight loss below 150 ^{o}C for all samples may be due to the removal physically adsorbed water or ethanol which remained in the washing step. The weight loss in the temperature range of 150 – 450 ^{o}C for all samples is due to the removal of surfactant molecules. The very small weight loss in the calcined materials indicates the surfactant molecules are effectively removed in the calcination step. The weight loss in the temperature range of 450 – 750 ^{o}C for all samples is due to the removal of framework ethane (-CH_2CH_2-) groups and probably Cp groups. In this temperature range, equivalent amounts of weight are removed in both calcined and non-calcined materials of both types. This indicates that the framework ethane group is not affected by the calcination process. The small weight loss above 750 ^{o}C for all samples may be due to the dehydroxylation of surface hydroxyl groups. Therefore calcination at 350 ^{o}C for 5 h is an optimum condition to selectively remove the surfactant molecules without affecting the framework ethane group.

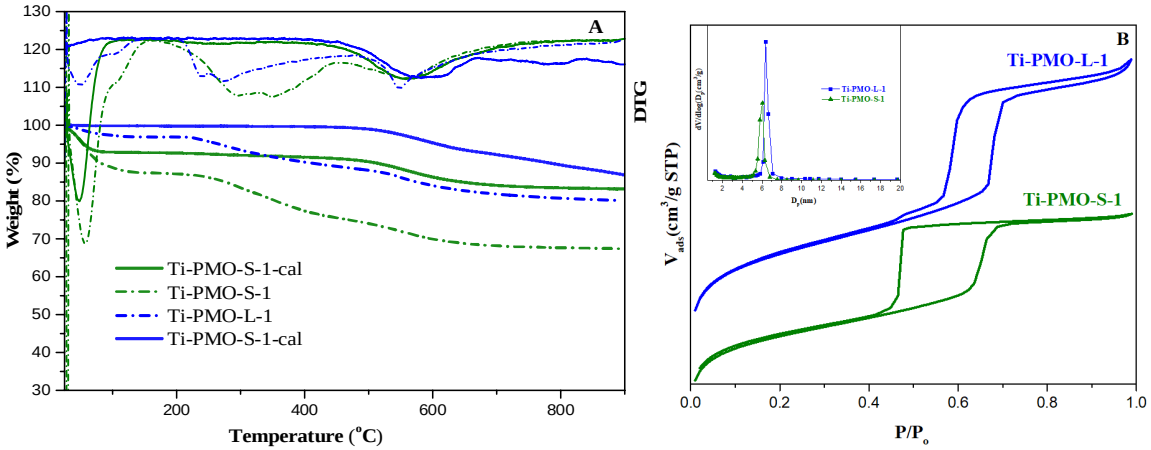

Figure 84. TGA profile (A) and N_2 adsorption-desorption isotherm (B) for Ti-PMO-L-1 and Ti-PMO-S-1 materials

These materials have also been characterized by N_2 adsorption-desorption measurements to characterize the textural properties and to confirm its mesoporosity (Figure 84 (B)). Based on the IUPAC classification of porous materials, both materials show type IV isotherms indicating that they are mesoporous materials. Ti-PMO-L-1 material has H1 type hysteresis loop, indicating the presence of uniformly distributed cylindrical mesopores. However, Ti-PMO-S-1 shows H2 type (a) hysteresis loop. This may be due to the presence of partially blocked pores or bottlenecks. The BJH pore size distribution plot (Figure 84 (B), inset), supports this fact. The summary of the structural and textural properties of both materials is given in Table 16.

Table 16. Structural and textural properties of the Ti-containing PMO materials

Catalyst	a_0 (nm)	Pore size (nm)	Pore wall (nm)	Ti (wt. %)	Pore volume (cm^3/g)	S_{BET} (m^2g^{-1})
Ti-PMO-L-1	11.0	6.6	4.4	0.23	0.79	748
Ti-PMO-S-1	12.1	6.1	6	0.62	0.59	640

The unit cell dimension and the pore wall thickness Ti-PMO-S-1 is slightly higher than Ti-PMO-L-1. This may be due to the presence of a higher hydrophilic PEO/hydrophobic PPO block ratio in the P104 surfactant that may increase its pore wall thickness. On the other hand, the pore diameter of Ti-PMO-L-1 is slightly higher than Ti-PMO-S-1 due to the presence of higher hydrophobic PPO/hydrophilic PEO block ratio in P123 surfactant. The pore volume and surface area of Ti-PMO-L-1 are higher than Ti-i-PMO-S-1 because it is better in mesopores arrangement and uniformity.

The pore size of the materials of both types should be expanded to increase the adsorption and diffusion rate of bulky vernonia oil in the pore channels of the materials. As shown in Figure 78, large pore size materials of both types (Ti-EPMO-L-1 and Ti-EPMO-S-1) were synthesized by using titanocene dichloride as a titanium source and TIPB as a micelle expander. These materials have also characterized by the above mentioned characterization techniques.

The XRD patterns of Ti-EPMO-L-1 and Ti-EPMO-S-1 materials were shown in Figure 85 (A). Only the XRD peak (100) appears, the other two weak peaks are not well resolved. This indicates that both materials have moderately ordered hexagonal structure due to the effect of pore expanders regardless of the titanium source. Ti-EPMO-L-1 has more intense XRD peaks than Ti-EPMO-S-1, i.e. It has a better ordered pore arrangement.

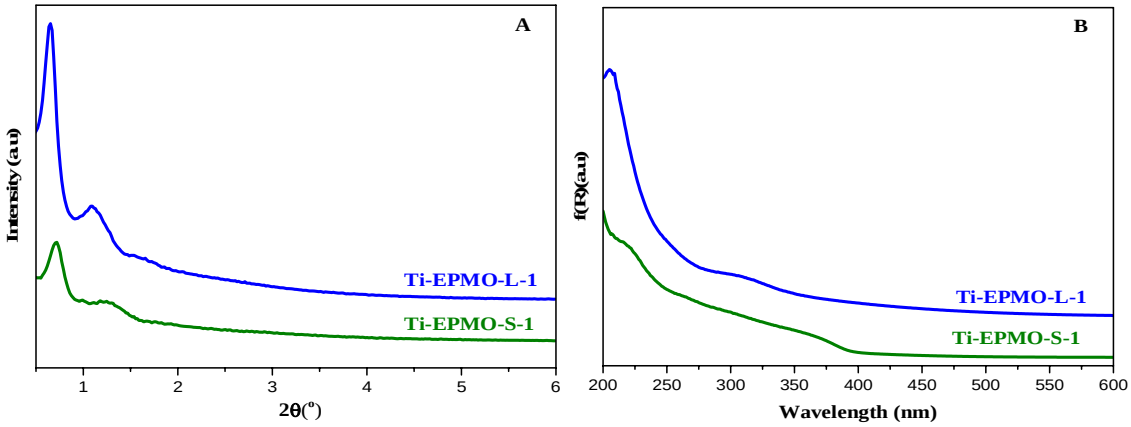

Figure 85. Low angle XRD patterns recorded (A) and DR UV-vis spectra (B) for Ti-EPMO-L-1 and Ti-EPMO-S-1

Figure 85 (B) shows the DR UV-vis spectra recorded for the Ti-EPMO-L-1 and Ti-EPMO-S-1 materials. The presence of a weak UV-vis absorption band in the wavelength range of 200 – 220 nm is due to the electronic transitions occurring in isolated tetrahedrally coordinated titanium species bonded to oxygen atoms. This weak absorption is due to the presence of small amount of Ti found in the final material. Although, all Ti-incorporated PMO materials showed weak UV-vis absorption band in the wavelength range of 200 – 220 nm, due to the incorporation of a small amount of Ti in the framework/channel of the material, the samples which have been synthesized using titanocene dichloride as a titanium source showed better absorption band intensity than their corresponding materials which have been synthesized by using Ti (IV) isopropoxide as a titanium source. This scenario works in both types of surfactants with and without pore expanders. The main reason for this happening is, as we have explained in the case of SBA-15 materials is the presence of cyclopentadienyl groups within the titanocene dichloride precursor, which gives a special advantage to incorporate titanium on the wall of the micelle by hydrophobic interaction between this group and the center of the micelle. From this result, we conclude

that the titanium source influences the incorporation of titanium on the framework/channel of the PMO materials. The absorption broad band at 320 nm is probably due to the electronic transition from Cp, to the vacant d-orbitals of Ti (IV) ion.

Both materials, i.e. Ti-EPMO-L-1 and Ti-EPMO-S-1 are also characterized by the N_2 adsorption- desorption isotherms (Figure 86) to study to what extent the pore is expanded and to evaluate the effect of pore expanders on the other textural properties of the materials.

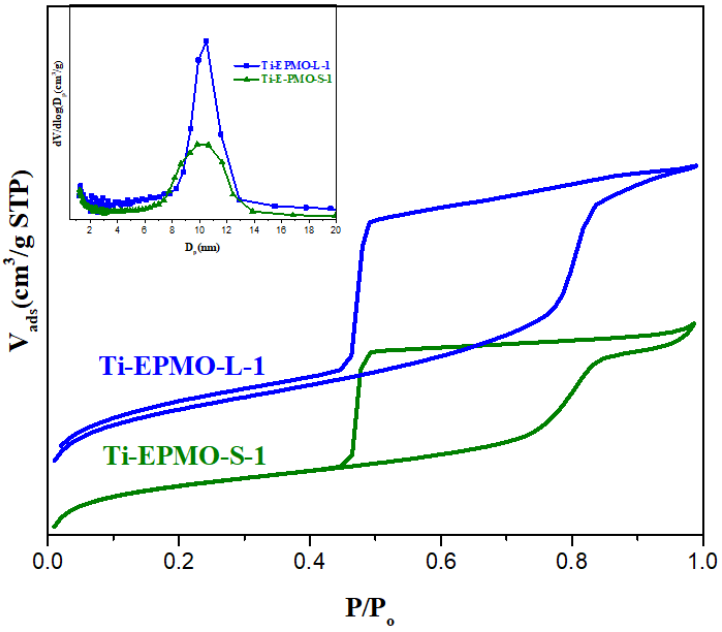

Figure 86. N_2 adsorption-desorption isotherm and BJH pore size distribution (inset) of Ti-E-PMO-L-1 and Ti-E-PMO-S-1 materials

From the N_2 adsorption-desorption results, both materials show type IV isotherms. The hysteresis loop is very large when compared to the parent materials synthesized without pore expander. This indicates the presence of pores larger than the parent one. The hysteresis loops of both materials seem to be of the H2 (a) type, indicating the presence of partially blocked pore mouths or bottlenecks. BJH pore size distribution plot (Figure 86

(inset)) confirms the pore size of materials of both types is increased when compared to the same materials synthesized without pore expanders (Ti-PMO-L-1 and Ti-PMO-S-1). The structural and textural properties of both materials are summarized in Table 16. Both Ti-EPMO-L-1 and Ti-EPMO-S-1 have roughly similar unit cell dimensions and average pore diameter. However, Ti-EPMO-L-1 has higher pore volume and surface area due to its more ordered and uniform pore structure. The pore diameter of both materials is increased by an average value of 4 nm when compared to the parent materials, although its pore arrangement is less ordered.

As we can see from the scheme in Figure 78, we tried to synthesize PMO materials which have a relatively high content of Ti in the final material by increasing the Ti-content in the synthesis gel (Ti/Si = 0.05 and 0.1) and by using titanocene dichloride as a titanium source. All materials were characterized by X-ray diffraction, TGA, N_2 adsorption-desorption isotherm, Inductively Coupled Plasma Optical Emission Spectroscopy (ICP-OES), DR UV-vis Spectroscopy, SEM and TEM.

Figure 87 (A & B) show the low angle and large angle XRD results of the calcined Ti-containing PMO type of materials. Figure 87 (A) shows that the hexagonal arrangement pore structure Ti-containing PMO materials are unaffected by the Ti content of the synthesis gel when using the P123 surfactant. However, when the Ti/Si ratio of the synthesis increases, there is an agglomeration of Ti-species (TiO_2 (anatase), observed in Figure 88 (A)). On the other hand, any attempt of *in situ* pore expansion and Ti-incorporation leads to the loss of the hexagonal structure of the material.

As shown in Figure 87 (B), the material which has been synthesized by using P104 surfactant, only the lowest content of Cl_2TiCp_2 in the synthesis gel (0.01 Ti/Si ratio; sample Ti-PMO-S-1) produced the hexagonally arranged pore structure. Any attempt to obtain higher loading of Ti with a short channel, or to expand pores by adding TIPB to the synthesis gel, resulted in less ordered mesoporous materials with foam type of porous structure having hindered access to the pore cavities. In our opinion, it may be the incorporation of a higher amount of organic groups ($-CH_2CH_2-$ and Cp) can result in a loss of the mesoscopic structure of the final material as a consequence of the distortion of the micelles. The pore wall amorphization (broad band) and the presence of agglomerated anatase (TiO_2) species on the surface of the material (sharp peaks) was observed in the large angle XRD measurements Figure 88 (A & B)).

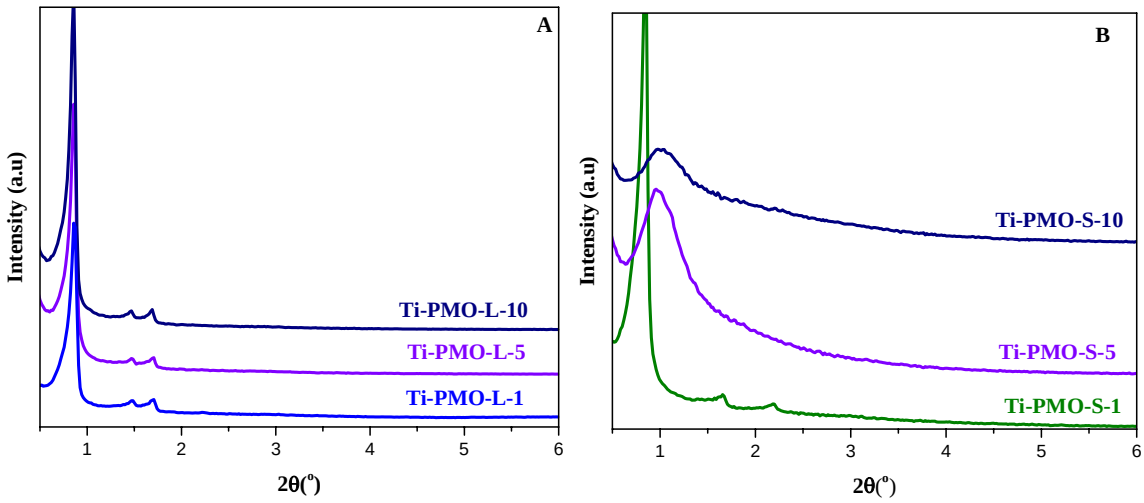

Figure 87. Low angle (A & B) of Ti-incorporated PMO materials by using P123 and P104 surfactants, respectively

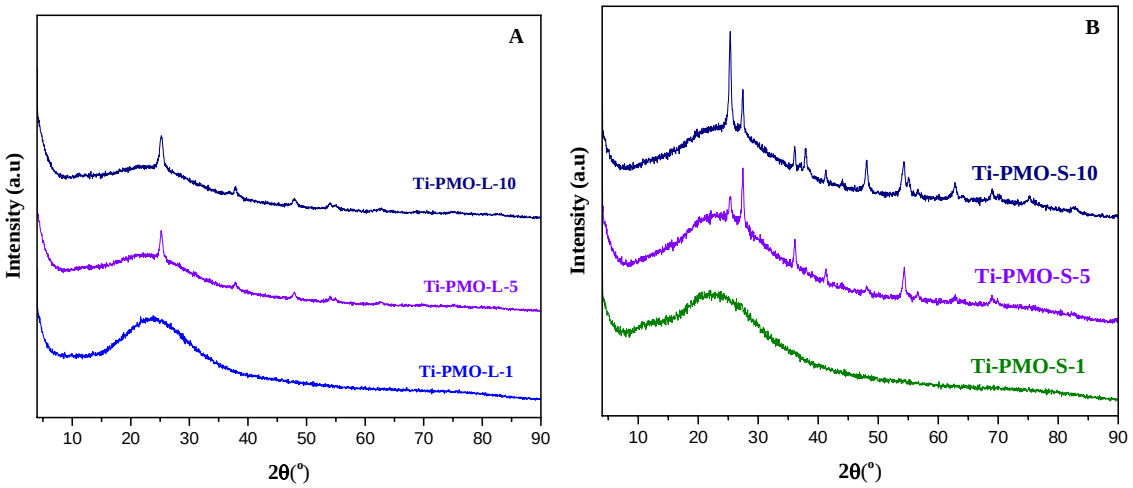

Figure 88. Large angle XRD (A & B) of Ti-incorporated PMO materials by using P123 and P104 surfactants, respectively

In order to create porosity, the surfactant has been removed from the final material by calcination at 350 ^{o}C for 5 h. Calcination at this temperature also promote the removal of cyclopentadienyl to create acidic Ti (IV) center and to avoid steric hindrance. The TGA profile of selected Ti-containing PMO materials before and after calcination is given in Figure 89 (A and B).

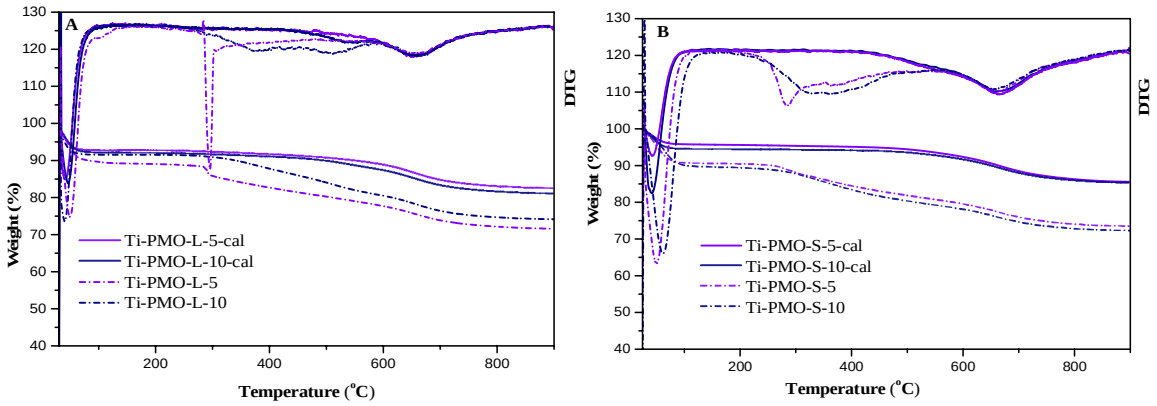

Figure 89. TGA profiles of selected Ti-containing PMO materials of before and after calcination

Table 17.The weight loss in different temperature ranges for Ti-containing PMO materials

Catalyst	Weight loss (%) in different temperature ranges				
	< 150 ^{o}C	150 – 450 ^{o}C	450 – 580 ^{o}C	580 - 780 ^{o}C	>780 ^{o}C
Ti-PMO-L-5	10.82	7.78	3.15	5.89	0.75
Ti-PMO-L-5-cal	7.35	1.45	1.9	6.13	0.7
Ti-PMO-L-10	8.03	6	4.91	6.19	0.7
Ti-PMO-L-10-cal	8.03	1.43	2.7	6.11	0.71
Ti-PMO-S-5	9.51	7.55	3.03	5.72	0.8
Ti-PMO-S-5-cal	4.31	0.81	2.02	6.29	0.99
Ti-PMO-S-10	10.48	7.99	3.05	5.58	0.72
Ti-PMO-S-10-cal	5.6	0.5	1.81	5.97	0.87

Figure 89 (A & B) shows the TGA profiles of Ti-containing PMO materials which have been synthesized using P123 and P104 surfactants. The TGA of each sample before and after calcination is plotted for comparison purposes. The weight loses of all samples in Figure 89 (A & B), in different temperature ranges are given in Table 17. The weight losses below 150 ^{o}C for all samples is due to the loss of physically adsorbed water or ethanol residue that remain in the washing step. The weight losses in the temperature range of 150 – 450 ^{o}C for all samples is due to the removal of the surfactant molecules. This weight losses are very low for calcined samples, confirming the removal of the surfactant during the calcination process. The weight losses in the temperature range of 450 – 580 ^{o}C for all samples may be due to the removal of the cyclopentadienyl group which is coordinated with Ti species and dehydroxylation of surface hydroxyl groups. The weight losses in the

calcined samples is lower when compared to their corresponding non-calcined samples due to the removal of cyclopentadienyl molecules during calcination. The weight losses in the temperature range of 580 – 780 ^{o}C for all samples is due to the removal of the framework ethane (-CH_2CH_2-) groups and probably the dehydroxylation of surface hydroxyl groups. An equivalent amount of weight is removed in this temperature range for all materials before and after calcination. This indicates, calcination doesn't affect the framework of the material; it selectively removes the surfactant molecule. The small weight loss above 780 ^{o}C for all samples is due to the dehydroxylation of surface hydroxyl groups. In general, calcination at 350 °C for 5 h is an optimum condition to selectively remove surfactant molecules without affecting the framework of Ti-containing PMO materials.

The mesoporosity and textural properties of Ti-containing PMO materials were systematically studied by N_2 adsorption-desorption isotherms (Figure 90 (A & B)). The isotherms of all materials are type IV. The materials which have been synthesized using P123 surfactant (Figure 90 (A)), show type H1 hysteresis loop, which is often associated with porous materials consisting of well-defined cylindrical-like pore channels. However, the materials which have been synthesized by using P104 show different types of hysteresis loop (Figure 90 (B)). The isotherm of Ti-PMO-S-5 sample shows type H3 hysteresis loop, which is often associated with porous materials with non-rigid aggregates of plate-like particles. The isotherms of Ti-PMO-S-10 show H4 type hysteresis loop, which is often associated with porous materials that have mesopores with narrow pore diameter and made from aggregated crystals. This fact is also confirmed by BJH pore size distribution (Figure 90 (A & B, inset)). The actual pore size in each sample (Table 18) varies upon the purity and degree of the structuring of the samples.

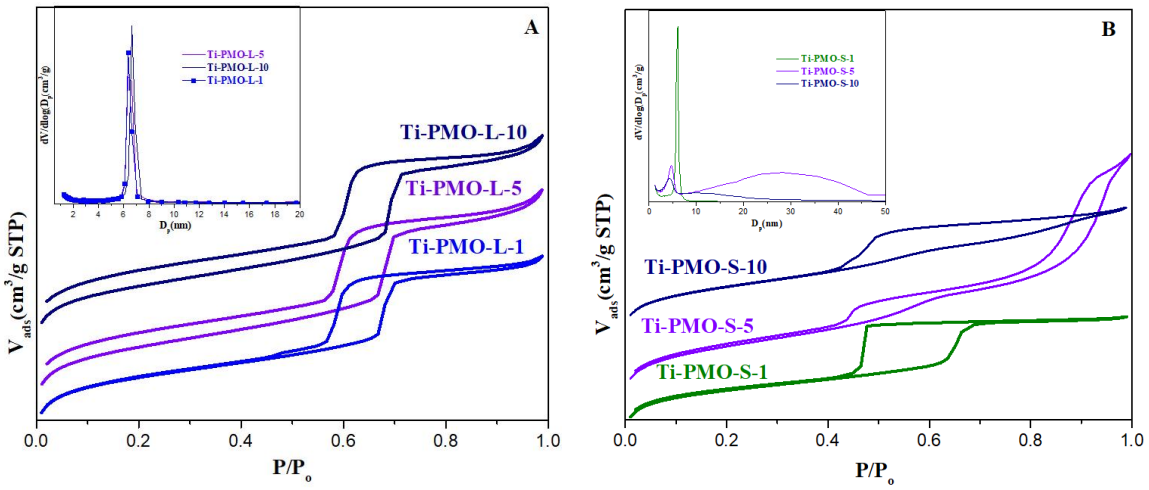

Figure 90. N_2 adsorption-desorption isotherm and BJH pore size distribution (inset) (A) using P123 and (B) using P104 for Ti-containing PMO materials

All the Ti-containing PMO materials have narrow pore diameters (< 7 nm), which is shown in Table 18. This may hinder the diffusion of bulky vernonia oil and its product epoxidized vernonia oil. As a result, further investigation of Ti-containing large pore size material is necessary. In general the difference of structural and textural properties among materials may be due to their difference in purity.

Table 18. Structural and textural properties of the Ti-containing PMO materials

Catalyst	a_0 (nm)	Pore size (nm)	Pore wall (nm)	Ti (wt. %)	Pore volume (cm^3/g)	S_{BET} (m^2g^{-1})
Ti-PMO-L-1	11.0	6.6	4.4	0.23	0.79	748
Ti-PMO-L-5	11.0	6.7	4.3	3.04	0.94	795
Ti-PMO-L-10	11.2	6.8	4.4	4.59	0.90	755
Ti-PMO-S-1	12.1	6.1	6	0.62	0.59	640
Ti-PMO-S-5	10.3	4.8	5.5	3.34	1.05	686
Ti-PMO-S-10	10.1	4.5	5.6	6.60	0.59	618

The amount of Ti found in the final material was quantified by ICP-OES and the results given in wt. % in Table 18. In both types of materials, high amount of Ti was incorporated. The type of Ti-species which is present in the final material of Ti-containing PMO materials of both types are studied by DR UV-vis spectroscopy (Figure 91 (A & B)). The DR UV–vis spectra of all the samples show a band at 200 – 230 nm, due to the presence of isolated T_d Ti (IV) species. This absorption band could be assigned to a charge transfer from the oxide ion (O^{2-}) to a central Ti (IV) ion (Ti^{4+}) with tetrahedral coordination in isolated species. However, the band intensity in this wavelength range is significantly different among the samples, this may be due to the difference of the amount of T_d Ti (IV) species found in the final material of each sample. Although more Ti is incorporated into the channel walls of the samples (Table 18) prepared with both types of surfactants, their quality is decreased due to the heterogeneity of the sample in terms of Ti species (Figure 88 (A & B), large angle XRD and Figure 91 (A & B), DR UV-vis) and the material

synthesized with P104 also loses its structure. This may limit the accessibility of the active sites.

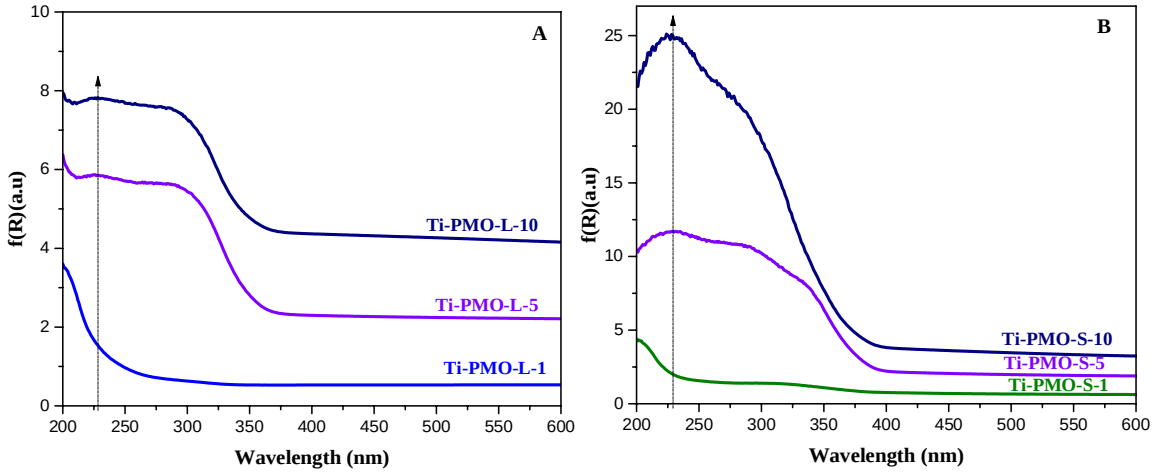

Figure 91. DR UV-vis spectra of Ti-containing PMO type of materials by using (A) P123 (B) P104 surfactants

Figure 91 (A and B) show the DR UV–vis of the samples obtained in the presence of Pluronic P123 and Pluronic P104. When the Ti loading increases, the absorption band intensity also increases due to the incorporation of a high amount of Ti (IV) isolated sites, shifting the band towards $\lambda \geq 230$ nm indicates an extension of the coordination number to five or six. The shoulders observed between 300 - 350 nm, showed the presence of anatase TiO_2-like clusters as observed in the large-angle XRD measurements in Figure 88 (A & B). Like in the SBA-15, the same thing happens in PMO, the incorporation of Ti in the T_d structure is more efficient when using Pluronic P104 surfactant. However, the material loses its structure due to the high incorporation of T_d Ti (IV) in the framework. When using Pluronic P123 less amount of Ti incorporated in the framework retained its structure and agglomeration of TiO_2 species when increasing the Ti content in the synthesis gel.

The particle morphology of Ti-containing PMO materials was evaluated systematically by scanning electron microscopy. Figure 92 shows the SEM micrographs of selected catalysts obtained with different channel length and particle morphology.

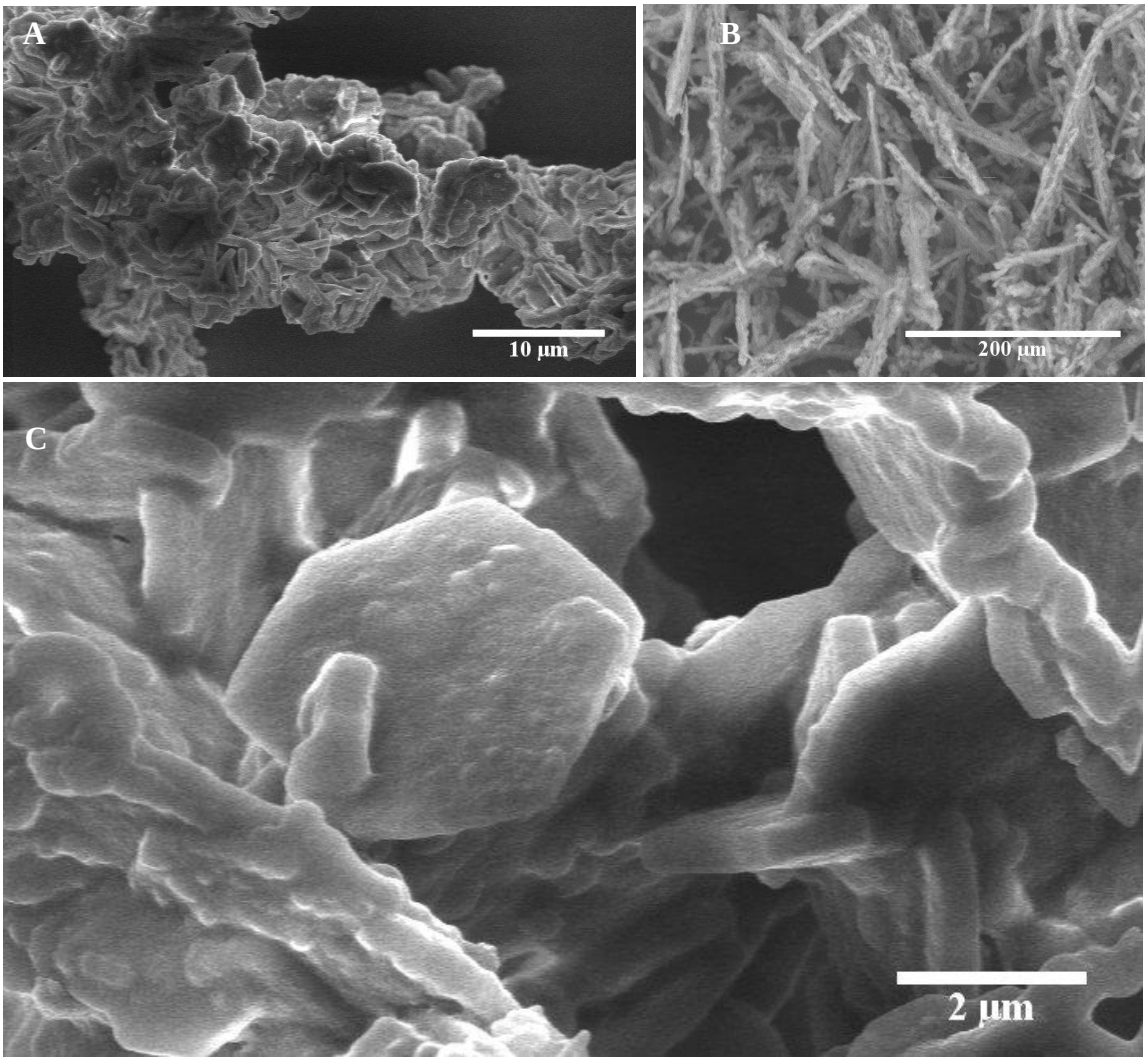

Figure 92. SEM images of selected Ti-containing (A & C) Ti-PMO-S-1 and (B) Ti-PMO-L-5 materials

Figure 92 (A & C) shows Ti-containing PMO material with hexagonal plate-like particle morphology was synthesized by using the Pluronic P104 surfactant. The particles have on average 4 µm diameter with 530 nm channel length. This short path length is convenient

to improve the diffusion of reagents during the reaction. However, when Pluronic P123 surfactant was used, materials with conventional fiber-like particle morphology were synthesized. This indicates Pluronic P104 is a suitable surfactant to produce Ti-containing PMO materials with short path length.

The orientation of the channels' alignment within the crystals was verified by TEM. Figure 93 (A and B) shows a typical image of Ti-PMO-S-1 material. This TEM study confirms Ti-PMO-S-1 material has ordered pore structure and short channel length (~ 550 nm), as we have discussed in its SEM image.

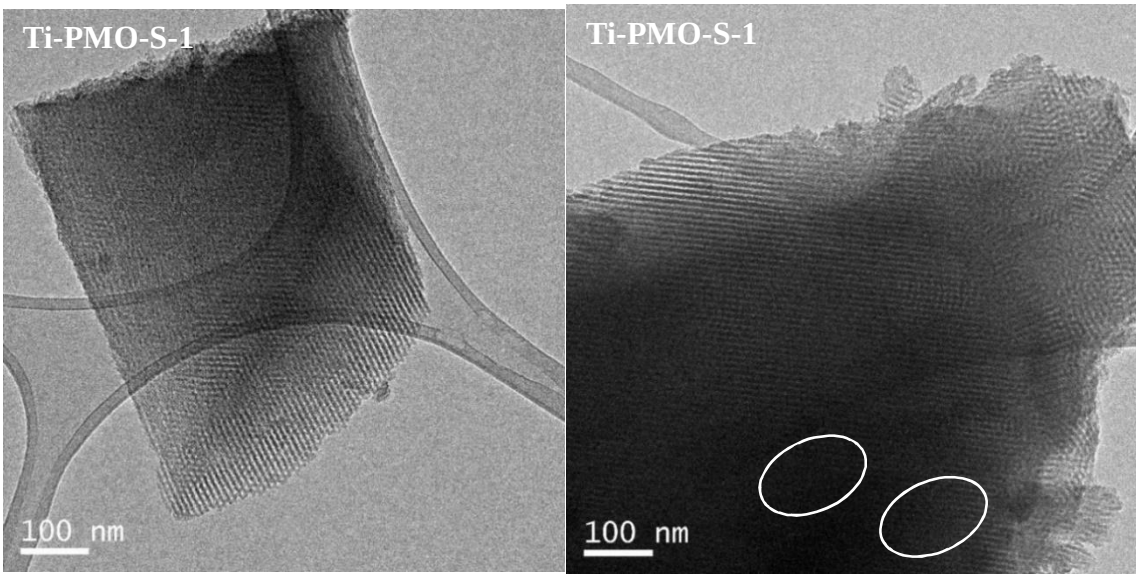

Figure 93. TEM images of calcined Ti-PMO-S-1 material

We tried to increase the Ti content in the final material by using the Ti/Si ratio of the synthesis gel 0.05 during the synthesis of large pore size PMO materials (in the presence of TIPB micelle expander) as it is shown the scheme in Figure 78.

Figure 94 (A and B) shows the low angle XRD results of the calcined Ti-containing large pore size PMO type of materials. In both types of materials, any attempt of *in situ* pore

expansion and Ti-incorporation loses the hexagonal structure of the material. Only the main peak of 100 appears the two weak peaks of 110 and 200 are not well resolved. Any attempt to obtain higher loading of Ti with a short channel, or to expand pores by adding TIPB to the synthesis gel, resulted in less ordered mesoporous materials with foam type of porous structure having hindered access to the pore cavities. In our opinion, it may be the incorporation of a higher amount of organic groups (-CH_2CH_2- and Cp) that can result in a loss of the mesoscopic structure of the final material as a consequence of the distortion of the micelles.

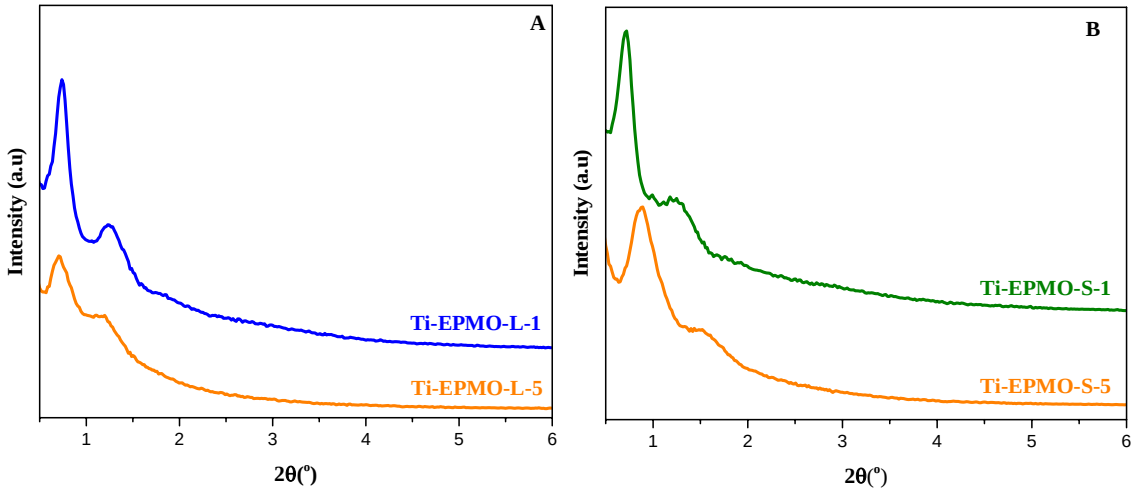

Figure 94. Low angle (A & B) of Ti-containing large pore size PMO materials by using TIPB micelle expander and P123 and P104 surfactants

Both materials are also characterized by large angle XRD measurements to study the homogeneity of Ti-species (whether anatase TiO_2 species are formed or not during the Ti-incorporation process). Ti-EPMO-L-5 in Figure 95 (A) shows only the broadband due to its amorphous pore wall and it is free from anatase species. However, the presence of sharp peaks in Ti-EPMO-S-5 material in Figure 95 (B) indicates the presence of anatase TiO_2

species on the surface of the material confirms the heterogeneity of Ti-species in this material.

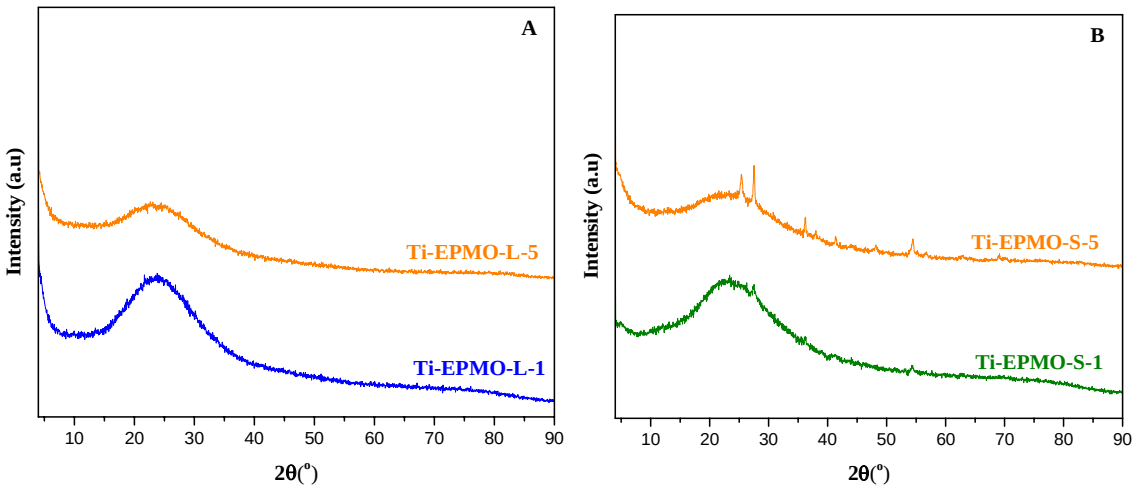

Figure 95. Large angle XRD (A & B) of Ti-containing large pore size PMO materials by using TIPB micelle expander and P123 and P104 surfactants

The TGA profile of large pore size Ti-containing PMO materials before and after calcination is given in Figure 96 (A and B).

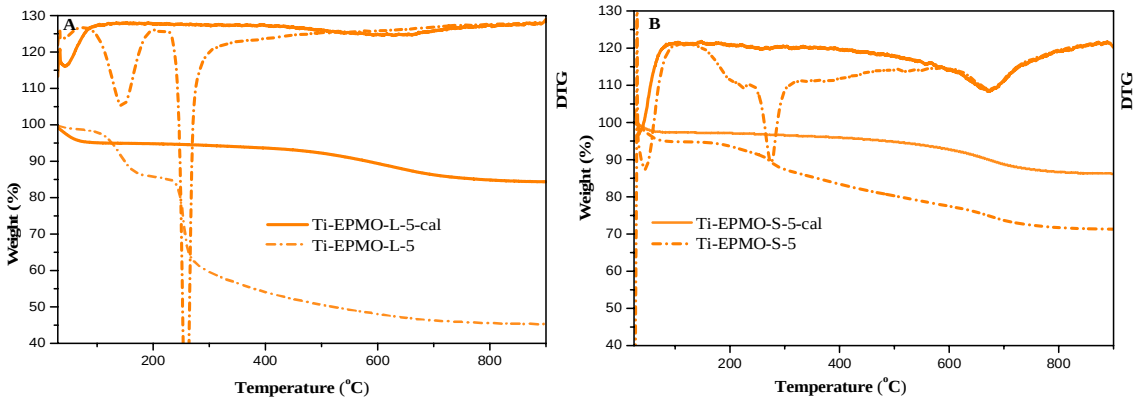

Figure 96. TGA profiles of Ti-EPMO-L-5 and Ti-EPMO-S-5 materials before and after calcination

Table 19.The weight loss in different temperature ranges for large pore size Ti-containing PMO materials

Catalyst	Weight loss (%) in different temperature ranges			
	< 150 ^{o}C	150 – 450 ^{o}C	450 – 780 ^{o}C	>780 ^{o}C
Ti-EPMO-L-5	10.17	37.84	6.54	0.37
Ti-EPMO-L-5-cal	5.07	1.78	8.1	0.65
Ti-EPMO-S-5	5.34	12.95	9.78	0.61
Ti-EPMO-S-5-cal	2.82	1.79	8.55	0.67

Figure 96 (A & B) and Table 19 show the TGA profiles of large pore size Ti-containing PMO materials and the weight losses in different temperature ranges. The weight losses below 150 ^{o}C for all samples is due to the loss of physically adsorbed water or ethanol residues that remain in the washing step. The weight loss in the temperature range of 150 – 450 ^{o}C for all samples is due to the removal of the surfactant molecules. The very small weight losses for calcined samples in this temperature range confirms the calcination process is effectively removes the surfactant molecule. The weight losses in the temperature range of 450 – 780 ^{o}C for all samples may be due to the removal framework ethane (-CH_2CH_2-) group, Cp groups probably coordinated the framework Ti (IV) active sites and dehydroxylation of surface hydroxyl groups. In this temperature range the weight losses for each sample before and after calcination are comparable. This indicates the framework ethane group is unaffected in the calcination process. The small weight loss above 780 ^{o}C for all samples is due to the dehydroxylation of surface hydroxyl groups. The mesoporosity and textural properties of Ti-containing PMO materials were systematically

studied by N_2 adsorption/desorption isotherm (Figure 97 (A and B)). The isotherms of both materials are type IV with H3 type hysteresis loop, which is often associated with porous materials with non-rigid aggregates of plate-like particles. As we can see from the BJH pore size distribution (Figure 97 (A & B, inset), the pore diameter is increased to 7 – 8.5 nm when the material is synthesized with TIPB micelle expander and with a Ti/Si ratio of synthesis gel 0.05 (Ti-EPMO-S-5 & Ti-EPMO-L-5). The pore size is not significantly increased. This may be due to the interaction of the TIPB with the cyclopentadienyl group of the titanocene dichloride on the interface of the micelle. This may hinder the interaction of TIPB with the center of the micelle, as a result the pore diameter is not significantly increased. However, the pore size is significantly increased when using less amount of Ti source in the synthesis gel (Ti/Si = 0.01) (Table 20).

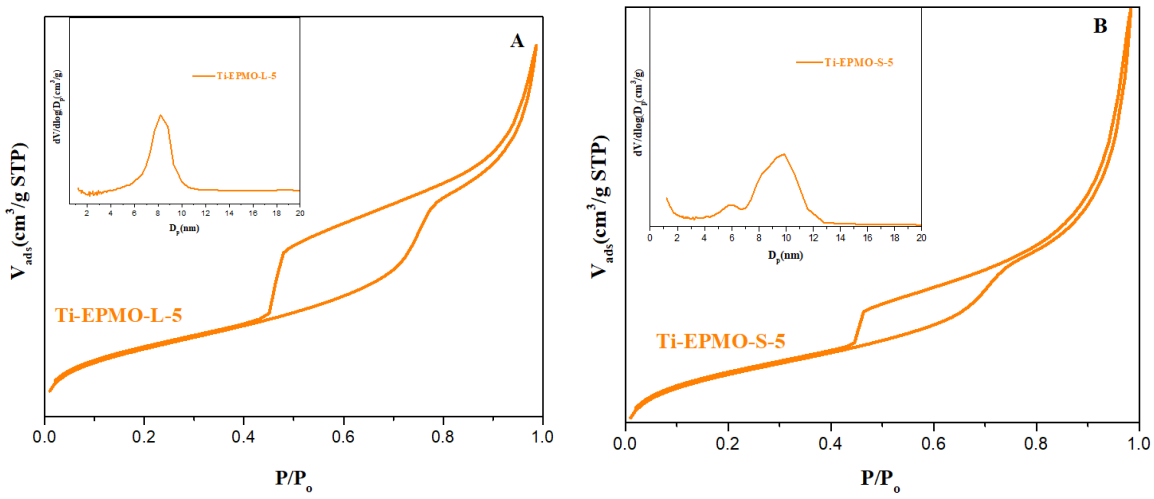

Figure 97. N_2 adsorption-desorption isotherm (A & B) and BJH pore size distribution (inset) of Ti-EPMO-L-5 and Ti-EPMO-S-5 materials

Table 20. Structural and textural properties of the large pore size Ti-containing PMO materials

Catalyst	a_0 (nm)	Pore size (nm)	Pore wall (nm)	Ti (wt. %)	Pore volume (cm^3/g)	S_{BET} (m^2g^{-1})
Ti-EPMO-L-1	13.7	10.8	2.9	-	1.16	826
Ti-EPMO-L-5	13.1	8.5	4.5	0.71	1.10	666
Ti-EPMO-S-1	14.0	11.0	3.0	-	0.66	593
Ti-EPMO-S-5	11.4	7.1	4.3	3.39	1.62	833

The bulk Ti content in the calcined materials of both types has been quantified by ICP-OES and is given in wt. % (Table 20). In the Ti-EPMO-S-5 sample higher amount of Ti was loaded when compared to Ti-EPMO-L-5 may be due to the difference the surfactants used during the synthesis. The type of Ti-species which is present in the final material of both types is studied by DR UV-vis Spectroscopy (Figure 98 (A & B)).

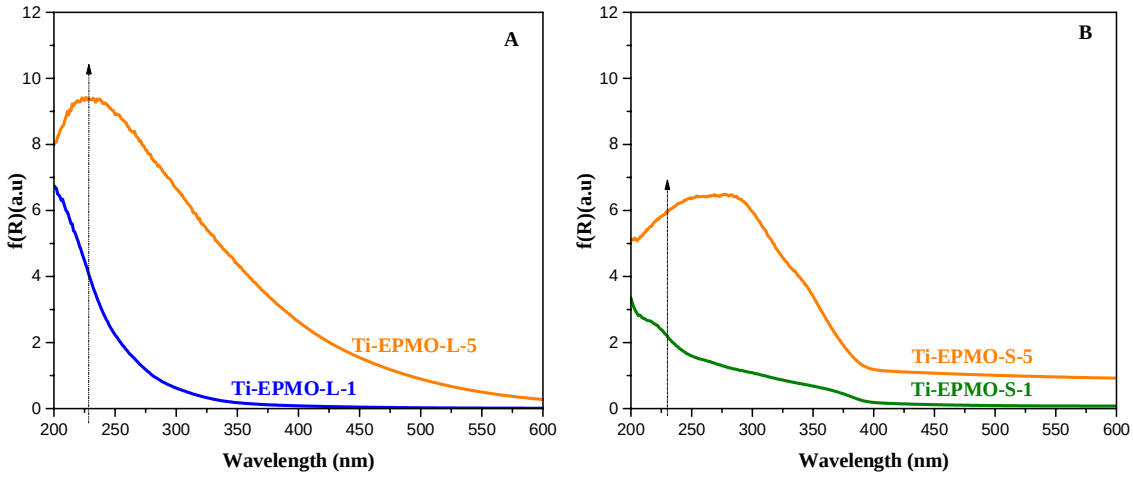

Figure 98. DR UV-vis of Ti-containing PMO type of materials by using (A) P123 (B) P104 surfactants

When the Ti/Si ratio of the synthesis gel increases, the DR UV-vis absorption band intensity also increases due to the incorporation of a high amount of Ti (IV) isolated sites, shifting the band towards $\lambda \geq 230$ nm indicates an extension of the coordination number to five or six. The shoulders observed between 300 - 350 nm, showed the presence of anatase TiO_2-like clusters as observed in the large-angle XRD measurements in Figure 95 (B). The small amount of Ti content in the final material when using the P123 surfactant (Ti-EPMO-L-5), however better band intensity in the range of 210 - 230 nm band due to the presence of a higher number of isolated Ti (IV) species. On the other hand, the use of TIPB micelle expander in the presence of Pluronic P104 allowed incorporating higher amount of Ti (see Table 20), although in a very broad range of coordination stages (210 – 400 nm) due to the presence of different types of Ti-species (it seems less number of T_d Ti (IV) species with high amount of five or six coordinated and TiO_2 anatase species. Therefore, the Ti-species found in Ti-EPMO-L-5 material seem more homogenous.

The particle morphology of Ti-containing Ti-EPMO-L-5 and Ti-EPMO-S-5 were evaluated systematically by scanning electron microscopy (Figure 99). Both materials have similar particle morphology, an aggregation of small particles.

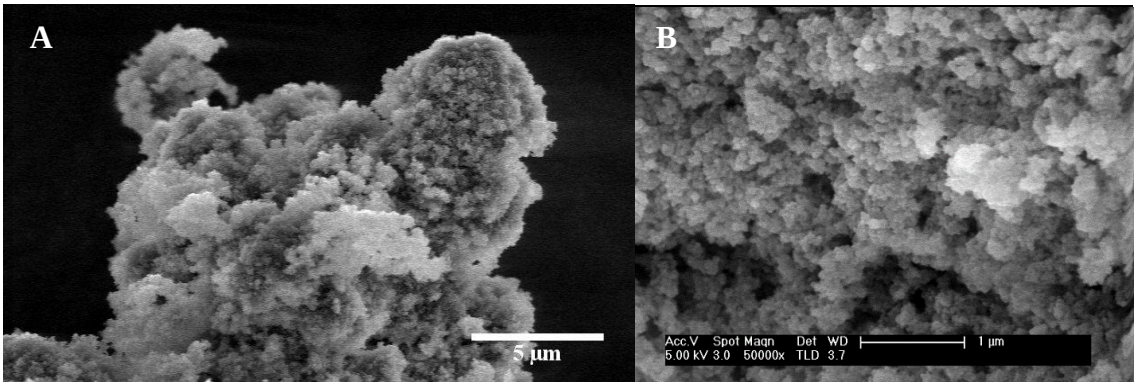

Figure 99. SEM images of (A) Ti-EPMO-L-5 (B) Ti-EPMO-S-5 materials

The internal structure of both materials were verified by TEM. TEM images of Ti-EPMO-L-5 and Ti-EPMO-S-5 (Figure 100 (A & B) show both materials have moderately ordered structure and the presence of some anatase crystal growths are also observed in Ti-EPMO-S-5 material.

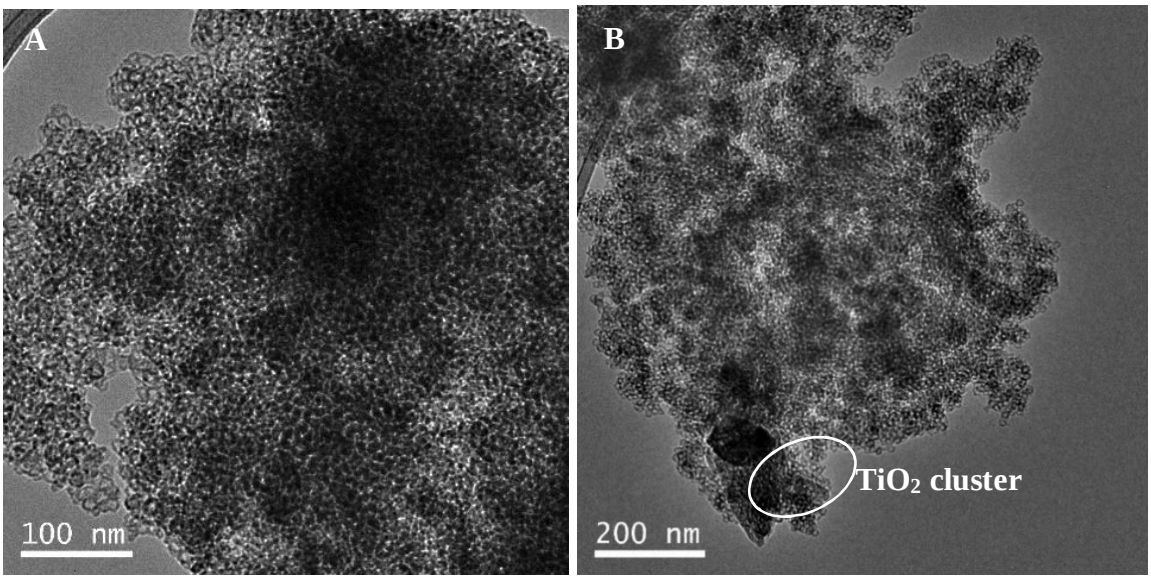

Figure 100. TEM images of Ti-EPMO-L-5 (A) and Ti-EPMO-S-5 (B) materials

Summary

- ✓ Ti-containing PMO type ordered mesoporous materials with an isolated T_d Ti-species environment were prepared in a direct synthesis method.
- ✓ Ti-containing PMO materials which have hexagonal pore arrangements with conventional fiber like particle morphology and different Ti-content were synthesized by using P123 surfactant and by varying the Ti/Si ratio of the synthesis gel.
- ✓ Ti-containing PMO material which has hexagonal pore arrangement with hexagonal plate-like particle morphology and 530 nm channel length was synthesized by using the Pluronic P104 surfactant and the Ti/Si ratio of the synthesis gel is 0.01.

- ✓ Moderately ordered Ti-containing PMO material with a large pore size (8.5 nm) and isolated T_d Ti (IV) species was synthesized by using Pluronic P123 surfactant, TIPB micelle expander and Ti/Si ratio of the synthesis gel is 0.05.
- ✓ Ti content above 2-2.5 wt%, polymeric TiO_2-like species are formed together with isolated Ti species.
- ✓ Optimization of the synthesis condition of Ti-containing PMO material which has ordered pore structure, high content T_d Ti (IV) species (> 2 wt. %), controlled particle morphology and large pore diameter (> 8 nm) needs further investigation.

CHAPTER FIVE

5. CATALYTIC APPLICATIONS

5.1. Epoxidation of cyclohexene

The oxidation of cyclohexene with anhydrous tert-Butyl hydroperoxide was employed as a test reaction to evaluate the catalytic activity of the synthesized materials. Figure 101 illustrates some of the typical products of cyclohexene oxidation. The 1, 2-epoxycyclohexane, generated by the heterolytic epoxidation of the cyclohexene double bond, and the 1, 2-cyclohexanediol side product, formed by hydrolysis of the epoxide ring, generally reflect a concerted process. In contrast, the allylic oxidation side products, 2-cyclohexen-1-one and 2- cyclohexen-1-ol, are often ascribed to a homolytic radical pathway [134, 135].

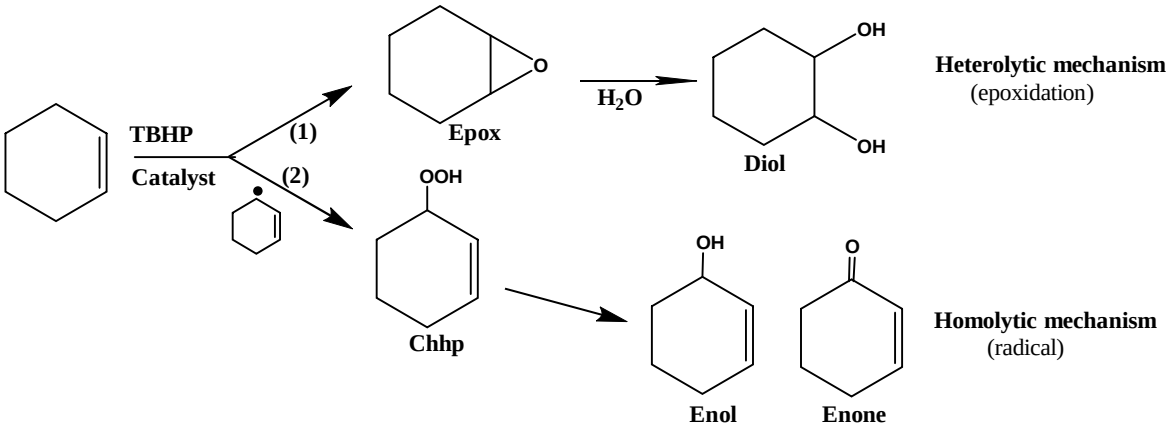

Figure 101. Reaction routes in the oxidation of cyclohexene according to the possible mechanisms of O – O bond breaking in the TBHP molecule

Currently, epoxide chemicals, which are produced by epoxidation of olefinic organic groups, have become considerably more vital, valued and useful intermediates in industrial

organic synthesis. Among epoxides, 1, 2-epoxycyclohexane, which could be synthesized by epoxidation of cyclohexene is an attractive chemical intermediate with multiple applications. For example, an alicyclic molecule, which is synthesized from 1, 2-epoxycyclohexane, used to produce pesticides, plant-protection agents, pharmaceuticals, perfumery, and dyestuffs in industry. Various authors studied the catalytic performance of Ti-containing microporous and mesoporous catalysts in the oxidation reaction of cyclohexene using hydrogen peroxide (H_2O_2) as an oxidant. H_2O_2 is commercially available at low cost, has a small molecular size, i.e. could be easily diffused in the channels of microporous materials and it is a green oxidant, i.e. its byproduct is only H_2O. However, H_2O_2 gives low epoxide selectivity due to ring-opening reaction facilitated by the byproduct H_2O. Besides, it facilitates the leaching of Ti from the support. Furthermore, the byproduct H_2O competes with the reagents in its approach to titanium ions in the transition state and its ease to migrate through the channels of the catalyst decreases the activity of the catalyst. Therefore, the oxidation process is prevented in the presence of water given its competition with cyclohexene molecules (considerably less polar) to cross the hydrophilic channels of the material. As a result, the catalyst may lose its activity irreversibly after only one cycle of reaction[136]. Appropriate selection of oxidants is necessary to improve the conversion and yield of the target products when using Ti-containing ordered mesoporous materials as catalysts. According to Xie *et al.*[137], Ti-MCM-41 and Ti-SBA-15 materials show better catalytic activity and epoxide selectivity in reactions when using tert-Butyl hydroperoxide (TBHP) rather than aqueous H_2O_2. Thus, in this study TBHP is used as an oxidant due to its many advantages, such as its stability, mild oxidation, non-corrosive, non-hazardous properties and good compatibility with alkenes,

which provide high activity. The diffusion problem of this molecule could be improved by controlling the catalyst's pore diameter and particle morphology.

Reaction mechanisms: it is widely accepted that the isolated Ti centre of titano-silicates needs to be coordinated in a specific geometry in order to be catalytically active. The catalytic mechanism, however, has been a topic of controversy and much debate. The mechanism of alkene epoxidation by titano-silicates was further investigated by Notestein *et al.* via theoretical and experimental studies (Figure 102). They describe a general catalytic mechanism, applicable for titano-silicates of the TS-type, and other catalysts with isolated Ti centres with 4-fold coordination.

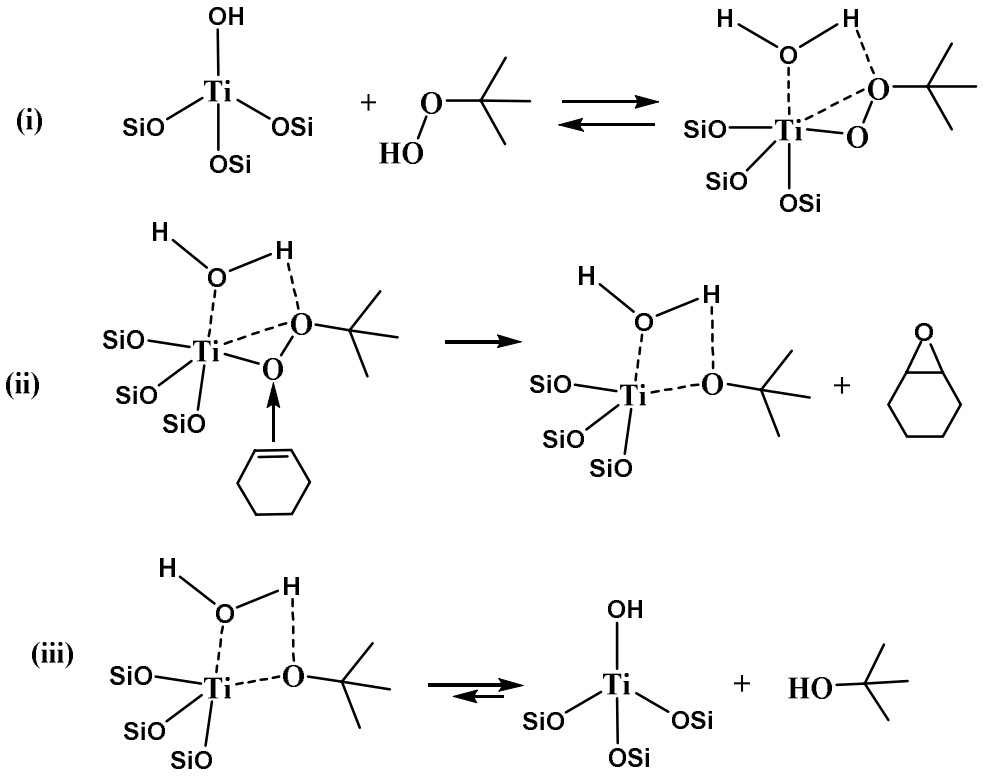

Figure 102. Mechanism of alkene epoxidation by titano-silicates according to Notestein *et al.* (A)[138]

According to this catalytic mechanism, described with TBHP as oxidant, there are three basic steps: (1) reversible coordination of hydroperoxide to the Ti active site, (2) electrophilic attack of alkene to O1 oxygen in bound peroxide, and (3) dissociation of alcohol by-products.

The titanium peroxide, Ti(OOR), which is proposed as active intermediate is exotic, as the titanium is coordinated with both oxygen atoms. The double bond on the olefin directly attacks the activated oxygen atom of the Ti(OOR), the titanium complex removes the oxygen atom as an epoxide and leaves a titanium alkoxide behind.

5.1.1. Results and discussion on epoxidized cyclohexene

The epoxidation of cyclohexene can be catalyzed over isolated T_d Ti species in Ti-containing ordered mesoporous materials[139]. The type of Ti-species and their concentration on the catalyst pore surfaces affect the conversion of cyclohexene and selectivity of the epoxide formation. Here, we are able to control the environment and concentration of Ti on the ordered mesoporous silica surfaces. Ti-containing materials, which have been synthesized using only Ti/Si ratio of the synthesis gel 0.01 regardless of the type of Ti source and surfactant used have not been tested in epoxidation of cyclohexene due to the presence of a very low amount of T_d Ti (IV) species (weak absorption bands in UV-vis). The catalytic activity of the synthesized Ti-containing SBA-15 and Ti-containing PMO materials prepared via co-condensation using Ti/Si ratio of the synthesis gel 0.05 and 0.1 were evaluated in the epoxidation of cyclohexene with TBHP as the oxidant as a reaction test, allowing us to select the best catalysts for the epoxidation of vernonia oil (chapter 5.2). Table 21 shows the catalytic results achieved with SBA-15 materials functionalized with

different loading of Ti and different particle morphology. The catalytic assay using pure silica SBA-15 material has also been included as blank.

Table 21. Catalytic results in the epoxidation of cyclohexene with TBHP in the presence of Ti-containing SBA-15 materials

Run[a]	Catalyst	Ti[b] (wt %)	Initial reaction rate (mmol/h)[c]	Conversion[d] (%)	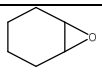	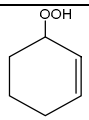	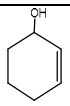	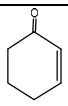	TON[e]
1	SBA-15[f]	-	-	5.04	6.2	23.5	16.7	53.5	-
2	Ti-SBA-L-5	1.25	0.69	19.05	86.9	4.7	3.3	5.0	77
3	Ti-SBA-L-10	2.97	0.35	13.47	81.6	8.9	4.7	4.7	21
4	Ti-SBA-S-5	2.83	0.67	21.39	88. 5	2.5	4.5	4.4	39
5	Ti-SBA-S-10	5.51	0.51	22.1	88.6	2.9	3.9	4.5	21
6	Ti-ESBA-L-5	2.25	0.19	11.77	60.9	3.5	9.7	25.7	19
7	Ti-ESBA-S-5	0.22	0.34	15.62	76.5	2.9	5.9	14.5	322
8	Ti-ESBA-S-10	0.52	0.38	18.27	68.1	3.7	8.9	19.2	140

[a] Reactions carried out using catalyst to substrate mass ratio of 1:10 and TBHP to cyclohexene molar ratio of 1.1:1, 70 ºC, 24 h.
[b] Ti content in weight by ICP.
[c] Estimated from the cyclohexene conversion level measured within the first 2 h of reaction.
[d] cyclohexene conversion calculated by the total addition of the yields of the resultant products.
[e] Turnover number mole of epoxide produced per mole of Ti.
[f] Blank reaction performed in the absence of any catalyst.

All of the selected materials are catalytically active in the epoxidation of the cyclohexene under the employed reaction conditions. The products obtained are 1, 2-cyclohexene epoxide, 2-cyclohexenyl-1-hydroperoxide, 2-cyclohexen-1-ol, and 2-cyclohexen-1-one. Being 1, 2-cyclohexane epoxide the main product detected by gas chromatography (Figure

119, appendix) so that a very high percentage selectivity of the catalyst in the transformation of the olefin towards the oxirane has been assumed.

Pure silica SBA-15 materials produced only 0.3 % 1, 2-cyclohexane epoxide (5 % of cyclohexene conversion with 6 % of epoxide selectivity, Table 21). This result is due to the homogeneous oxidation reaction and is very low when compared to those obtained using the Ti-containing materials under the same reaction conditions.

Figure 103 shows the conversion versus time (A) and cyclohexene oxide selectivity versus conversion (B) of the reaction conducted with selected Ti-containing SBA-15 materials synthesized with different surfactants aiming to change the particle morphology, and different Ti/Si ratio to change the Ti-loading in the final material.

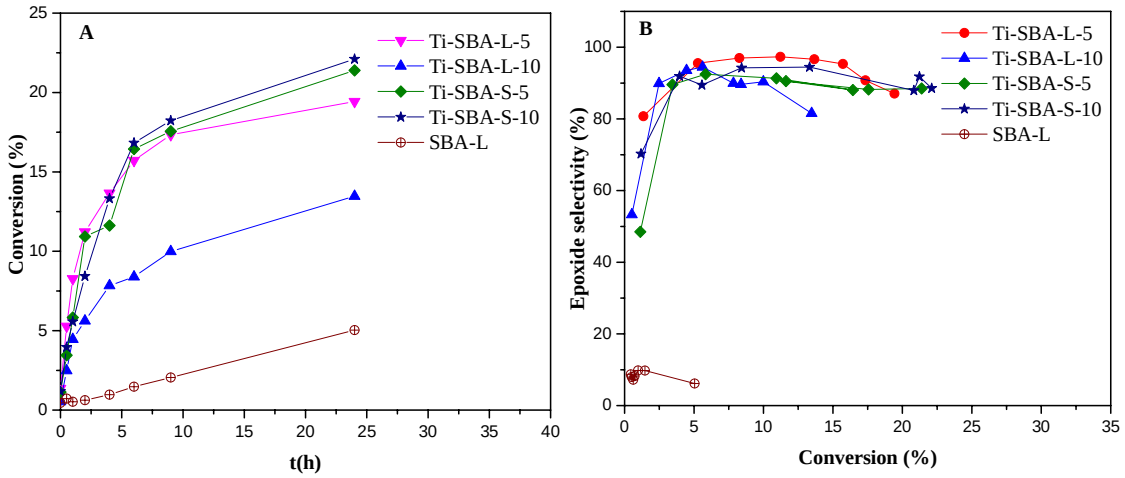

Figure 103. Reactions kinetics of cyclohexene conversion (A) and epoxide selectivity (B) in presence of Ti-containing SBA-15 catalysts under anhydrous conditions

When we compare the catalytic activity of "L" types Ti-containing SBA-15 materials in Figure 103 (Ti-SBA-L-5 and Ti-SBA-L-10), which have similar particle morphology i.e. both are fibers but different Ti-loadings in the final material i.e. Ti-SBA-L-5 (1.25 wt %) and Ti-SBA-L-10 (2.97 wt %), the former material (Ti-SBA-L-5) has high initial rate of

reaction after 2 h reaction and better conversion of cyclohexene after 24 h reaction. This is probably due to the presence of highly dispersed and accessible T_d Ti (IV) active sites on the mesopores surfaces of the channels of this material. Although higher Ti content is incorporated in the Ti-SBA-L-10 material, its accessibility maybe limited, i.e. more Ti may be incorporated in the walls of the micropores. This is probably due to the covering up of Ti with the thick amorphous pore wall of Ti-SBA-L-10. Different authors have reported that the catalytic activity of Ti-incorporated ordered mesoporous materials in epoxidation reaction could be affected by its amorphous pore wall thickness[18, 52]. Thus, the access of the reactants to Ti active sites could be partially hindered because of partial covering by the SBA-15 thick amorphous pore wall. However, when the Ti content is lower, the beneficial aspects of a more dispersed micro environment of Ti sites are noticeable, favoring the accessibility of the active sites towards the reagents and finally leading to an increase catalytic activity per Ti sites, overcoming the trouble of the covering of Ti species. As shown in Figure 103 (B), Ti-SBA-L-5 also has better epoxide selectivity than Ti-SBA-L-10 material, which may be attributed to the better accessibility of T_d Ti (IV) active sites that facilitate reaction in the heterolytic reaction mechanism (Figure 101). The Turnover Number (TON) of Ti-SBA-L-5 material (77) is higher than the Ti-SBA-L-10 ones (21). The TON values are calculated based on the total amount of Ti in the final titanosilica materials. This means that inaccessible Ti species within the pore walls are also included for the calculation.

When we compare the catalytic activity of “S” types of materials (Ti-SBA-S-5 and Ti-SBA-S-10) which have roughly similar particle morphology, i.e. both are platelets, but different Ti-loading in the final material, Ti-SBA-S-5 (2.83 wt %) and Ti-SBA-S-10 (5.51

wt %) have similar catalytic performance (Figure 103 and Table 21). Both materials (Ti-SBA-S-5 and Ti-SBA-S-10) have roughly similar catalytic activity in the rate of cyclohexene conversion and epoxide selectivity after 24 h reaction. However, we expect that the catalytic activity of Ti-SBA-S-10 material will be improved due to the presence of significantly higher Ti-loading and T_d Ti (IV)-species (UV-vis, Figure 70 (A)). This may be due to the presence of significant amounts of catalytically inactive anatase species (large angle XRD, Figure 64 (A) and SEM, Figure 67 (C)) in the Ti-SBA-S-10 material that hinder its catalytic activity. Furthermore, the presence of blocked pores or bottlenecks in Ti-SBA-S-10 material (desorption curve, Figure 66 (A)) may also hinder the accessibility of the Ti (IV) active sites. As a result, the TON of Ti-SBA-S-5 material (39) is significantly higher than the Ti-SBA-S-10 ones (21), although both materials have similar catalytic activity.

When we compare the catalytic activity of Ti-SBA-L-10 and Ti-SBA-S-5 materials which have equivalent Ti loading in the final material (2.97 and 2.83 wt %, respectively) and similar pore wall thickness (4.1 nm) (Table 12), the latter sample has a better catalytic performance. This may be due to its short channel platelets particle morphology of Ti-SBA-S-5 gives high surface area 842 m^2/g for the better accessibility of the Ti active sites than the Ti-SBA-L-10 material which has been discussed to have less efficient Ti species.

In general, all Ti-containing materials have very high selectivity of cyclohexene epoxide, although there is no significant difference due to the modification of the particle morphology from fibers to plates, which indicates that cyclohexene is too small to be affected by diffusion problems in these type of ordered mesoporous materials.

Despite this conclusion, we used the same catalytic activity to evaluate larger pore size catalysts in order to evaluate the efficiency in the surface location of isolated Ti active sites during the direct co-condensation synthesis procedure (*in situ* Ti-incorporation and pore expansion). Selected large pore size Ti-containing SBA-15 materials were also tested in the epoxidation of cyclohexene and the products obtained are given in Figure 104 and Table 21.

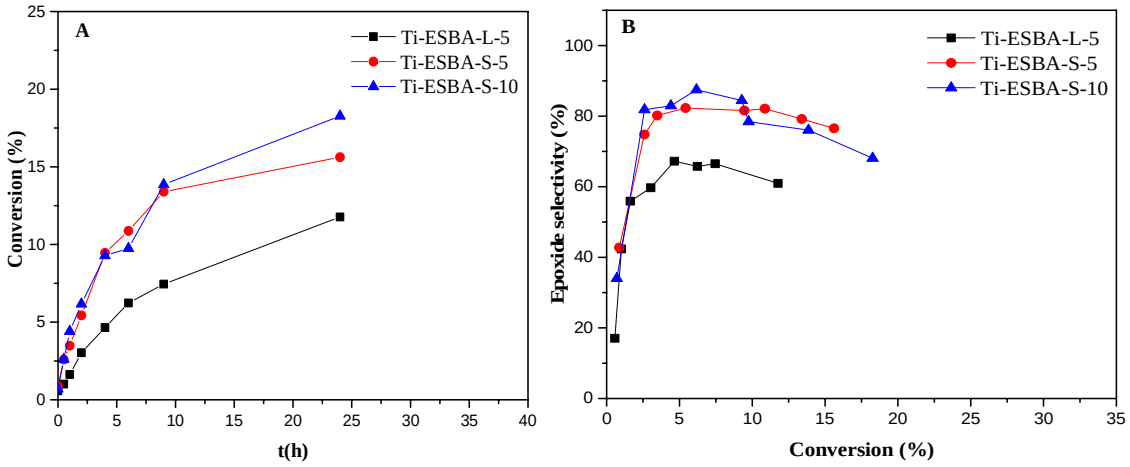

Figure 104. Reactions kinetics of cyclohexene conversion (A) and epoxide selectivity (B) in the presence of large pore size Ti-containing SBA-15 materials under anhydrous conditions

When we compare the catalytic activity of large pore size Ti-containing "S" type of materials (Ti-ESBA-S-5 and Ti-ESBA-S-10), which have similar particle morphology, i.e. both have short channel cylindrical like but different Ti-loading in the final material, i.e. Ti-ESBA-S-5 (0.22 wt %) and Ti-ESBA-S-10 (0.52 wt %), the latter material has better reaction rate in cyclohexene conversion due to the presence of relatively higher Ti-content with larger T_d Ti (IV) species (intense UV-vis band, Figure 77 (A)). However, the reaction rate is not as high as would be expected, this probably due to the less accessibility of Ti

(IV) active-sites by bottlenecks delay of diffusion of reagents. This fact also confirmed by its lower epoxide selectivity. The rate of reaction, as well as epoxide selectivity in Ti-ESBA-L-5, is too low this may be due to the presence of significant amounts of catalytically inactive anatase species.

The catalytic performance of large pore size Ti-containing SBA-15 materials is lower than their corresponding standard pore size materials due to the general lower Ti content and pore blockage. On the other hand, Ti-ESBA-L-5 does not exhibit a high catalytic performance despite the highest Ti loading; the Turnover Number (TON) is only 19. This is due to the presence of catalytically inactive anatase TiO_2 species (Figure 72 (B) and Figure 77 (B). This proved that P104 surfactant is more convenient than P123 to synthesize large pore size Ti-containing materials via co-condensation to improve their catalytic activity. This indicates that the type and concentration of Ti-species is very important rather than pore size of the support in such type of reaction because cyclohexene and TBHP could easily diffuse as well in the channel.

It is important to note that all catalysts demonstrate a high epoxide selectivity although there is a significant difference between the samples. In both “L” and “S” type of materials, the Ti/Si ratio of the synthesis gel 0.05 seem to be the optimum, further increasing the Ti/Si ratio does not have a significant value to the catalytic performance of the material. The UV-vis spectra of the materials given in the previous sections clearly show that in many cases, and in particular for Ti content above 2-2.5 wt%, a large fraction Ti(IV) is present in octahedral coordination and it is therefore no active for this reaction. It can be clearly seen according to the results collected in Table 21 that the TON values strongly decreases

as the Ti increase, which is in agreement with the nature of the Ti sites as derived from the UV-vis spectra.

Ti-containing PMO materials were also tested in epoxidation of cyclohexene under the same reaction conditions to study the effect of surface hydrophobicity on catalysis, although only the best Ti-PMO samples were selected based on the amount of T_d Ti (IV) species and degree of pore ordering. Table 22 collects the summary of all the samples tested and the results obtained.

Table 22. Catalytic results in the epoxidation of cyclohexene with TBHP in the presence of Ti-containing PMO materials

Run[a]	Catalyst	Ti[b] (wt %)	Initial reaction rate (mmol/h)[c]	Conversion[d] (%)	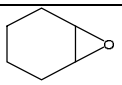	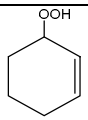	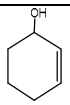	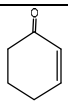	TON[e]
1	Ti-PMO-L-5	3.04	0.14	10.57	65.9	7.2	8.9	17.9	13
2	Ti-PMO-L-10	4.59	0.23	16.7	80.5	2.0	6.3	11.2	17
3	Ti-PMO-S-5	3.34	0.44	28.03	93.9	0.7	2.0	3.4	46
4	Ti-PMO-S-10	6.60	0.55	30.45	93.8	0.5	2.4	3.2	25
5	Ti-EPMO-S-5	3.39	0.24	18.81	66.1	3.4	7.5	23.0	22
6	Ti-EPMO-L-5	0.71	0.27	17.7	79.7	1.5	6.6	12.2	113

[a] Reactions carried out using catalyst to substrate mass ratio of 1:10 and TBHP to cyclohexene molar ratio of 1.1:1, 70 ^{o}C, 24 h.
[b] Ti content in weight by ICP.
[c] Estimated from the cyclohexene conversion level measured within the first 2 h of reaction.
[d] cyclohexene conversion calculated by the total addition of the yields of the resultant products.
[e] Turnover number mole of epoxide produced per mole of Ti.

Figure 105 plots the reaction results for samples of Ti-containing PMO materials prepared by using P123 and P104 surfactants and different Ti-loading in the final material.

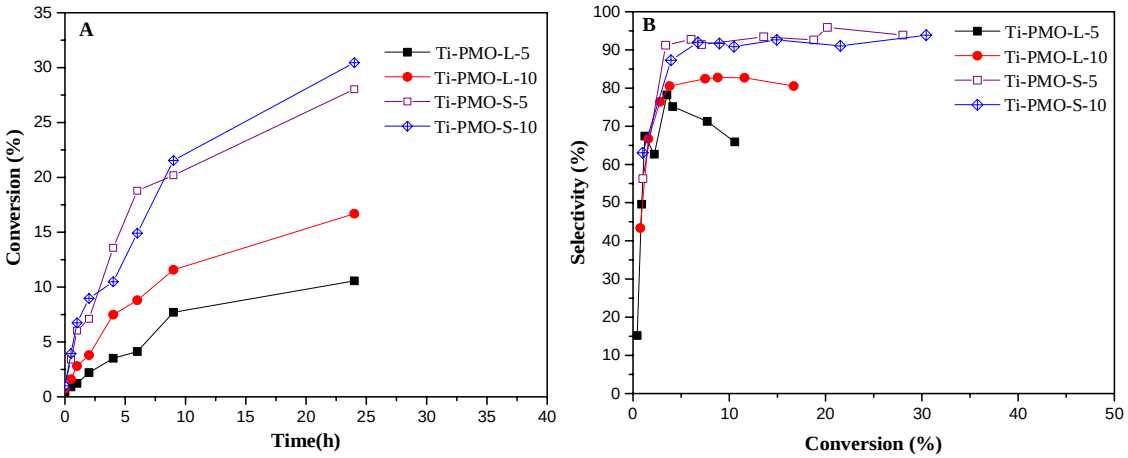

Figure 105. Reaction kinetics of cyclohexene conversion (A) and epoxide selectivity (B) in presence of Ti-containing PMO materials under anhydrous conditions

When we compare the catalytic activity of "L" types of Ti-containing PMO materials (Ti-PMO-L-5 and Ti-PMO-L-10), which have similar particle morphology i.e. both are fibers (Figure 92 (B)) and roughly similar textural properties (Table 18) but different Ti-content 3.04 wt % and 4.59 wt %, respectively, the latter sample has higher catalytic activity in cyclohexene conversion and better cyclohexene epoxide selectivity. This may be due to the presence of relatively high content T_d Ti (IV) species in the Ti-PMO-L-10 sample (relatively intense UV-vis band, Figure 91 (A). The catalytic activity of "S" type of PMO materials were also tested, although both materials have less degree of ordering. When we compare Ti-PMO-S-5 and Ti-PMO-S-10 materials, which have similar particle morphology i.e. aggregation of platelets like particles and significantly different Ti-content in the final material. The latter sample (Ti-PMO-S-10) has a relatively higher rate of cyclohexene conversion than the former sample. This may be due to the presence of relatively higher T_d Ti (IV) species in Ti-PMO-S-10 material (intense UV-vis band, Figure 91 (B)). However, the catalytic activity of Ti-PMO-S-10 material is not as high as would

be expected from its Ti-content. This may be due to the partial blockage of mesopores decreasing its surface area and pore volume significantly (Table 18) which hinders the accessibility of the Ti (IV) active sites. As a result, Ti-PMO-S-10 has lower TON than Ti-PMO-S-5, although both materials have high selectivity to cyclohexene epoxide (Table 22).

As shown in Figure 105, Ti-containing PMO materials which have been synthesized using Pluronic P123 as a surfactant (Ti-PMO-L-5 and Ti-PMO-L-10), have lower reaction rate in cyclohexene conversion and lower epoxide selectivity than their corresponding "S" types prepared with Pluronic P104 (Ti-PMO-S-5 and Ti-PMO-S-10). This may be due to the presence of less amount of T_d Ti (IV) species in the final "L" types of materials, lowers its catalytic activity in epoxidation of cyclohexene. On the other hand, the presence of relatively higher number T_d Ti (IV) active sites in the final "S" type of materials, intense UV bands at ~ 220 nm (Figure 91 (B)), exhibits better catalytic activity.

The Ti-PMO-S materials also produced better yield of epoxide as compared to their corresponding SBA-15 type of materials indicating that there is a positive effect due to their higher surface hydrophobicity improving the adsorption and diffusion rate of cyclohexene molecule. However, the catalytic performance of the materials is not significantly enhanced (lower TON) due to lower degree of ordering of the material that in turn limit the accessibility of Ti (IV) active sites.

The catalytic activity of large pore size Ti-containing PMO materials of both "L" and "S" types, were tested in epoxidation of cyclohexene (Figure 106, Table 22). These materials

have similar particle morphology, i.e. aggregation of particle and significantly different Ti content in the final material.

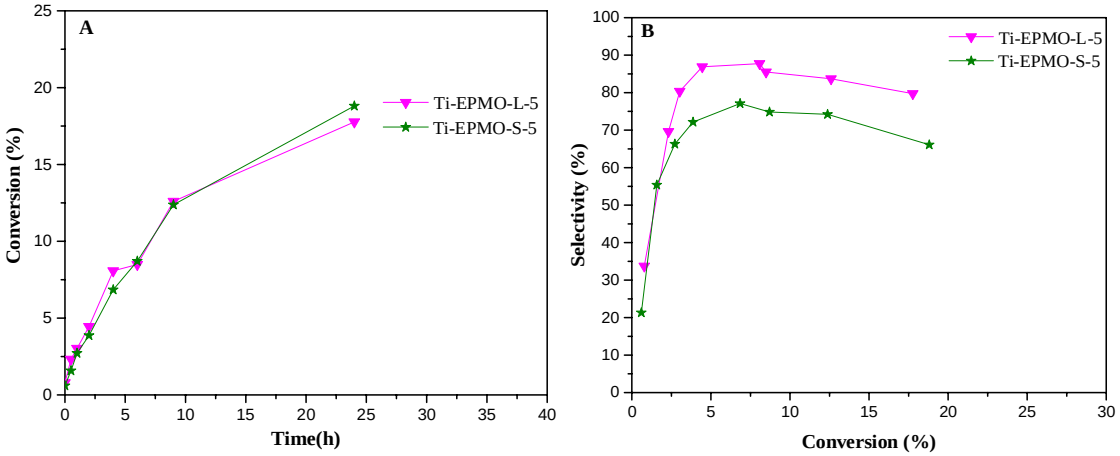

Figure 106. Reaction kinetics of cyclohexene conversion (A) and epoxide selectivity (B) in the presence of large pore size Ti-containing PMO materials under anhydrous conditions

Although Ti-EPMO-S-5 material has higher Ti content (3.39 wt %), both materials show similar catalytic activity in cyclohexene conversion. This may be due to the presence of less amount of T_d Ti (IV) species and high amount catalytically inactive Ti-species (octahedrally coordinated and anatase TiO_2 species) in Ti-EPMOS-5 material hinders its catalytic activity as would be expected from its Ti-content. The presence of higher T_d Ti (IV) species in Ti-EPMO-L-5 material (intense UV-vis band, Figure 98) makes this material to have better selectivity towards cyclohexene epoxide. On the other hand, the presence of anatase TiO_2 species in Ti-EPMO-S-5 material could participate in oxidant decomposition to facilitate allylic oxidation and thereby decreasing epoxide yield. The Ti-EPMO-L-5 material has the highest TON value. This may be due to its large pore diameter (8.5 nm) and its low Ti content revealing highly dispersed Ti (IV) species (Table 22).

Finally, the Ti-grafted materials were also tested during the epoxidation of cyclohexene under the same reaction conditions of the Ti-containing materials synthesized by co-condensation. As we have discussed in section 4.2, the Ti-grafted materials have high Ti contents in the final materials with 4-coordinated Ti-species (T_d Ti (IV)), and no detected anatase TiO_2 species. In this method of Ti-incorporation, we expect that all the Ti (IV) active sites are on the pore surface of the channel, with no possibility for the buried Ti species in the pore wall of the material. As a result, the catalytic activities of these materials have better performance in cyclohexene conversion as well as selectivity of cyclohexene epoxide (Table 23) as compared to the previous materials which have been synthesized by co-condensation. This may be due to the high accessibility of the Ti-species on the pore surface and may not be buried in the pore wall of the material because they were grafted on the surface.

Table 23. Catalytic results in the epoxidation of cyclohexene with TBHP in the presence of Ti-containing SBA-15 materials

Run[a]	Catalyst	Ti[b] (wt %)	Initial reaction rate (mmol/h)[c]	Conversion[d] (%)	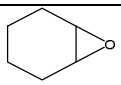	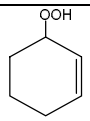	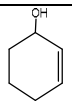	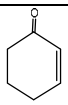	TON[e]
1	TiG-SBA-L	4.65	0.93	25.92	89.5	1.6	3.7	5.1	30
2	TiG-ESBA-L	3.31	1.81	44.62	97.4	0.8	0.7	1.0	78
3	TiG-PMO-L	1.87	0.54	26.17	92.5	0.9	2.8	3.8	76
4	TiG-EPMO-L	2.46	0.50	25.42	93.6	0.7	2.8	2.9	57

[a] Reactions carried out using catalyst to substrate mass ratio of 1:10 and TBHP to cyclohexene molar ratio of 1.1:1, 70 °C, 24 h.

[b] Ti content in weight by ICP.

[c] Estimated from the cyclohexene conversion level measured within the first 2 h of reaction.

[d] cyclohexene conversion calculated by the total addition of the yields of the resultant products.

[e] Turnover number mole of epoxide produced per mole of Ti.

When we compare the catalytic activity of Ti-grafted SBA-15 materials (TiG-SBA-L and TiG-ESBA-L), which have similar particle morphology and different pore size and Ti content in the final material. Ti-grafted large pore size SBA-15 (TiG-ESBA-L) have significantly higher conversion and cyclohexene epoxide selectivity probably due to the high accessibility and dispersion of Ti (IV) active sites, its large pore diameter (10.5 nm) and high degree of ordering for better mass transfer and accessibility of the active sites. Although TiG-SBA-L has higher Ti-content in the final material, its narrow pore diameter (8.4 nm) may decrease the dispersion of Ti-active sites during the functionalization process. This probably lowers the catalytic performance of the material. As a result, TiG-ESBA-L material has a higher TON than TiG-SBA-L material.

When we compare the catalytic activity of Ti-grafted PMO types of materials (TiG-PMO-L and TiG-EPMO-L), which have similar particle morphology, i.e. fibers-like and different in pore diameter and Ti-content in the final material. As shown in Figure 107 both materials have similar catalytic activity in cyclohexene conversion as well as cyclohexene epoxide selectivity. This may be due to the presence of some blocked mesopores in TiG-EPMO-L material (Figure 53 (B), desorption curve) may hinder the accessibility of some Ti (IV) active sites. Thus, the catalytic activity of TiG-EPMO-L materials is not as high as would be expected from its high Ti-content and large pore diameter (Table 10). As a result, TiG-EPMO-L has a lower TON than TiG-PMO-L although both materials have similar catalytic activity. It is difficult to extract clear conclusions in this section on the relative influence of pore size and hydrophobicity on the catalytic activity due basically to the presence of Ti both as isolated active sites and polymeric octahedral sites.

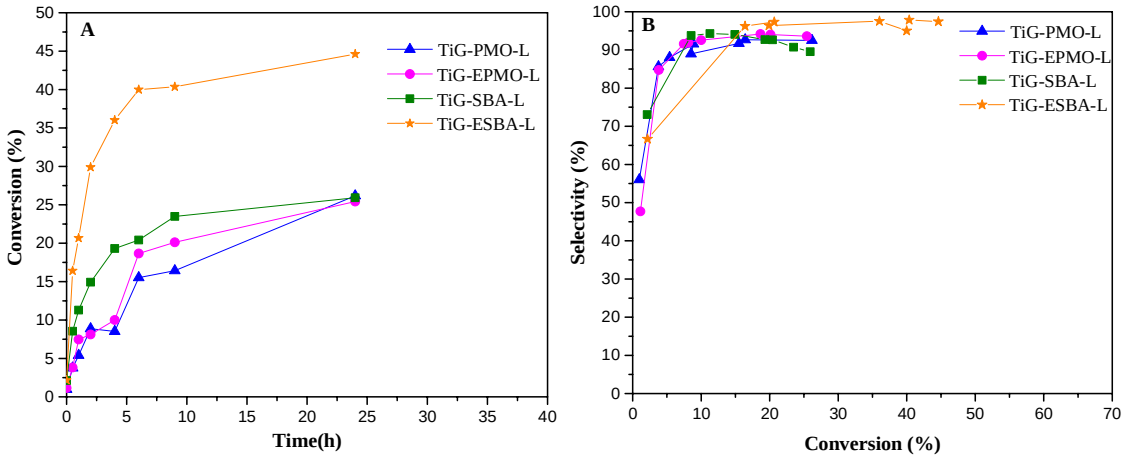

Figure 107. Reaction kinetics of cyclohexene conversion (A) and epoxide selectivity (B) in the presence of Ti-containing SBA-15 catalysts under anhydrous conditions

Considering together the conversion of cyclohexene and epoxide selectivity after a particular reaction period allows to predict the catalytic performance of the synthesized materials (Figure 108). Besides this the Turnover Number of the materials was also calculated to study the catalytic activity per Ti active sites. The materials which have lower Ti loading give the higher TON. This may be due to the better dispersion of Ti active sites on the silica support. The cyclohexene conversion and cyclohexene epoxide selectivity of all catalysts after 24 h reaction is drawn together in Figure 108 for comparison purpose. Ti-grafted materials seem to be better in cyclohexene conversion and cyclohexene epoxide selectivity than their corresponding materials synthesized in direct synthesis method using Pluronic P123 surfactant. Figure 108 also show that the Ti-containing “S” type materials synthesized using P104 surfactant seem to be better in catalytic conversion and epoxide selectivity than their corresponding “L” types of materials synthesized using P123 surfactant regardless of the silica source. Especially the Ti-PMO-S materials show very

high conversion and epoxide selectivity, maybe due to the easier adsorption and diffusion of reagents in its hydrophobic pore surface and short channel pathlengths.

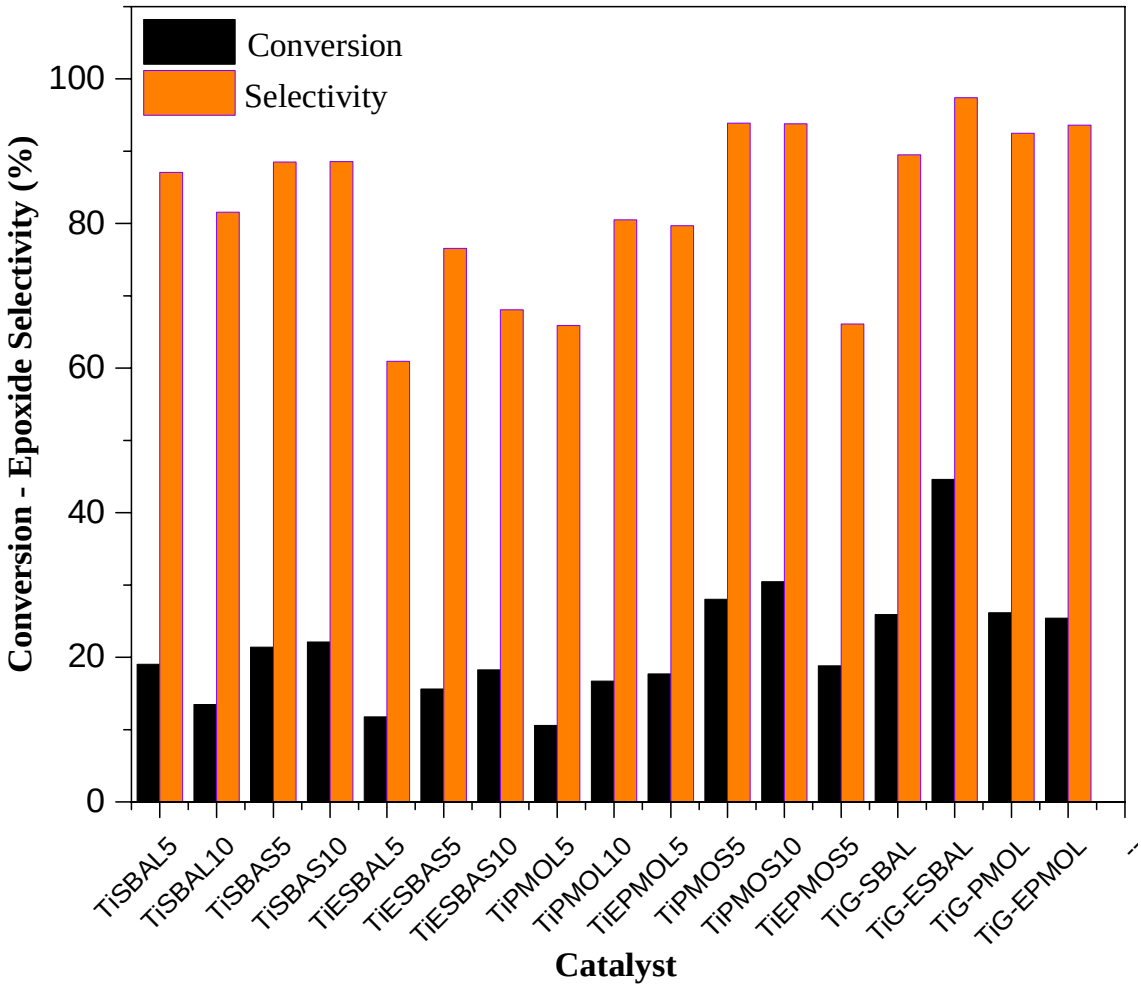

Figure 108. Cyclohexene conversion and epoxide selectivity after 24 h reaction in presence of Ti-containing SBA-15 catalysts under anhydrous conditions

Summary

- ✓ Ti-containing SBA-L material (Ti-SBA-L-5) with lower Ti loading (1.25 wt %) has better catalytic activity and higher TON than Ti-SBA-L-10 with higher loading Ti (2.97 wt %) and slightly lower pore diameter and surface area.

- ✓ Ti-containing SBA-S material (Ti-SBA-S-5) which has hexagonal plate-like particle morphology has better catalytic performance and higher TON than Ti-containing SBA-L material (Ti-SBA-L-10) material which has fiber-like particle morphology. Both materials have a roughly equivalent amount of Ti in the final material.
- ✓ Ti-containing PMO-S materials that have a relatively higher T_d Ti (IV) species with short channel plates-like particle morphology have better catalytic performance than Ti-containing PMO-L materials, which have a relatively lower T_d Ti (IV) species with long channel fiber-like particle morphology.
- ✓ Large pore size Ti-containing SBA-15 and PMO materials which have been synthesized by the co-condensation method have lower catalytic activity due to the heterogeneity of Ti-species or the very small Ti-loading in the final material.
- ✓ Ti grafted SBA-15 materials have better catalytic performance in cyclohexene conversion as well as epoxide selectivity than the corresponding materials synthesized by co-condensation. Ti-grafted large pore size SBA-15 material (TiG-ESBA-L) has the highest catalytic activity.
- ✓ Ti grafted PMO materials have better catalytic performance in cyclohexene conversion and epoxide selectivity than their corresponding “L” type of materials synthesized by co-condensation.
- ✓ Ordered Mesoporous Materials which have high content of T_d Ti species either with large pore diameter or short diffusion pathlengths with hydrophobic surfaces have good catalytic activity.

5.2. Epoxidation of Vernonia Oil with TBHP

As the fast development of the transformation of biomass to bulk and fine chemicals, green conversion processes for biomass utilization become particularly important. Vegetable oils with high content of epoxides are highly reactive intermediates that are also readily converted to other functional groups through ring-opening reactions and have an application for the synthesis of thermoplastic materials such as polyamide, thermoset materials such as polyurethanes and as stabilizers of PVC. For the application of a thermosetting polymers, vegetable oil with a high content of epoxides is desirable, because more functional groups that facilitate more highly crosslinked structures for better thermal and mechanical strengths. Therefore, further epoxidation of the unsaturated carbon of vernonia oil by using environmentally friendly catalysts and methods is desirable to increase its epoxide concentration.

5.2.1. Characterization of the starting material (vernonia oil)

Vernonia oil was extracted by using a supercritical carbon dioxide extraction technique and characterized by using ^{1}H and ^{13}C-NMR and ATR-FTIR spectroscopy.

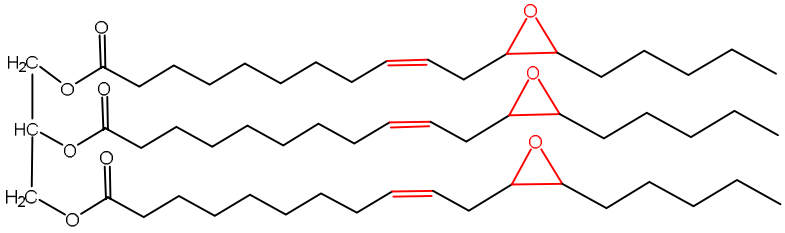

Figure 109. Trivernolin structure of vernonia oil

In this study, the starting material (vernonia oil) and the product (epoxidized vernonia oil) were characterized by ^{1}H & ^{13}C NMR spectroscopic techniques (in ppm) (Bruker AVANCE 300 MHz, $CDCl_3$). The ^{1}H NMR data of the vernonia oil show the presence of

olefinic protons (CH=CH) and glycerol methine proton (CH) at 5.24 – 5.60, glycerol methylene proton (CH_2) at 4.07 – 4.30, epoxy protons (O-C-H) at 2.74 – 2.94 characteristic of vernolic acid moiety in the trivernolin structure, protons of methylene attached to olefinic group (-**CH_2**-CH=CH-**CH_2**-) and methylene attached to epoxy group (-**CH_2**-CHOCH-**CH_2**-) at 1.99 – 2.39, protons of the rest methylene groups $(CH_2)n$ at 1.23 –1.60, protons of methyl (CH_3) group at 0.83 – 0.90. The results obtained indicate that the major functional groups such as a double bond, epoxy group and triglyceride ester characteristic components of vernonia oil remained intact throughout the extraction processes.

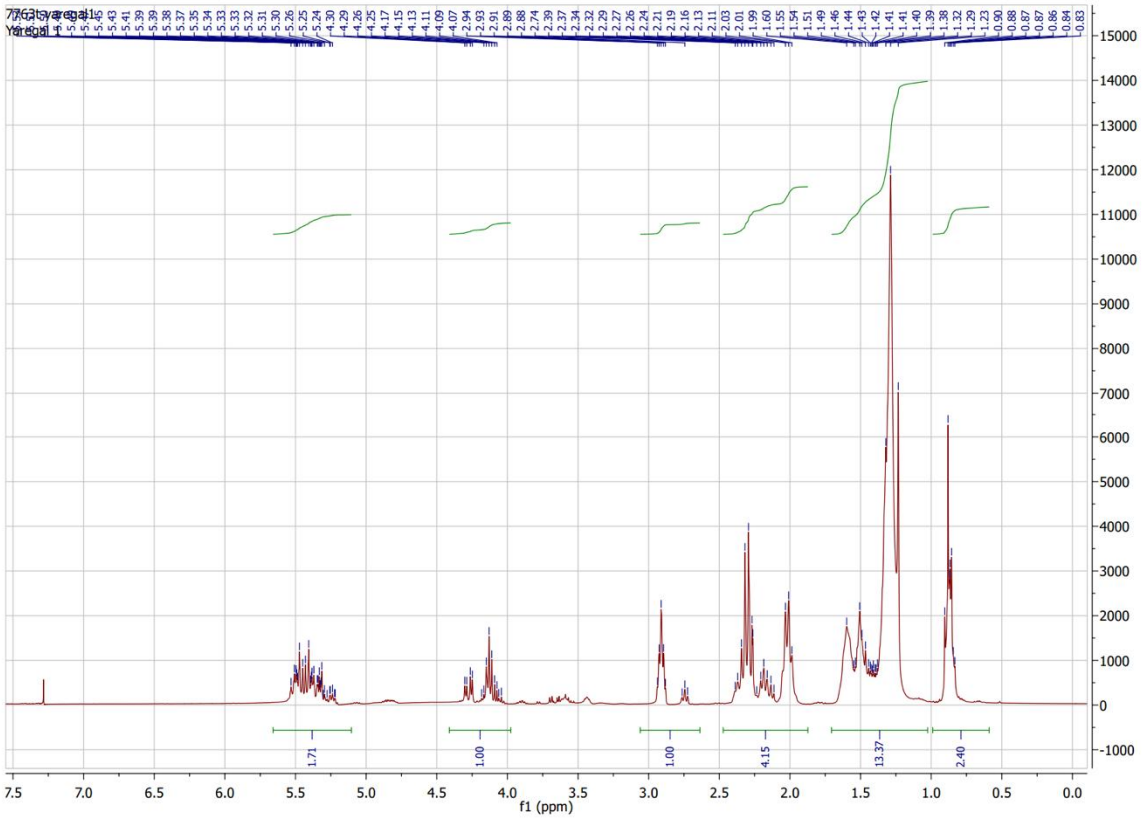

Figure 110. ^{1}H NMR of supercritically extracted vernonia oil

The ^{13}C NMR data (ppm) (Bruker AVANCE 300 MHz, $CDCl_3$): The ^{13}C NMR of the vernonia oil shows the presence of ester carbonyl carbon (C=O) of fatty acids at 178.08,

ester carbonyl carbon (C=O) triglyceride at 173.04, olefinic carbons (CH=CH) at 123.87 – 132.47, glyceral (CH) at 68.88, and glyceral (CH_2) at 62.06 – 64.97, epoxy carbons (O-C-H) at 56.58 – 57.25, methylene carbons $(CH_2)_n$ at 22.54 – 33.95, and methyl carbon (CH_3) at 14.02. This data are in agreement with the literature report[140].

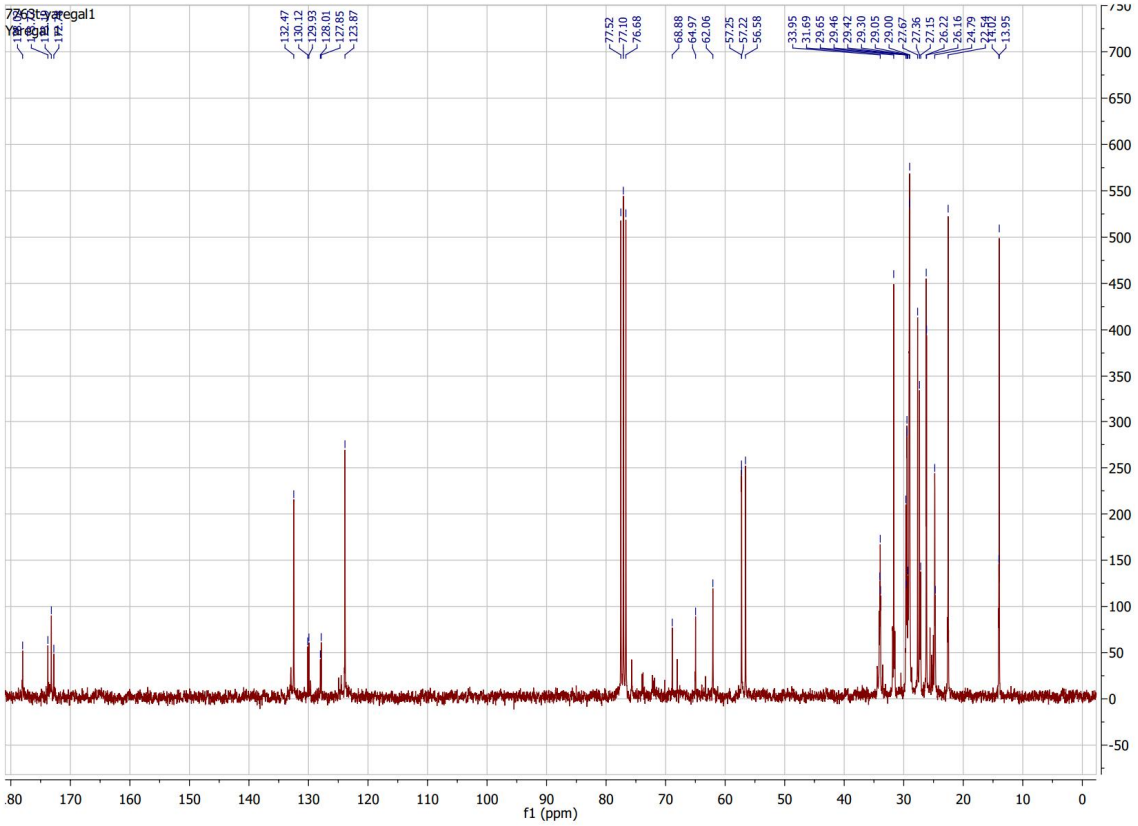

Figure 111. ^{13}C NMR of $scCO_2$ extracted vernonia oil

ATR-FTIR spectrum analysis

Fourier transform infrared (FT-IR) spectroscopy deals with the vibration of chemical bonds in a molecule at various frequencies depending on the elements and types of bonds. After absorbing electromagnetic radiation the frequency of vibration of a bond increases leading to transition between ground state and several excited states. These absorption frequencies represent excitations of vibrations of the chemical bonds and thus are specific to the type

of bond and the group of atoms involved in the vibration. The infrared region of the electromagnetic spectrum extends from 14,000 to 50 cm^{-1} and is divided into three areas: the far-infrared from 400 to 50 cm^{-1}; the mid-infrared region from 4000 to 400 cm^{-1}, the region of the spectrum widely used for the study of organic compounds, because the absorption bands are due to the vibration of a particular functional grouping; and the near-infrared (NIR) from 14,000 to 4000 cm^{-1}.

Table 24 summarizes the frequencies of the characteristic bands or shoulders, their assignment to functional groups, their vibration mode and their intensity in the spectrum of samples of vernonia oil which is shown in Figure 112.

Table 24. Summary of FTIR data of vernonia oil

No	Frequency (cm^{-1})	Assigned group	Mode of vibration	Intensity
1	3010	=C-H (cis-)	Stretching	Very weak
2	2925	-C-H (CH_3)	Stretching (asym)	Very strong
3	2890	-C-H (CH_2)	Stretching (sym)	Strong
4	1740	-C=O (ester)	Stretching	Very strong
5	1654	-C=C- (cis-)	Stretching	Very weak
6	1465	-C-H (CH_2)	Bending (Scissoring)	Medium
7	1377	-C-H (CH_3)	Bending (sym)	Medium
8	1259	-C-O, -CH_2-	Stretching, bending	Weak
9	1170	-C-O, -CH_2-	Stretching, bending	Strong
10	1100, 1097, 1033	-C-O	Stretching	Weak
11	840	-C-O (epoxy group)	stretching	Medium
12	823	-C-O (epoxy group)	stretching	Weak
13	723	-(CH_2)n,	Bending (rocking)	Medium

In the spectrum, the functional groups characteristic of the triglyceride structure of vernonia oil are clearly identified. Among these, the peak at 823, 840cm^{-1} correlated to the epoxy (or oxirane) group, the C=O stretching band obtained at 1740 cm^{-1} and the peak at 1654 cm^{-1} corresponding to C=C stretching mode, can be mentioned. The presence of very

weak broad peak at 3400 cm^{-1} in the spectrum of vernonia oil indicates partial hydrolysis of the epoxide group, which probably occurred during the extraction process. The FTIR spectrum of vernonia oil is in a good agreement with the literature reports[82, 141, 142]. The spectral data analysis result indicate that the vernonia oil is pure with less amount of free fatty acid.

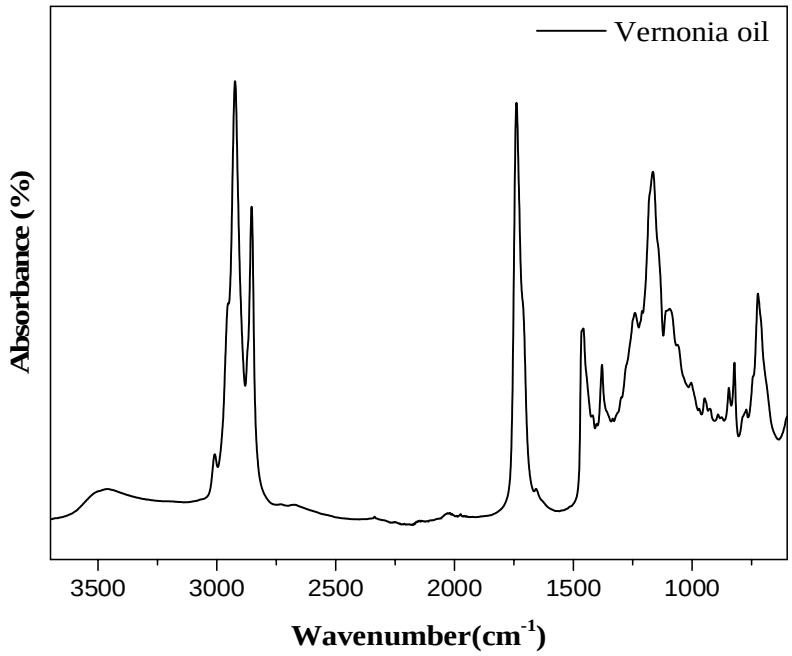

Figure 112. FT-IR spectra of vernonia oil

After characterization of the supercritically extracted vernonia oil, the unsaturated carbons were epoxidized using the following catalytic set up.

5.2.2. Reaction set up and characterization

Vernonia oil was obtained by supercritical carbon dioxide extraction and used as a starting material for epoxidation reaction. The oil is composed of a mixture of triacylglycerols containing on average 2.0 epoxy functionalities and 3.0 olefinic groups per glycerol molecule, as determined by ^{1}H-NMR analysis (see below for details on group quantification). The low viscosity of vernonia oil[143] motivated us to run the epoxidation

reaction without any organic solvent. The experimental conditions were developed from the work by Rios *et al.*[144] with some necessary modifications. Epoxidation of vernonia oil was carried out in the liquid phase at 70 °C in a 50 mL round-bottom flask equipped with a septum (Figure 113). Vernonia oil was used as a substrate and TBHP (5.5 M in decane solution) as the oxidant. In a typical experiment, 1.0 g (1.08 mmol) of vernonia oil and 0.32 g (3.56 mmol) of TBHP were mixed at room temperature (1.1 to 1.0, oxidant to olefinic groups molar ratio[91]). The reaction was started by adding the reaction mixture into the flask containing the catalyst (0.1 g) dried at 120 °C overnight in air prior to the experiment. The suspension was kept under magnetic stirring (400 rpm), and samples were taken periodically from the reaction mixture and analyzed by attenuated total reflection FT-IR (ATR-FTIR) spectroscopy to follow conversion of olefinic groups with time. ATR-FTIR spectra of oil samples were recorded using a Thermo Nicolet Nexus 670 FTIR spectrometer equipped with a PIKE GladiATR single-bounce monolithic diamond ATR accessory and a liquid nitrogen-cooled MCT detector. Each spectrum was obtained as the average of 128 scans recorded at room temperature with 4 cm^{-1} resolution in the wavenumber 4000 – 650 cm^{-1}. Conversion at any given reaction time was calculated as the fractional loss of absorbance of the C-H stretching band of olefinic groups (at ca. 3010 cm^{-1}) with respect to the initial reaction mixture. Products obtained after 24 h reaction were characterized by ^{1}H and ^{13}C NMR to evaluate epoxide selectivity's. A few drops of the oil were added to $CDCl_3$ and the solution analyzed using a Bruker AVANCE 300 MHz spectrometer with a 5 mm $^{1}H/^{13}C$ dual probe. ^{1}H-NMR spectra were used to quantify epoxide and olefinic groups in the oil. For quantitative analysis, methylene hydrogens of glyceryl groups (at positions 1 and 3) were used as internal standard, as they are unaffected during epoxidation and

oxidation reactions in the absence of water[145]. Conversion of olefinic groups and selectivity to epoxide groups were calculated from epoxide to glyceryl (EP/GL) and olefinic to glyceryl (OL/GL) molar ratios determined by ^{1}H-NMR, using the method of Hong, *et al.*[146] with some modifications. The integrated intensities of all protons were normalized by assigning to the signal of the 4 protons of the glyceryl methylene groups (δ 4.0 – 4.4 ppm) a value of 4. Thus, the number of glyceryl groups, which corresponds to ¼ of this latter value is assigned a value of 1. In this way, the integrated intensity of the protons in epoxide (-CH-O-CH-) groups (δ 2.7 – 3.0 ppm) is equivalent to twice the number of epoxide groups per glyceryl moiety (EP/GL). The signals of olefinic (-CH=CH-) protons (δ 5.2 – 5.6 ppm) overlap with that of the methine hydrogen of the glyceryl moiety (at position 2). Therefore, to determine the concentration of olefinic groups, the integrated signal in the 5.2 – 5.6 ppm chemical shift range was first corrected by subtracting 1 unit (one methine proton per glyceryl group). Thus, the resulting value, divided by 2, corresponds to the number of olefinic groups per glyceryl moiety (OL/GL). The conversion of olefinic groups and the selectivity to epoxide were then determined according to:

$$\text{Conversion (\%)} = \left[\frac{(OL/GL)_i - (OL/GL)_p}{(OL/GL)_i}\right] * 100 \qquad (1)$$

$$\text{Epoxide selectivity(\%)} = \left[\frac{(OL/GL)_p + (EP/GL)_p}{(OL/GL)_i + (EP/GL)_i}\right] * 100 \qquad (2)$$

where the subscripts *i* and *p* refer to the initial reaction mixture and the product after 24 h reaction, respectively.

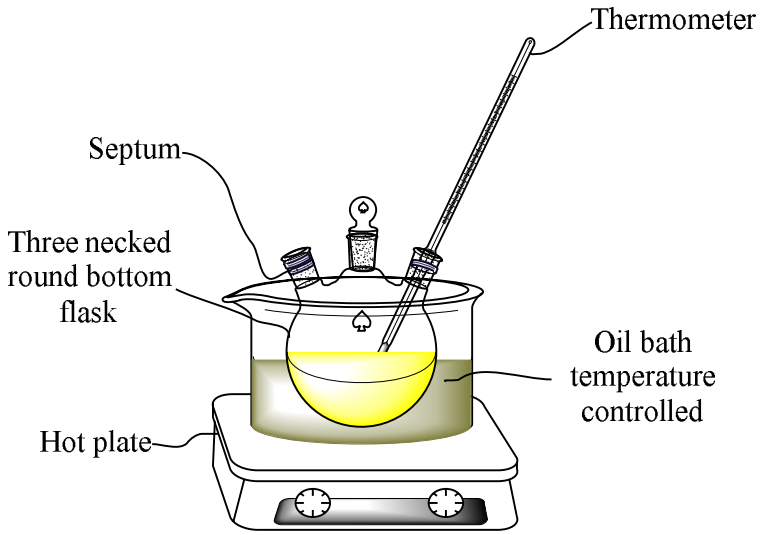

Figure 113. Catalytic set up of vernonia oil epoxidation

5.2.3. Results and discussion on epoxidized vernonia oil

Epoxidation of vernonia oil (Figure 114) would require large pore sizes and active Ti (IV) species to proceed. Our aim was initially to work with solvents and at low temperatures to avoid viscosity increase. In our first attempts, we tried to epoxidize vernonia oil at different reaction conditions using acetonitrile and heptane as solvents at 50, 60 and 70 ^{o}C. However, in all cases, the ATR-FTIR spectra of the reaction mixture showed no significant changes with time, indicating that negligible conversion levels were attained[147, 148]. This is probably due to the fact that both solvents are not suitable for mixing the oil, oxidant, and catalyst. Therefore, we tried to follow the epoxidation reaction at 70 ^{o}C without additional organic solvents, using the oxidant (TBHP, 5.5 M in decane solution) as a solvent.

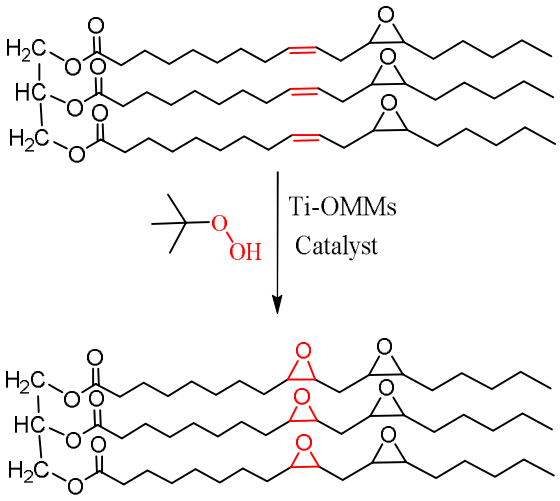

Figure 114. Schematic representation of epoxidation of vernonia oil using Ti-SBA-15 and Ti-PMO as a catalyst and TBHP as an oxidant

In all catalytic runs, the reaction was monitored by FT-IR (Figure 115 and Figure 120 in appendix). The significant disappearance of the bands at 3010 cm^{-1} (νC-H of unsaturated carbon) and 1650 cm^{-1} (νC=C) is an indication of the conversion of the olefinic carbon of the vernonia oil, while the increase of peak intensity at ca. 824 cm^{-1} supported the formation of epoxide groups. These spectra allowed determining the conversion of olefinic carbon groups along the reaction time by following the decrease of intensity of the νC-H stretching band at ca. 3010 cm^{-1}.

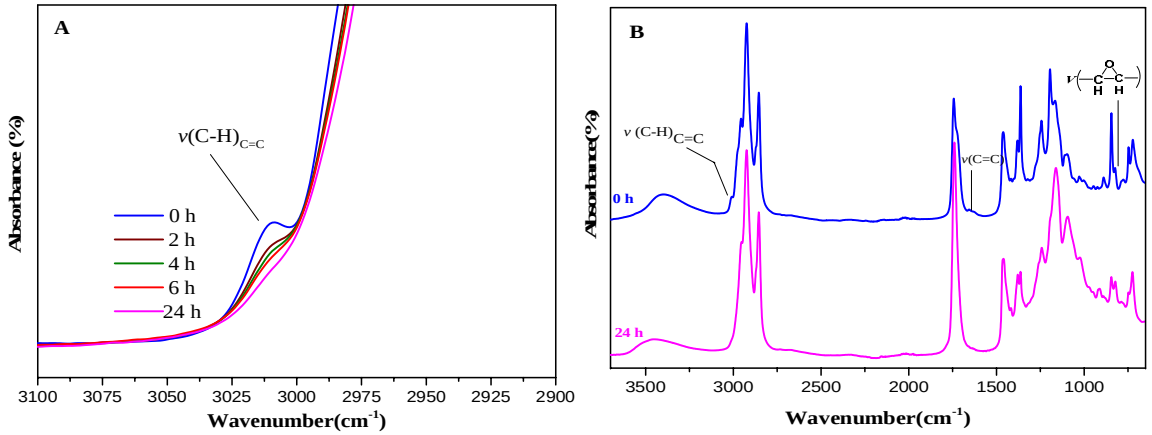

Figure 115. ATR-FTIR spectra of reaction mixture collected at different reaction time using TiG-ESBA-L as a catalyst, indicating the assignment of vibration bands corresponding to olefinic and epoxide groups in vernonia oil

The conversion versus time of the reaction conducted with selected catalysts followed by FTIR is shown in Figure 116 (initial reaction rates calculated from these curves are also included in Table 25).

Conversion of C=C double bond of the vernonia oil is determined by ATR-FTIR from the peak intensity of C-H stretching C=C group at ca. 3010 cm^{-1}. It is normalized by the peak intensity of C=O stretching of the ester –C=O group at ca. 1740 cm^{-1}.

$$\text{Conversion (\%)} = \frac{[I_o(C-H)_{C=C}/I_o(C=O)]-[I_t(C-H)_{C=C}/I_t(C=O)]}{[I_o(C-H)_{C=C}/I_o(C=O)]} * 100 \ldots\ldots\ldots\ldots (1)$$

where I_o is the peak intensity before the reaction (time zero reaction) and I_t is the peak intensity after certain time of reaction.

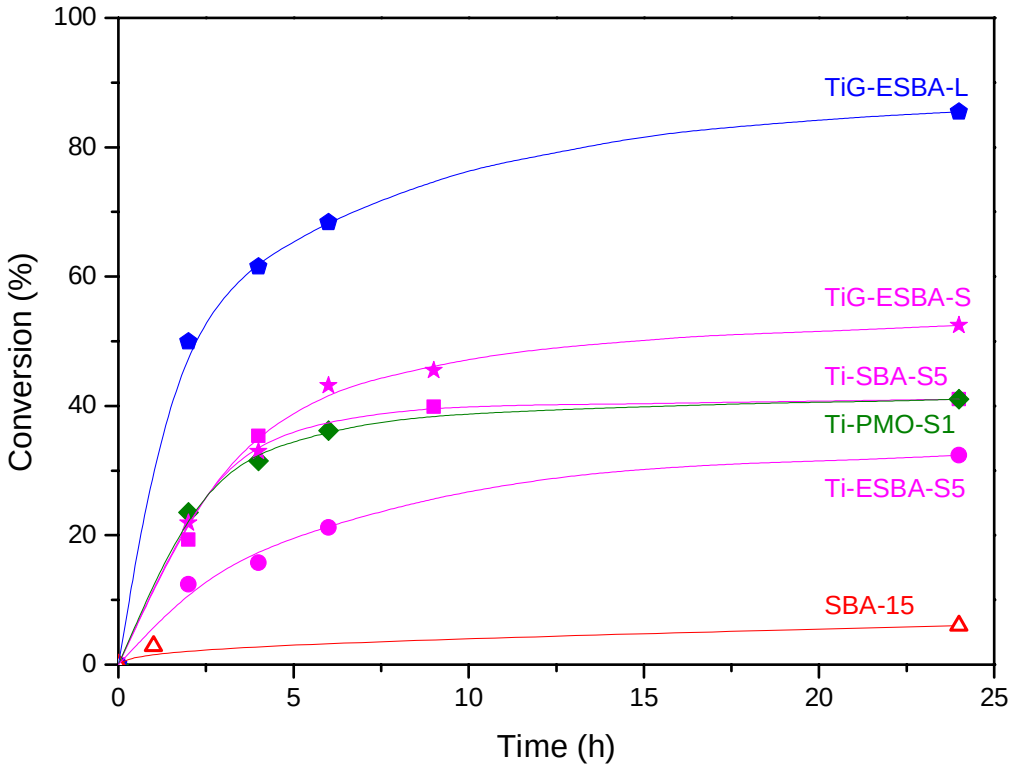

Figure 116.Vernonia oil conversion determined by ATR-FTIR analysis for selected catalysts

As can be observed, TiG-ESBA-L shows the highest initial reaction rate, probably due to the large pore diameter that allowed easy diffusion of reagents and products. The high content of isolated Ti (IV) active sites in this sample, together with the large pore size justifies the highest conversion obtained for this catalyst. When we compare the catalysts with short channels, a slight difference in the initial reaction rate is observed in favour of Ti-PMO-S over Ti-SBA-S-5 and Ti-ESBA-S-5, probably due to a higher affinity of the vernonia oil with the hydrophobic surface of the pores in this case, despite the very low amount of Ti (0.62 wt %) in this catalyst. In this group of catalysts, the highest conversion is achieved by the Ti-grafted sample (TiG-ESBA-S), justified once again by the higher content of Ti active sites (3.43 wt %). However, the activity of this latter sample is not as

high as would be expected when compared with those of the catalysts prepared by direct synthesis, which contain less than 1wt % Ti. In the case of Ti-SBA-S-5, the presence of anatase crystals in the sample hinders the catalytic activity, whereas in the Ti-ESBA-S-5, the low activity values are due to the presence of only 0.22 wt % Ti.

In summary, what seems to be clear from this plot is that large pore, and a Ti content in the range of 2-3 wt % yield high conversion in this reaction, regardless of the length of the channels, although a hydrophobic surface seems to have a major effect on the adsorption of the vernonia oil making the Ti sites more efficient.

Table 25. Results of epoxidation of vernonia oil by using selected catalysts (10% weight of catalyst relative to the oil) at 70 ºC for 24h

Catalyst	Ti (wt %)	Pore size (nm)	Initial reaction rate (mmol/h)[a]	Conversion (%)	Selectivity (%)	Yield (%)	TON
Ti-SBA-S-5	2.83	8	0.10	41	88	36	7.4
Ti-ESBA-S-5	0.22	12	0.07	26	94	24	64.8
Ti-ESBA-S-10	0.52	14.3	0.11	32	93	30	34.2
Ti-PMO-S-1	0.62	6.1	0.13	41	92	37	35
Ti-SBA-L-10	2.97	7.3	0.09	39	93	36	7.2
Ti-SBA-L-5	1.25	8	0.09	39	92	36	16.8
TiG-ESBA-S	3.43	12	0.12	45	83	37.6	6.4
TiG-PMO-S	2.39	5.4	0.07	28	90	25	6.15
TiG-SBA-L	4.65	8.4	0.05	49	84	41	5.06
TiG-ESBA-L	3.31	10.5	0.27	71	80	57	10
Ti-EPMO-L-5	0.71	8.5	-	32	95	30	24.6
TiG-PMO-L	1.87	7.5	-	39	96	37	12
TiG-EPMO-L	2.46	10	-	48	94	45	10
SBA-15	-	-	-	5.41	92	5.6	-
Blank	-	-	-	5.41	91	5.5	-

[a] Estimated from the vernonia oil conversion level measured within the first 2 h of reaction.

Upon stabilization (24 h of reaction), conversion, selectivity and yield to EVO were quantified using ^{1}H NMR. Identification of the different functional groups was also supported by ^{13}C NMR. The full ^{1}H and ^{13}C NMR spectra of vernonia oil and its epoxidation product are included in Figure 117 and Figure 118 by using TiG-ESBA-L as a catalyst and in Figure 121 (A-M) in the appendix by using other selected catalysts. The epoxidation of olefinic groups present in the oil is evidenced by the presence of ^{1}H resonances in the 2.87 – 3.11 ppm range and ^{13}C NMR peaks at ca. 54.15 – 57.18 ppm, with a concomitant depletion of the olefinic protons signals at δ 5.30 – 5.60 ppm and olefinic carbon signals in the range 123.87 – 132.47 ppm. Downfield shifts of ^{1}H atoms in epoxy groups were observed when the number of epoxy groups increased in the fatty acid chain. The formation of new ^{1}H-NMR peaks at ~ 1.75 ppm is due to -CH_2- protons signals bridged the two epoxide groups (the former and the new epoxide) this indicates the presence of diepoxides in the fatty acid chain after epoxidation reaction. From the ^{13}C NMR result of EVO the presence of new peaks at 54.15 – 54.32 ppm indicates the formation of new epoxy groups after the epoxidation reaction. The disappearance/the presence of weak peaks from 123.87 – 132.43 ppm also confirms the conversion of the part of the double bond of the vernonia oil into the epoxy group. The remaining ^{13}C NMR peaks of the starting material remains unchanged. This indicates that the triglyceride structure of the vernonia oil is not affected throughout the reaction process. In general the ^{1}H and ^{13}C NMR spectra show that, for all catalysts tests, the major product of reaction at 70 ^{o}C was epoxidized vernonia oil. ^{13}C-NMR confirms the absence of other side products like enol and enone esters (absence of peaks at around 200 ppm). Furthermore, NMR results showed that the triglyceride structure remained intact after epoxidation.

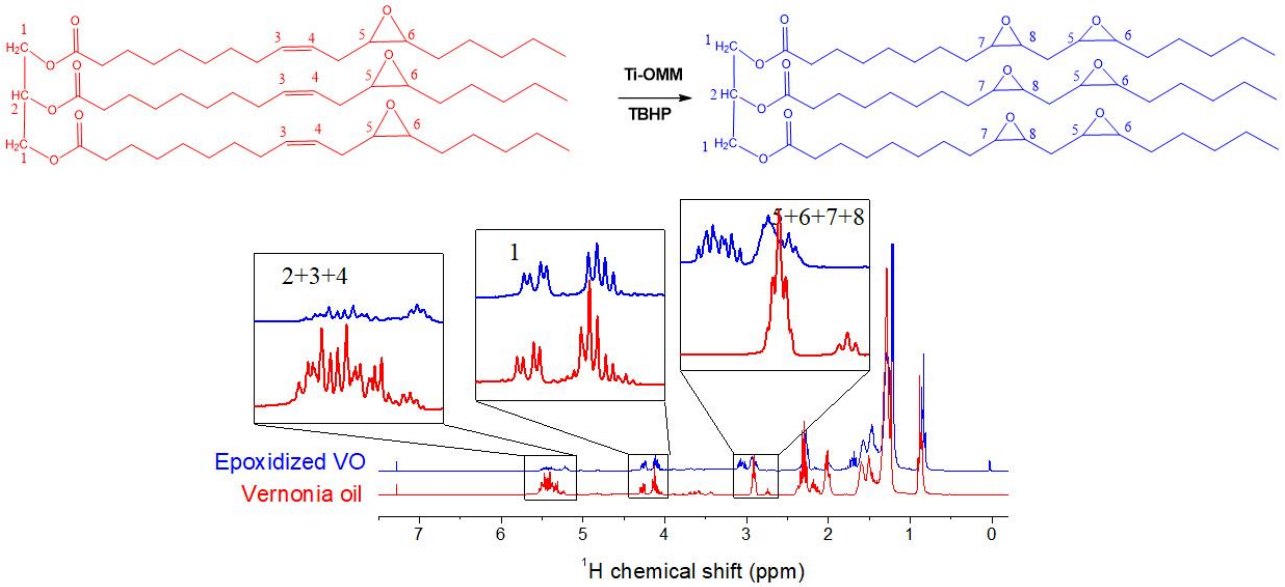

Figure 117. ^{1}H NMR spectra of vernonia oil and the epoxidized product obtained after 24 h reaction at 70 ° C using catalyst TiG-ESBA-L

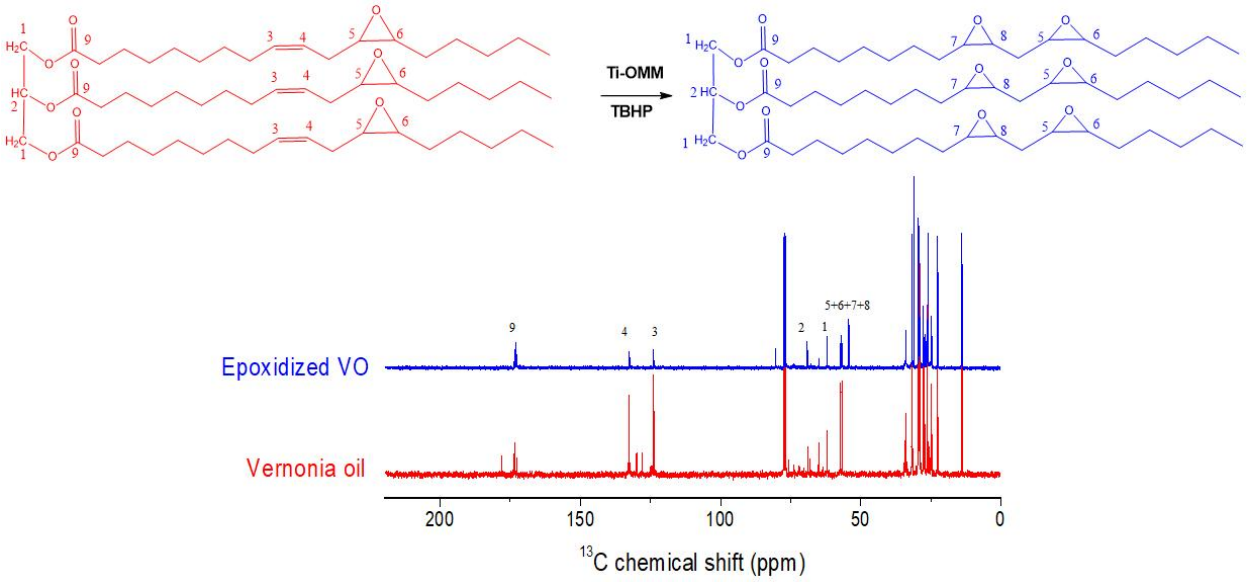

Figure 118. ^{13}C NMR spectra of vernonia oil and the epoxidized product obtained after 24 h reaction at 70 °C using catalyst TiG-ESBA-L

Conversion, selectivity and epoxide yield determined by ^{1}H NMR analysis of the products obtained after 24 h of reaction are collected in Table 25, along with turnover number

calculated as mol EVO/mol Ti for each catalyst. One has to bear in mind that we are working with the pure triglyceride oil, with relatively high viscosity, and without solvent, which explains the lower conversion values as compared to epoxidation of fatty acid methyl esters[132]. The conversions obtained do not follow any trend respect to Ti content of the catalysts, although values around 2 wt % Ti seem to be optimum to reach conversions above 40 %. However, it is remarkable the result given by the catalyst Ti-PMO-S which with only 0.62 wt % of Ti, gives a conversion of 41% at 24 h. If we compare only the "S" family (catalysts containing short pore channels), the increase of conversion follows the increase of Ti content, maintaining in all cases selectivities > 90%. The effect of the pore size is difficult to isolate because the catalysts do not contain the same amount of active Ti sites. Ti-SBA-S-5 with relatively narrow pores (8 nm) converts 41% with 88% selectivity has TON of 7.4, while Ti-ESBA-S-5, with 12 nm pore size, only converts 26 % of VO with 94 % selectivity has TON of 64.8. The lower conversion in Ti-ESBA-S-5 is due to the presence of very low amount of Ti actives sites in the final material (0.22 wt. %) and the higher selectivity and TON may be due to the better dispersion of Ti-active sites and higher diffusion rate of substrates. Ti-PMO-S is the most efficient catalyst (41% conversion, 92% selectivity and has TON 35) despite its narrow pore size of 6.1 nm. This indicates that the surface chemistry is more important than the actual pore size. The efficiency of the small amounts of Ti in Ti-ESBA-S-5 (0.22 wt%) and Ti-PMO-S (0.62 wt%), as indicated by the highest TON, corroborates with the presence of isolated Ti(IV) sites in these samples, against the mixture of several types of populations in Ti-SBA-S5 which contained small crystals of anatase. On the other hand, when Ti-ESBA-S-5 and Ti-PMO-S catalysts are compared with their Ti-grafted counterparts, TiG-ESBA-S and TiG-PMO-S, it can be seen

a significant drop of catalytic activity of the latter samples despite the successful increment of Ti content (3.43 and 2.39 wt %, respectively). This is probably due to the fact that grafting causes for the decrement in pore size in the case of TiG-PMO-S (5.4 nm). For the "L" group of catalysts, with pore sizes around 8 nm but with fiber-like particle morphology (long pore channels), conversion decreases to 39 % despite the higher Ti contents (1.25wt% for Ti-SBA-L-5 and 2.97 wt% for Ti-SBA-L-10) demonstrating that the fiber-like particle morphology may hinder the diffusion of VO and, therefore, decrease the efficiency of the catalyst (lower TON values). Finally, for Ti-grafted catalysts, the notable increase in Ti content achieved in these catalyst (4.65 wt% in TiG-SBA-L and 3.31 wt % in TiG-ESBA-L), does not produce a proportional increase of activity, which results in lower TON values. However, the highest conversion (71%) is achieved for TiG-ESBA-L, probably due to its large pore size (10.5 nm) together with the large amount of Ti active sites. These results, in our opinion, indicate that 2 wt% of Ti(IV) isolated sites is an optimum composition for this reaction, in a hydrophobic pore surface such as PMO, with pore sizes between 6 and 10 nm, and with a short-channel particle morphology. Although equivalent amount Ti (IV) isolated active sites (0.71 wt %) are incorporated in a large pore size (8.5 nm), TiEPMOL5 relative to Ti-PMO-S, the percent of conversion is lower (32 %) than the latter material (41 %). This may be due to the less degree of ordering of the former material and its foam-like particle morphology that hinders the accessibility of the active sites and diffusion of reagents. Ti-grafted PMO materials were also used to catalyse epoxidation of vernonia oil (TiG-PMO-L (1.87 wt %) & TiG-EPMO-L (2.46 wt %)) and conversion of 39 and 48 %, respectively were obtained; however, the TON value is low. The higher conversion by TiG-EPMO-L relative to TiG-PMO-L also confirms the importance of larger pore diameter for

diffusion of VO through the channel of the material, this effect is not observed during epoxidation of cyclohexene. In general, during epoxidation of vernonia oil, all PMO materials have very high epoxide selectivity (> 90 %) (Table 25), this confirms the more the surface hydrophobicity of the material, the higher the affinity for adsorption and diffusion of vernonia oil. Furthermore, the presence of limited surface hydroxyl groups minimize ring opening reaction that results high epoxide selectivity. However, in the case of SBA-15, the selectivity towards epoxides is significantly different from one material to another this may be due to the difference of their surface hydrophilicity (concentration of silanol groups).

Summary

- ✓ Solvent free epoxidation of vernonia oil with anhydrous tert-butyl hydroperoxide (5.5 M TBHP in decane solution) in the presence of Ti-containing SBA-15 and PMO catalysts was investigated.
- ✓ Ti-grafted large-pore conventional SBA-15 and PMO shows higher conversion and yield of epoxide probably due to the easy mass transfer of reactants and products throughout the channel.
- ✓ Ti-SBA-15 and Ti-PMO materials with hexagonal platelet morphologies having short pore channels give better conversion in epoxidation of vernonia oil than those with conventional fiber-like morphologies possessing longer channels.
- ✓ Ordered Mesoporous Materials which have high content of T_d Ti species either with large pore diameter or short diffusion pathlengths with hydrophobic surfaces are a good candidates for epoxidation of vernonia oil.

6. CONCLUSION

In this study, Ti-containing SBA-15 and PMO types of ordered mesoporous materials were assessed for catalysis. The effect of pore size and particle morphology of the support and the Ti content of the final material on catalysis were also evaluated. Prior to Ti-incorporation, the synthesis condition of mesoporous silica (SBA-15) and organosilica (PMO) molecular sieves with various pore sizes and particle morphologies has been optimized. Titanium was effectively incorporated either by grafting or co-condensation methods using titanocene dichloride as a titanium source. In the direct synthesis method: the synthesis conditions, the nature of the surfactant used, the Ti-source precursor and the swelling agent are important factors that have to be carefully selected to achieve properly structured and suitable particle morphology Ti-containing SBA-15 materials. In the co-condensation method, the Ti/Si ratio of the synthesis gel was varied 0.01, 0.05 and 0.1 with and without TIPB micelle expander in both pure silica SBA-15 and organosilica PMO type of materials. Elemental composition, particle morphology, structural and textural properties of the synthesized materials were studied using different characterization techniques.

The Ti content of the synthesis gel has a significant effect on the degree of ordering of the material as well as the morphology of the particle. Ti-containing SBA-15 and PMO materials with different pore sizes and particle morphology were synthesized. Grafting seems to be a more convenient method to incorporate more populated isolated T_d Ti (IV) species without anatase formation as compared with the co-condensation method.

The catalytic activities of these materials were tested for the epoxidation of cyclohexene using TBHP (5.5 M in decane solution) as an oxidant. The catalytic tests were carried out

by using four different groups of catalysts: Ti-grafted SBA-15 materials, Ti-grafted PMO materials, Ti-containing SBA-15 and Ti-containing PMO materials materials synthesized using co-condensation method. The selected catalysts were used for epoxidation of vernonia oil and the results showed promising results. Solvent-free epoxidation of vernonia oil with anhydrous tert-butyl hydroperoxide (5.5 M TBHP in decane solution) in the presence of titanium-containing SBA-15 and PMO catalysts was also investigated.

It was found that all Ti-grafted SBA-15 and PMO materials effectively catalyze the epoxidation reaction. Among them, TiG-ESBA-L, which has a large pore diameter and a high degree of ordering, has the highest catalytic activity. These catalysts also give promising results in the epoxidation of vernonia oil. TiG-ESBA-L catalyst also has the highest conversion with a high yield of epoxide among the tested materials.

Furthermore, all Ti-containing SBA-15 materials which have been synthesized by co-condensation showed a promising result in catalyzing the epoxidation of cyclohexene as well as vernonia oil. Among these group of materials, the one with a short channel and hexagonal particle morphology showed slightly higher catalytic activity than the corresponding materials which adopt fiber-like particle morphology. This difference is not significant due to the presence of catalytically inactive TiO_2 species in short channel material. As a result, the materials which have lower Ti content and free from anatase TiO_2 species have higher TON regardless of the particle morphology.

Ti-containing PMO materials also showed an effective catalytic performance. Among these catalysts, the one which has short channel path length showed higher catalytic activity with enhanced epoxide selectivity. Ti-PMO materials with hexagonal platelet

morphologies having short pore channels give better epoxide yield in the epoxidation of vernonia oil than those with conventional fiber-like morphologies possessing longer channels. These catalysts show promising epoxidation properties due to the short diffusion path obtained which could be further improved by achieving higher Ti loading as well as increased pore size which should be further studied in detail.

In general, Ti-containing SBA-15 and PMO materials showed promising results for epoxidizing the unsaturated carbon of the vernonia oil and its epoxy content enhanced significantly. The materials which have been synthesized by grafting method showed higher catalytic activity than their corresponding materials synthesized with the co-condensation method. This may attributed to the presence of more populated and accessible Ti active sites.

REFERENCES

1. C. K. Hong and R. P. Wool, *Journal of Applied Polymer Science*, 2005, **95**, 1524-1538.
2. Y. Shen, J. He, Z. Xie, X. Zhou, C. Fang and C. Zhang, *Industrial Crops and Products*, 2019, **140**, 1-6.
3. F. Haitz, S. Radloff, S. Rupp, M. Frohling, T. Hirth and S. Zibek, *Applied Biochemistry and Biotechnology*, 2018, **185**, 13-33.
4. S. G. Tan and W. S. Chow, *Polymer Plastics Technology and Engineering*, 2010, **49**, 1581-1590.
5. K. D. Carlson and S. P. Chang, *Journal of the American Oil Chemist' Society*, 1985, **62**, 934-939.
6. T. Baye, H. C. Becker and S. v. Witzke-Ehbrecht, *Industrial Crops and Products*, 2005, **21**, 257-261.
7. S. Dinda, A. V. Patwardhan, V. V. Goud and N. C. Pradhan, *Bioresource Technology*, 2008, **99**, 3737–3744.
8. E. Milchert, A. Smagowicz and G. Lewandowski, *Journal of Chemical Technology and Biotechnology*, 2010, **85**, 1099-1107.
9. N. Asfaw, Y. Chebude, A. Ejigu, B. B. Hurisso, P. Licence, R. L. Smith, S. L. Y. Tang and M. Poliakoff, *Green Chemistry*, 2011, **13**, 1059–1060.
10. S. M. Danov, O. A. Kazantsev, A. L. Esipovich, A. S. Belousov, A. E. Rogozhin and E. A. Kanakov, *Catalysis Science and Technology*, 2017, **7**, 3659-3675.
11. K. M. Choi, T. Yokoi, T. Tatsumi and K. Kuroda, *Journal of Materials Chemistry A*, 2013, **1**, 2485–2494.

12. M. Fukuda, N. Tsunoji, Y. Yagenji, Y. Ide, S. Hayakawa, M. Sadakane and T. Sano, *Journal of Materials Chemistry A*, 2015, **3**, 15280–15291.

13. N. Wilde, J. Přech, M. Pelz, M. Kubů, J. Čejka and R. Gläser, *Catalysis Science and Technology*, 2016, **6**, 7280-7288.

14. J. Přech, *Catalysis Reviews*, 2017, **60**, 71-131.

15. D. Zhao, J. Feng, Q. Huo, N. Melosh, G. H. Fredrickson, B. F. Chmelka and G. D. Stucky, *Science*, 1998, **279**, 548-552.

16. D. Zhao, Q. Huo, J. Feng, B. F. Chmelka and G. D. Stucky, *Journal of the American Chemical Society*, 1998, **120**, 6024-6036.

17. J. Iglesias, J. A. Melero and J. Sainz-Pardo, *Journal of Molecular Catalysis A: Chemical*, 2008, **291**, 75-84.

18. Y. Chen, Y. Huang, J. Xiu, X. Han and X. Bao, *Applied Catalysis A: General*, 2004, **273**, 185-191.

19. H. Chu, Y. Wan and D. Zhao, *Catalysis Today*, 2009, **148**, 19-27.

20. E. Gianotti, C. Bisio, L. Marchese, M. Guidotti, N. Ravasio, R. Psaro and S. Coluccia, *Journal of Physical Chemistry C*, 2007, **111**, 5083-5089.

21. W. Zhan, J. Yao, Z. Xiao, Y. Guo, Y. Wang, Y. Guo and G. Lu, *Microporous and Mesoporous Materials*, 2014, **183**, 150-155.

22. V. Gascon, I. Diaz, C. Marquez-Alvarez and R. M. Blanco, *Molecules*, 2014, **19**, 7057-7071.

23. J. A. Melero, J. Iglesias, J. M. Arsuaga, J. Sainz-Pardo, P. de Frutos and S. Blazquez, *Journal of Materials Chemistry*, 2007, **17**, 377-385.

24. I. Díaz, C. Márquez-Alvarez, F. Mohino, J. n. Pérez-Pariente and E. Sastre, *Journal of Catalysis*, 2000, **193**, 283-294.

25. I. Díaz, C. Márquez-Alvarez, F. Mohino, J. n. Pérez-Pariente and E. Sastre, *Journal of Catalysis*, 2000, **193**, 295-302.

26. K. Kosuge, T. Tetsu Sato, N. Kikukawa and M. Takemori, *Chemistry of Materials*, 2004, **16**, 899-905.

27. C. T. Kresge, M. E. Leonowicz, W. J. Roth, J. C. Vartuli and J. S. Beck, *Nature*, 1992, **359**, 710-712.

28. L. Cao, T. Man and M. Kruk, *Chemistry of Materials*, 2009, **21**, 1144–1153.

29. X. S. Zhao, X. Y. Bao, W. Guo and F. Y. Lee, *Materials Today*, 2006, **9**, 32-39.

30. W. Li and D. Zhao, *Chemical Communications*, 2013, **49**, 943-946.

31. Y. Wan and D. Zhao, *Chemical Reviews*, 2007, **107**, 2821-2860.

32. G. J. Soler-Illia, C. Sanchez, B. Lebeau and J. Patarin, *Chemical Reviews*, 2002, **102**, 4093−4138.

33. S. A. Bagshaw, E. Prouzet and T. J. Pinnavaiat, *Science*, 1995, **269**, 1242-1244.

34. S. Che, K. Lund, T. Tatsumi, S. Iijima, S. H. Joo, R. Ryoo and O. Terasaki, *Angewandte Chemie International Edition*, 2003, **42**, 2182 – 2185.

35. L. Han, J. Ruan, Y. Li, O. Terasaki and S. Che, *Chemistry of Materials*, 2007, **19**, 2860-2867.

36. E. Serra, Á. Mayoral, Y. Sakamoto, R. M. Blanco and I. Díaz, *Microporous and Mesoporous Materials*, 2008, **114**, 201-213.

37. E. M. Johansson, *Linköping Studies in Science and Technology*, 2010, 1-79.

38. R. Narayan, U. Y. Nayak, A. M. Raichur and S. Garg, *Pharmaceutics*, 2018, **10**, 1-49.

39. F. Hoffmann, M. Cornelius, J. Morell and M. Froba, *Angewandte Chemie International Edition*, 2006, **45**, 3216-3251.

40. E. M. Johansson, J. M. Córdoba and M. Odén, *Microporous and Mesoporous Materials*, 2010, **133**, 66-74.

41. P. Linton, H. Wennerstrom and V. Alfredsson, *Physical Chemistry Chemical Physics*, 2010, **12**, 3852-3858.

42. M. Ide, M. El-Roz, E. De Canck, A. Vicente, T. Planckaert, T. Bogaerts, I. Van Driessche, F. Lynen, V. Van Speybroeck, F. Thybault-Starzyk and P. Van Der Voort, *Physical Chemistry Chemical Physics*, 2013, **15**, 642-650.

43. D. He, C. Bai, C. Jiang and T. Zhou, *Powder Technology*, 2013, **249**, 151-156.

44. A. Gawarecka and A. Wróblewska, *Reaction Kinetics, Mechanisms and Catalysis*, 2018, **124**, 523-543.

45. M. Guidotti, *Journal of Catalysis*, 2003, **214**, 242-250.

46. Z. Luan and L. Kevan, *Microporous and Mesoporous Materials*, 2001, **44-45**, 337-344.

47. P. Célestin Bakala, E. Briot, L. Salles and J.-M. Brégeault, *Applied Catalysis A: General*, 2006, **300**, 91-99.

48. G. Du, S. Lim, M. Pinault, C. Wang, F. Fang, L. Pfefferle and G. L. Haller, *Journal of Catalysis*, 2008, **253**, 74-90.

49. S. Dworakowska, C. Tiozzo, M. Niemczyk-Wrzeszcz, P. Michorczyk, N. Ravasio, R. Psaro, D. Bogdał and M. Guidotti, *Journal of Cleaner Production*, 2017, **166**, 901-909.

50. A.-L. Adedigba, G. Sankar, C. R. A. Catlow, Y. Du, S. Xi and A. Borgna, *Microporous and Mesoporous Materials*, 2017, **244**, 83-92.

51. K. Lin, P. Pescarmona, H. Vandepitte, D. Liang, G. Vantendeloo and P. Jacobs, *Journal of Catalysis*, 2008, **254**, 64-70.

52. J. A. Melero, J. M. Arsuaga, P. de Frutos, J. Iglesias, J. Sainz and S. Blázquez, *Microporous and Mesoporous Materials*, 2005, **86**, 364–373.

53. W.-H. Zhang, J. Lu, B. Han, M. Li, J. Xiu, P. Ying and C. Li, *Chemistry of Materials*, 2002, **14**, 3413-3421.

54. N. Mizoshita, T. Tani and S. Inagaki, *Chemical Society Reviews*, 2011, **40**, 789-800.

55. Q. Yang, J. Liu, L. Zhang and C. Li, *Journal of Materials Chemistry*, 2009, **19**, 1945-1955.

56. R. M. Blanco, P. Terreros, M. Fernández-Pérez, C. Otero and G. Díaz-González, *Journal of Molecular Catalysis B: Enzymatic*, 2004, **30**, 83-93.

57. D. Esquivel, P. Van Der Voort and F. J. Romero-Salguero, *AIMS Materials Science*, 2014, **1**, 70-86.

58. S. Inagaki, S. Guan, Y. Fukushima, T. Ohsuna and O. Terasaki, *Journal of the American Chemical Society*, 1999, **21**, 9611-9614.

59. V. Gascón, I. Díaz, R. M. Blanco and C. Márquez-Álvarez, *RSC Advances*, 2014, **4**, 34356–34368.

60. S. Z. Qiao, C. Z. Yu, Q. H. Hu, Y. G. Jin, X. F. Zhou, X. S. Zhao and G. Q. Lu, *Microporous and Mesoporous Materials*, 2006, **91**, 59-69.

61. F. Lin, X. Meng, E. Kukueva, M. Kus, M. Mertens, S. Bals, S. Van Doorslaer and P. Cool, *Microporous and Mesoporous Materials*, 2015, **207**, 61-70.

62. N. Suriyanon, P. Punyapalakul and C. Ngamcharussrivichai, *Materials Chemistry and Physics*, 2015, **149-150**, 701-712.

63. E. De Canck, I. Dosuna-Rodriguez, E. M. Gaigneaux and P. Van Der Voort, *Materials (Basel)*, 2013, **6**, 3556-3570.

64. F. Goethals, I. Ciofi, O. Madia, K. Vanstreels, M. R. Baklanov, C. Detavernier, P. Van Der Voort and I. Van Driessche, *Journal of Materials Chemistry*, 2012, **22**, 8281-8286.

65. E. De Canck, L. Lapeire, J. De Clercq, F. Verpoort and P. Van der Voort, *Langmuir*, 2010, **26**, 10076-10083.

66. E. Serra, E. Díez, I. Díaz and R. M. Blanco, *Microporous and Mesoporous Materials*, 2010, **132**, 487-493.

67. A. Bhaumik, M. P. Kapoor and S. Inagaki, *Chemical Communications*, 2003, 470-471.

68. H. Chu, Y. Wan and D. Zhao, *Catalysis Today*, 2009, **148**, 19-27.

69. A. Gandini and T. M. Lacerda, *Progress in Polymer Science*, 2015, **48**, 1-39.

70. G. p. o. v. o. f. t. Statista, a. a. h. 2018/19 (in million metric tons), www.statista.com/statistics/263978/global-vegetable-oil- and a. b. J. production-since-2000-2001/, 2019.

71. L. Maisonneuve, T. Lebarbé, E. Grau and H. Cramail, *Polymer Chemistry*, 2013, **4**, 5472.

72. M. A. R. Meier, J. O. Metzger and U. S. Schubert, *Chemical Society Reviews*, 2007, **36**, 1788-1802.

73. H. N. Cheng and A. Biswas, *Green Polymer Chemistry: Biobased Materials and Biocatalysis*, 2015, **1192**, 235-247.

74. S.-C. Chua, X. Xu and Z. Guo, *Process Biochemistry*, 2012, **47**, 1439-1451.

75. H. A. Shimelis, M. T. Labuschagne and A. Hugo, *South African Journal of Plant and Soil*, 2006, **23**, 62-63.

76. R. E. Perdue, K. D. Carlson and M. G. Gilbert, *Economic Botany*, 1986, **40**, 54-68.

77. T. Desalegn, I. J. V. Garcia, J. Titman, P. Licence, I. Diaz and Y. Chebude, *Starch - Stärke*, 2014, **66**, 385-392.

78. S. Grinberg, V. Kolot and D. Mills, *Industrial Crops and Products*, 1994, **3**, 113-119.

79. T. Baye and H. C. Becker, *Genetic Resources and Crop Evolution*, 2005, **52**, 805-811.

80. V. Kolot and S. Grinberg, *Journal of Applied Polymer Science*, 2004, **91**, 3835-3843.

81. H. Shimelis and E. T. Gwat, *African Center for Crop Improvement*, 2013, 131-148.

82. F. O. Ayorinde, B. D. Butler and M. T. Clayton, *Journal of the American Oil Chemists' Society*, 1990, **67**, 844-845.

83. H. L. Bhardwaj, A. A. Hamama and D. A. Dierig, *Journal of the American Oil Chemists' Society*, 2007, **84**, 393-397.

84. K. F. Adekunle, *Open Journal of Polymer Chemistry*, 2014, **04**, 95-101.

85. J. R. Kim and S. Sharma, *Industrial Crops and Products*, 2012, **36**, 485-499.

86. M. Guidotti, E. Gavrilova, A. Galarneau, B. Coq, R. Psaro and N. Ravasioa, *Green Chemistry*, 2011, **13**, 1806–1811.

87. T. Vlček and Z. S. Petrović, *Journal of the American Oil Chemists Society*, 2006, **83**, 247-252.

88. P. T. Wai, P. Jiang, Y. Shen, P. Zhang, Q. Gu and Y. Leng, *RSC Advances*, 2019, **9**, 38119–38136.

89. S. M. Danov, O. A. Kazantsev, A. L. Esipovich, A. S. Belousov, A. E. Rogozhin and E. A. Kanakov, *Catalysis Science & Technology*, 2017, 1-16.

90. W. Cheng, Y. Jiang, X. Xu, Y. Wang, K. Lin and P. P. Pescarmona, *Journal of Catalysis*, 2016, **333**, 139-148.

91. A. Campanella, M. A. Baltanás, M. C. Capel-Sánchez, J. M. Campos-Martín and J. L. G. Fierro, *Green Chemistry*, 2004, **6**, 330-334.

92. M. Guidotti, N. Ravasio, R. Psaro, E. Gianotti, L. Marchese and S. Coluccia, *Green Chemistry*, 2003, **5**, 421–424.

93. D. Kumar and A. Ali, *Energy & Fuels*, 2012, **26**, 2953-2961.

94. X. Ye, P. Jiang, P. Zhang, Y. Dong, C. Jia, X. Zhang and H. Xu, *Catalysis Letters*, 2010, **137**, 88-93.

95. M. Guidotti, I. Batonneau-Gener, E. Gianotti, L. Marchese, S. Mignard, R. Psaro, M. Sgobba and N. Ravasio, *Microporous and Mesoporous Materials*, 2008, **111**, 39-47.

96. Y. Shen, P. Jiang, P. T. Wai, Q. Gu and W. Zhang, *Catalysts*, 2019, **9**, 31.

97. S. N. Khot, J. J. Lascala, E. Can, S. S. Morye, G. I. Williams, G. R. Palmese, S. H. Kusefoglu and R. P. Wool, *Journal of Applied Polymer Science*, 2001, **82**, 703-723.

98. S. Miao, W. Zhu, N. J. Castro, M. Nowicki, X. Zhou, H. Cui, J. P. Fisher and L. G. Zhang, *Scientific Reports*, 2016, **6**, 1-10.

99. G. Karmakar, P. Ghosh and B. Sharma, *Lubricants*, 2017, **5**, 1-17.

100. J. L. Zheng, P. Tolvanen, B. Taouk, K. Eränen, S. Leveneur and T. Salmi, *Chemical Engineering Research and Design*, 2018, **132**, 9-18.

101. L. Poussard, J. Mariage, B. Grignard, C. Detrembleur, C. Jérôme, C. Calberg, B. Heinrichs, J. De Winter, P. Gerbaux, J. M. Raquez, L. Bonnaud and P. Dubois, *Macromolecules*, 2016, **49**, 2162-2171.

102. K. Błażek and J. Datta, *Critical Reviews in Environmental Science and Technology*, 2019, **49**, 173-211.

103. S. Doley and S. K. Dolui, *European Polymer Journal*, 2018, **102**, 161-168.

104. J. K. Cockcroft and A. N. Fitch, *Powder Diffraction: Theory and Practice, The Royal Society of Chemistry*, 2008, 20-57.

105. R. E. Dinnebier and S. J. L. Billinge, *Powder Diffraction: Theory and Practice, The Royal Society of Chemistry*, 2008, 1-19.

106. R. Sharma, D. P. Bisen, U. Shukla and B. G. Sharma, *Recent Research in Science and Technology*, 2012, **4**, 77-79.

107. K. S. W. Sing, D. H. Everett, R. A. W. Haul, L. Moscou, R. A. Pierotti, J. Rouquerol and T. Siemieniewska, *Pure and Applied Chemistry*, 1985, **57**, 603 -619.

108. M. Thommes, K. Kaneko, A. V. Neimark, J. P. Olivier, F. Rodriguez-Reinoso, J. Rouquerol and K. S. W. Sing, *Pure and Applied Chemistry*, 2015, **87**, 1051-1069.

109. J. P. Bonnelle, *Surface Properties and Catalysis*, 1983, 237-272.

110. M. L. Myrick, M. N. Simcock, M. Baranowski, H. Brooke, S. L. Morgan and J. N. McCutcheon, *Applied Spectroscopy Reviews*, 2011, **46**, 140–165.

111. V. L. P. Somsubhra Ghosh, B. Sowjanya, P. Srivani, M. Alagaraja, David Banji *Asian Journal of Pharmaceutical Analysis*, 2013, **3**, 24-33.

112. K. R. J. Mamatha Veeramachaneni, *Journal of Advanced Pharmacy Education & Research*, 2013, **3**, 516-522.

113. D. J. E. A. Michael Dunlap, *Facility for advanced instrumentation,U. C. Davis*, 1997, 1-51.

114. T. Radeti, *Fundamentals of Scanning Electron Microscopy and Energy Dispersive X-ray Analysis in SEM and TEM*, University of Belgrade Faculty of Technology and Metallurgy, Beograd, Serbia, 2011.

115. W. Wan, C. Xiao and X. Zou, *in Mesoporous Zeolites, Wiley-VCH Verlag GmbH & Co. KGaA*, 2015, 425-460.

116. D. J. Smith, in *Nanocharacterisation*, The Royal Society of Chemistry, 2015, DOI: 10.1039/9781782621867-00001, pp. 1-29.

117. A. R. Lupini, S. N. Rashkeev, M. Varela, A. Y. Borisevich, M. P. Oxley, K. van Benthem, Y. Peng, N. de Jonge, G. M. Veith, T. J. Pennycook, W. Zhou, R. Ishikawa, M. F. Chisholm, S. T. Pantelides and S. J. Pennycook, *Chapter 2 Scanning Transmission Electron Microscopy pp. 30-79 in Nanocharacterisation 2nd Edition. Book serious RSC Nanoscience and nanotechnology No 37. Editors: Angus I Kirkland, Sarah J Haigh. Publisher: The Royal Society of Chemistry 2015. ISBN: 978-1-84973-805-7.*

118. J. Czarnecki and J. Šesták, *Journal of Thermal Analysis and Calorimetry*, 2000, **60**, 759-778.

119. G. Gómez, J. Á. Botas, D. P. Serrano and P. Pizarro, *Catalysis Today*, 2016, **277**, 152-160.

120. L. Cao and M. Kruk, *Colloid Surface A*, 2010, **357**, 91-96.

121. J. M. Kim, Y.-J. Han, G. D. Stucky and B. F. Chmelka, *Chemical Communications*, 2000, 2437-2438.

122. J. A. Melero, J. Iglesias, J. M. Arsuaga, J. Sainz-Pardo, P. de Frutos and S. Blazquez, *Journal of Materials Chemistry*, 2007, **17**, 377-385.

123. S. Z. Qiao, H. Djojoputro, Q. Hu and G. Q. Lu, *Progress in Solid State Chemistry*, 2006, **34**, 249-256.

124. A. Alfayate, C. Márquez-Álvarez, M. Grande-Casas, B. Bernardo-Maestro, M. Sánchez-Sánchez and J. Pérez-Pariente, *Catalysis Today*, 2013, **213**, 211-218.

125. V. Sazo, C. M. López, M. De Quesada and J. M. Vieira, *Catalysis Today*, 2011, **172**, 8-12.

126. V. Meynen, P. Cool and E. F. Vansant, *Microporous and Mesoporous Materials*, 2009, **125**, 170-223.

127. T. P. B. Nguyen, J.-W. Lee, W. G. Shim and H. Moon, *Microporous and Mesoporous Materials*, 2008, **110**, 560-569.

128. Y. Yao, J. Feng, L. Han and S. Che, *RSC Advances*, 2015, **5**, 102256-102260.

129. P. Yuan, S. Yang, H. Wang, M. Yu, X. Zhou, G. Lu, J. Zou and C. Yu, *Langmuir*, 2008, **24**, 5038-5043.

130. M. C. Capel-Sanchez, J. M. Campos-Martin, J. L. G. Fierro, M. P. de Frutos and A. P. Polo, *Chemical Communications*, 2000, 855-856.

131. R. V. Grieken, G. Calleja, G. D. Stucky, J. A. Melero, R. A. Garcia and J. Iglesias, *Langmuir*, 2003, **19**, 3966-3973.

132. Z. Alothman, *Materials (Basel)*, 2012, **5**, 2874-2902.

133. Z. Wang and K. J. Balkus, *Microporous and Mesoporous Materials*, 2017, **243**, 76-84.

134. G. Eimer, S. Casuscelli, G. Ghione, M. Crivello and E. Herrero, *Applied Catalysis A: General*, 2006, **298**, 232-242.

135. G. A. Eimer, S. G. Casuscelli, C. M. Chanquia, V. Elías, M. E. Crivello and E. R. Herrero, *Catalysis Today*, 2008, **133-135**, 639-646.

136. L. Y. Chen, G. K. Chuah and S. Jaenicke, *Catalysis Letter*, 1998, **50**, 107-114.

137. H. L. Xie, Y. X. Fan, C. H. Zhou, Z. X. Du, E. Z. Min, Z. H. Ge and X. N. Lia, *Chemical and Biochemical Engineering Quarterly*, 2008, **22**, 25–39

138. J. M. Notestein, A. Solovyov, L. R. Andrini, F. G. Requejo, A. Katz and E. Iglesia, *Journal of the American Chemical Society*, 2007, **129**, 15585-15595.

139. J. M. Thomas, R. Raja and D. W. Lewis, *Angewandte Chemie International Edition*, 2005, **44**, 6456-6482.

140. S. Grinberg, V. Kolot and D. Mills, *Industrial Crops and Products*, 1994, **3**, 113-119.

141. P. Muturi, D. Wang and S. Dirlikov, *Progress in Organic Coatings*, 1994, **25**, 85-94.

142. M. D. Guillén and N. Cabo, *Journal of the American Oil Chemists Society*, 1997, **74**, 1281-1286.

143. B. M. Wamalwa, E. N. Njuguna, P. M. Shiundu and G. N. Kamau, *Bulletin Chemical Society of Ethiopia*, 2000, **14**, 161-168.

144. L. Rios, P. Weckes, H. Schuster and W. Hoelderich, *Journal of Catalysis*, 2005, **232**, 19-26.

145. W. Xia, S. M. Budge and M. D. Lumsden, *Journal of Agricultural and Food Chemistry*, 2015, **63**, 5780-5786.

146. M. Hong, M.-Y. Yao and H. Pan, *RSC Advances*, 2015, **5**, 91558–91563.

147. T. D. Zeleke and Y. M. Ayana, *American Journal of Applied Chemistry*, 2017, **5**, 1-6.

148. A. Sammaiah, K. V. Padmaja and R. B. Narayna Prasad, *Journal of Oleo Science*, 2014, **63**, 637-643.

APPENDICES

A

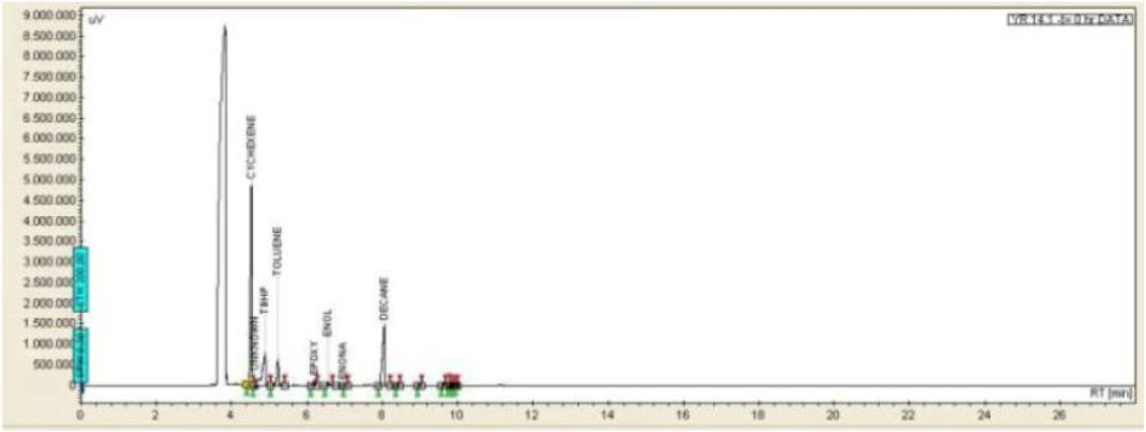

B

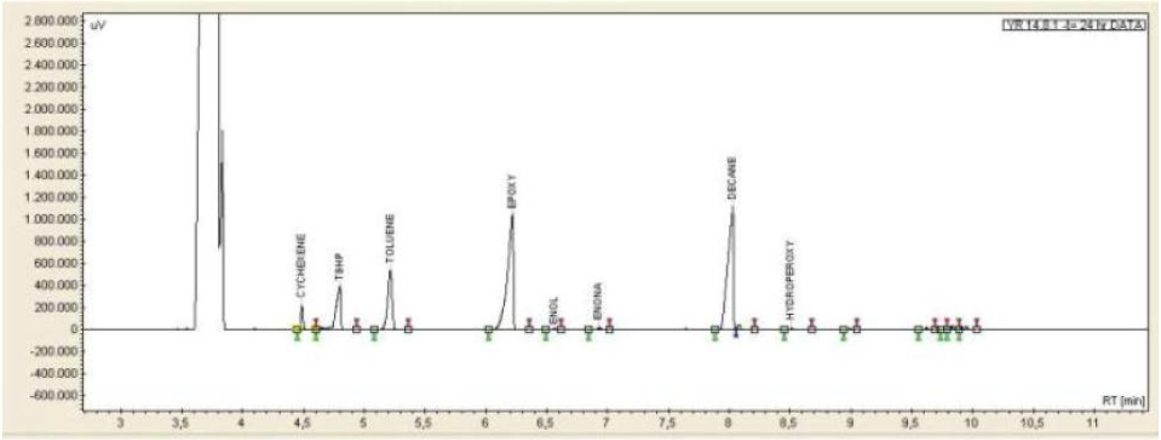

Figure 119. The spectra of gas chromatography of epoxidation of cyclohexene at 0 h (A) and 24 h (B) reaction time

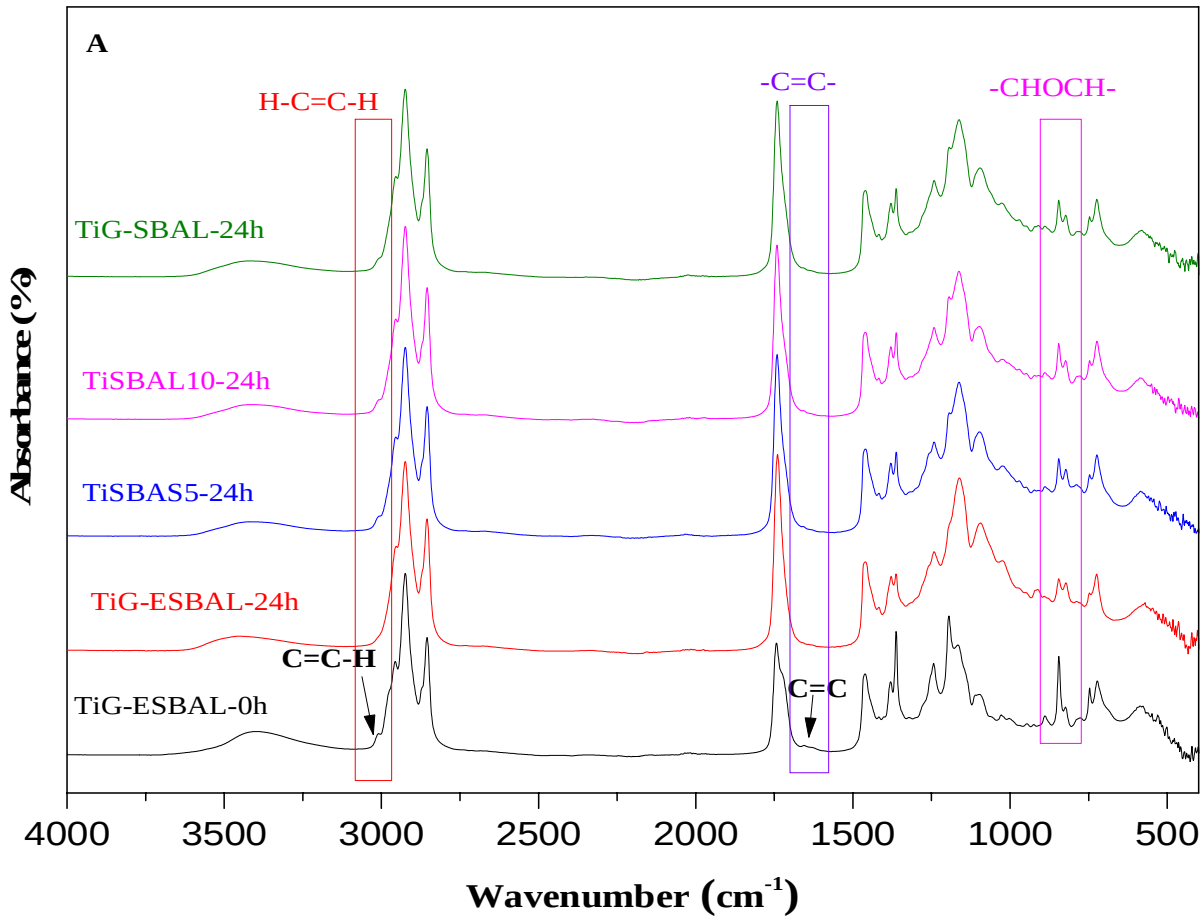
A
H-C=C-H
-C=C-
-CHOCH-
TiG-SBAL-24h
TiSBAL10-24h
TiSBAS5-24h
TiG-ESBAL-24h
TiG-ESBAL-0h
C=C-H
C=C
Absorbance (%)
4000
3500
3000
2500
2000
1500
1000
500
Wavenumber (cm-1)

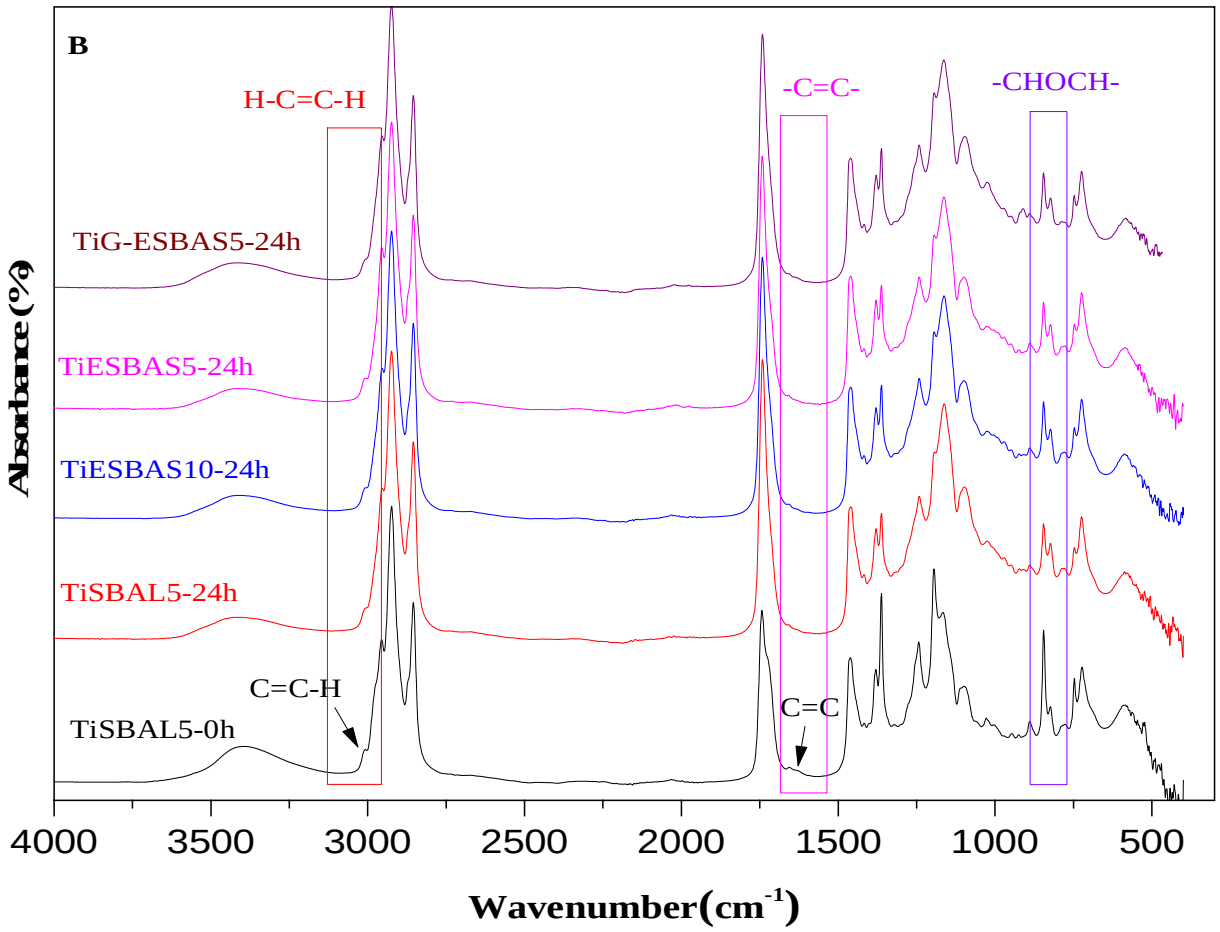
B
H-C=C-H
-C=C-
-CHOCH-
TiG-ESBAS5-24h
TiESBAS5-24h
TiESBAS10-24h
TiSBAL5-24h
C=C-H
TiSBAL5-0h
C=C
Absorbance (%)
4000
3500
3000
2500
2000
1500
1000
500
Wavenumber(cm-1)

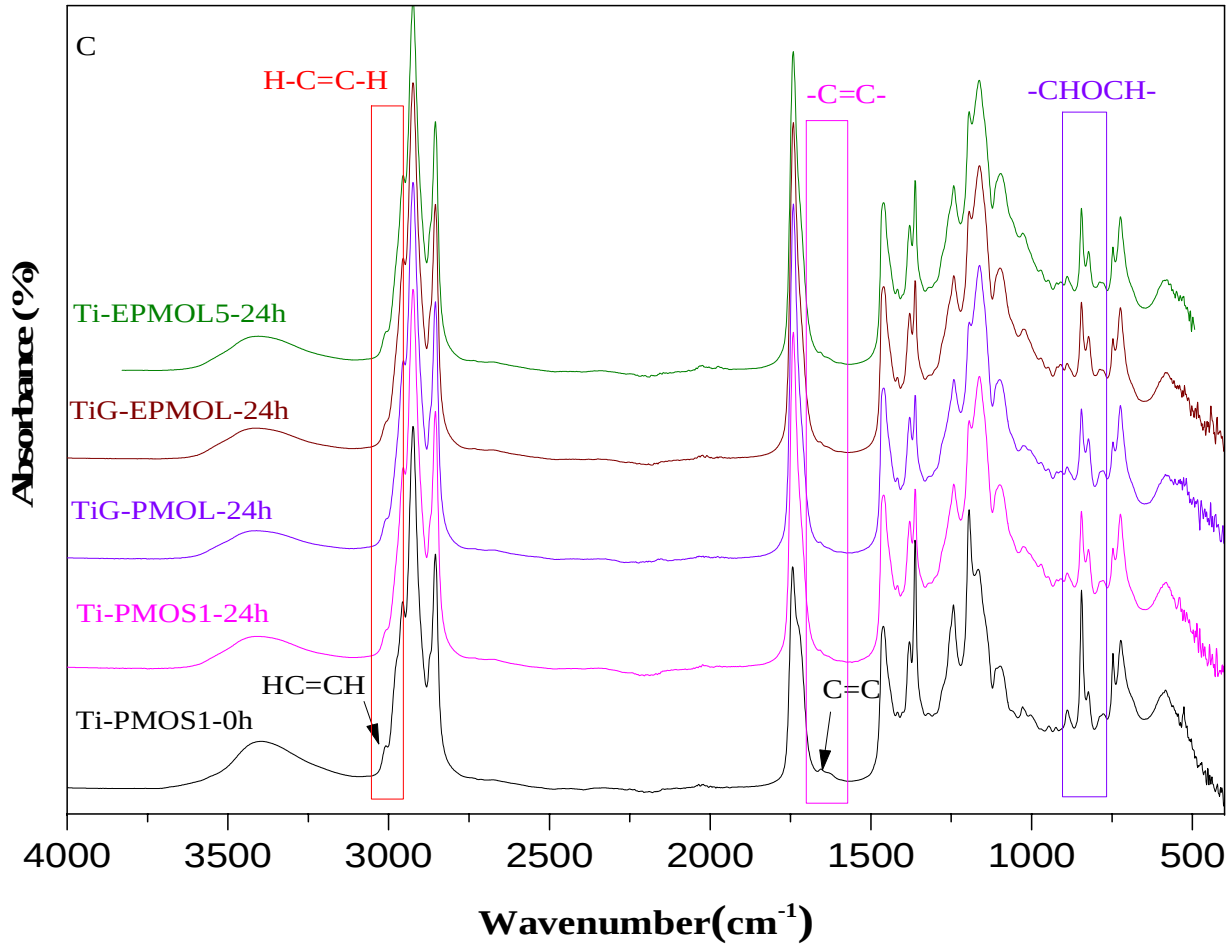

Figure 120 (A-C). ATR-FTIR spectra of reaction mixture collected using different catalysts, indicating the assignment of vibration bands corresponding to olefinic and epoxide groups in vernonia oil. Only the zero and 24 h reaction time products are included in the figure to show the decrease of olefinic peak intensities and increase of the epoxide peak intensities. The overlapping of C-O stretching of the oxidant TBHP at the same region of C-O stretching of epoxy group disturbs the comparison of epoxide group's intensity before and after the reaction.

(A) ^{1}H and ^{13}C NMR of vernonia oil (VO)

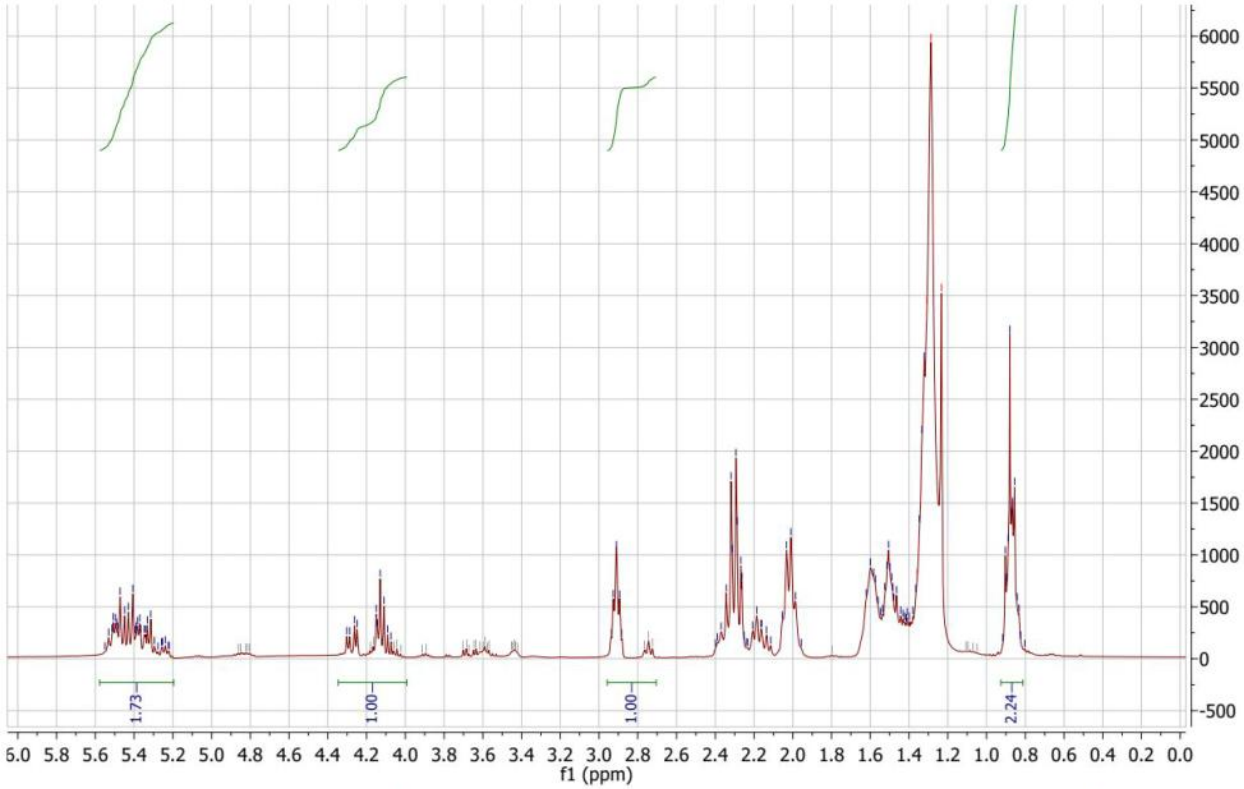

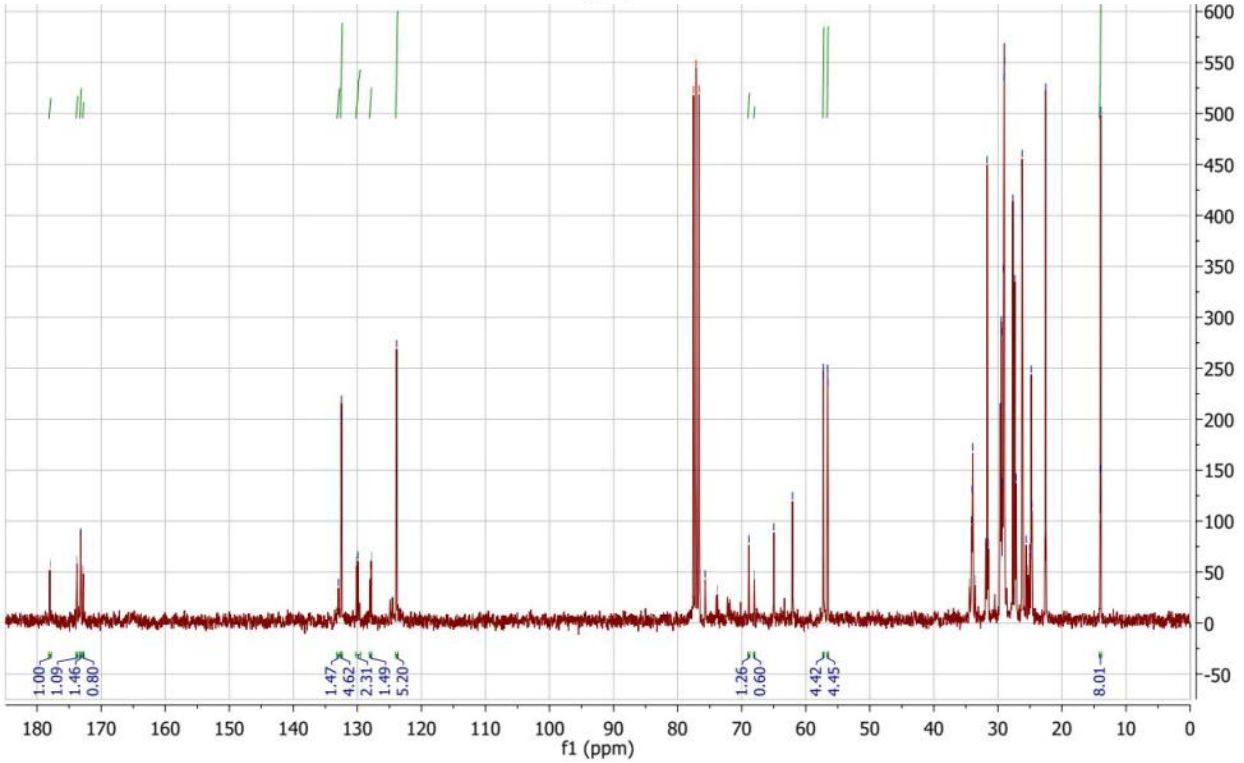

(B) ^{1}H and ^{13}C NMR of EVO by using TiG-ESBA-L as a catalyst at 70 ^{o}C for 24 h

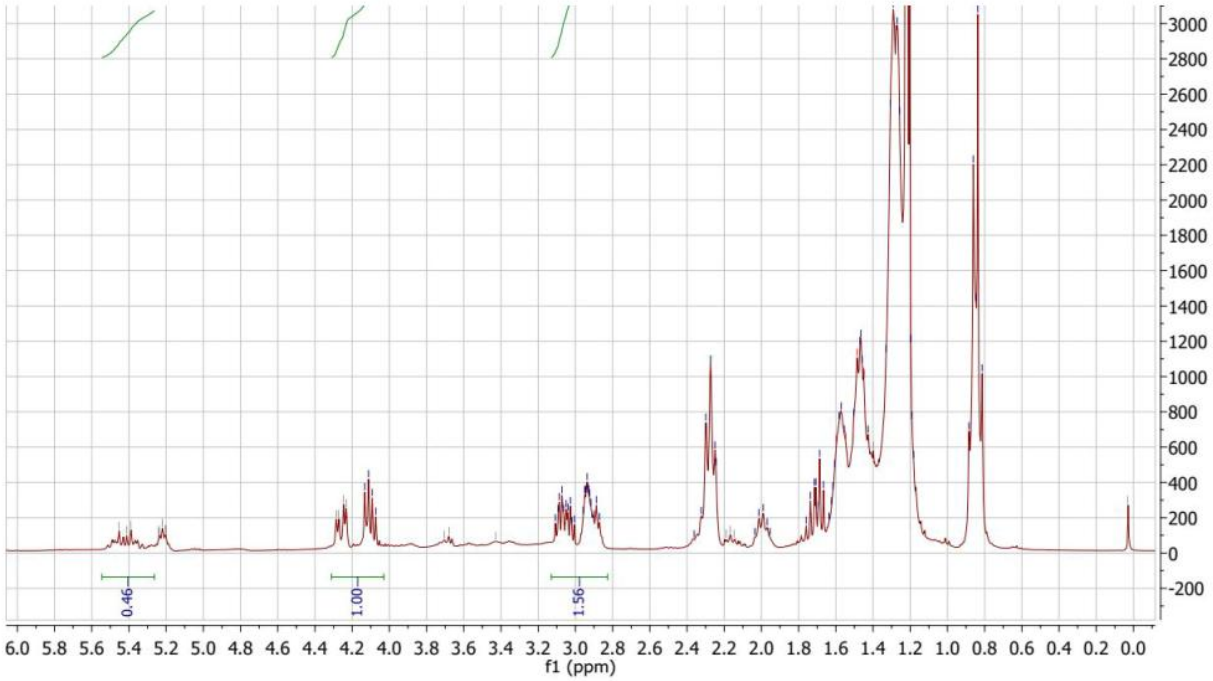

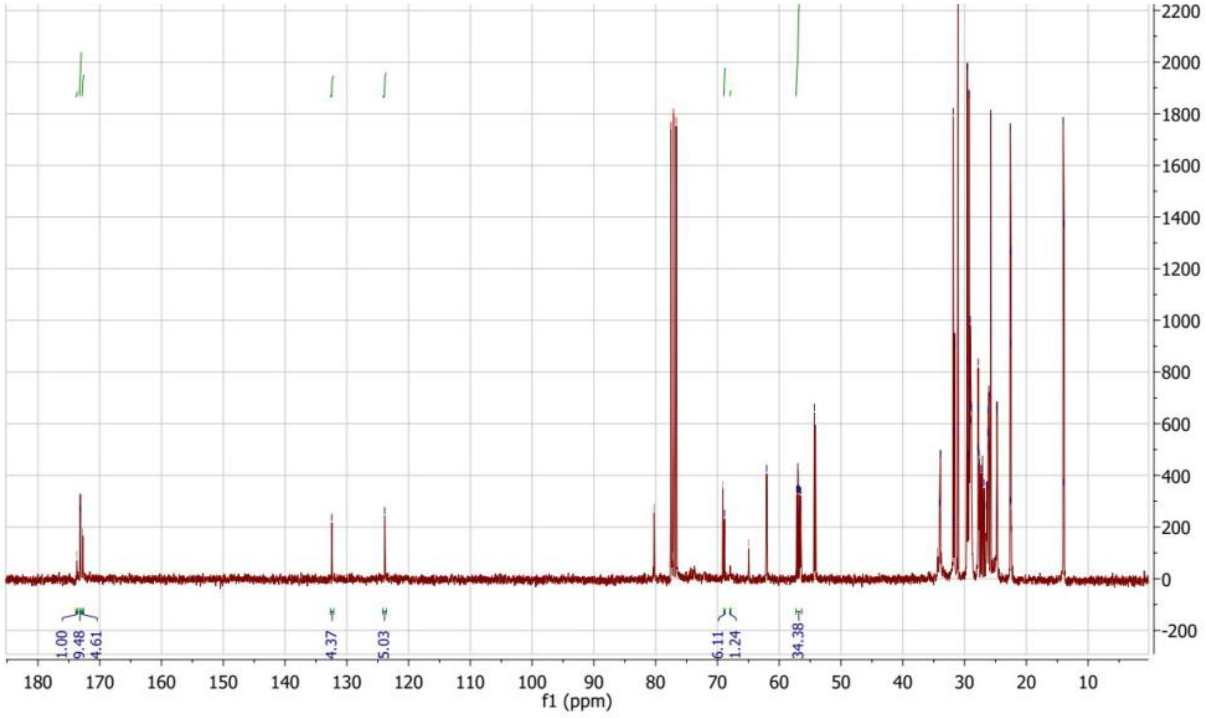

(C) ^{1}H and ^{13}C NMR of EVO by using TiG-SBA-L as a catalyst at 70 ^{o}C for 24 h

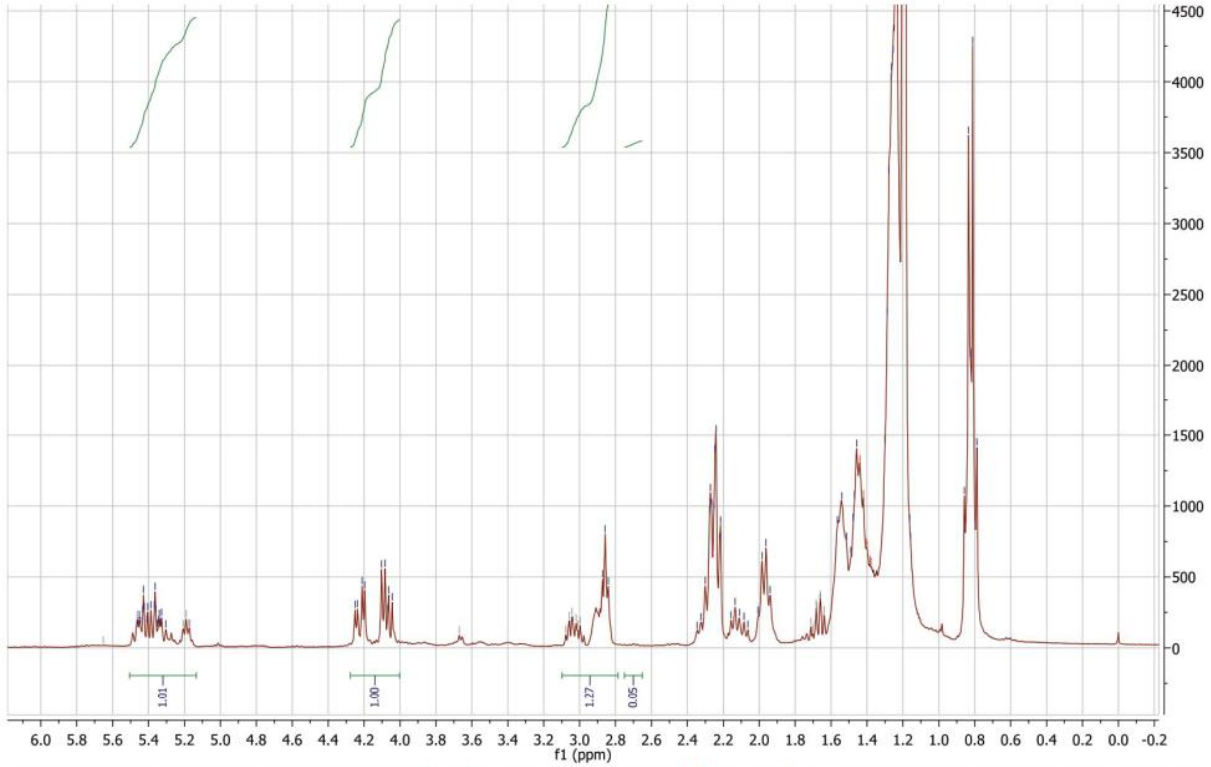

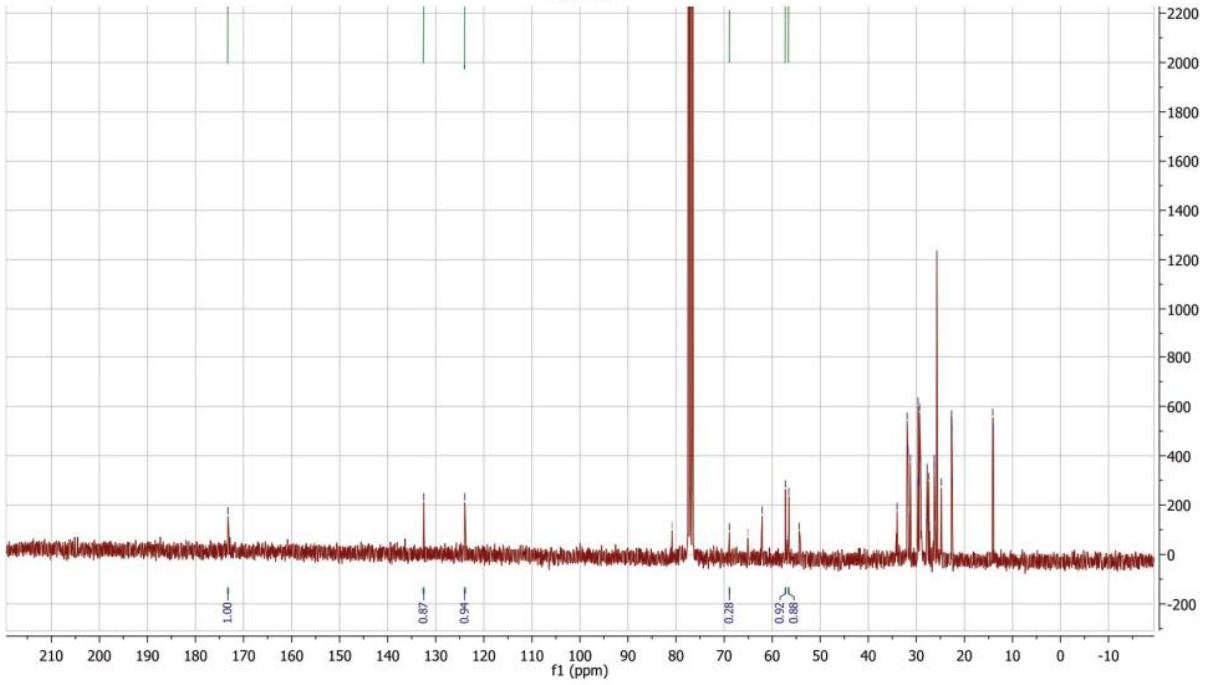

(D) ^{1}H and ^{13}C NMR of EVO by using TiG-ESBA-S5 as a catalyst at 70 ^{o}C for 24 h

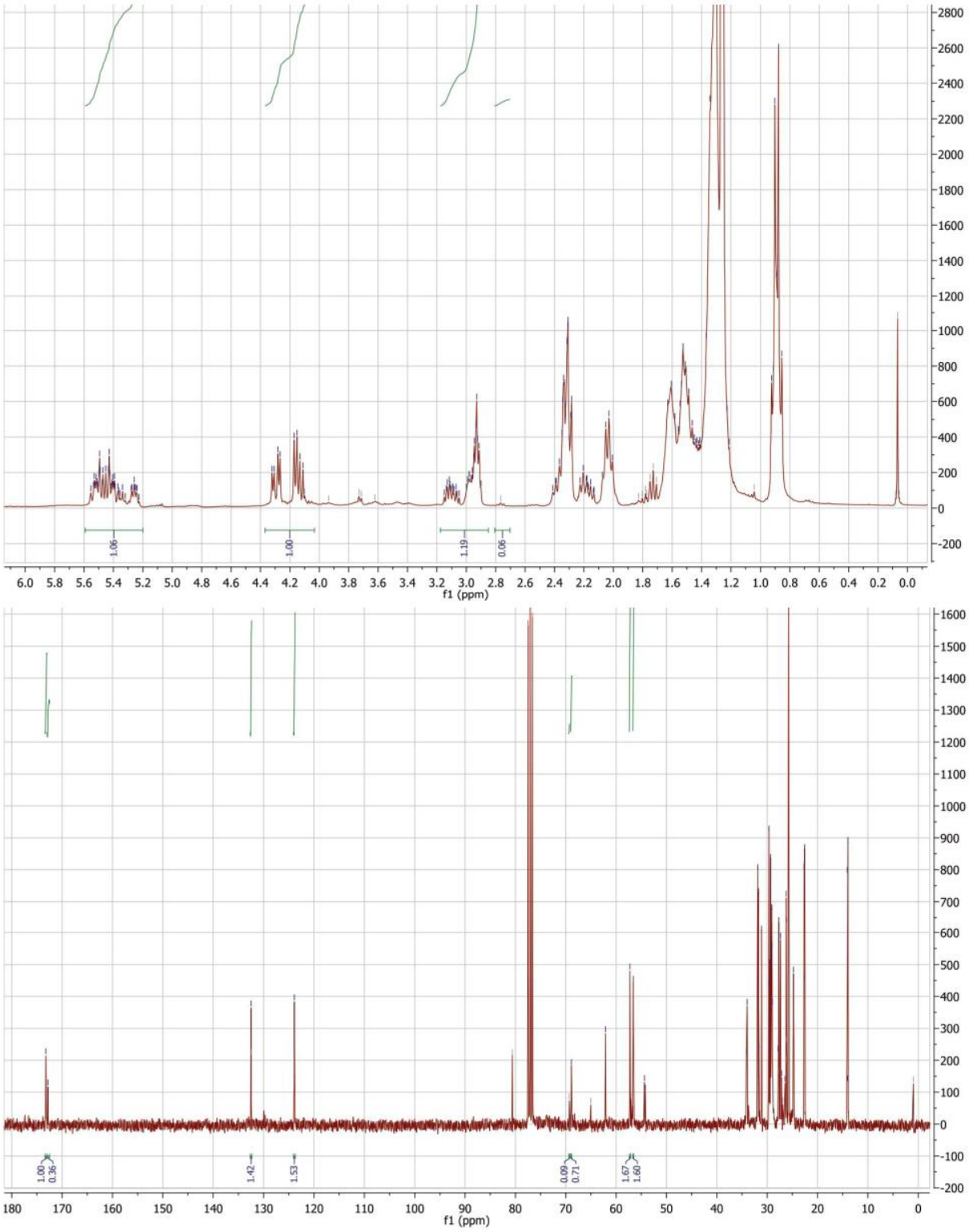

(E) ^{1}H and ^{13}C NMR of EVO by using TiSBAS5 as a catalyst at 70 ^{o}C for 24 h

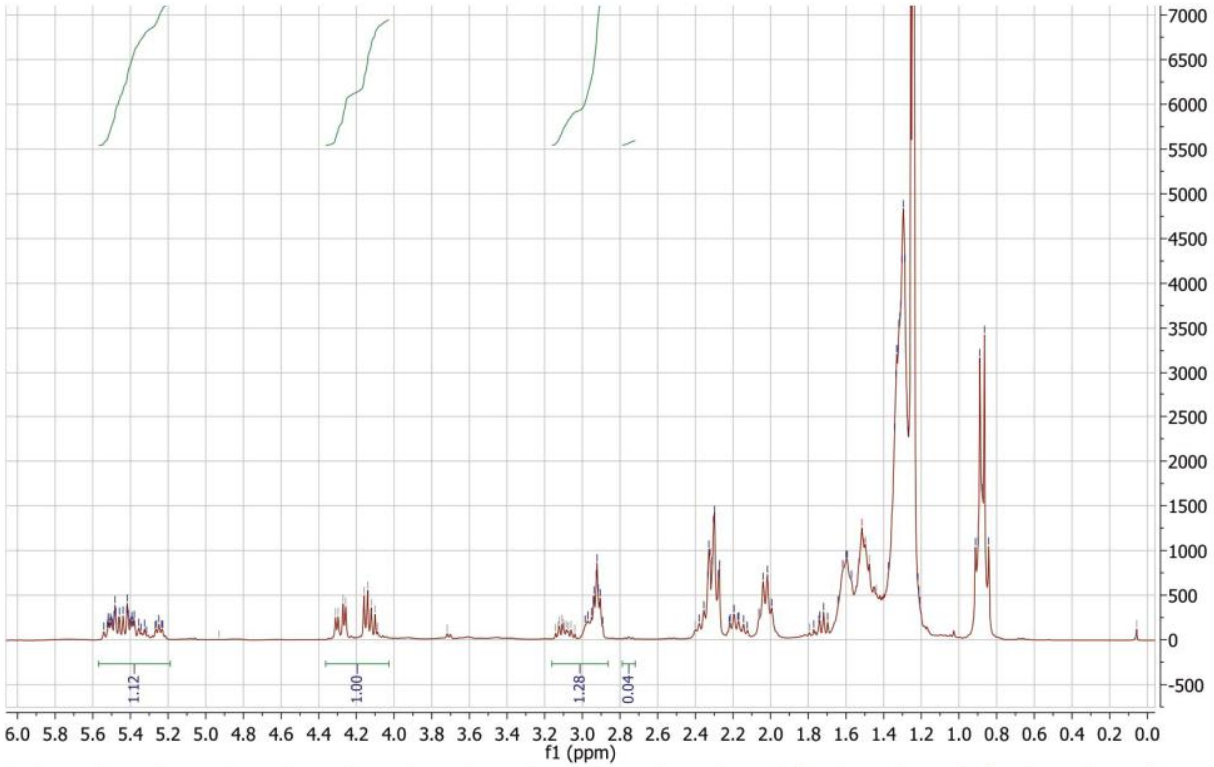

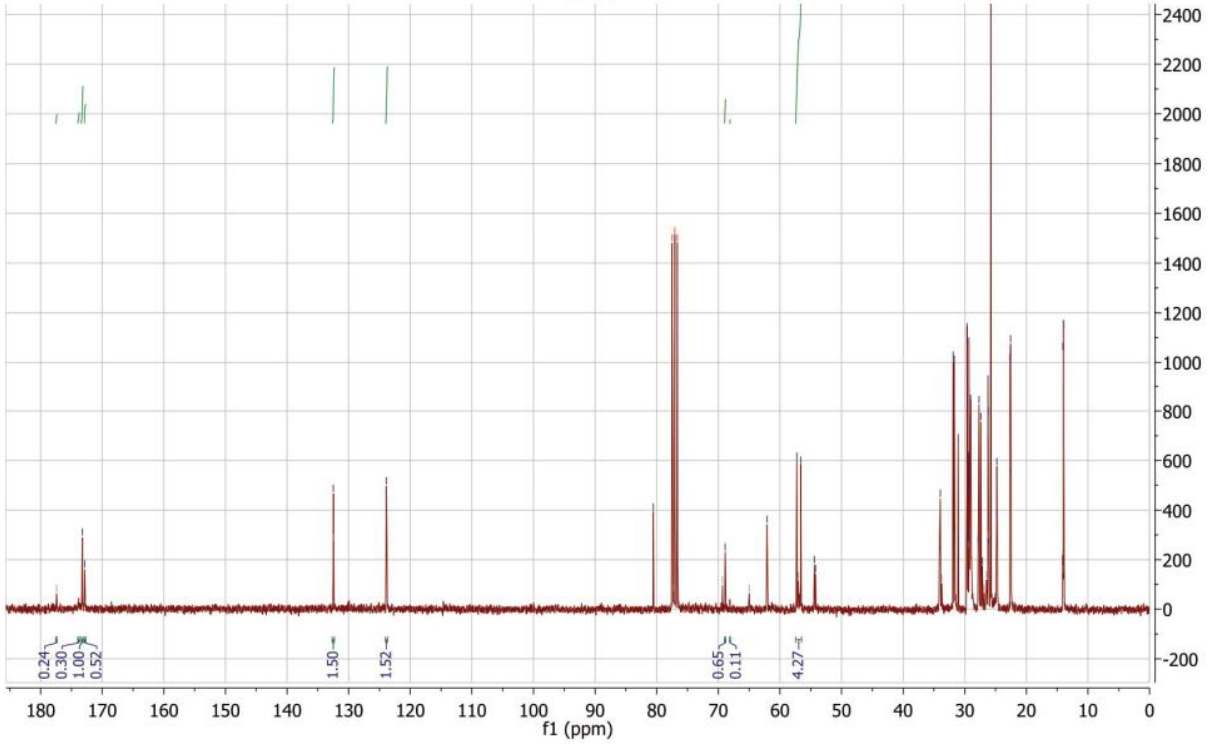

(F) ^{1}H and ^{13}C NMR of EVO by using Ti-ESBA-S5 as a catalyst at 70 ^{o}C for 24 h

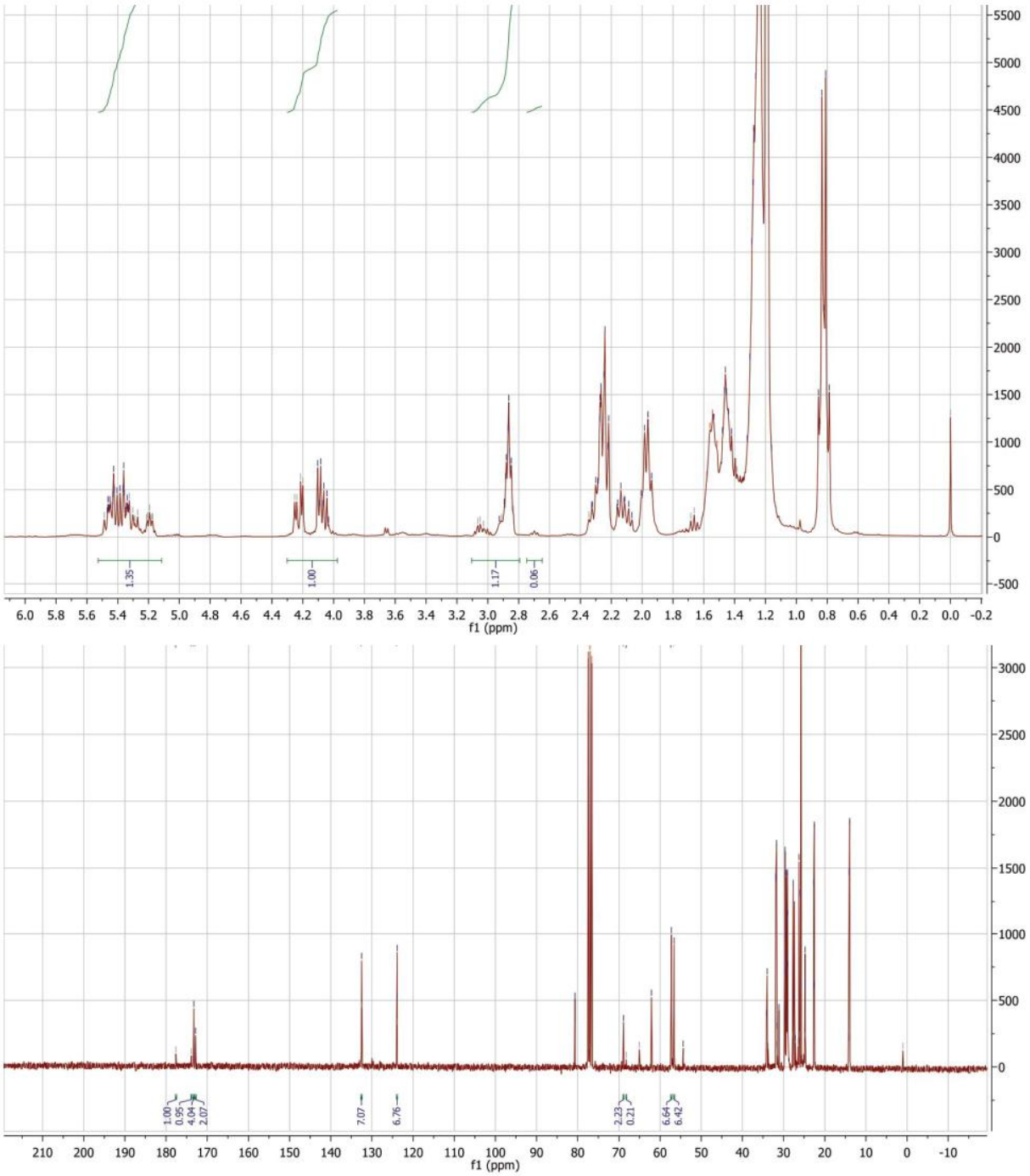

(G) ^{1}H and ^{13}C NMR of EVO by using Ti-ESBA-S10 as a catalyst at 70 ^{o}C for 24 h

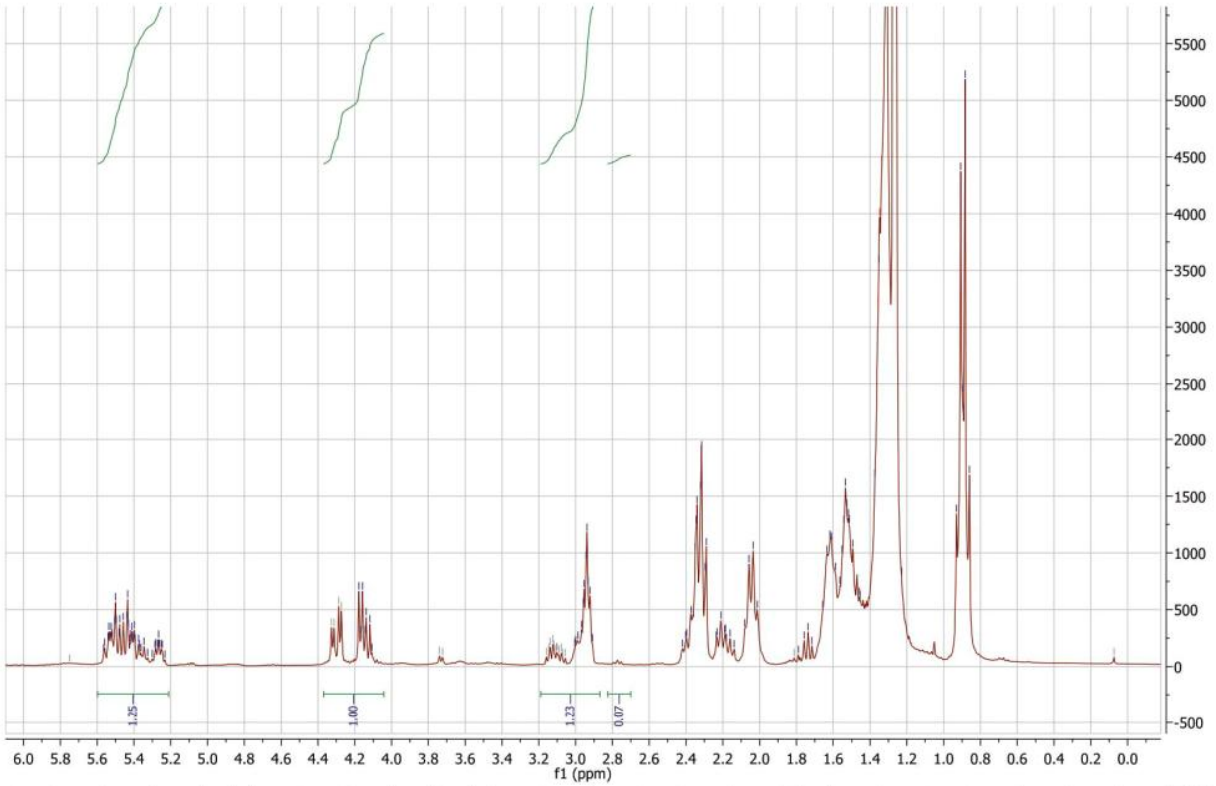

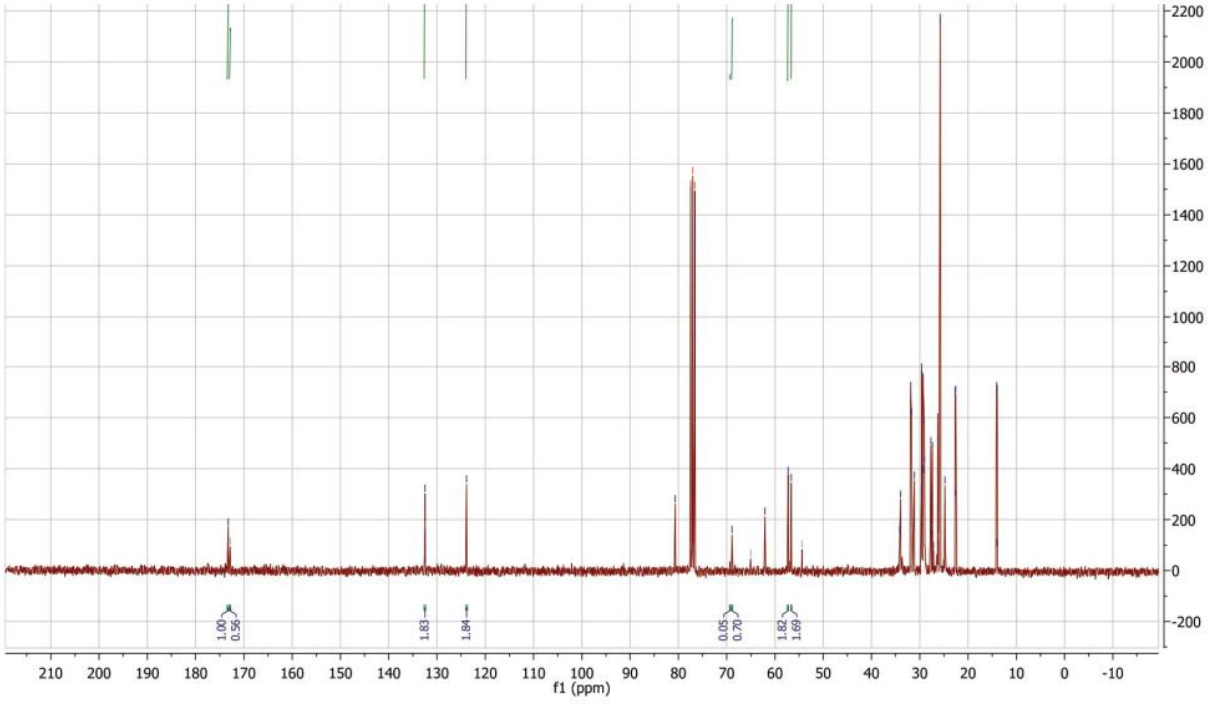

(H) ^{1}H and ^{13}C NMR of EVO by using TiSBAL5 as a catalyst at 70 ^{o}C for 24 h

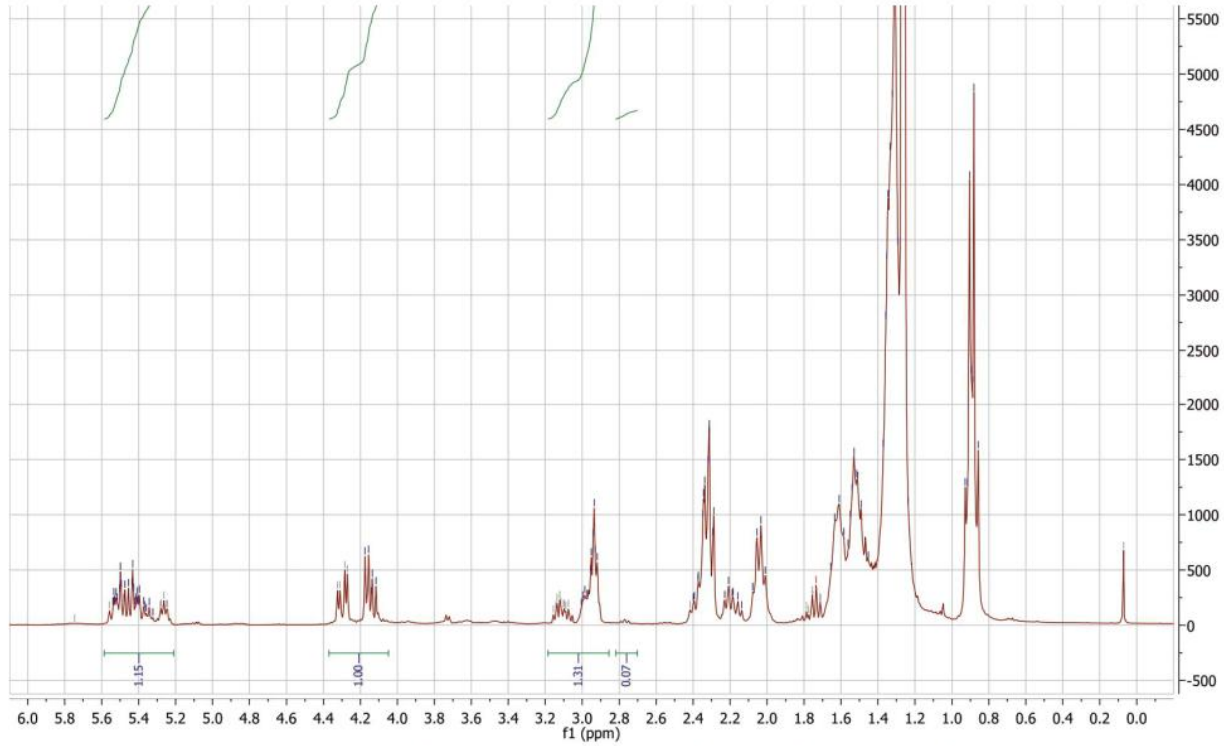

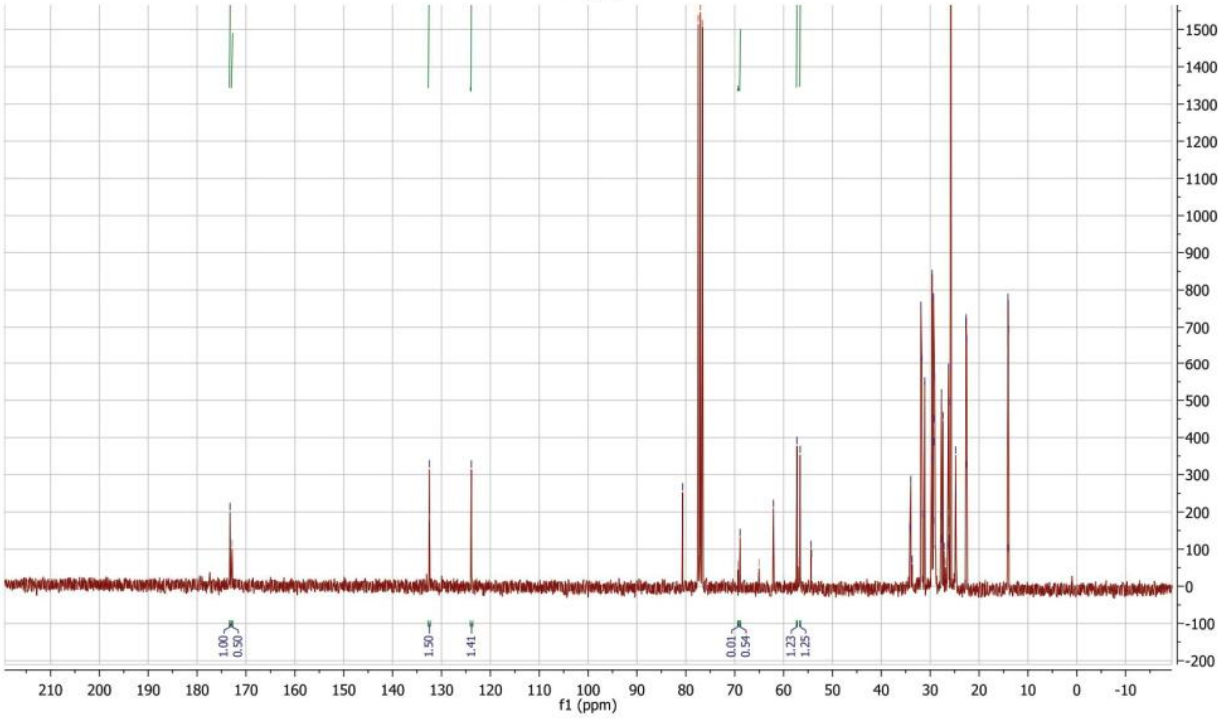

(I) ^{1}H and ^{13}C NMR of EVO by using TiSBAL10 as a catalyst at 70 ^{o}C for 24 h

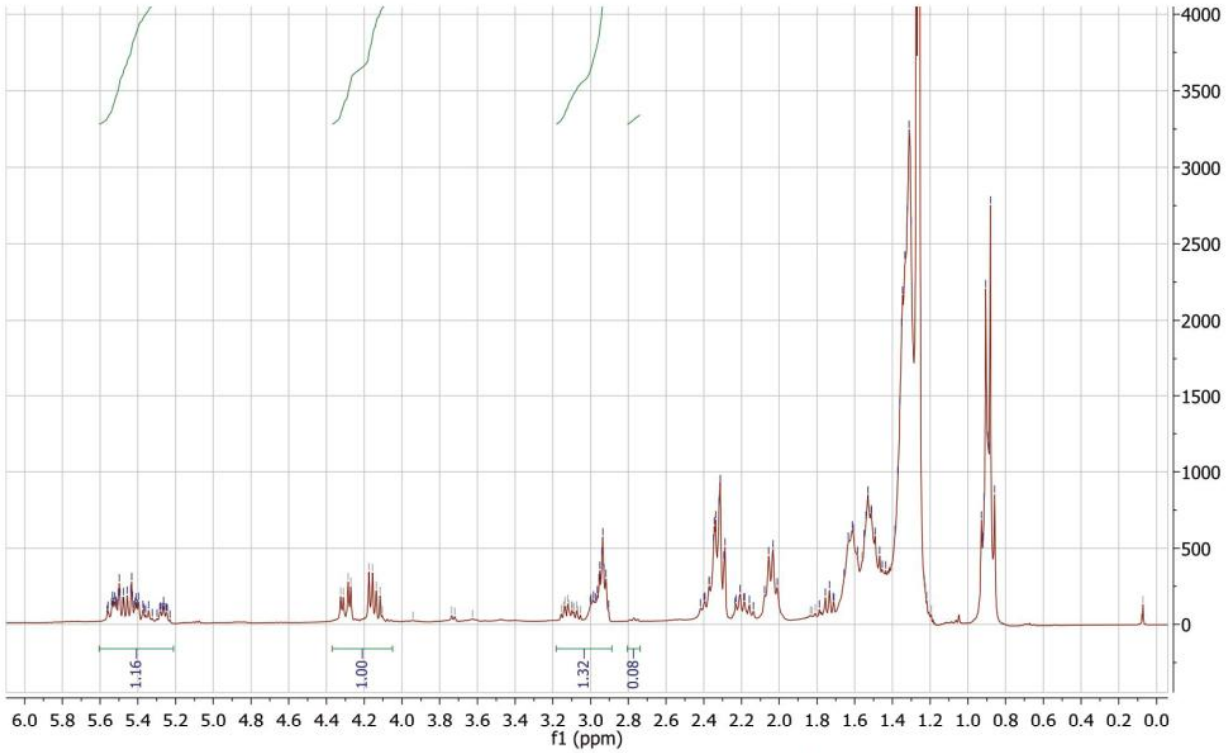

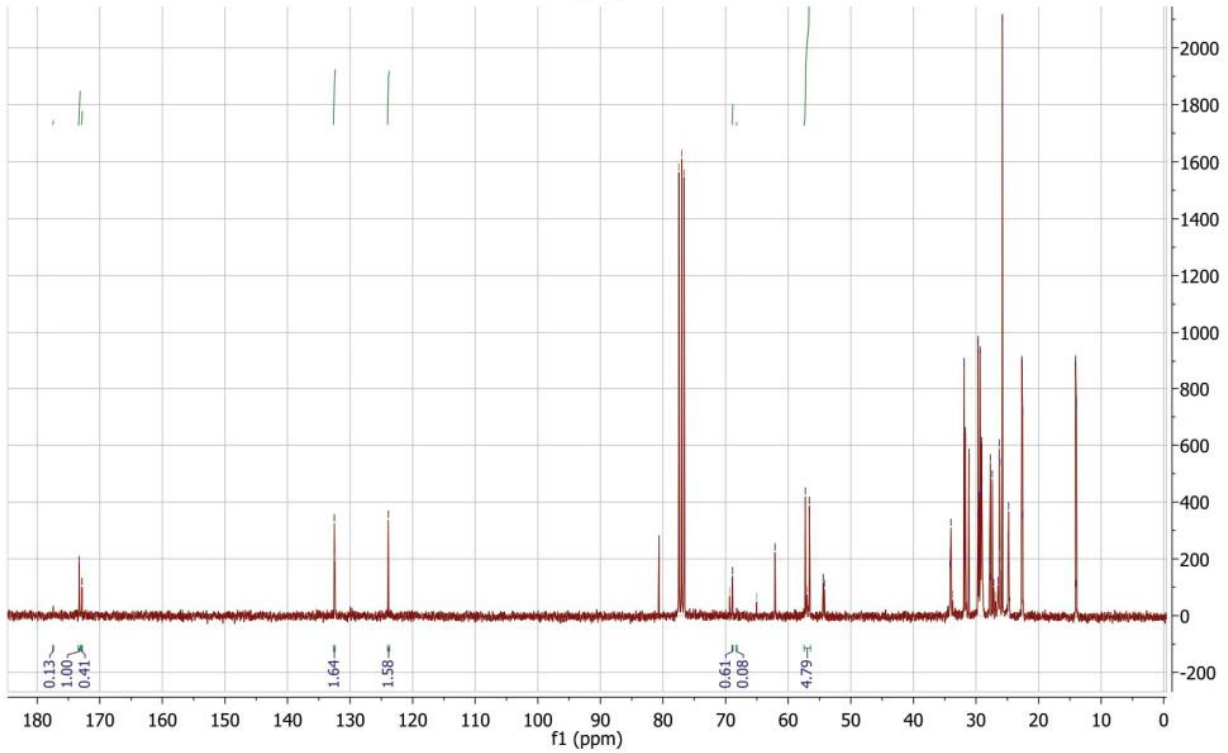

(J) ^{1}H and ^{13}C NMR of EVO by using TiPMOS1 as a catalyst at 70 ^{o}C for 24 h

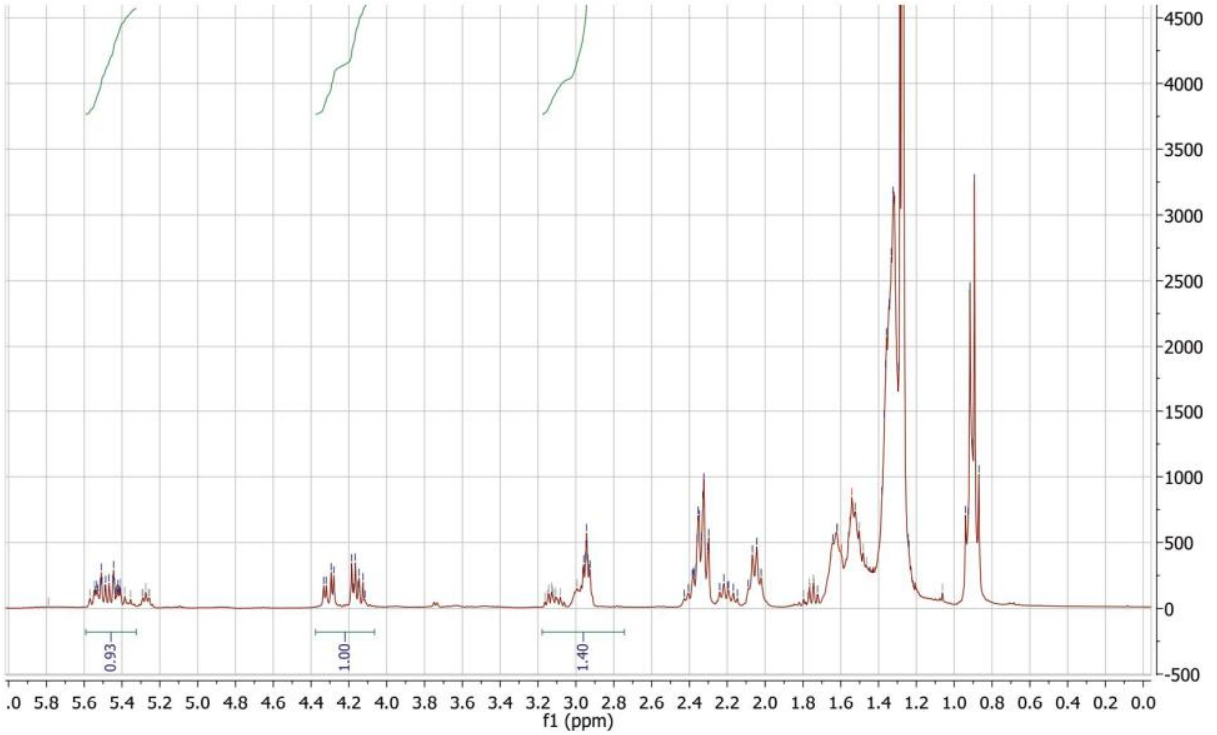

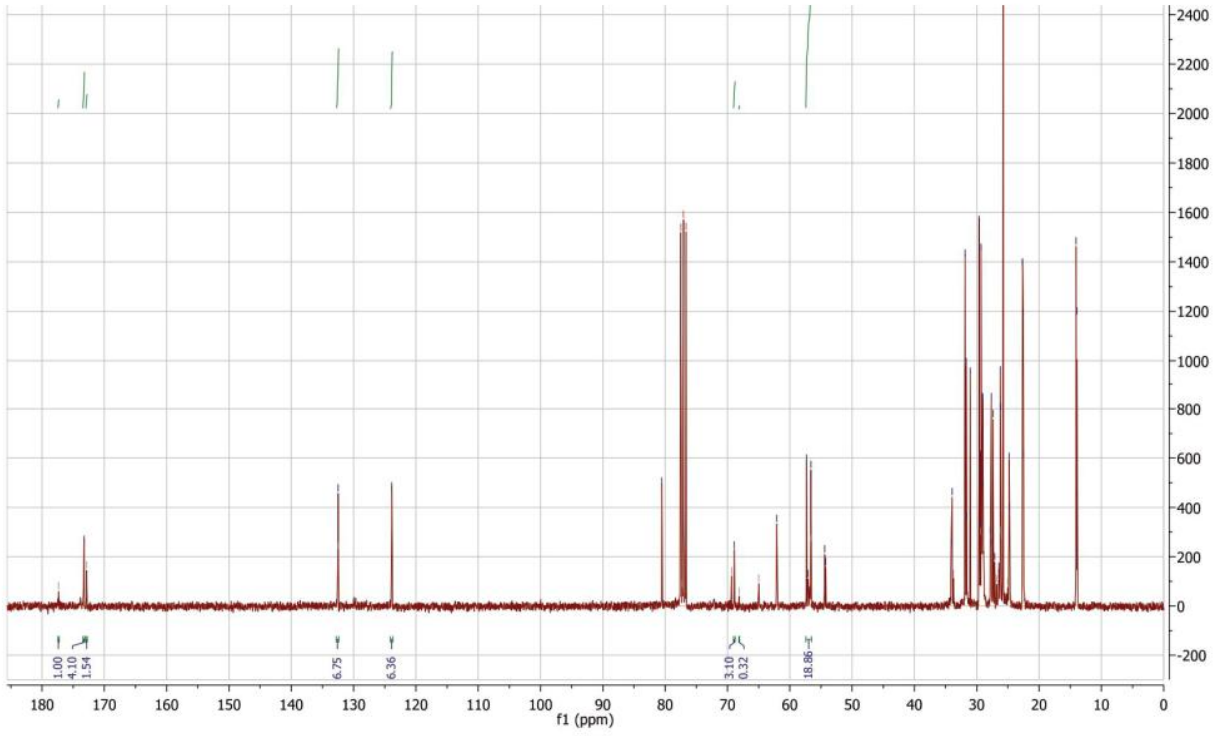

(K) ^{1}H and ^{13}C NMR of EVO by using TiG-PMO-L as a catalyst at 70 ^{o}C for 24 h

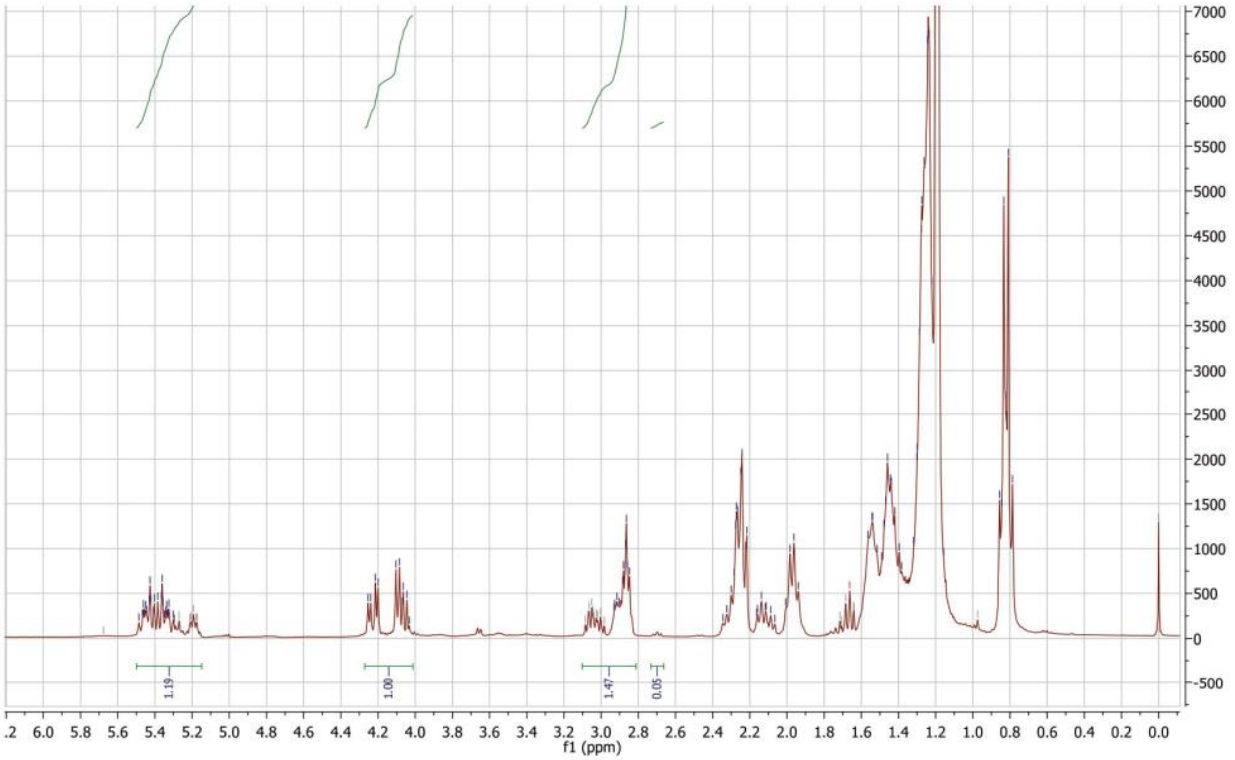

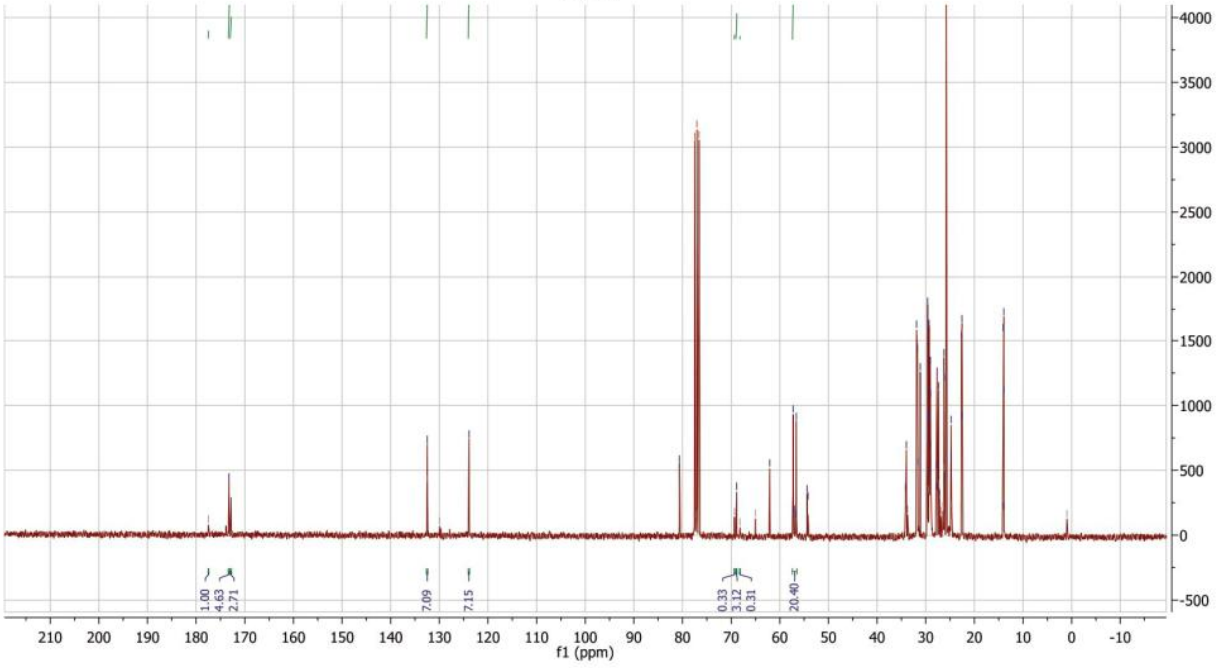

(L) ^{1}H and ^{13}C NMR of EVO by using TiG-EPMO-L as a catalyst at 70 ^{o}C for 24 h

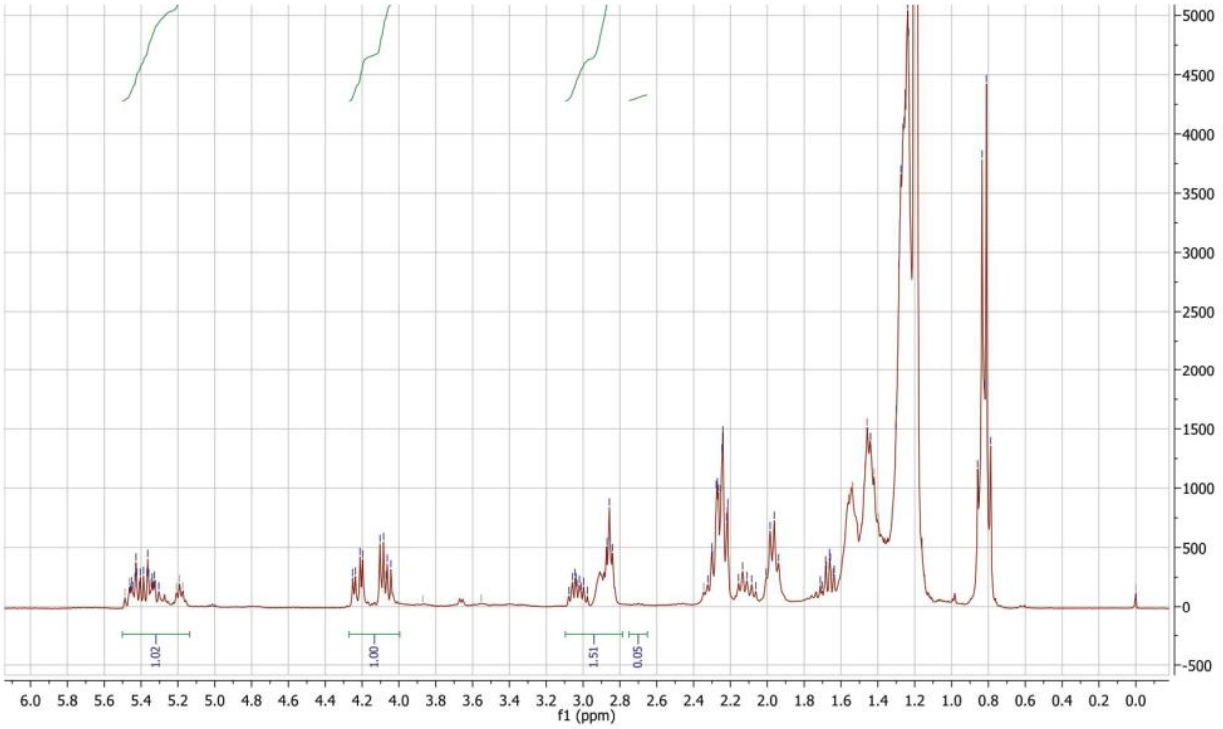

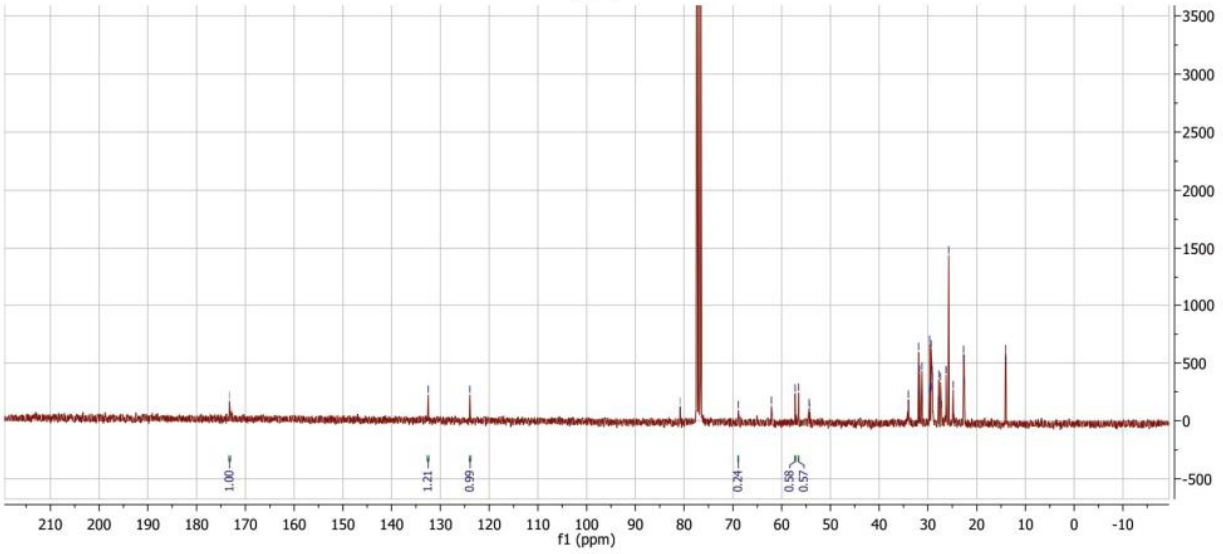

(M) ^{1}H and ^{13}C NMR of EVO by using TiEPMOL5 as a catalyst at 70 ^{o}C for 24 h

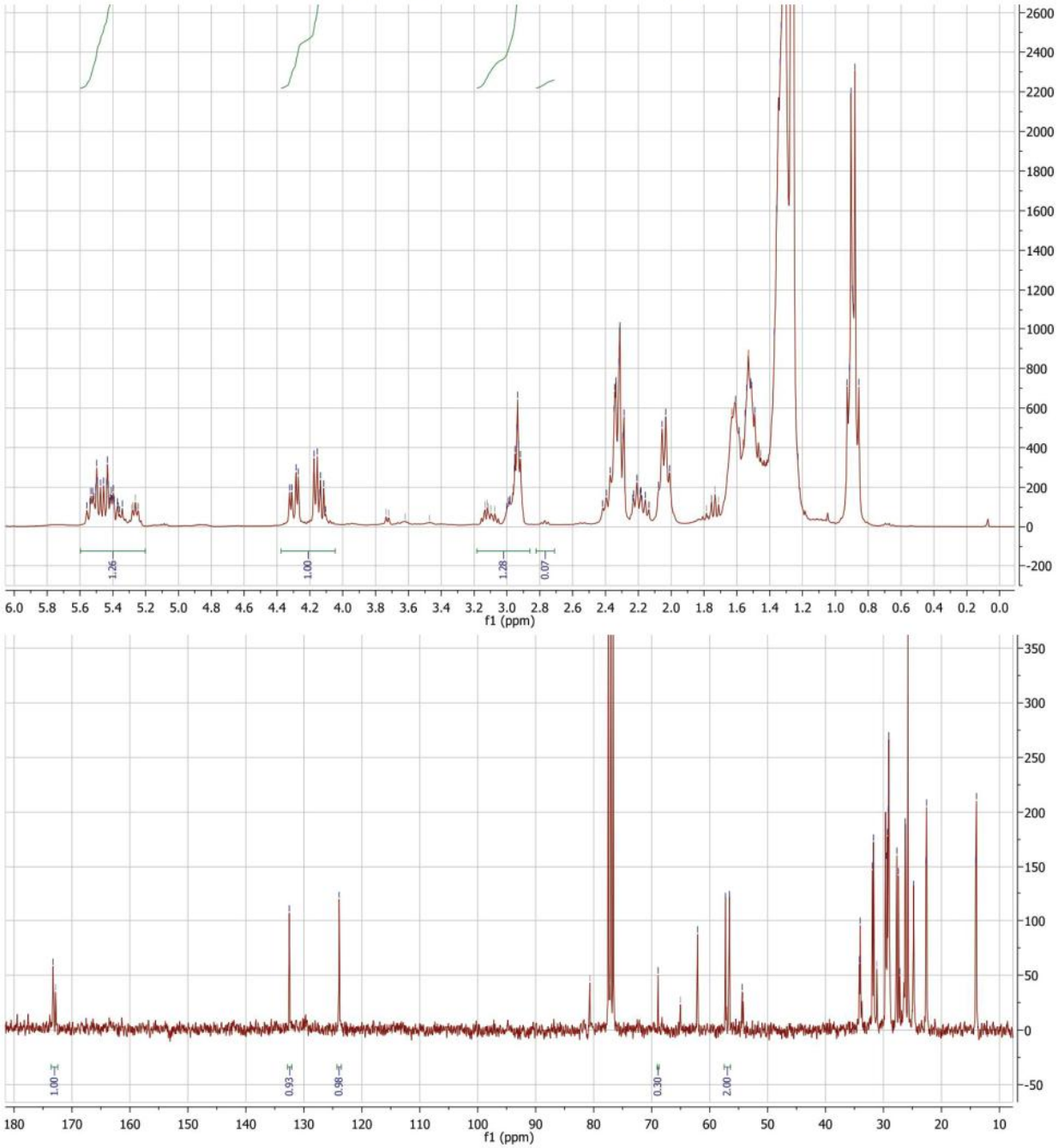

Figure 121 (A-M). ^{1}H and ^{13}C NMR of EVO products after 24 h reaction at 70 ^{o}C by using different catalysts